



HAL
open science

CISS Tsinghua-Princeton, 2019

Philippe Dagaut

► **To cite this version:**

Philippe Dagaut. CISS Tsinghua-Princeton, 2019: Combustion chemistry. Doctoral. Combustion Institute Summer School, Tsinghua University, Beijing, China. 2019. hal-04054394

HAL Id: hal-04054394

<https://hal.science/hal-04054394>

Submitted on 18 Apr 2023

HAL is a multi-disciplinary open access archive for the deposit and dissemination of scientific research documents, whether they are published or not. The documents may come from teaching and research institutions in France or abroad, or from public or private research centers.

L'archive ouverte pluridisciplinaire **HAL**, est destinée au dépôt et à la diffusion de documents scientifiques de niveau recherche, publiés ou non, émanant des établissements d'enseignement et de recherche français ou étrangers, des laboratoires publics ou privés.

Public Domain

1/ INTRODUCTION

What is combustion?

Why combustion?

Statistics

Chemical Kinetics and Modeling

Global fuel properties

Composition of Fuels

2/ EXPERIMENTAL TECHNIQUES FOR KINETIC MODELS ASSESSMENT

Introduction

Shock-tubes and rapid compression machines

Flow reactors: Tubular Flow Reactors and Stirred Reactors

Flames

Some conclusions and perspectives

3/ MODELING

Modeling: General information

Temperature dependencies of elementary reactions

Pressure dependencies

Kinetic analyses

Brute force method and 1st order sensitivity analyses

Pressure/Temperature dependencies and reaction pathways

Oxidation at low-T

Pyrolysis and high-T oxidation

Single-fuel vs. multi-fuel components

4/ POLLUTANTS: NO_x formation (thermal, prompt, N₂O, NNH) and reduction (SNCR, reburning)

NO_x formation

NO_x reduction

UHC and soot

Effect of trace species on ignition: NO_x, ozone

5/ SURROGATES, COMMERCIAL FUELS, BIOFUELS

Gasoline

Diesel

Jet fuel

Biofuels

INTRODUCTION



La Guerre du Feu, Jean-Jacques Annaud, 1981

Where is combustion?



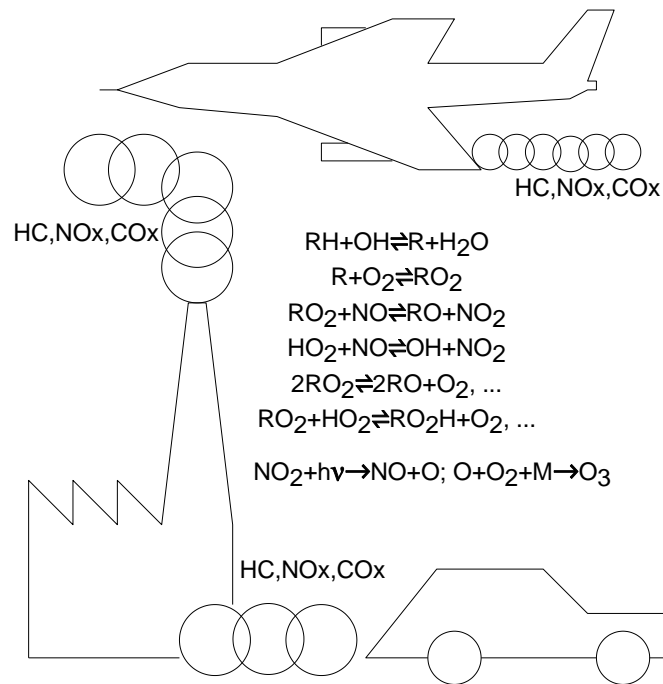
What is combustion? (1/2)

The **oxidation** of a fuel, ultimately leads to the formation of carbon dioxide, water, and heat in the case of organic fuels (e.g. hydrocarbons).

Other definition: an exothermic redox reaction between a fuel (reductant) and an oxidant (e.g., oxygen from air)

Incomplete combustion yields UHC and soot. 

NOx resulting from nitrogen oxidation can also be released. 



What is combustion? (2/2)

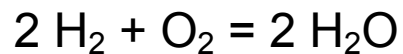
Combustion involves chemical reactions, thermochemistry, kinetics, heat and mass transfer, radiation...

The overall/global chemical equation, e.g. $2 \text{H}_2 + \text{O}_2 = 2 \text{H}_2\text{O}$, $\text{CH}_4 + 2\text{O}_2 = \text{CO}_2 + 2\text{H}_2\text{O}$, is a mass balance that does inform on the reaction pathways to products.

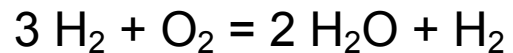
Equivalence ratio and excess air:

$$\phi = \{[\text{Fuel}]/[\text{O}_2]\} / \{[\text{Fuel}]/[\text{O}_2]\}_{\text{at stoichiometry}}$$

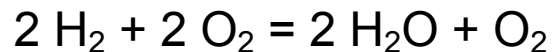
$$\lambda = 1/\phi$$



$\phi=1$ and $\lambda = 1$ (stoichiometric mix)



$\phi>1$ and $\lambda < 1$ (fuel-rich, excess of fuel, some left over)



$\phi<1$ and $\lambda > 1$ (fuel-lean, excess of oxygen, some left over)

The combustion of methane involves a long sequence of elementary reactions (*initiation, propagation, branching, and termination*). They involve stable species and labile species (*atoms, radicals*). These reactions proceed with reaction rates ranging from slow (e.g., $\text{RH}+\text{O}_2$) to very fast ($\text{R}+\text{R}'$).

Why combustion?

Transport accounts for ca. 20% of the total global primary energy consumed, ca. 23% of CO₂ emissions, ca. 7 billion tons of CO₂, ca. from livestock farming.

> 99.9% Transport is powered by I.C. engines (land and marine) and air transport by GT.

G. Kalghatgi

Applied Energy 225 (2018) 965–974

Table 2

Fuel capacity and equivalent battery pack size for three different types of aircraft.

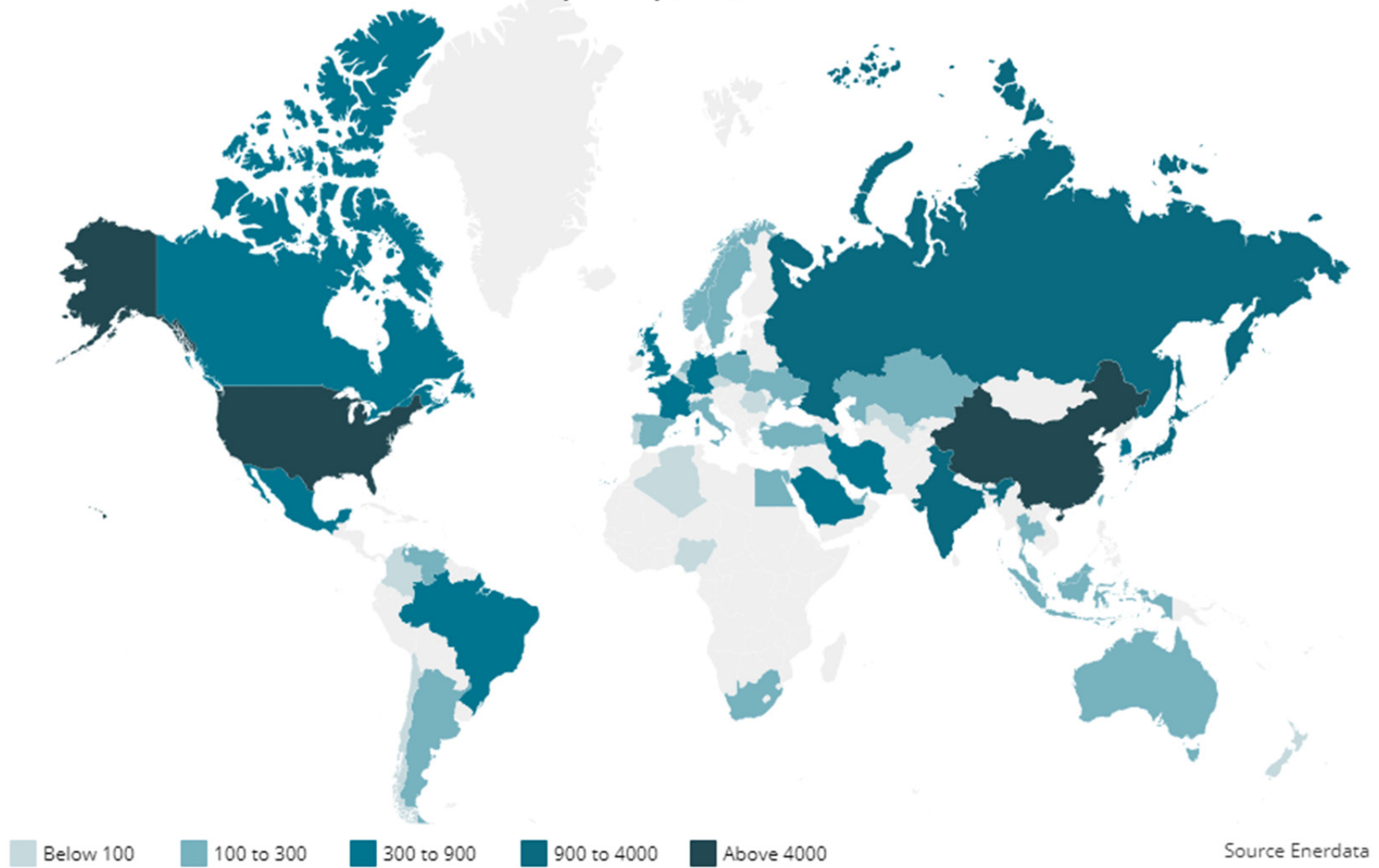
	Maximum Take-off Weight (MTOW), kg	Volume of fuel, liters	Weight of fuel ^a , kg	Energy content of fuel (ECF) ^a , MWh	Weight of battery pack with the same ECF ^b (WBP), kg	WBP/MTOW
Embraer 135 [41]	20,000	5146	4168	51	284,831	14
Airbus A320 Neo [42]	76,000	26,730	21,651	266	1,479,506	19
Airbus A380-800 [43]	576,000	323,545	262,071	3223	17,908,216	31

The global demand for transport energy is ca. 105 TWh of liquid fuel energy/day (**38,325 TWh/year**)

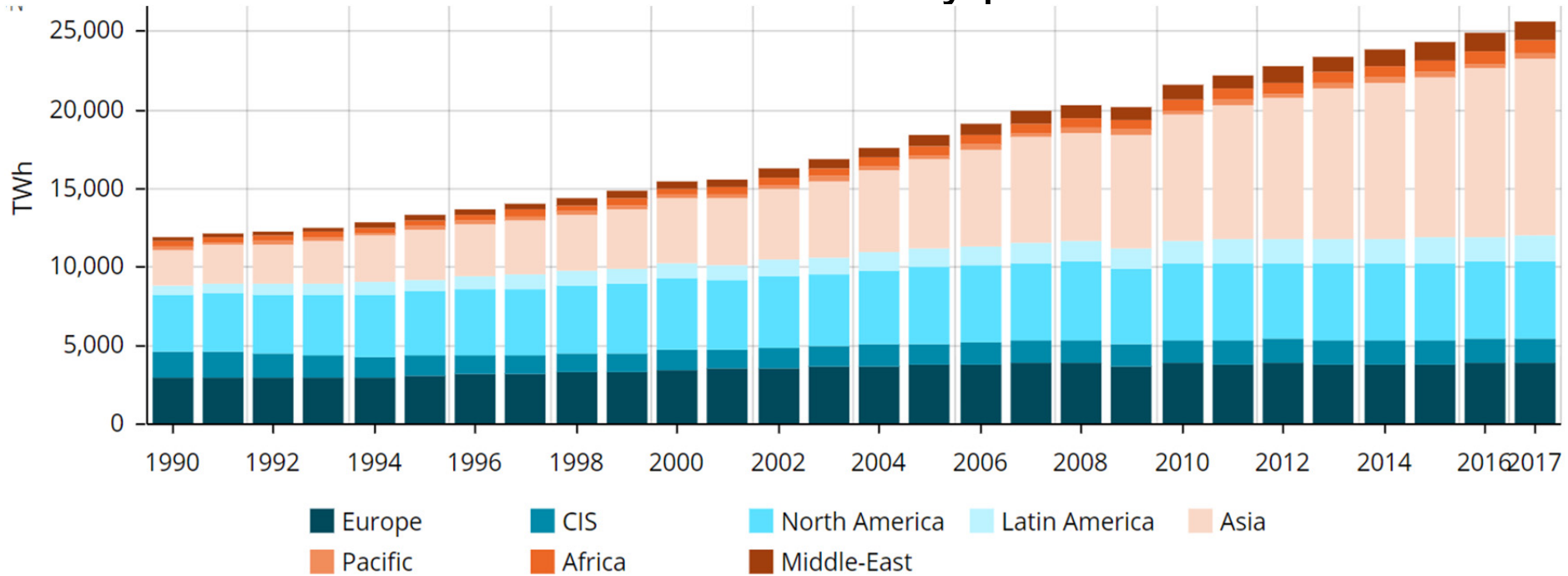
In 2016 the consumption of wind and solar energy together reached **1,292 TWh/year**.

In 2016 the consumption of electricity reached almost **25,000 TWh/year**. 

Breakdown by country (TWh) World - 2017



World electricity production



% in electricity production (2017)

From Global Energy Statistical Yearbook 2018

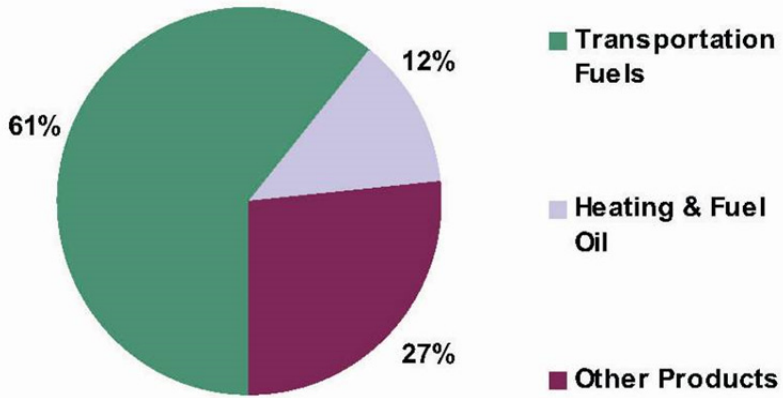


Renewables Non renewables



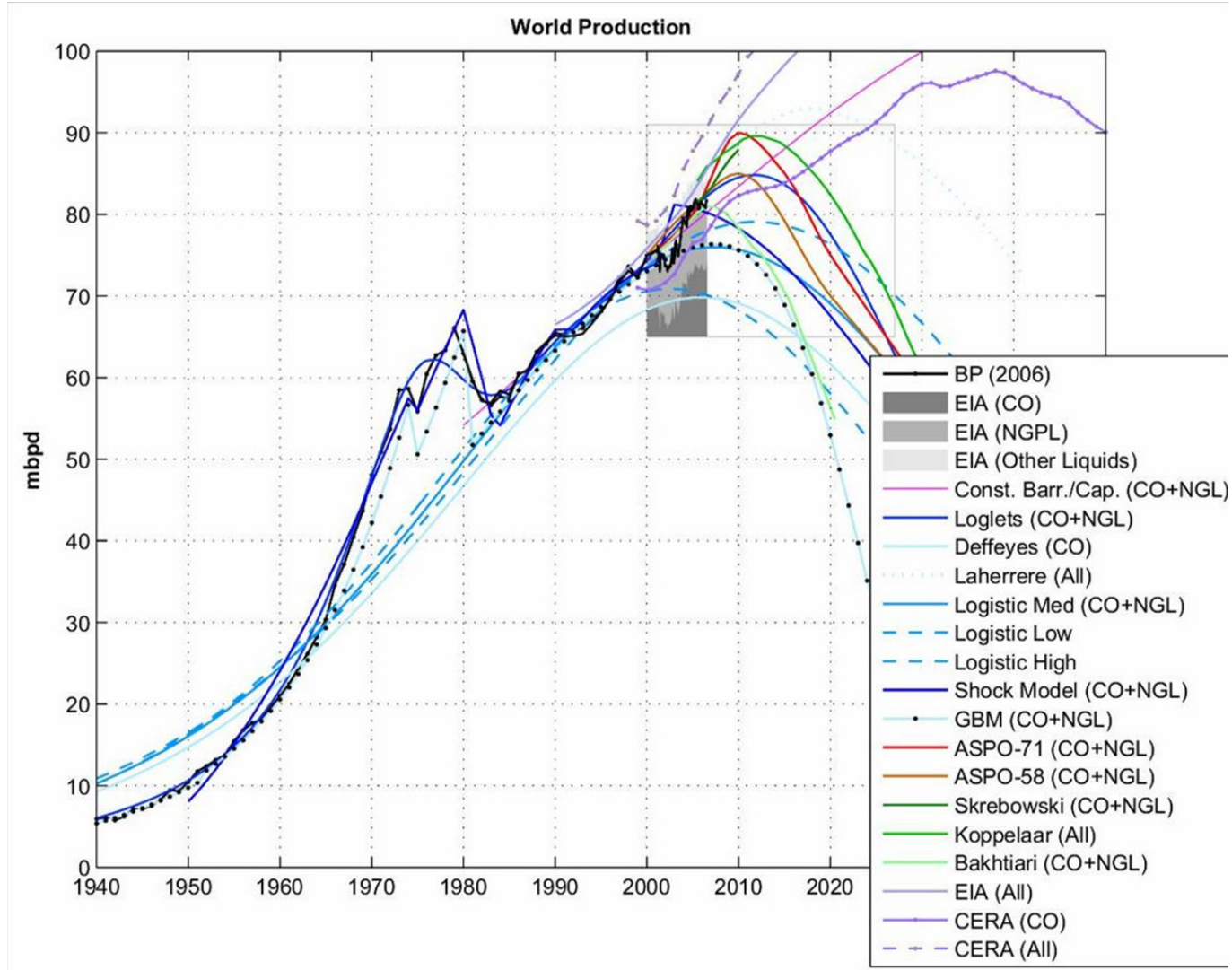
What do we burn?

World: Total Oil Product Demand by Type of Product, 2014

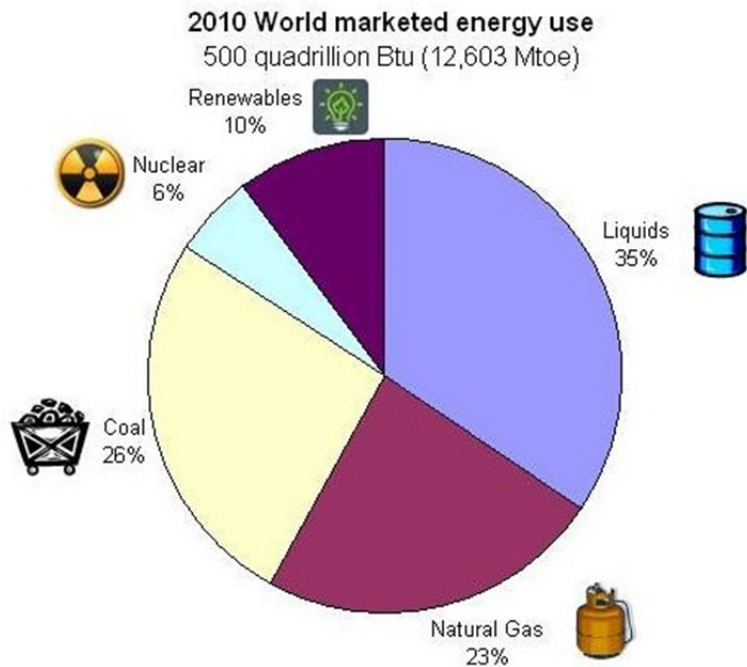


IEA, 2009

98% transport fuels are oil-derived



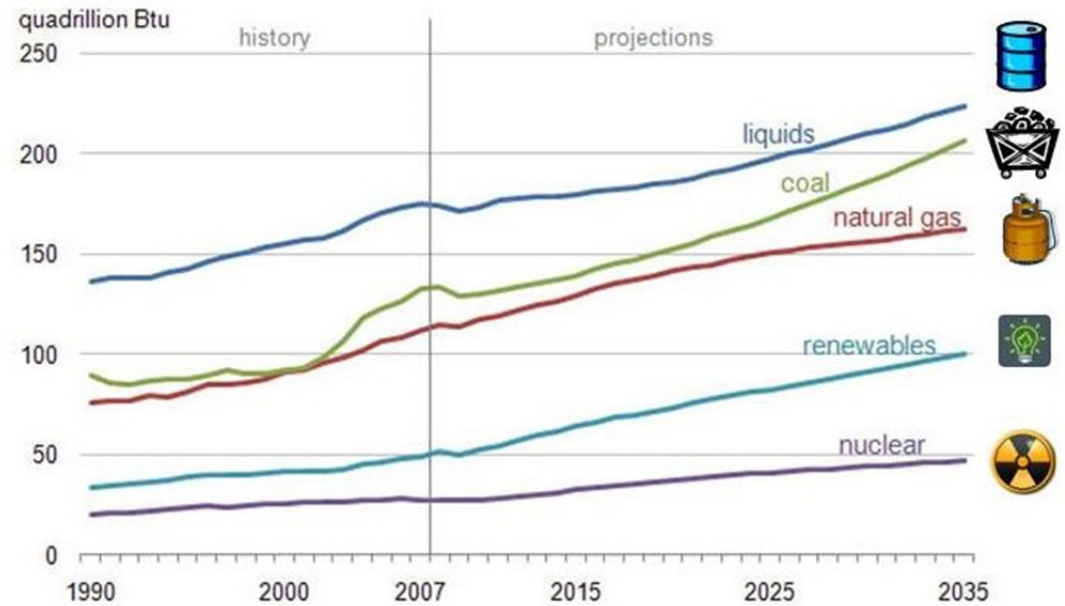
Primary Energy Use



Source: U.S. Energy Information Administration
(Report #DOE/EIA-0484(2010))

Primary Energy Use

Figure 2. World marketed energy use by fuel type



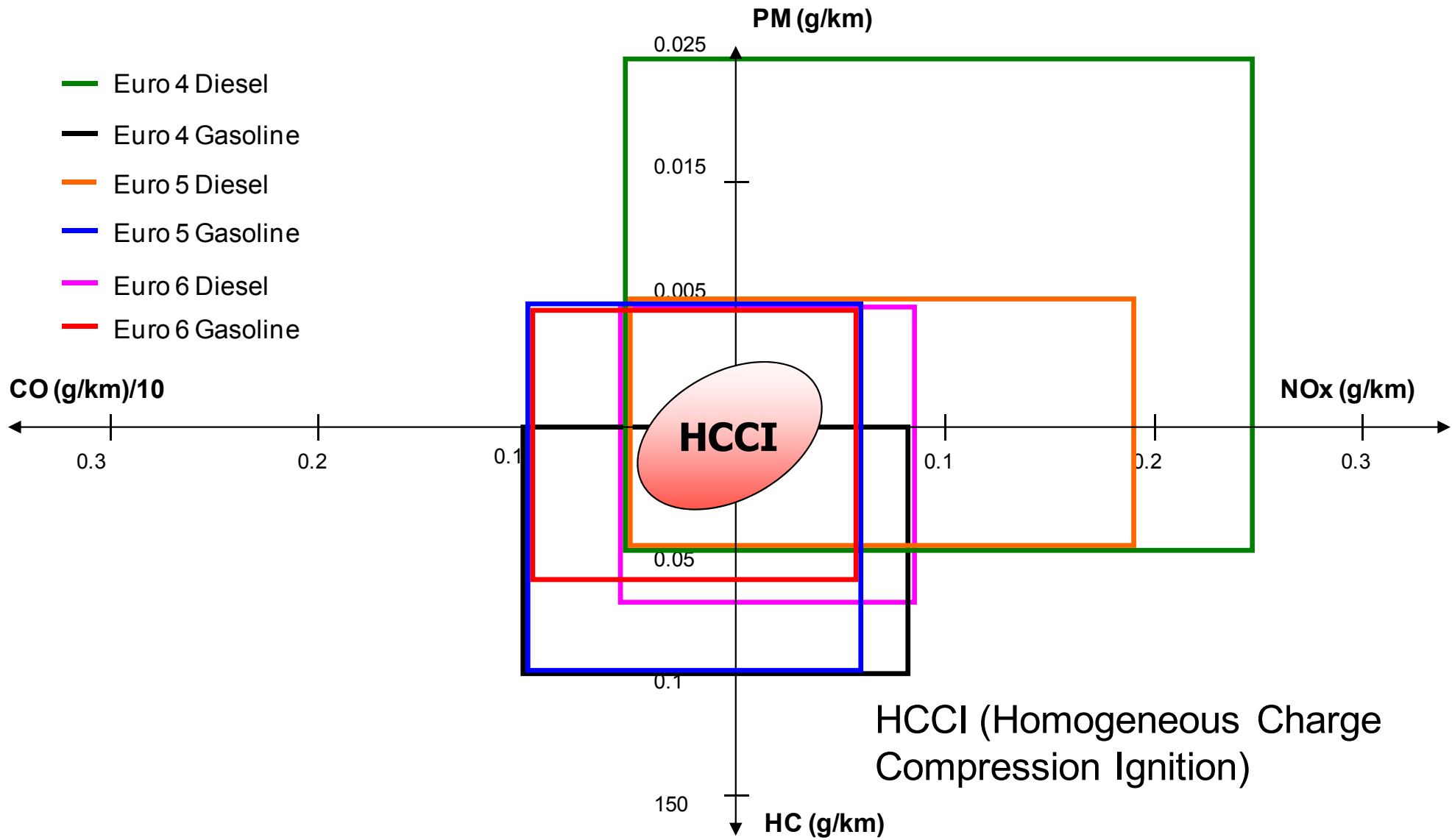
Source: U.S. Energy Information Administration
(Report #DOE/EIA-0484(2010))

Sustainability:

We need to burn cleaner

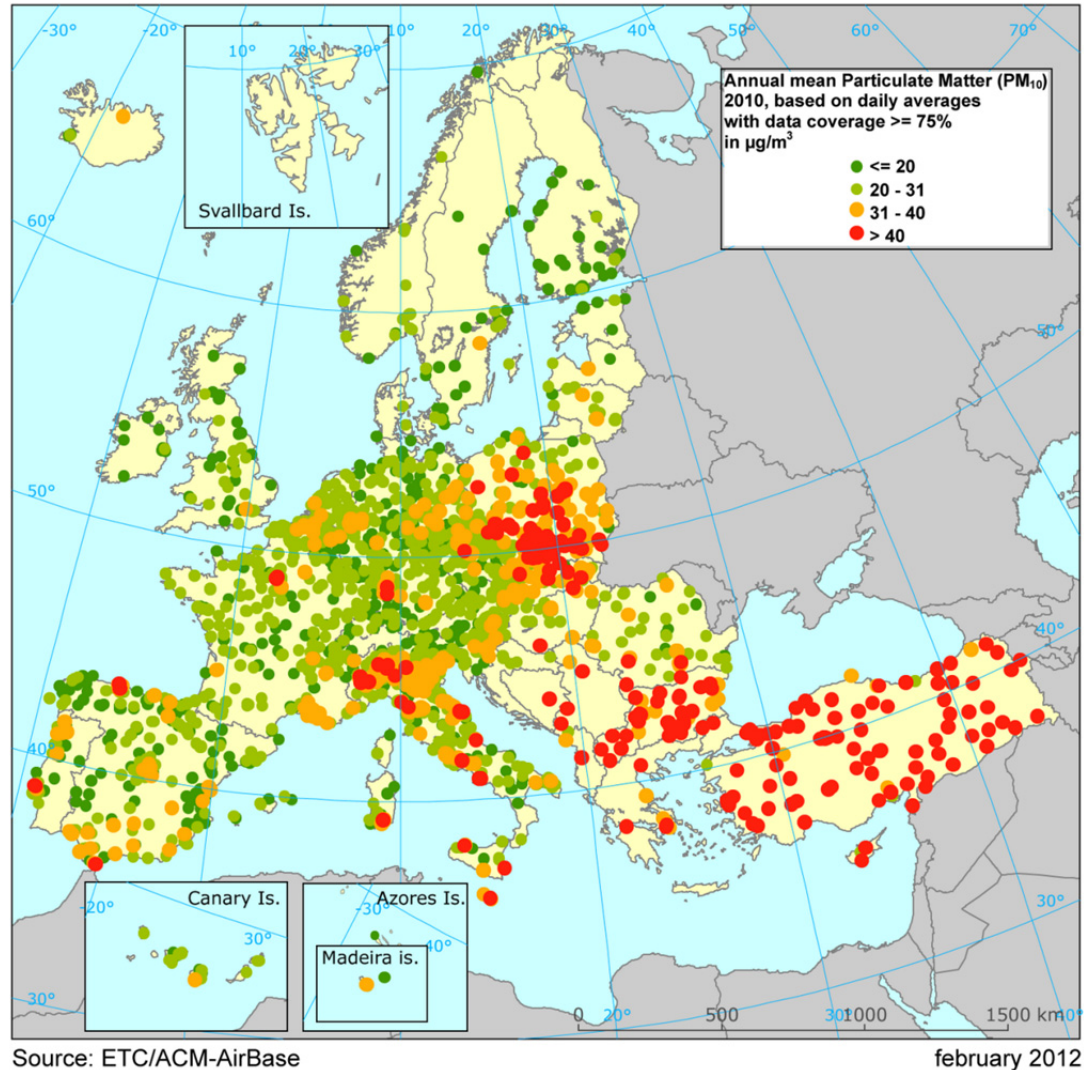
We need more efficient combustion (energy production)

EU regulations



HCCI (Homogeneous Charge
Compression Ignition)

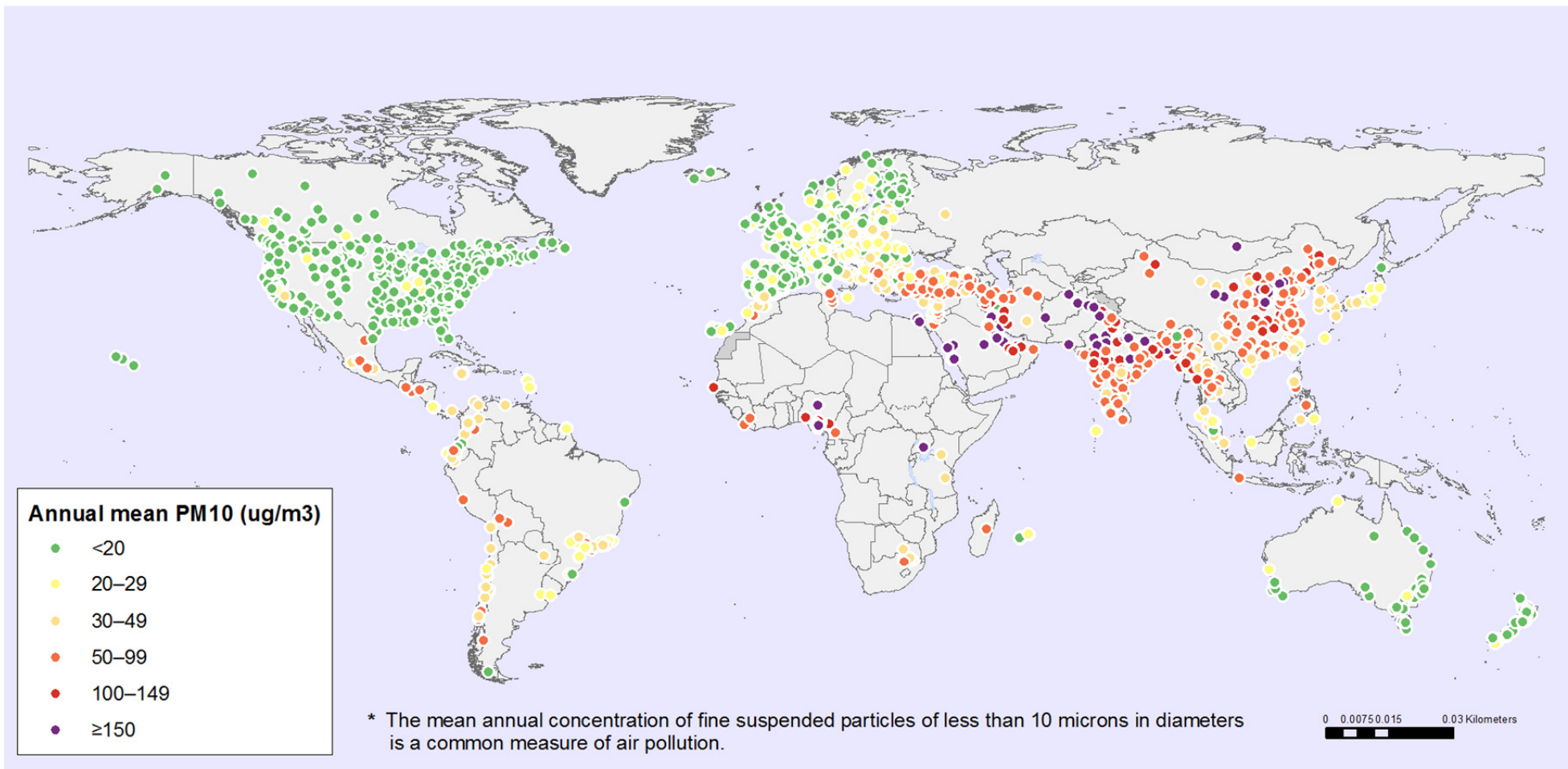
PM₁₀ (<10 microns)



Sources of particulates: industry, agriculture, air and ground transportation (soot, tires, brakes), homes, wild fires, volcanoes, soil erosion and hurricanes/tornados, sea salts...

PARTICULATES

Concentration of particulate matter with an aerodynamic diameter of 10 μm or less (PM₁₀) in nearly 3000 urban areas*, 2008–2015



The boundaries and names shown and the designations used on this map do not imply the expression of any opinion whatsoever on the part of the World Health Organization concerning the legal status of any country, territory, city or area or of its authorities, or concerning the delimitation of its frontiers or boundaries. Dotted and dashed lines on maps represent approximate border lines for which there may not yet be full agreement.

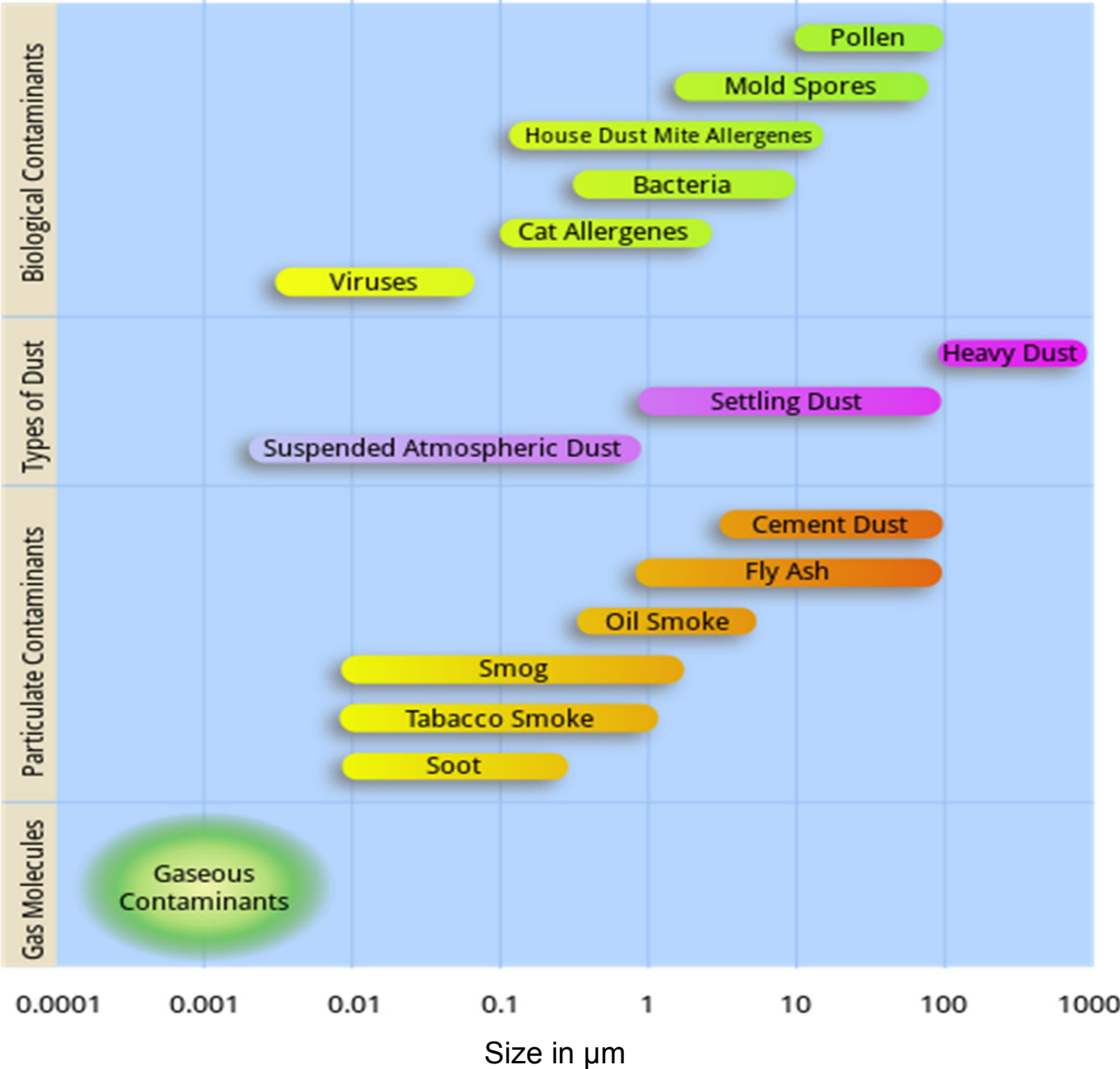
Data Source: World Health Organization
Map Production: Information Evidence and Research (IER)
World Health Organization



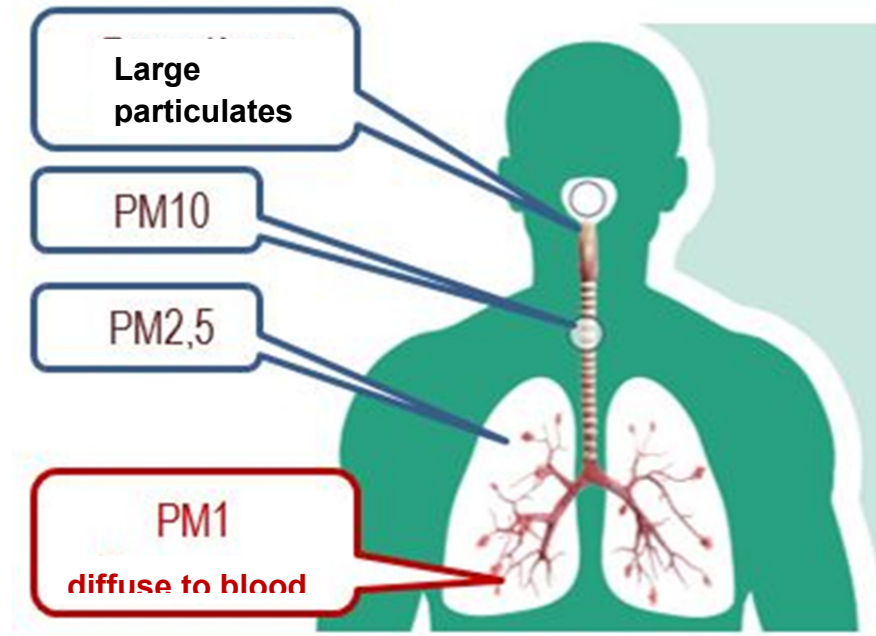
© WHO 2016. All rights reserved.

See also <https://www.conserve-energy-future.com/causes-and-effects-of-particulate-matter.php>

PARTICULATES and health



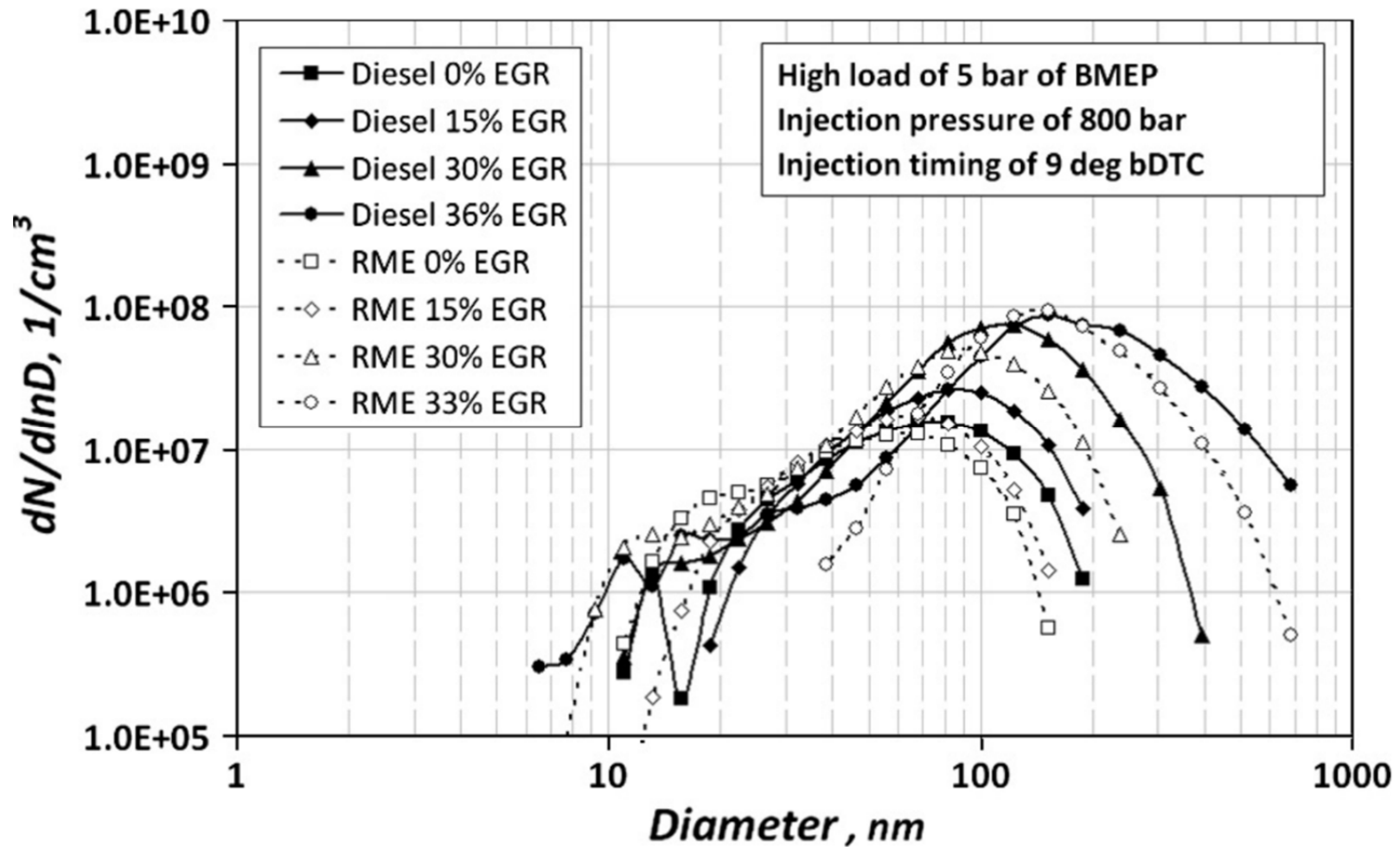
PARTICULATES and health



Source: produits.xpair.com

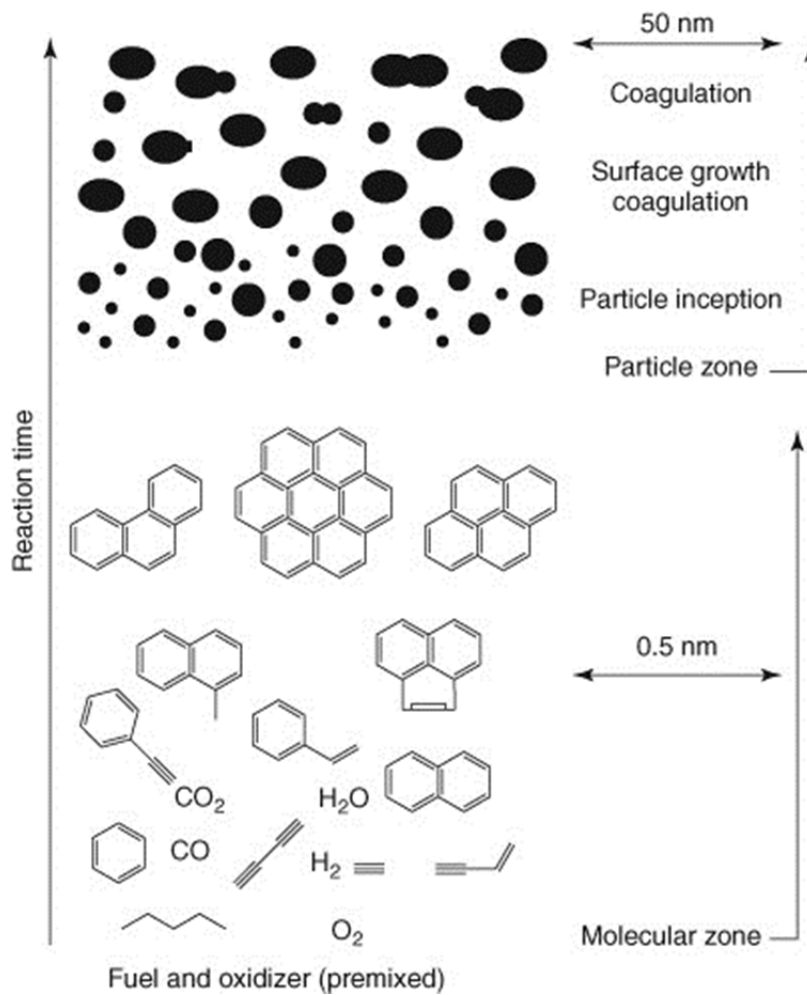
N.B. PM1 (< 1 μm or 1000 nm)

PARTICULATES from i.c. engines

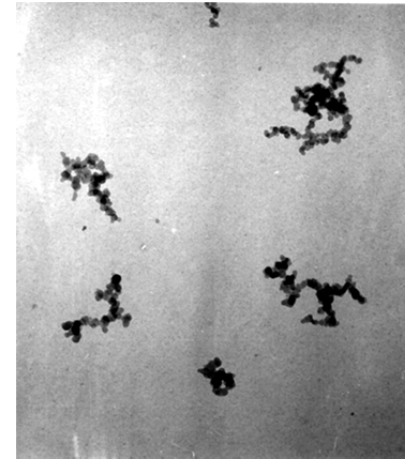


Source: Labecki et al., *Fuel* (2013) <https://doi.org/10.1016/j.fuel.2013.05.013>

PARTICULATES



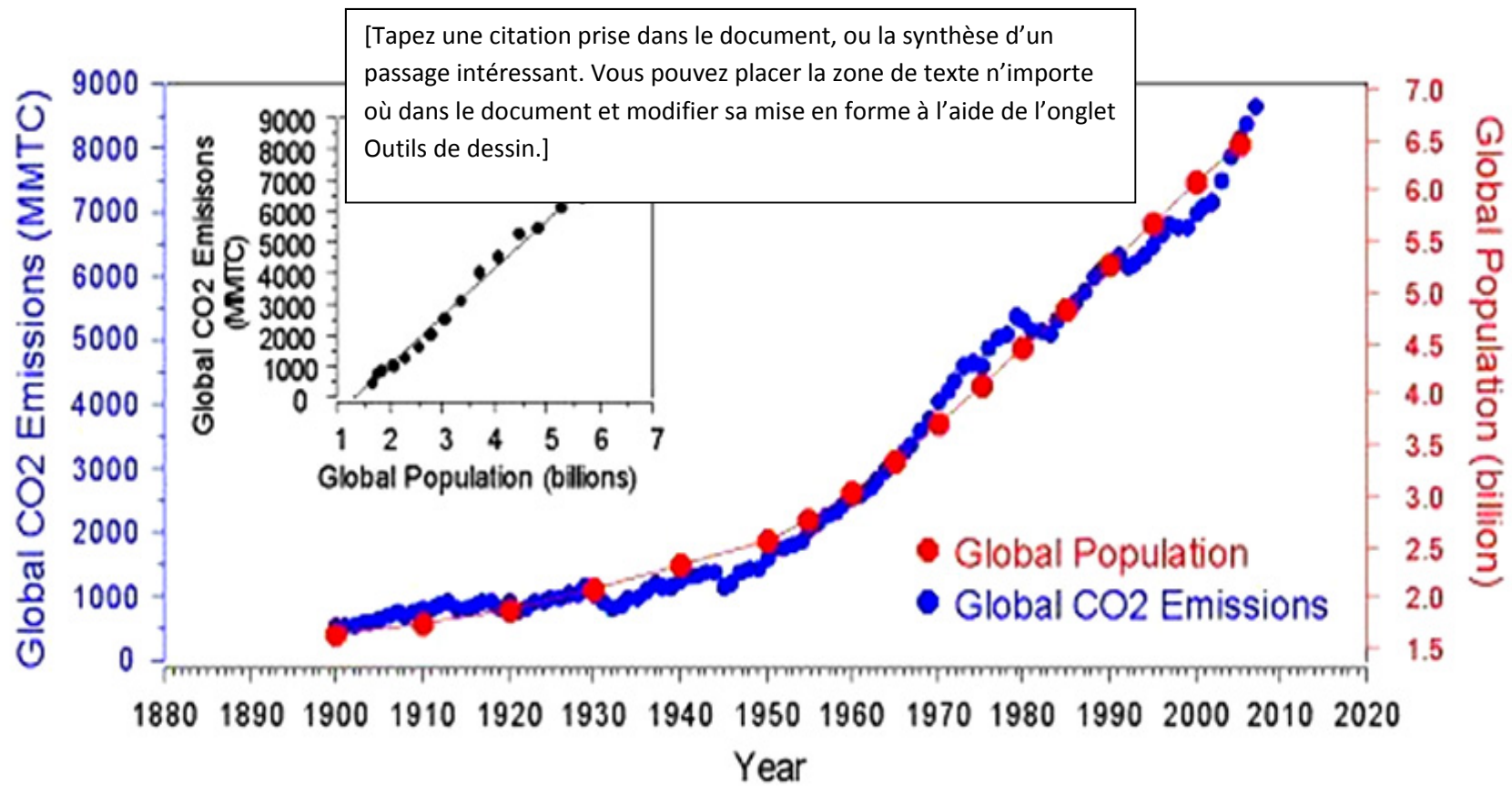
Source: H. Bockhorn (1986)



TEM image of soot particles generated by CAST

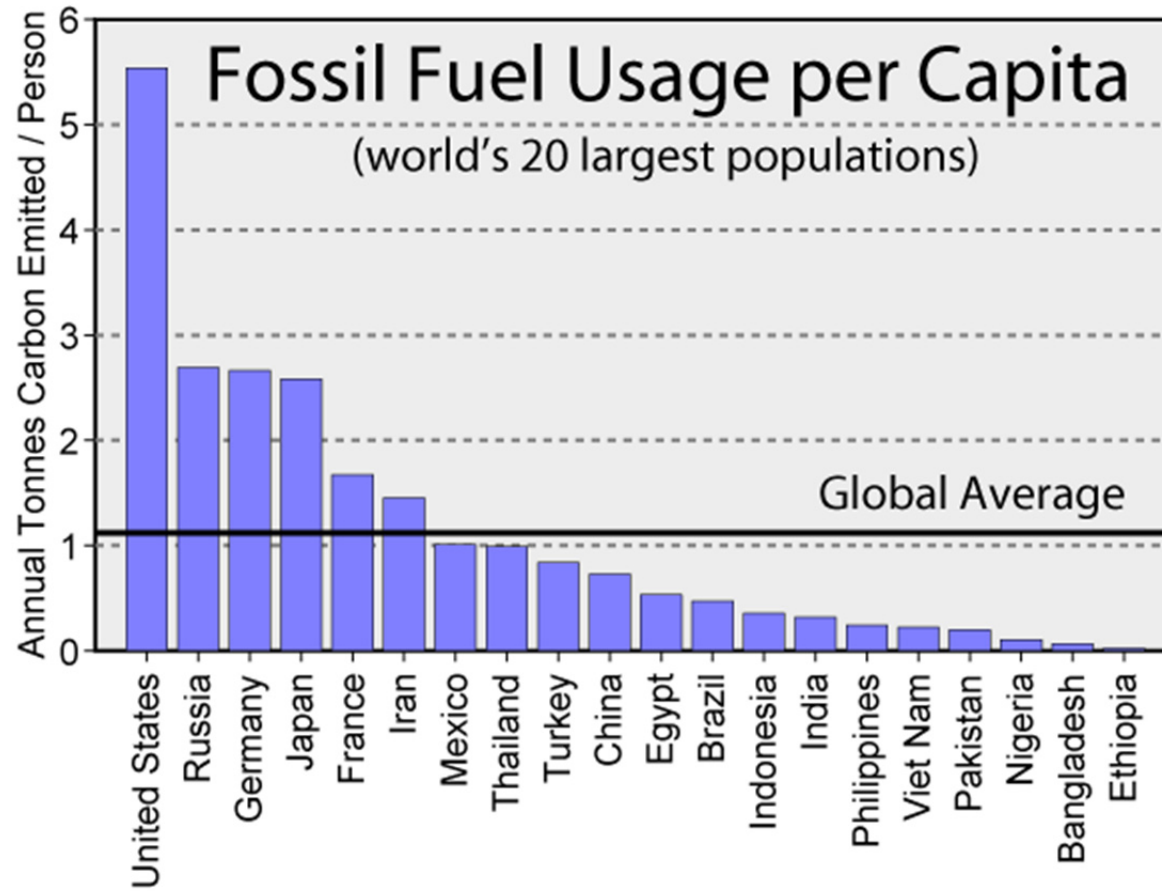
Source: <http://www.sootgenerator.com>

GHG: CO₂

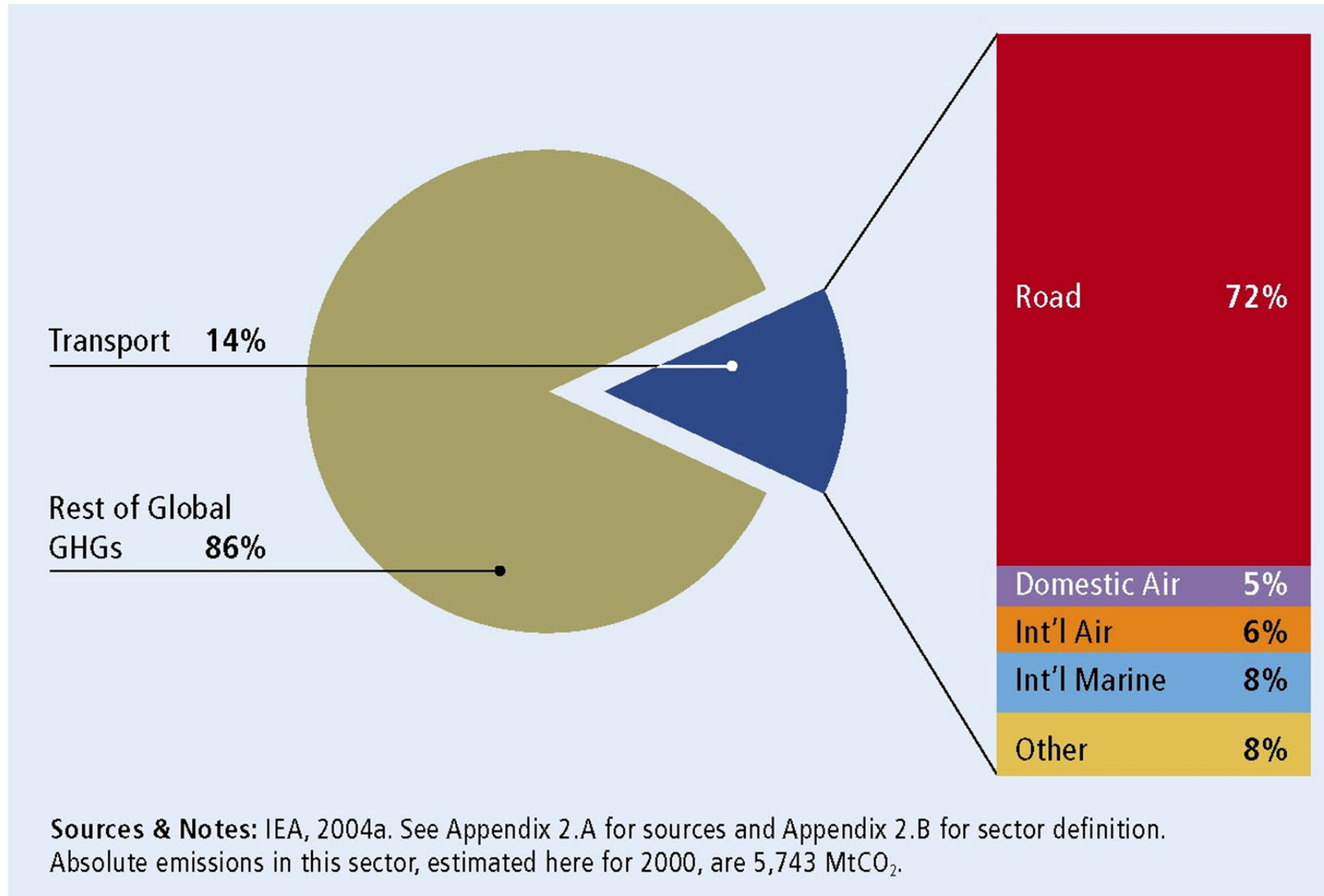


<http://www.worldclimatereport.com>

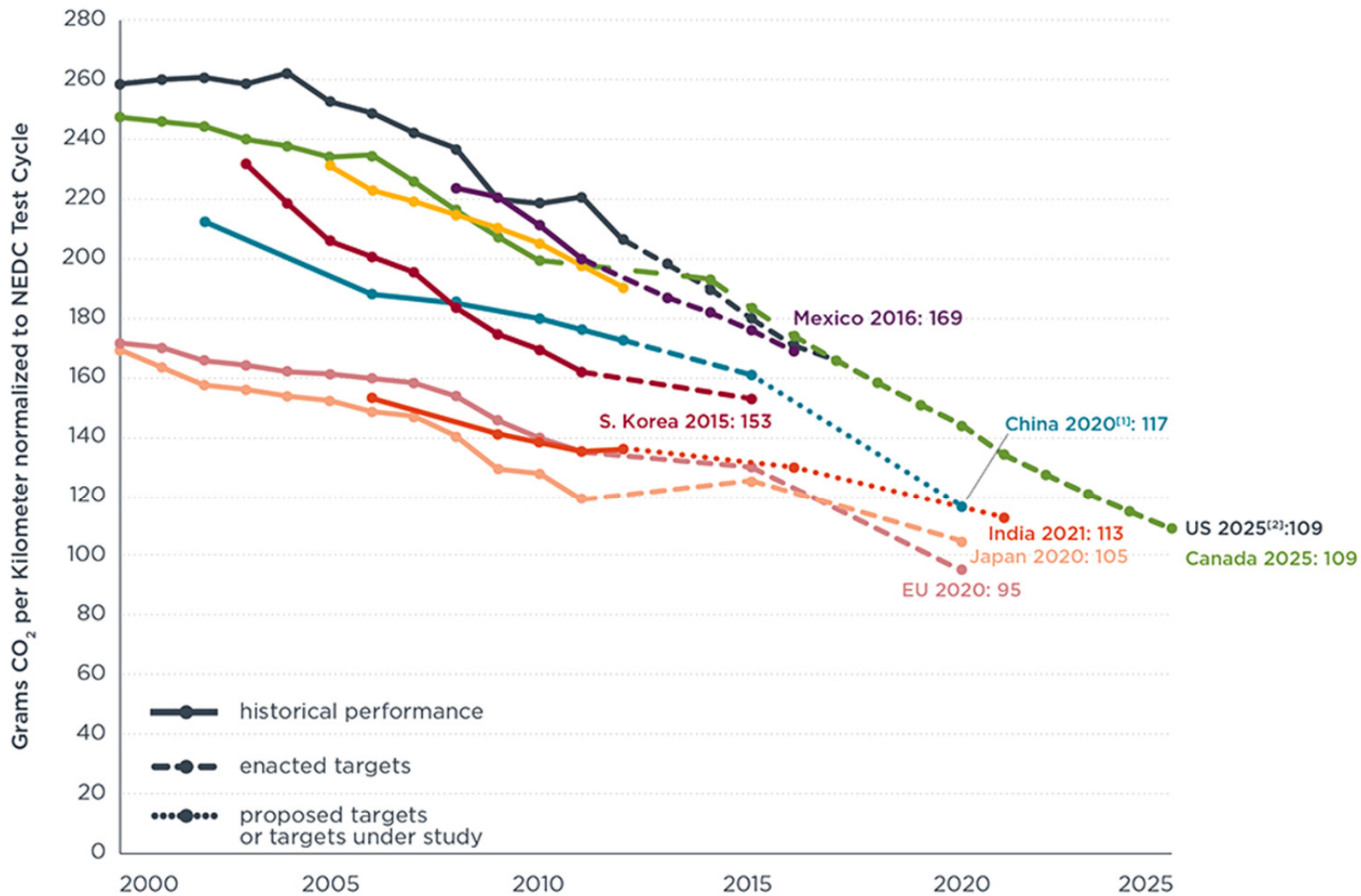
GHG: CO₂



GHG



REDUCE CO₂ EMISSIONS

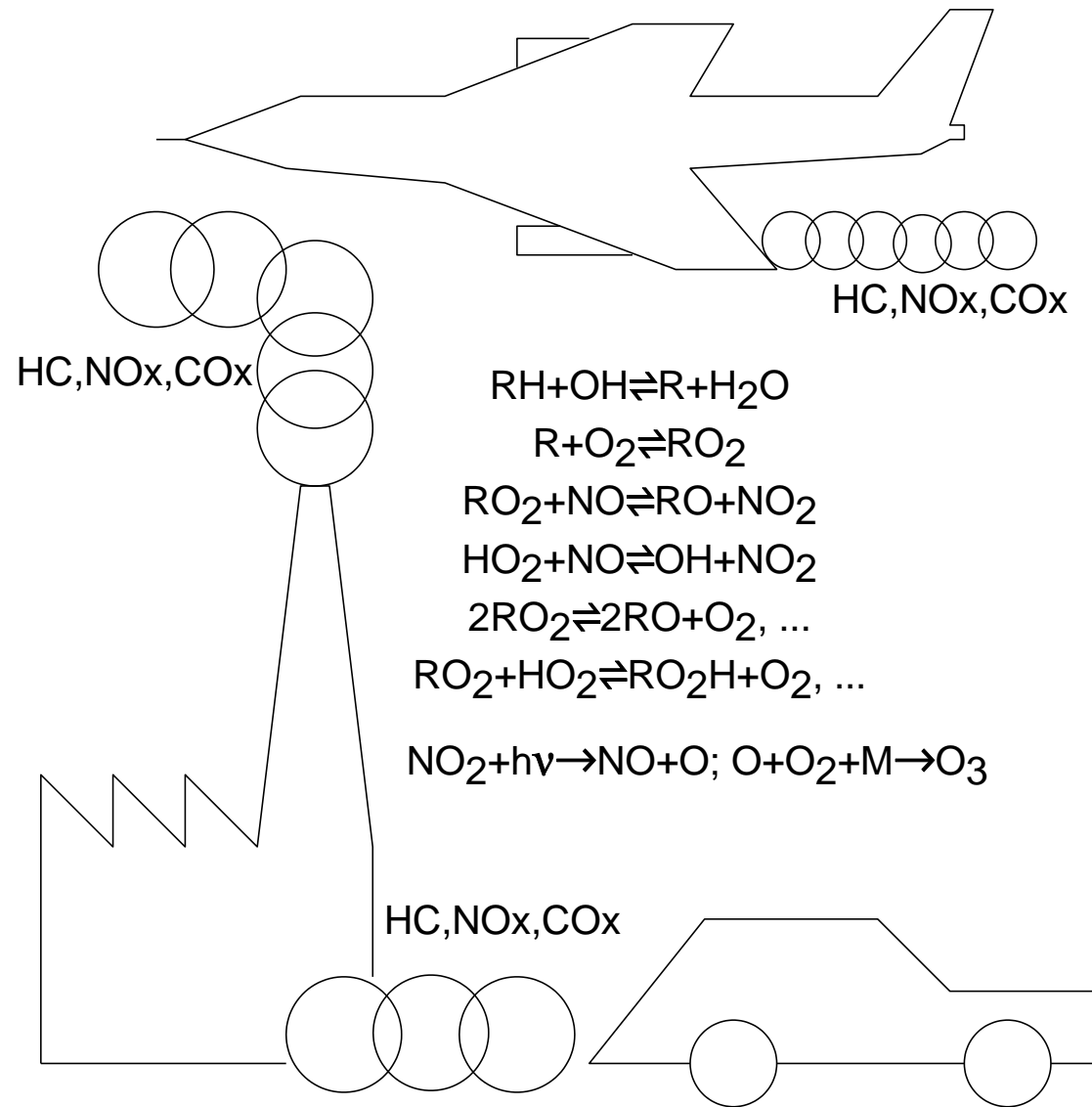


[1] China's target reflects gasoline vehicles only. The target may be higher after new energy vehicles are considered.

[2] US, Canada, and Mexico light-duty vehicles include light-commercial vehicles.

[3] Supporting data can be found at: <http://www.theicct.org/info-tools/global-passenger-vehicle-standards>

Chemical Kinetics and Modeling



Experimental data ↔ Model

Constrain the model by using

☞ **Global parameters:** Ignition delays (initiation reactions, $R+O_2$)
Burning velocities (H fluxes)

☞ **Detailed information:** Species concentrations (~ all processes)

Initiations: $RH \rightleftharpoons R + H$

$RH \rightleftharpoons R' + R''$

$RH + O_2 \rightleftharpoons R + HO_2$

Propagations: $RH + X \rightleftharpoons R + HX$ (X= H, O, OH, HO₂, CH₃, HCO, ...)

Terminations: $R + H \rightleftharpoons RH$

$R' + R'' \rightleftharpoons RH$

☞ **Different types of 'reactors':** ST, PF, PSR, Flames (laminar premixed, opposed flow), RCM, engines

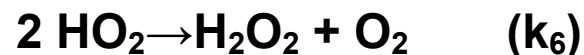
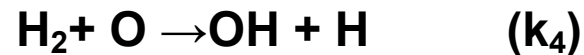
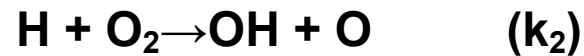
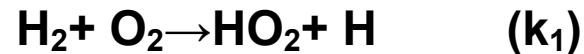
Introduction

Global vs. detailed chemistry

$\text{H}_2 + \frac{1}{2} \text{O}_2 = \text{H}_2\text{O}$: mass balance; misrepresents reaction pathways

$$\text{Global Rate} = A T^n \exp[-E / R T] [\text{Fuel}] [\text{O}_2]^{\frac{1}{2}}$$

In reality, many more reactions:



• • •

The value of k_i indicates how fast the reaction can proceed

Such sets of reactions constitute a “chemical kinetic reaction mechanism”

Kinetics

Forward reaction $A + B \rightarrow C + D$

$$\text{Rate} = -d[A]/dt = k_+ [A][B] = A_+ T^n \exp[-E/RT][A][B]$$

Reverse reaction $C + D \rightarrow A + B$

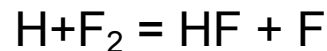
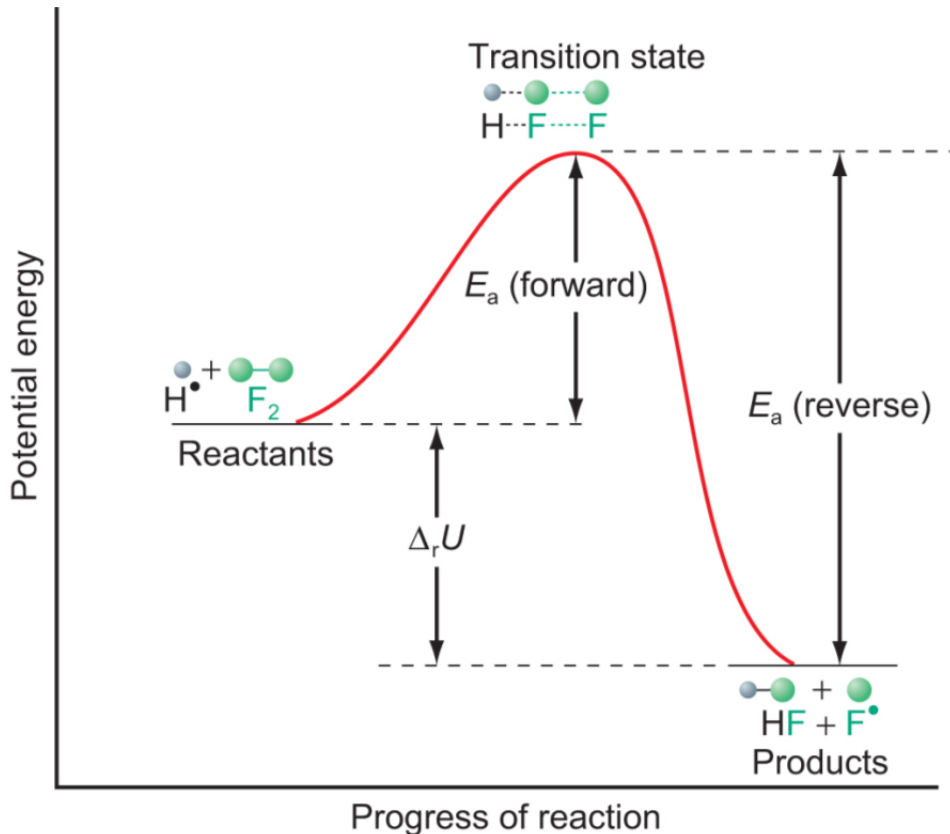
$$\text{Rate} = -d[C]/dt = k_- [C][D] = A_- T^{n'} \exp[-E'/RT][C][D]$$

Equilibrium constant computed from thermochemistry $K_{\text{eq}} = k_+ / k_-$

k_+ and/or k_- are determined experimentally or computed

K can be obtained in tabulations (JANAF, NASA ...)

Thermodynamics



As H approaches F₂, the F-F bond extends and electron density moves from that F-F bond into the newly forming F-H bond. This involves an increase in potential energy.

1st law: The energy U of an isolated system is constant

$dU = dQ + dW$; Q = heat absorbed by the system; W = work done on system

2nd law: Mechanical energy can be transferred completely into heat but heat cannot be transformed completely into mechanical energy

$dS \geq dQ/T$; S = entropy

$dS = dQ_{rev}/T$ and $dS > dQ_{irrev}/T$

3rd law: The entropy of a perfectly crystalline substance at 0°K is 0

$S = 0$ at $T = 0^\circ\text{K}$ ($\lim_{T \rightarrow 0}(S) = 0$)

Thermodynamics

Gibbs energy: $G = H - TS$

At constant T , $\Delta G = \Delta H - T\Delta S$

Equilibrium occurs at minimum G (at constant T, P)

Equilibrium constant: $\Delta G^\circ = -RT \ln(K)$ ($^\circ$ refers to the standard state)

Heat capacities ($_p$ at constant pressure; $_v$ at constant volume):

$$C_v = (\partial U / \partial T)_v \quad C_p = (\partial U / \partial T)_p \quad C_p = C_v + R \text{ (ideal gas)}$$

$$H(T_2) = H(T_1) + \int_{T_1}^{T_2} C_p dT$$

$$\Delta_r H(T_2) = \Delta_r H(T_1) + \int_{T_1}^{T_2} \Delta_r C_p dT$$

Thermodynamics

Gibbs Energy (G) indicates the spontaneity of a reaction

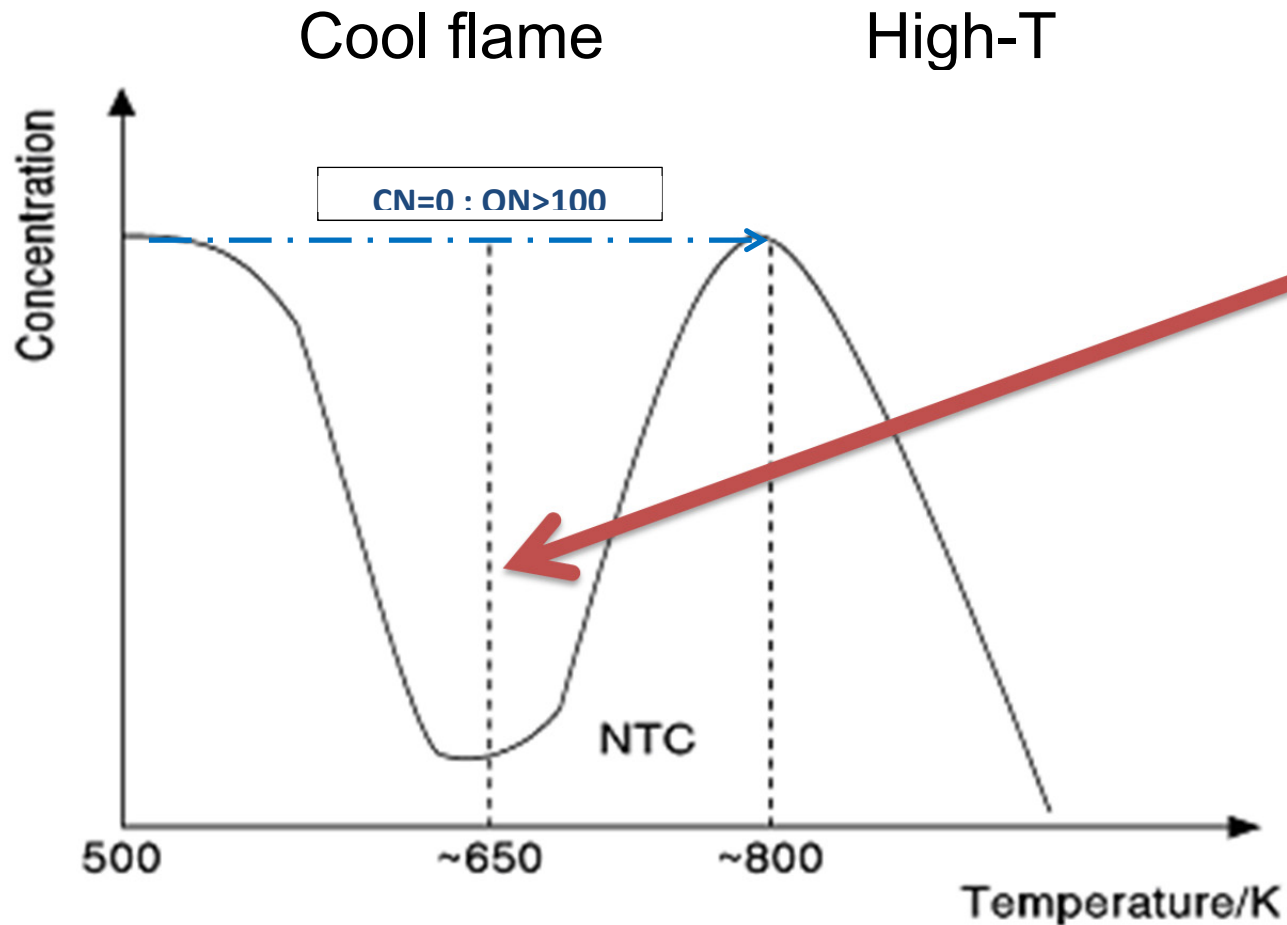
G depends on Enthalpy and Entropy

Entropy contribution increases as T increases: $G = H - TS$

$\Delta_r G < 0$ for spontaneous reaction

$\Delta_r G > 0$ for non-spontaneous reaction

Cetane number, Octane number



piston damaged by strong knock (LLNL)

Fuel concentration vs. temperature

S.I. engines: ON=100 for iso-octane and ON=0 for n-heptane (C_8H_{18})

C.I. engines: CN=100 for n-hexadecane ($C_{16}H_{34}$) and CN=0 for 1-methylnaphthalene ($C_{11}H_{10}$)

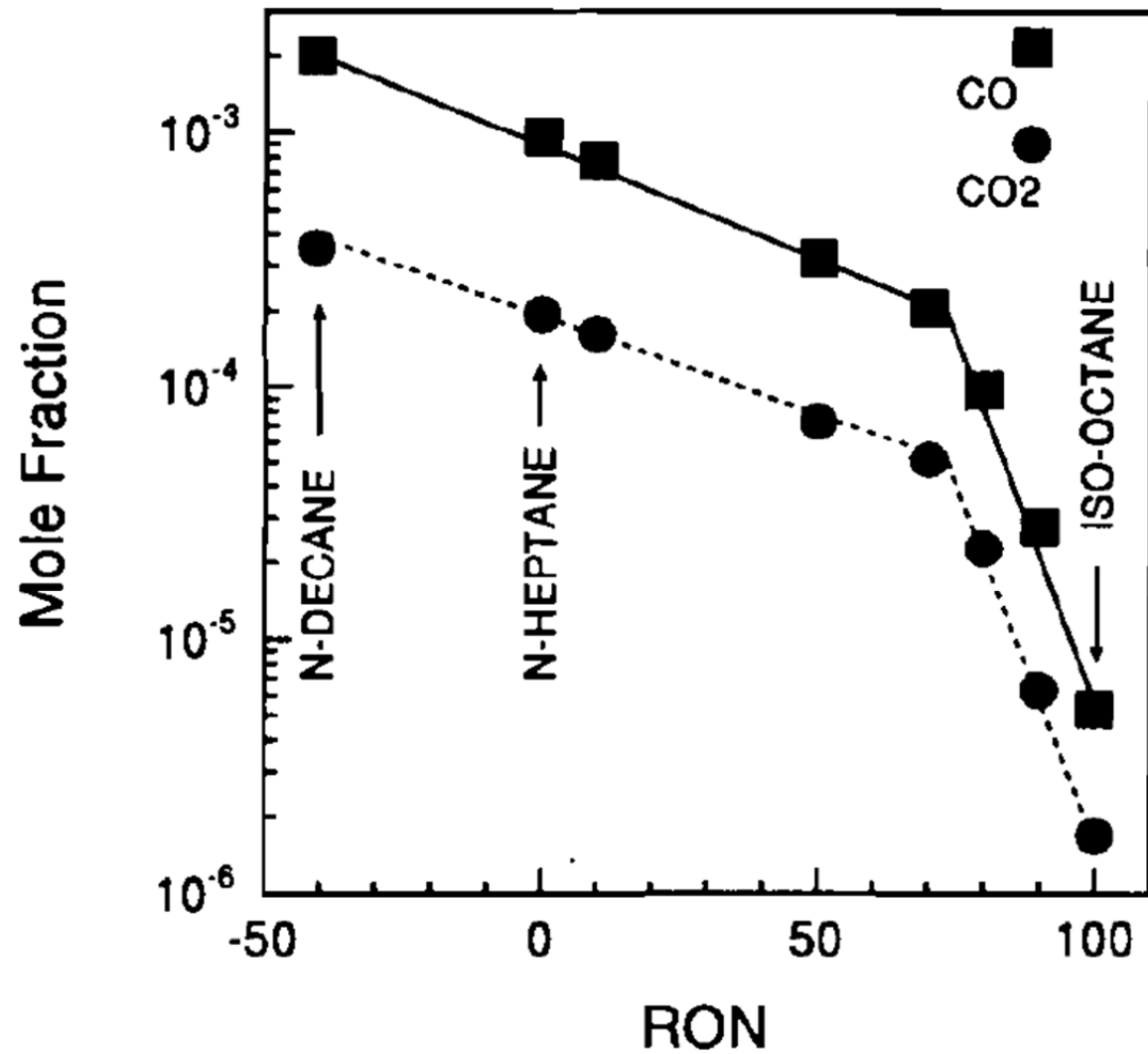
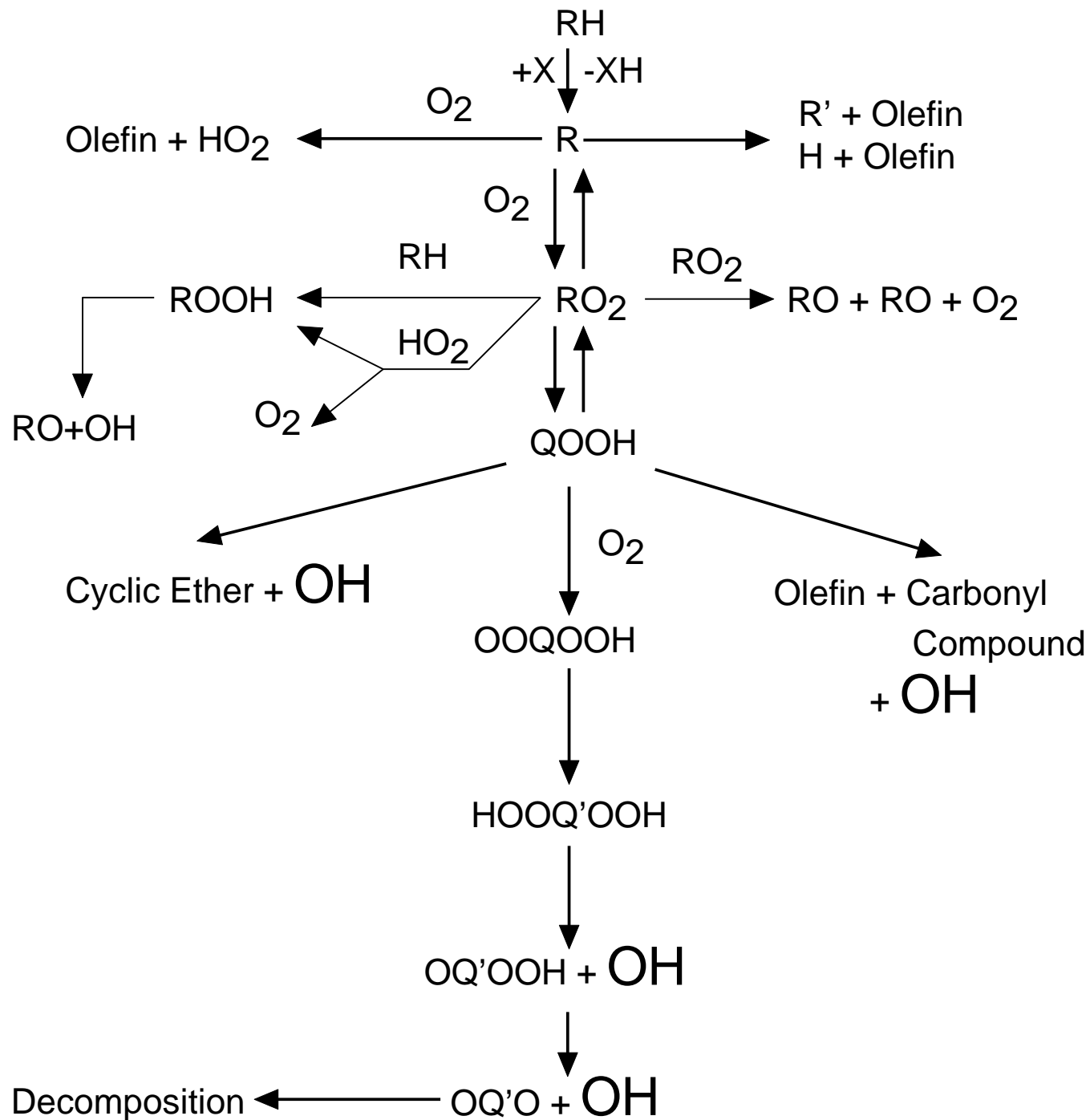
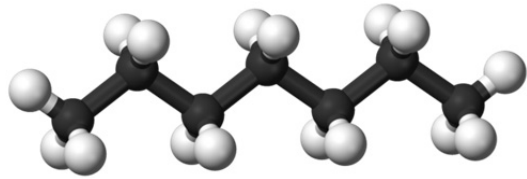


FIGURE 6 Carbon monoxide and carbon dioxide maximum mole fraction at low temperature, as a function of RON.

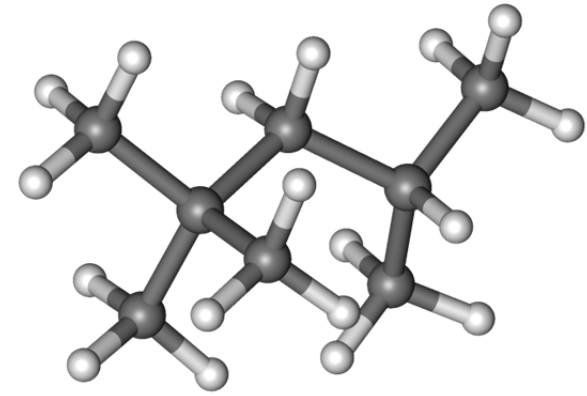
Dagaut et al., CST 103:1-6, 315-336 (1994).



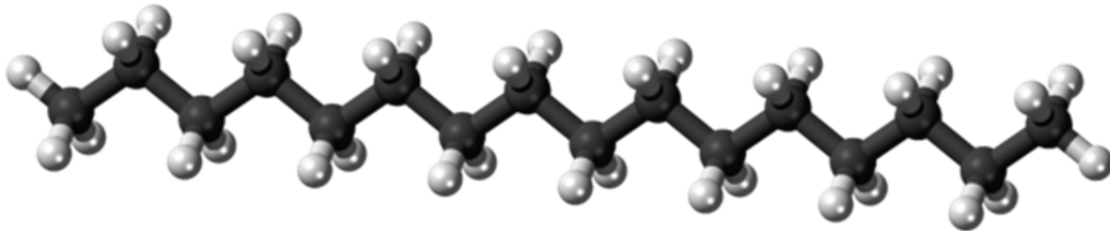
Structure-reactivity



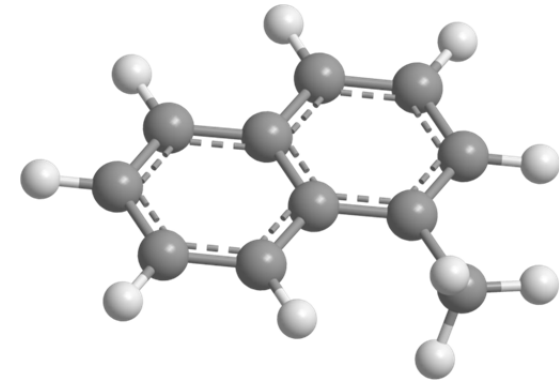
ON=0



ON=100



CN=100



CN=0

S.I. engines: ON=100 for iso-octane and ON=0 for n-heptane (C_8H_{18})

C.I. engines: CN=100 for n-hexadecane ($C_{16}H_{34}$) and 0 for 1-methylnaphthalene ($C_{11}H_{10}$)

Hydrocarbons

CN

Paraffins

2-Méthylpentane

33

3-Méthylpentane

30

n-Heptane

56

2,2,4-Triméthylpentane

12

n-Décane

76

n-Dodécane

80

3-Éthyldécane

48

4,5-Diéthyloctane

20

2,3,4,5,6-Pentaméthylheptane

9

n-Tridécane

88

2,5-Diméthylundécane

58

Hydrocarbons

CN

<i>n</i> -Hexadécane	100
Heptaméthylnonane	15
5-Butyldodécane	45
7,8-Diméthyltétradécane	40
<i>n</i> -Heptadécane	105
7-Butyltridécane	70
<i>n</i> -Octadécane	110
9-Méthylheptadécane	66
8-Propylpentadécane	48
7,8-Diéthyltétradécane	67
5,6-Dibutyldécane	30
<i>n</i> -Nonadécane	110
<i>n</i> -Eicosadécane	110
9,10-Diméthyl-octadécane	59
7-Hexylpentadécane	83
2,9-Diméthyl-5,6-diisoamyldécane	48
9,10-Dipropyloctadécane	47
10,13-Diméthyl-docosane	56
9-Heptylheptadécane	87
Oléfines	
Diisobutylène	10
Tétradéc-1-ène	79
Hexadéc-1-ène	88
4-Butyldodéc-4-ène	45
Tétraisobutylène	4



Hydrocarbons

CN

<i>n</i> -Nonylbenzène	50
<i>n</i> -Octylxylène	20
2-Phénylundécane	51
2-Phénylundéc-2-ène	23
2-Méthyl-2-(2-naphtyl)hexane	10
<i>n</i> -Dodécylbenzène	68
4-Phényldodécane	42
2- <i>n</i> -Octylnaphtalène	18
4-Méthyl-4-(2-naphtyl)heptane	9
7-Phényltridécane	41
<i>n</i> -Tétradécylbenzène	72
2-Phényltétradécane	49
3,6-Diméthyl-3-(2-naphtyl)octane	18
5-Méthyl-5-(2-naphtyl)nonane	12
2-Méthyl-2-(2-naphtyl)décane	18
3-Éthyl-3-(2-naphtyl)nonane	13
2-Méthyl-4-isobutyl-4-phénylundécane	38
2-Méthyl-2-phénylpentadécane	39
5-Butyl-5-phényltétradécane	58
1,2,4-Triméthyl-5-hexadécylbenzène	42
5-Phényleicosane	39



Hydrocarbons

RON

MON

Paraffins

Méthane	> 100	110,0
Éthane	> 100	104,0
Propane	> 100	100,0
<i>n</i> -Butane	95,0	92,0
2-Méthylpropane	> 100	99,0
<i>n</i> -Pentane	61,7	61,9
2-Méthylbutane	92,3	90,3
2,2-Diméthylpropane	85,5	80,2
<i>n</i> -Hexane	24,8	26,0
2-Méthylpentane	73,4	73,5
3-Méthylpentane	74,5	74,3
2,2-Diméthylbutane	91,8	93,4
2,3-Diméthylbutane	103,5	94,3
<i>n</i> -Heptane	0,0	0,0
2-Méthylhexane	42,4	46,4
3-Méthylhexane	52,0	55,0
3-Éthylpentane	65,0	69,3
2,2-Diméthylpentane	92,8	95,6
2,3-Diméthylpentane	91,1	88,5
2,4-Diméthylpentane	83,1	83,8
3,3-Diméthylpentane	80,8	86,6

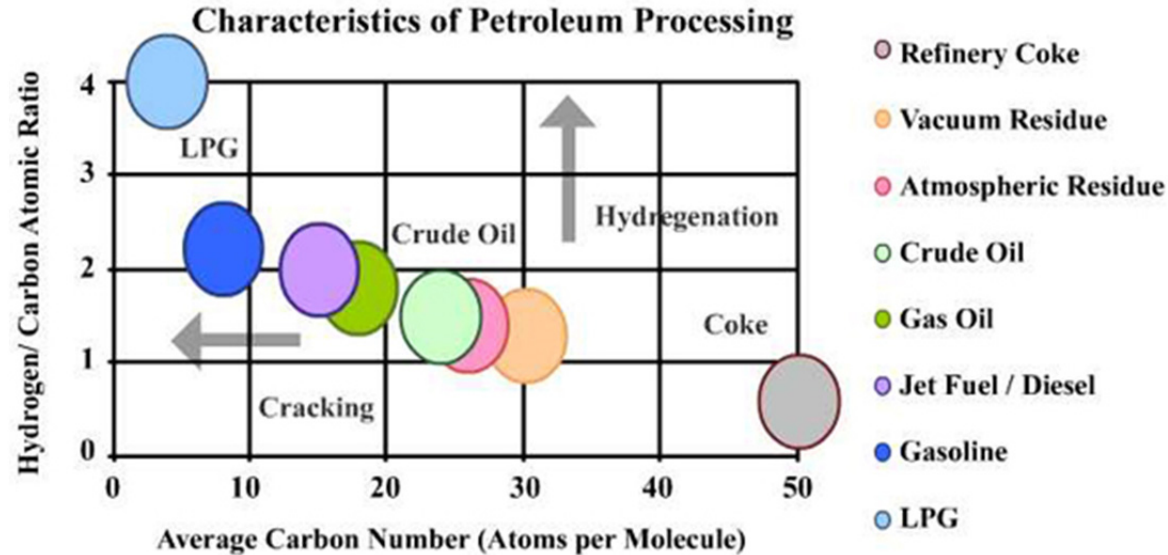
Hydrocarbons

RON

MON

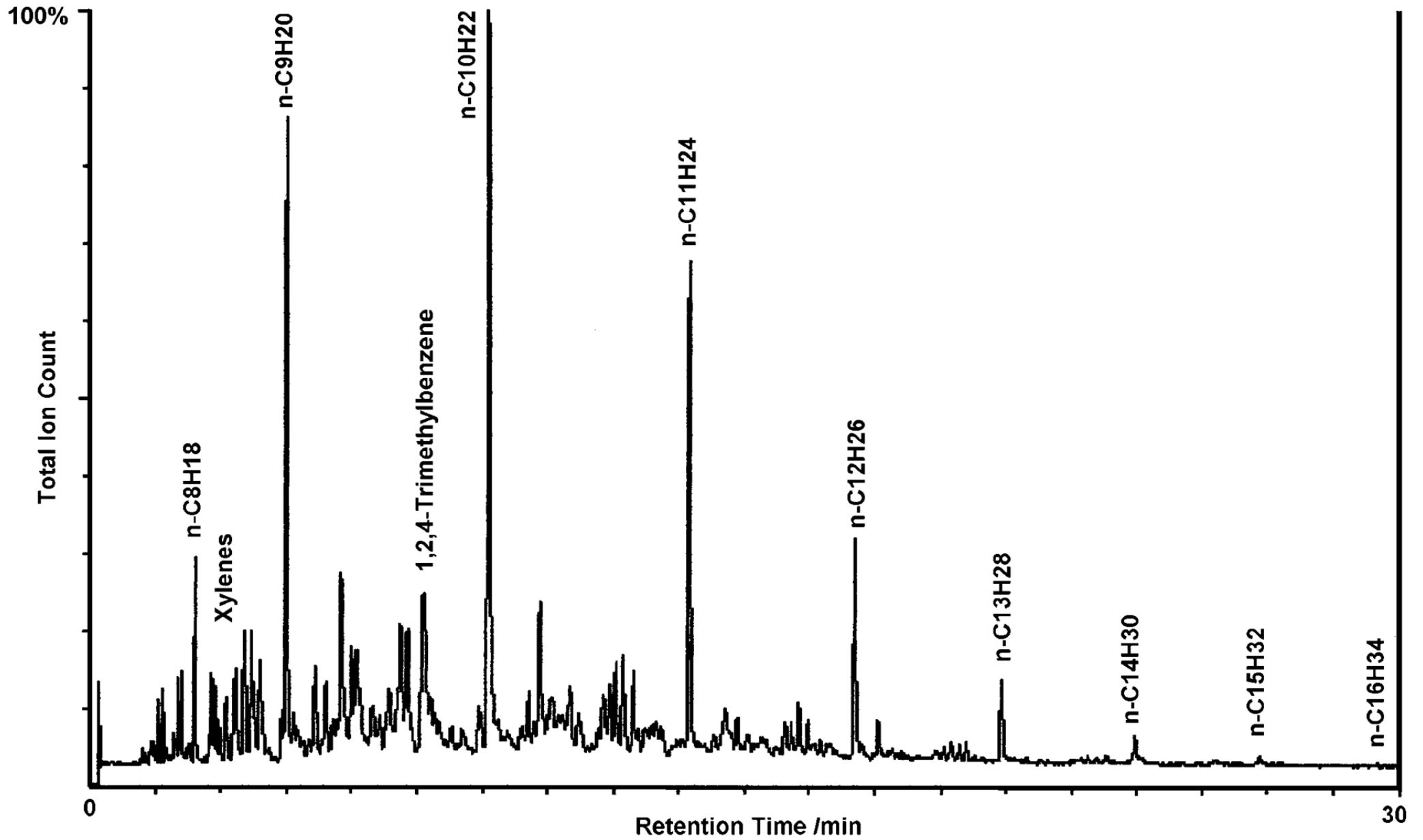
2,2,3-Triméthylpentane	108,7	99,9
2,2,4-Triméthylpentane	100,0	100,0
2,3,3-Triméthylpentane	106,1	99,4
2,3,4-Triméthylpentane	102,7	95,9
2-Méthyl-3-éthylpentane	87,3	88,1
3-Méthyl-3-éthylpentane	80,8	88,7
<i>n</i> -Nonane et <i>n</i> -alcanees supérieurs	< 0	< 0
Oléfines		
Éthylène	100,0	81,0
Propylène	102,0	85,0
But-1-ène	—	80,0
But-2-ène	100,0	83,0
Pent-1-ène	90,9	77,1
Pent-2-ène	98,0	80,0
2-Méthylbut-1-ène	102,5	81,9
2-Méthylbut-2-ène	97,3	84,7
Hex-1-ène	76,4	63,4
Hex-2-ène	92,7	80,8
Hex-3-ène	94,0	80,1
2-Méthylpent-1-ène	95,1	78,9
3-Méthylpent-1-ène	96,0	81,2
4-Méthylpent-1-ène	95,7	80,9
2-Méthylpent-2-ène	97,8	83,0
3-Méthylpent-2-ène	97,2	81,0
4-Méthylpent-2-ène	99,3	84,3
2-Éthylpent-1-ène	98,3	79,4
3,3-Diméthylbut-1-ène	111,7	93,5
2,3-Diméthylbut-2-ène	97,4	80,5
2,3-Diméthylbut-1-ène	101,3	82,8
Hept-1-ène	54,5	50,7
Hept-2-ène	73,4	68,8

Composition of Fuels

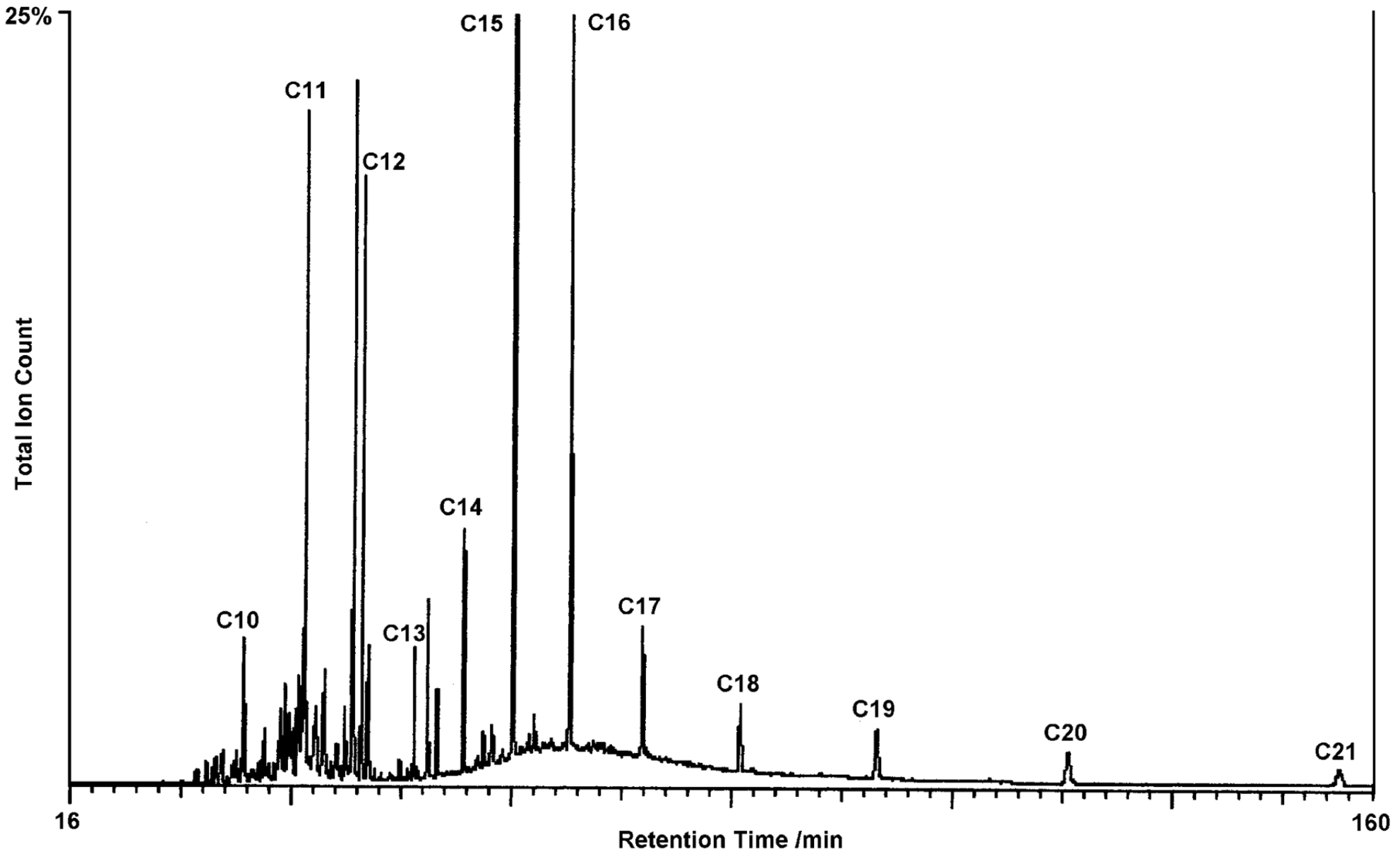


- NG: methane + higher alkanes (ca. C_8)
- LPG: region-dependent; C_3 – C_4 alkanes and alkenes
- Gasoline: C_4 – C_{12} hydrocarbons. Mixture of paraffins (alkanes), olefins (alkenes), cycloalkanes (naphthenes), aromatics
- Kerosene (Jet A-1 fuel), standard AFQRJOS (Aviation Fuel Quality Requirements for Jointly Operated Systems): C_6 – C_{16} hydrocarbons. Mixture of paraffins (alkanes), cycloalkanes (naphthenes), aromatics and <2% alkenes.
- Diesel: C_6 – C_{28} hydrocarbons. Mixture of paraffins (alkanes), olefins (alkenes), cycloalkanes (naphthenes), aromatics, naphtheno-aromatics
- Additives: EtOH, ETBE

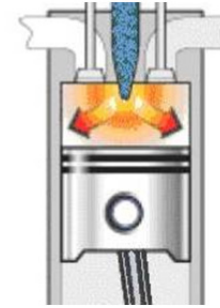
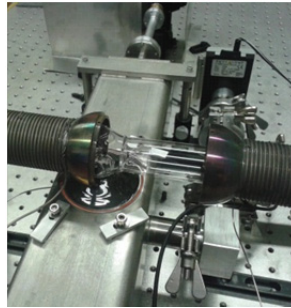
GC analysis of a Jet fuel sample



GC analysis of a diesel fuel sample



EXPERIMENTAL TECHNIQUES FOR KINETIC MODELS ASSESSMENT



1. Introduction

Chemical kinetic reaction mechanisms for combustion, either hand-written or automatically generated, rely on experimental data obtained over a large range of conditions.

However, combustion is a complex, generally exothermic, phenomenon involving strongly coupled chemical processes (reaction kinetics) and physical processes (diffusion and heat transfer). Thus, in order to better assess chemical kinetic reaction mechanisms, it is preferable to design experiments where the complexity of physical processes is minimized and the accuracy of the data is maximized.

This is the case for ideal reactors such as plug-flow reactors, perfectly stirred reactors, and shock-tubes.

In practice, the experiments should be performed under conditions where ideal reactor models can be used, e.g., operating a JSR under highly diluted conditions, under near-isothermal conditions).

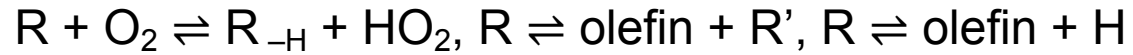
Indeed, such kinetic reaction mechanisms need to be validated through extensive comparison of modeling predictions and experimental results obtained under well-defined conditions. A wide range of experimental facilities can provide such data which are usually described as 'global' and 'detailed'. By combining data obtained from several techniques and conditions, one can check their consistency and use them to constrain chemical kinetic reaction mechanisms.

Global data include ignition delay times which can be obtained using shock-tubes, rapid compression machines, or plug-flow reactors, and laminar burning velocities or flame speeds determined using several types of experiments such as spherical flames in combustion vessels, Bunsen burners, stagnation-flow flames, counter-flow flames, or heat-flux burners. Ignition experiments are particularly useful for probing initiation and termination reactions and reactions of molecular oxygen with radicals whereas they are usually less useful for probing the kinetics of propagation reactions involving atoms and radicals.

Initiations reactions:



Propagation reactions:

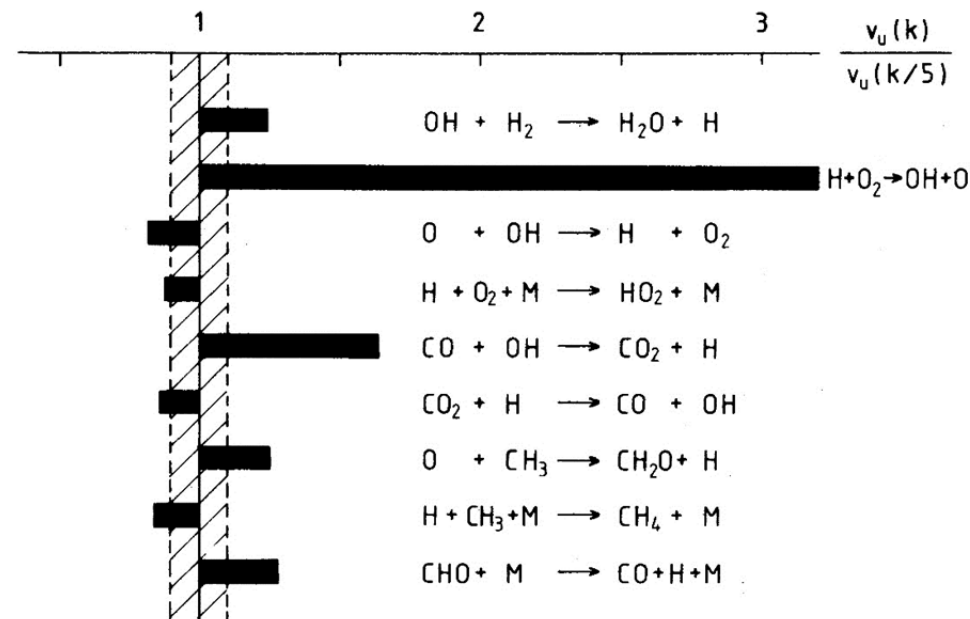


Termination reactions:



The paramount importance of H-atoms has been recognized long ago (Tanford, C., J. Chem. Phys., 1947. 15(7): p. 433-439.).

Burning velocity experiments are very valuable for probing reactions involving H-atoms such as $\text{RH} (+\text{M}) \rightleftharpoons \text{R} + \text{H} (+\text{M})$ and $\text{R} (+\text{M}) \rightleftharpoons \text{product} + \text{H} (+\text{M})$. Burning velocities are also very sensitive to the main branching reaction in combustion, i.e., $\text{H} + \text{O}_2 \rightleftharpoons \text{OH} + \text{O}$



Sensitivity of computed laminar burning velocity of a methane-air flame at 1 bar and $T_u = 298$ K to reaction kinetics. From Warnatz, J., The structure of laminar alkane-, alkene-, and acetylene flames. Symposium (International) on Combustion, 18(1), p. 380, 1981.


Detailed data are mostly concentration profiles of stable and unstable chemical species observed during the oxidation and combustion of fuels. Many reactors in conjunction with sampling methods and analytical techniques have been used to acquire such data.

Analytical techniques are often used after gas sampling performed using a range of probes (e.g., low-pressure, cooled, molecular beam) or traps (cold trap, bubblers, traps containing absorbents). These probes should stop chemical reactions and transfer a chemical sample to appropriate analyzers without changing its composition. This assumption needs to be verified.

Low-pressure probes reduce reactions rates by lowering molecular concentrations and temperature after gas expansion.

Cooled probes reduce reaction rates which are exponentially temperature-dependent, according to the Arrhenius equation.

Probes are responsible for disturbance of the reaction medium (flow, temperature) which can result in additional complications for interpreting the experimental results.

Many cool traps can be used to collect the condensable compounds at the temperature of the trap (water ice: 273 K; CO₂ dry ice: 194.65 K; liquid nitrogen: 77.2 K). The use of liquid nitrogen traps oxygen (O₂ boiling temperature = 90.2 K) and requires particular care to prevent hazards. 

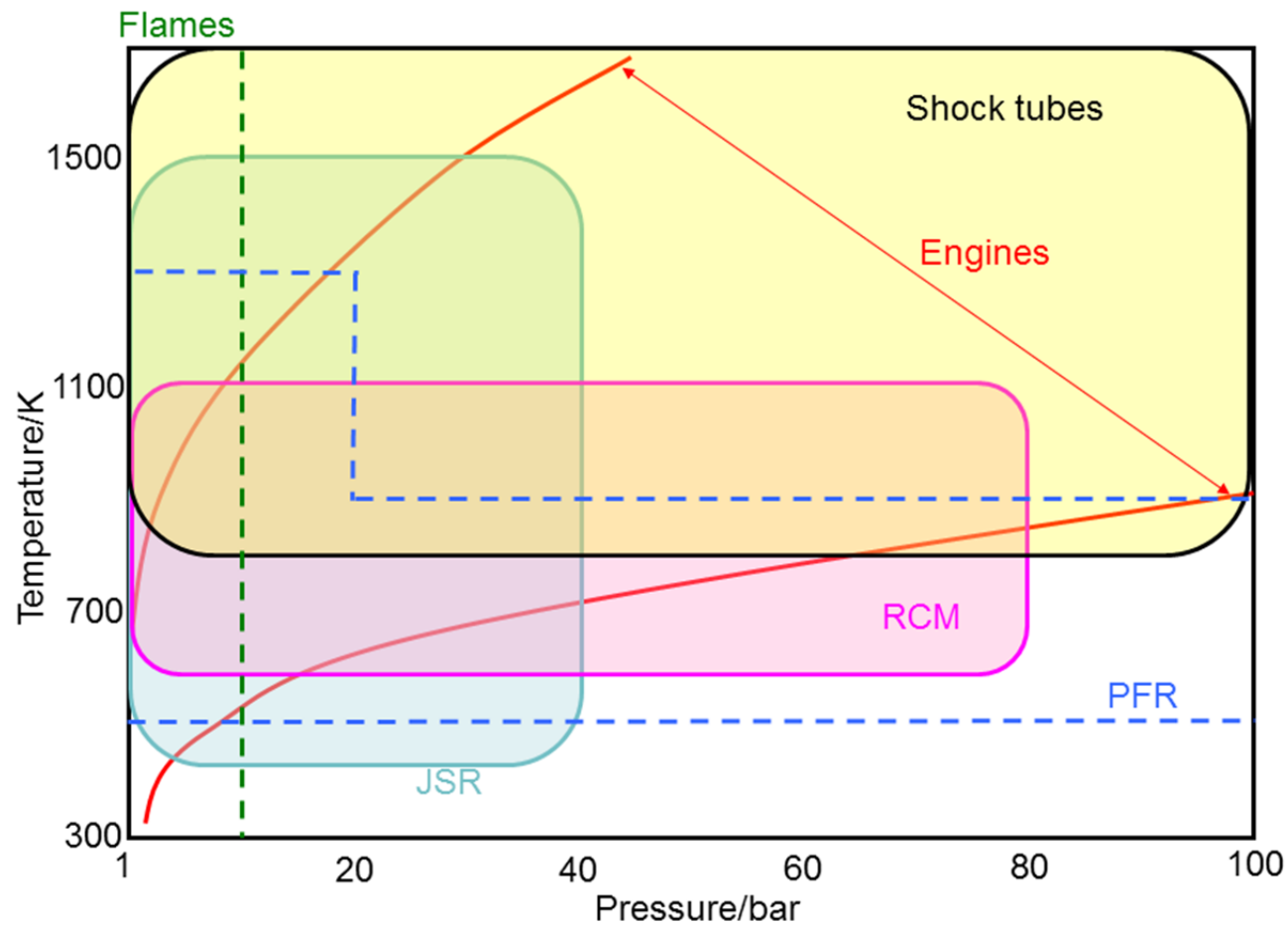
Nowadays, the most **popular experimental techniques** used are flow reactors (jet-stirred reactors, tubular flow reactors), burner stabilized laminar flames (premixed low-pressure flames, opposed flow diffusion flames), and shock-tubes. These techniques by themselves are useful because they cover a wide range of conditions (temperature, pressure, equivalence ratio, initial concentrations, residence time, recirculation rate) allowing to probe the complexity of combustion chemical kinetics. But this is through their coupling to a large range of analytical techniques that one can acquire the data needed to validate detailed kinetic combustion models.

Among these **analytical techniques**, some are very popular whereas others are less frequently used:

Gas chromatography (with thermal conductivity detector, flame ionization detector, mass spectrometry), molecular-beam mass spectrometry, Fourier transform infrared spectrometry are commonly used. They are commercially available, reliable, and easy to use.

Other **spectroscopy techniques** are also used in laboratory experiments. They are mostly used to measure radicals, atoms, and unstable molecular species in the UV or the infrared. Recent coupling of synchrotron-sourced photoionization with mass spectrometry allowed very detailed probing of oxidation and combustion processes. Several mass spectrometry techniques are used in laboratory experiments. They mostly differ by the use of different types of mass separation (time-of-flight, quadrupole, ion trap, Orbitrap®), and ionization mode (electronic, chemical, photonic).

By combining the above-mentioned laboratory experiments, one can cover a very broad range of conditions relevant to practical applications such as internal combustion engines and gas turbines.



By combining shock-tubes and RCM experiments, one can probe fuels ignition under internal combustion engine conditions. The measurements of burning velocities and flame structures are limited to about 10 bar. Whereas individual reactor experiments have limited operating ranges, by combining them, one can provide detailed data over almost the entire range of pressure and temperature pertinent to I.C. engines and GT.

2. Shock-tubes and rapid compression machines

Shock-tubes and RCM are **batch reactors** which can provide both global and detailed combustion data, i.e, ignition delay times and speciation.

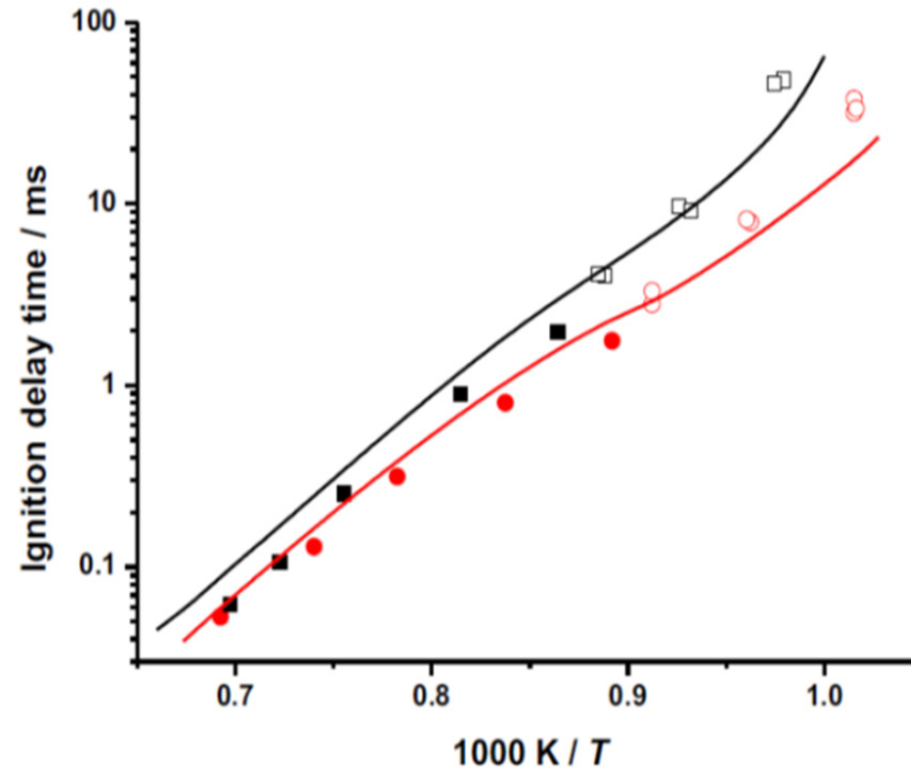
These techniques have been used for several decades. In 1890, Vieille started using compression driven shock tubes (*Vieille, P., Comptes Rendus de l'Académie des Sciences, 1890. 111 p. 639-641*)

In 1906, Falk used a RCM to determine ignition temperatures (*Falk, K.G., J. Am. Chem. Soc., 1906. 28 p. 1517*).

Major improvements have been made over the years, allowing the acquisition of very useful global and detailed data for kinetic modelers (*Hanson, R.K. and D.F. Davidson, PECS, 2014. 44: p. 103-114; Sung, C.J. and H.J. Curran, PECS, 2014. 44: p. 1-18; Goldsborough, S.S. et al., PECS, 2017. 63: p. 1-78*).

2.1 Ignition data from RCM and ST.

RCM are limited to the investigation of relatively long ignition delays (5–100's ms) at moderate-T, c.a. 1000 K, and to $P < 100$ bar, shock-tubes can operate over a wider range of P (up to 100's bar) and to very high-T (1000's K) where ignition delays are rather short (ca. 1–100's ms).



Experimental (symbols) and modeled (lines) ignition delay times for a $\phi = 0.5$ NG/air mix measured using a RCM (open symbols) and a shock-tube (closed symbols) at 8–10 atm (black) and 19–20 atm (red). From Sung, C.J. and H.J. Curran, Using rapid compression machines for chemical kinetics studies. Progress in Energy and Combustion Science, 44: p. 10, 2014.

However, modelers must be aware of a complication when trying to combine ignition data obtained in a shock-tube and a RCM. At first, they can look irreconcilable. In fact, it is necessary to consider facility-dependent effects before combining ignition delay times measured in shock-tubes and RCMs.

These have been described with great details in several publications and have been reviewed recently (*Sung, C.J. and H.J. Curran, PECS, 2014. 44: p. 1-18*).

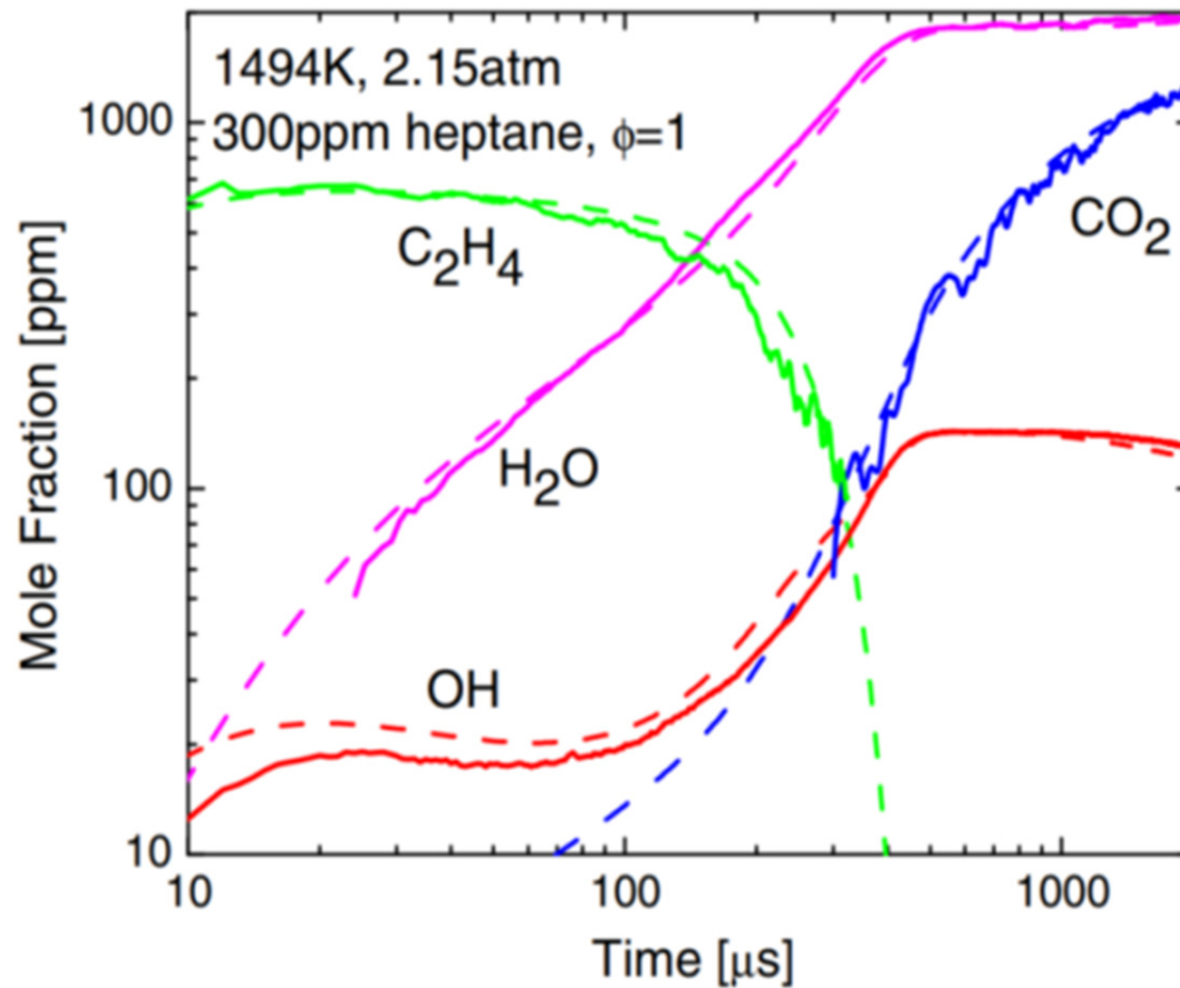
Up to now, a large set of data is available for the ignition of fuels ranging from hydrogen to practical fuels such as jet fuels or biodiesel (*Dagaut, P., et al., CNF, 2014. 161(3): p. 835-847; Ramirez-Lancheros, H.P., et al., CNF, 2012. 159(3): p. 996-1008*). These data have been extensively used to propose detailed and simple kinetic models.

2.2 Species measurements from ST and RCM.

Whereas speciation in shock-tubes has received much attention (studies concern both oxidation and pyrolysis), a more limited database is available from RCM experiments.

Several research groups have used shock tubes to measure species concentrations using spectroscopy (*Hanson, R.K., PROCI, 2011. 33(1): p. 1-40; Roth, P., Forsch. Ing.-Eng. Res., 1980. 46(3): p. 93-102*) and gas-chromatography (*Tranter, R.S. et al., Rev. Sci. Instr., 2001. 72(7): p. 3046-3054; Tranter, R.S. et al., PCCP, 2002. 4(11): p. 2001-2010*).

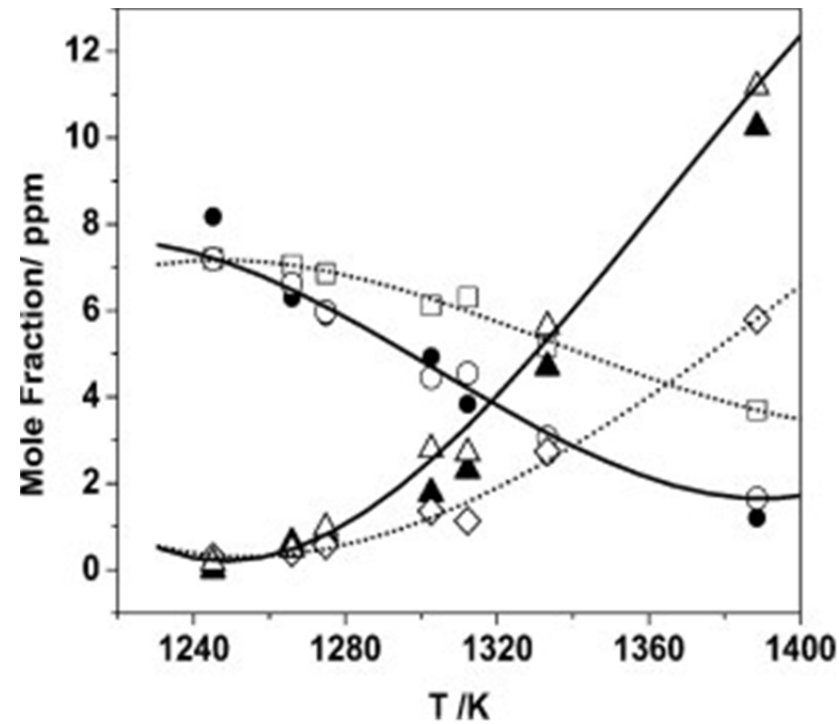
Hanson and co-workers have recently reported laser-absorption-based measurements in shock-tubes of time-histories of reactants, small-radicals, stable intermediates, and combustion products:



Time-history for stable and labile species measured during the oxidation of n-heptane in a shock-tube (continuous lines) are compared to kinetic modeling (dashed lines). From: Hanson, R.K., Applications of quantitative laser sensors to kinetics, propulsion and practical energy systems. Proceedings of the Combustion Institute, 33(1), p. 10, 2011.

Such data are particularly useful for improving kinetic reactions schemes. This is also true for data coming from single-pulse shock-tube experiments with gas-sampling and GC analyses (Sivaramakrishnan,

R. et al., *PROCI*, 2005. 30(1): p. 1165-1173):



*Toluene oxidation at $\phi = 1$ and 610 bar in a shock-tube. (●) Experimental data $C_6H_5CH_3$; (▲) Expt. CO; (□) KBG model $C_6H_5CH_3$; (◇) KBG model CO; (○) STB model $C_6H_5CH_3$; (Δ) STB model CO; (···) fit to KBG model predictions; and (—) fit to STB model predictions. From Sivaramakrishnan, R., R.S. Tranter, and K. Brezinsky, A high pressure model for the oxidation of toluene. *Proceedings of the Combustion Institute*, 30(1), p. 1169, 2005*

More recent developments:

A miniature with high-repetition rate shock-tube was recently introduced by Tranter (*Tranter, R.S. and P.T. Lynch, Rev. Sci. Instr., 2013. 84(9): p. 094102*) who used it to probe pyrolysis chemistry of dimethyl ether at high temperature (1400 –1700 K) and high pressure (3 –16 bar) with a tunable synchrotron-generated photoionization time-of-flight mass spectrometer (*Lynch, P.T. et al., Analytical Chemistry, 2015. 87(4): p. 2345-2352*). This new set-up opens up new horizons for chemical kinetics.

Data obtained with shock-tubes have been extensively used to propose detailed and simple kinetic models for the oxidation of fuels ranging from hydrogen to large hydrocarbons and practical fuels (gasoline and jet fuel, *Zhu, Y. et al., in 53rd AIAA Aerospace Sciences Meeting. 2015; Li, Y., Ph.D., School of Chemistry. 2017, Nat. Univ. of Ireland: Galway; Javed, T. et al., CNF, 2017. 185(Sup. C): p. 152-159*).

Species measurements in RCM through **gas-sampling** started in the 1960's (Roblee, L.H.S., *CNF*, 1961.

5(Sup. C): p. 229-234; Martinengo, A. et al., Symp. (Int.) Combust., 1965. 10(1): p. 323-330; Fish, A. et al., Proc. Royal Soc. London. A. Math. Phys.

Sci., 1969. 313(1513): p. 261). Several groups have performed such experiments for the ignition of

hydrocarbons, alkyl nitrates, and oxygenated fuels. GC has been used in most of RCM experiments;

exhaust gas analyzers for CO, CO₂, NO_x, and unburned hydrocarbons have also been used (*Ribaucour,*

M. et al. J. Chim. Phys. Phys.-Chim. Biol., 1992. 89(11-12): p. 2127-2152; Minetti, R. et al., CNF, 1994. 96(3): p. 201-211; Minetti, R. et al., CNF, 1995.

102(3): p. 298-309; Van Blarigan, P. et al., SAE Tech Pap 982484, 1998).

Spectroscopic methods in the UV and IR have also been used after Fish et al. (*Fish, A. et al., Proc. Royal Soc.*

London. A. Math. Phys. Sci., 1969. 313(1513): p. 261). These data have been used to propose detailed and simple

kinetic models for the oxidation of fuels (from H₂ to oxygenates and large HC (*Sung, C.J. and H.J. Curran, PECS,*

2014. 44: p. 1-18), but also served to identify the products of low-temperature oxidation of a range of fuels

(*Minetti, R et al., CNF, 1994. 96(3): p. 201-211; Minetti, R. et al., CNF, 1995. 102(3): p. 298-309; Walton, S.M. et al., Fuel, 2011. 90(5): p. 1796-1804;*

Karwat, D.M.A. et al., J. Phys.I Chem. A, 2011. 115(19): p. 4909-4921).

Advantages:

Can be run with very little fuel compared to flames and reactors experiments.

A wide range of operating conditions, in terms of P , T , and ϕ , is covered by combining these techniques.

Limitations/weaknesses:

Batch reactor experiments are time consuming because they involve mixture preparation, pumping after each ignition experiment, replacement of the shock-tube diaphragm (needing disassembling / reassembling).

Also, pressure history must be well characterized to allow accurate kinetic modeling.

3. Flow reactors: Tubular Flow Reactors and Stirred Reactors

Flow reactors are particularly useful for measuring the concentration of reactants, intermediates species, and final products of fuels oxidation or pyrolysis or interaction of fuels with other species, e.g., NO_x, SO_x, CO₂, H₂O.

They usually operate at temperatures below 1500 K and pressure less than 50 bar.

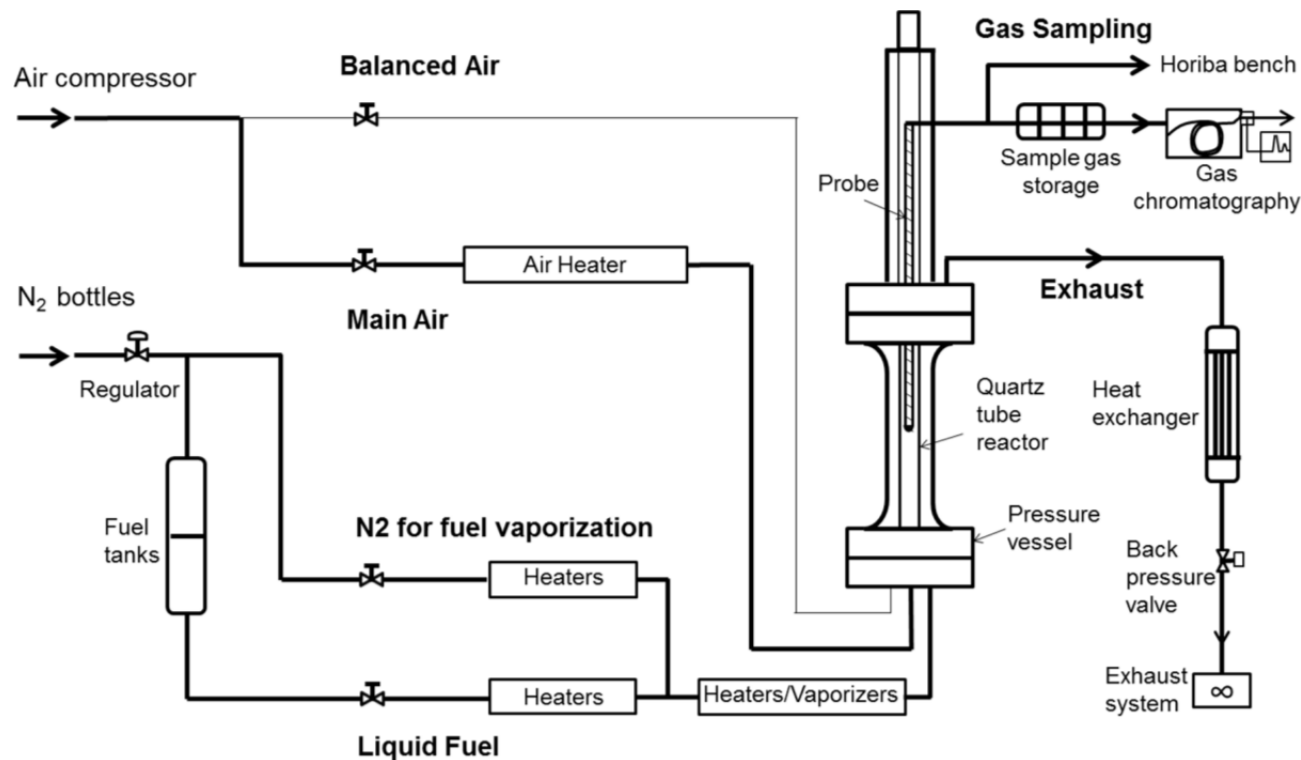
They are particularly useful for studying the low-T oxidation chemistry of fuels. In most of the experiments, high fuel dilution (100–1000's ppm) is used to avoid flame occurrence and large temperature gradients. Nevertheless, experiments are also performed with higher initial fuel concentrations (1–few mole %).

Whereas in **tubular flow reactors**, ideally called plug-flow reactors (PFRs), one can observe chemical reactions along the reactor axis; in jet-stirred reactors the chemical composition is ideally homogeneous. Flow reactors are usually heated by external ovens. Temperature measurements are of great importance for running accurate modeling. In tubular reactors, this means that measurements must be made along the reactors axis.

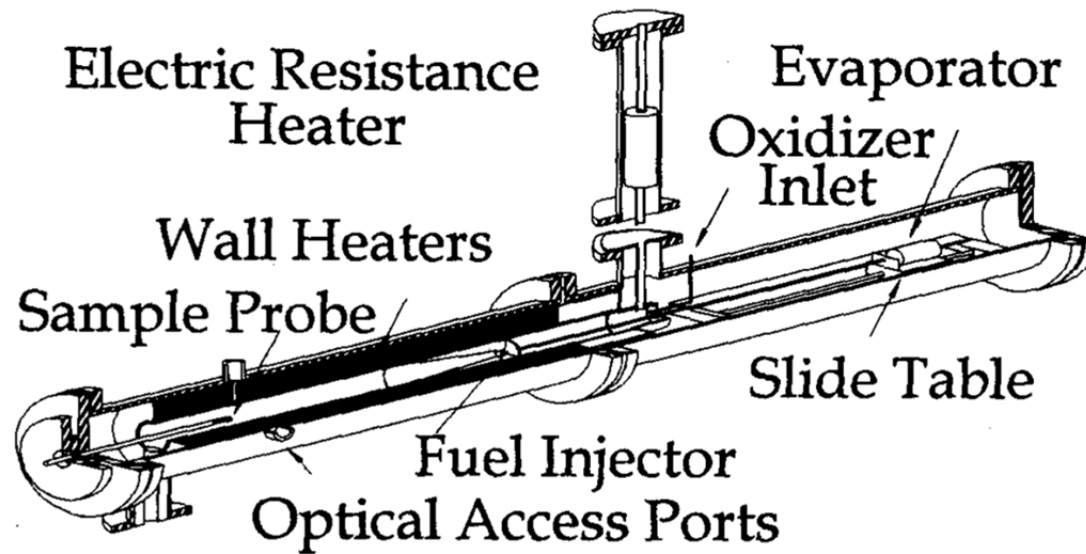
In **JSR**, temperature homogeneity is usually verified along the reactor main axis and measurements used as input in isothermal perfectly stirred reactor model. Compared to flame experiments, flow reactors are not limited to flammability limits. As shock-tubes, they allow studying fuel-lean oxidation to pyrolysis. Although this is not very common, tubular-flow reactors operating under plug-flow conditions can be used to determine ignition delays, as presented in Section 3.2.

3.1 Species measurements.

Two types of flow reactors are mainly used in recent kinetic studies. **Tubular flow reactors** consist of a tube where reactants are injected and heated from the outside. The flow inside the tube can be laminar (*Rasmussen, C.L. et al., IJCK, 2008, 40(8): p. 454-480; Zhang, T.C. et al., J.Phys .Chem. A, 2008. 112(42): p. 10487-10494*) or turbulent (*Allen, M.T. et al., I.J.C.K., 1995. 27(9): p. 883-909; Kim, T.J. et al., Symp. (Int.) Combust., 1994. 25(1): p. 759-766; Zhewen, L. et al, Meas. Sci. Technol., 2017. 28(10): p. 105902*):



Schematic of the Melbourne University high-pressure tubular flow reactor that operates up to 50 bar. From Zhewen, L., C. Julien, L. Nicolas, Y. Yi, and J.B. Michael, Measurement Science and Technology, 28(10), 105902, p. 3, 2017.



Schematic of the Princeton variable pressure tubular flow reactor that operates up to 20 atm and ca. 1200 K. From Kim, T.J., R.A. Yetter, and F.L. Dryer, Symposium (International) on Combustion, 25(1), p. 760, 1994.

Whereas most of the currently used PRFs use conventional analytical instruments (e.g., GC, GC-MS, FTIR) to probe the chemistry, molecular-beam mass spectrometry and tunable synchrotron VUV photoionization have been introduced recently (Zhang, T.C. et al., *J. Phys. Chem. A*, 2008. 112(42): p. 10487-10494), opening new horizons for the understanding and validation of chemical kinetic reaction mechanisms.

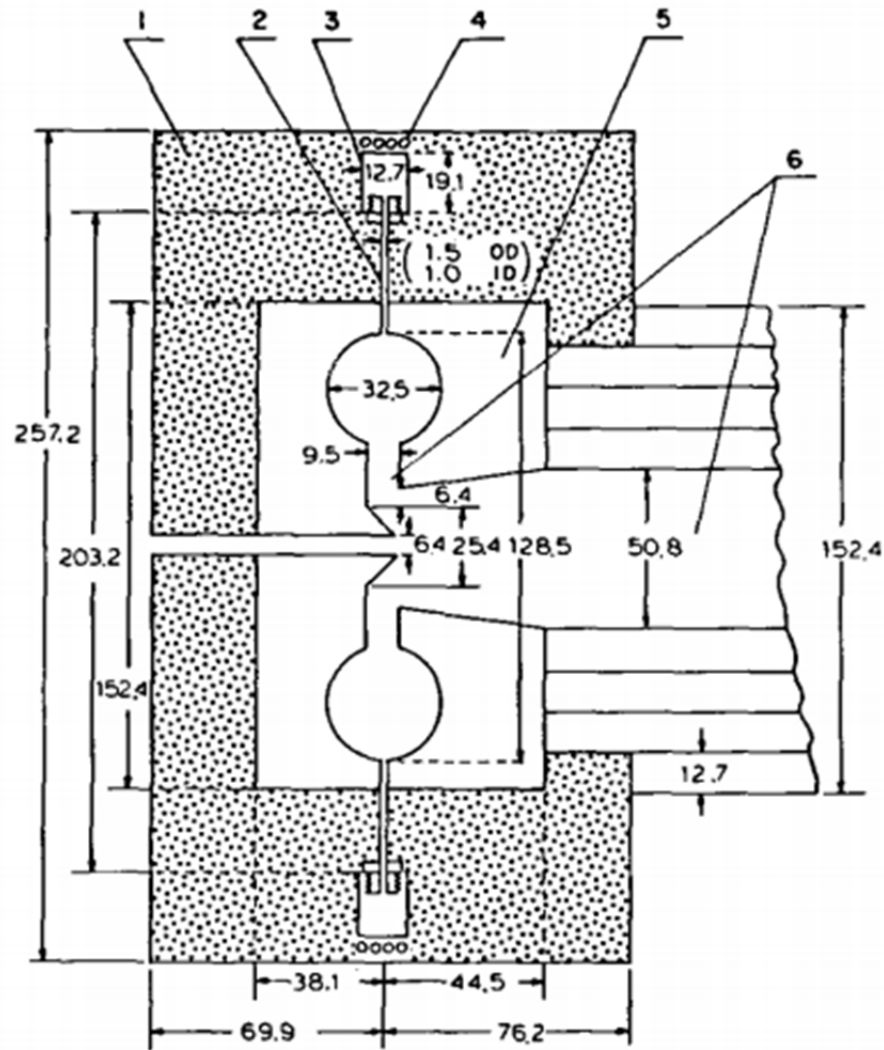
Several **jet-stirred reactor** (JSR) geometries have been used (spherical, hemispherical, toroidal, near-conical), but the most popular design is a spherical reactor of less than 50 cm³. This technique potentially allows operation over a wide range of residence time (from few milliseconds to several seconds), depending on the reactor geometry (David, R. and D. Matras, Can. J. Chem. Eng., 1975. 53(3): p. 297-300).

Temperature homogeneity is improved through preheating to a temperature close to the reactor operating temperature (Dagaut, P. et al., J. Phys. E-Sci. Instr., 1986. 19(3): p. 207-209; Rota, R. et al., Chem Eng Sci, 1994. 49(24A): p. 4211-4221).

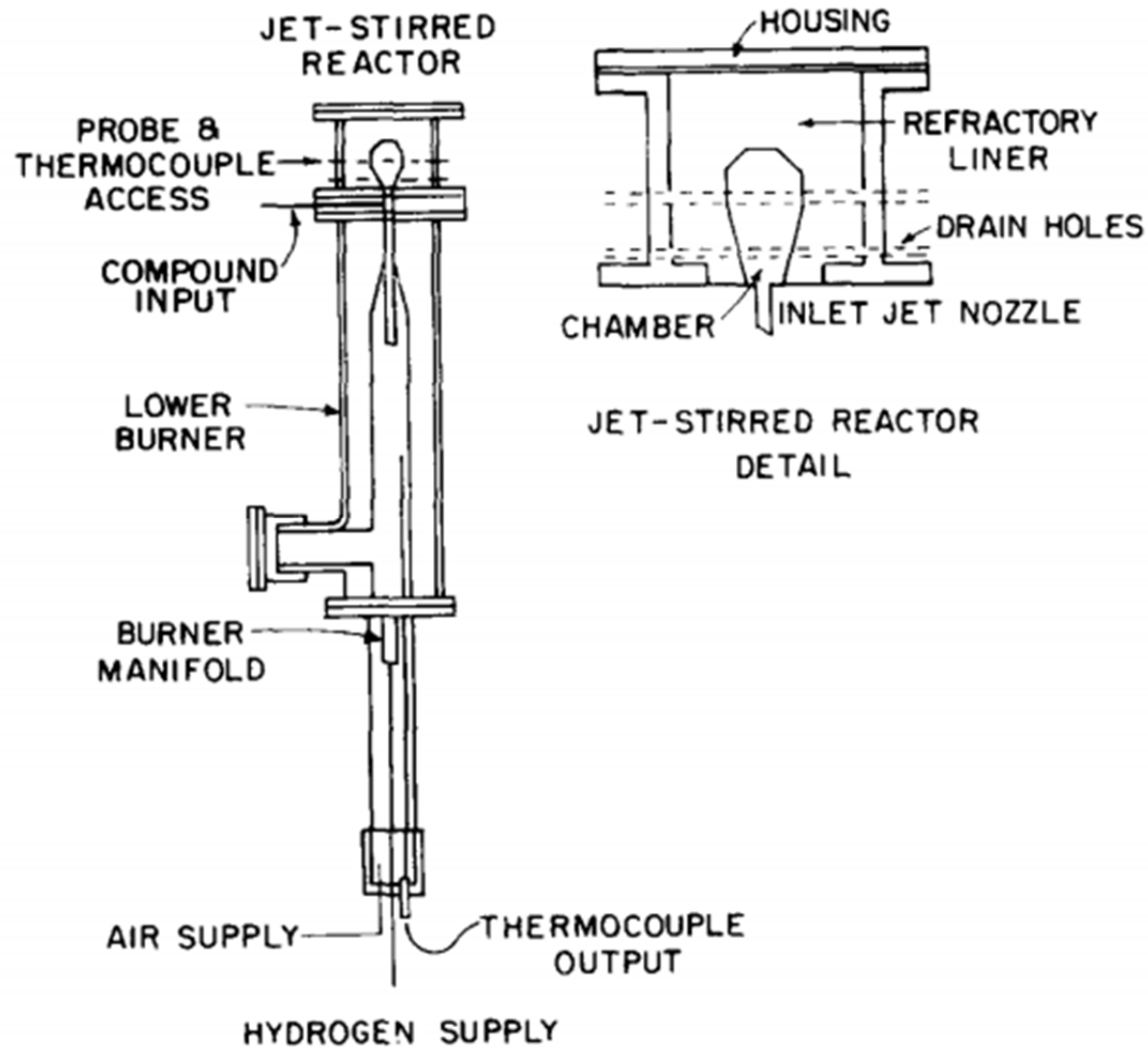
Composition homogeneity was shown to be easier to achieve.



Picture of a fused-silica JSR used at CNRS Orléans. Stirring is provided by 4 injectors. With this reactor, one can operate from 40 ms to 3s.



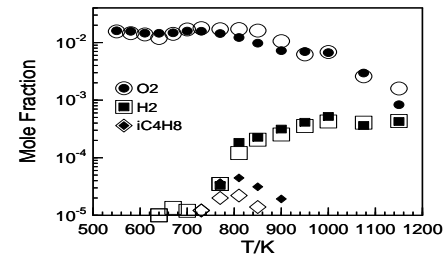
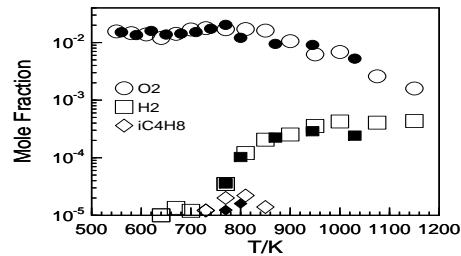
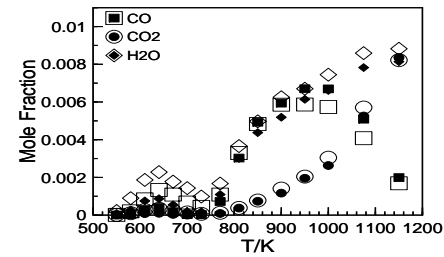
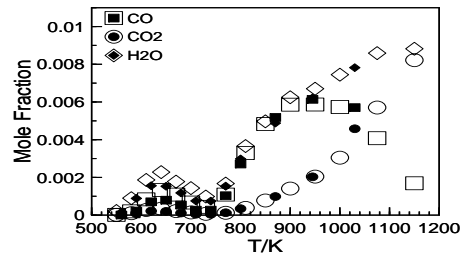
Schematic of the MIT alumina toroidal jet-stirred reactor. Stirring is provided by 32 injectors. From Nenniger, J.E., A. Kridiotis, J. Chomiak, J.P. Longwell, and A.F. Sarofim, Characterization of a toroidal well stirred reactor. Symposium (International) on Combustion, 20(1), p. 474, 1985.



*Schematic of the ceramic jet-stirred reactor developed at the University of Washington, Seattle. Stirring is provided by a single injector. From Westbrook, C.K., W.J. Pitz, M.M. Thornton, and P.C. Malte, *Combustion and Flame*, 72(1), p. 47, 1988.*

These reactors have been used to provide useful data for modeling the pyrolysis and oxidation of a wide range of fuels, i.e. hydrogen, ammonia, carbon monoxide, syngas, hydrocarbons, oxygenates, and complex fuels such as gasoline, jet-fuels, Diesel-fuels, synthetic fuels, and biodiesel.

An example of such results is given next for the oxidation of a **conventional jet A-1 and 2 synthetic jet-fuels** (*Dagaut, P. et al., CNF, 2014. 161(3): p. 835-847*).



(a)

(b)

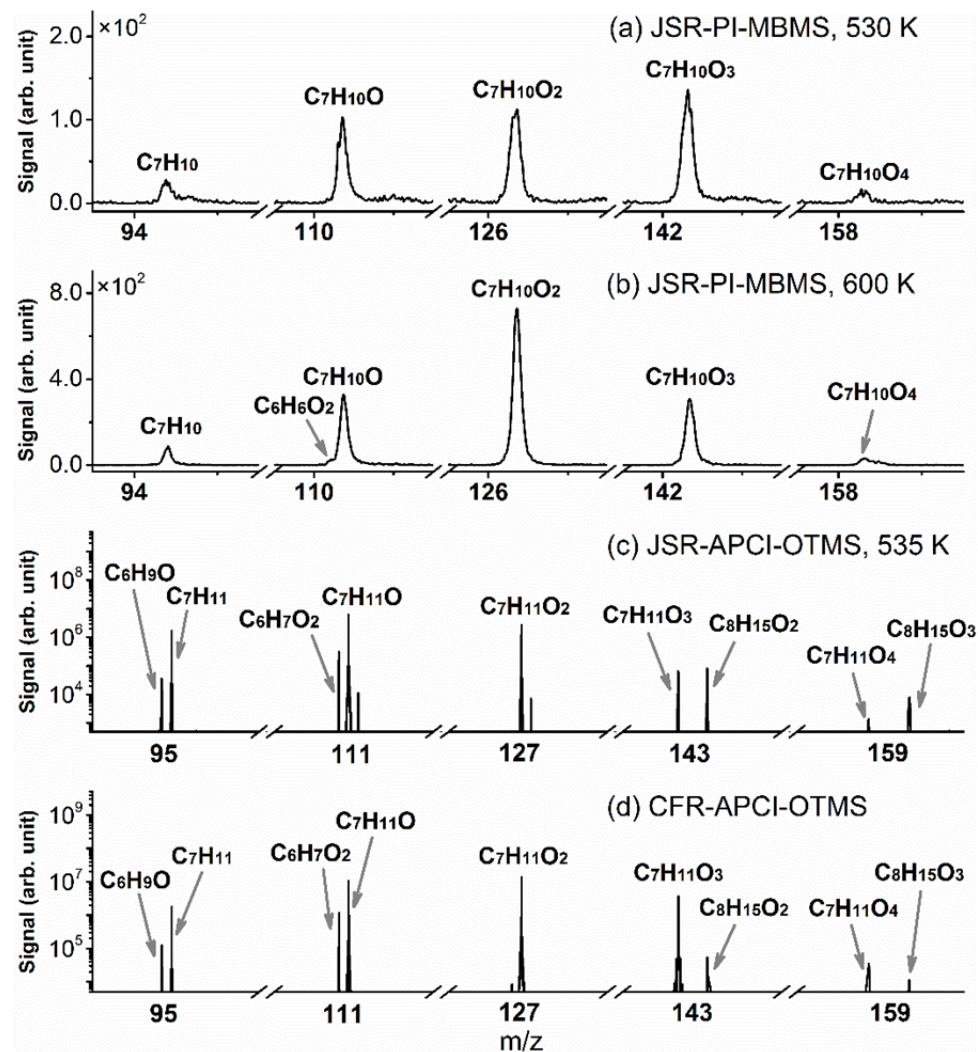
Comparison of experimental data obtained from the JSR oxidation of (a) Jet A-1 (closed symbols) and GtL (open symbols) and (b) CtL (closed symbols) and GtL jet fuel (open symbols) at $\phi = 1.0$, 10 bar, and a mean residence time of 1 s. From Dagaut, P., CNF, 2014, 161(3), p. 840.

These data show differences in terms of reactivity and formation of intermediate products that can be explained through detailed kinetic modeling (Dagaut, P. et al., CNF, 2014. 161(3): p. 835-847; CST, 2014. 186(10-11): p. 1275-1283; GT2015-42004 in ASME Turbo Expo 2015; CST 2016. 188(11-12): p. 1705-1718; PROCI, 2017. 36(1): p. 433-440).

Whereas gas chromatography and FTIR spectrometry are usually used in conjunction with small sonic probes in JSRs experiments to probe the chemistry (*Herbinet, O. and G. Dayma, in Cleaner Combustion: Developing Detailed Chemical Kinetic Models, 2013, Springer-Verlag, London*), molecular-beam mass spectrometry and tunable synchrotron VUV photoionization have been introduced recently, allowing deeper investigations of combustion chemistry (*Battin-Leclerc, F. et al., PROCI, 2011. 33(1): p. 325-331; Moshhammer, K. et al., J. Phys. Chem. A, 2015. 119(28): p. 7361-7374; Wang, Z. et al., PNAS, 2017. 114(50): p. 13102-13107*).

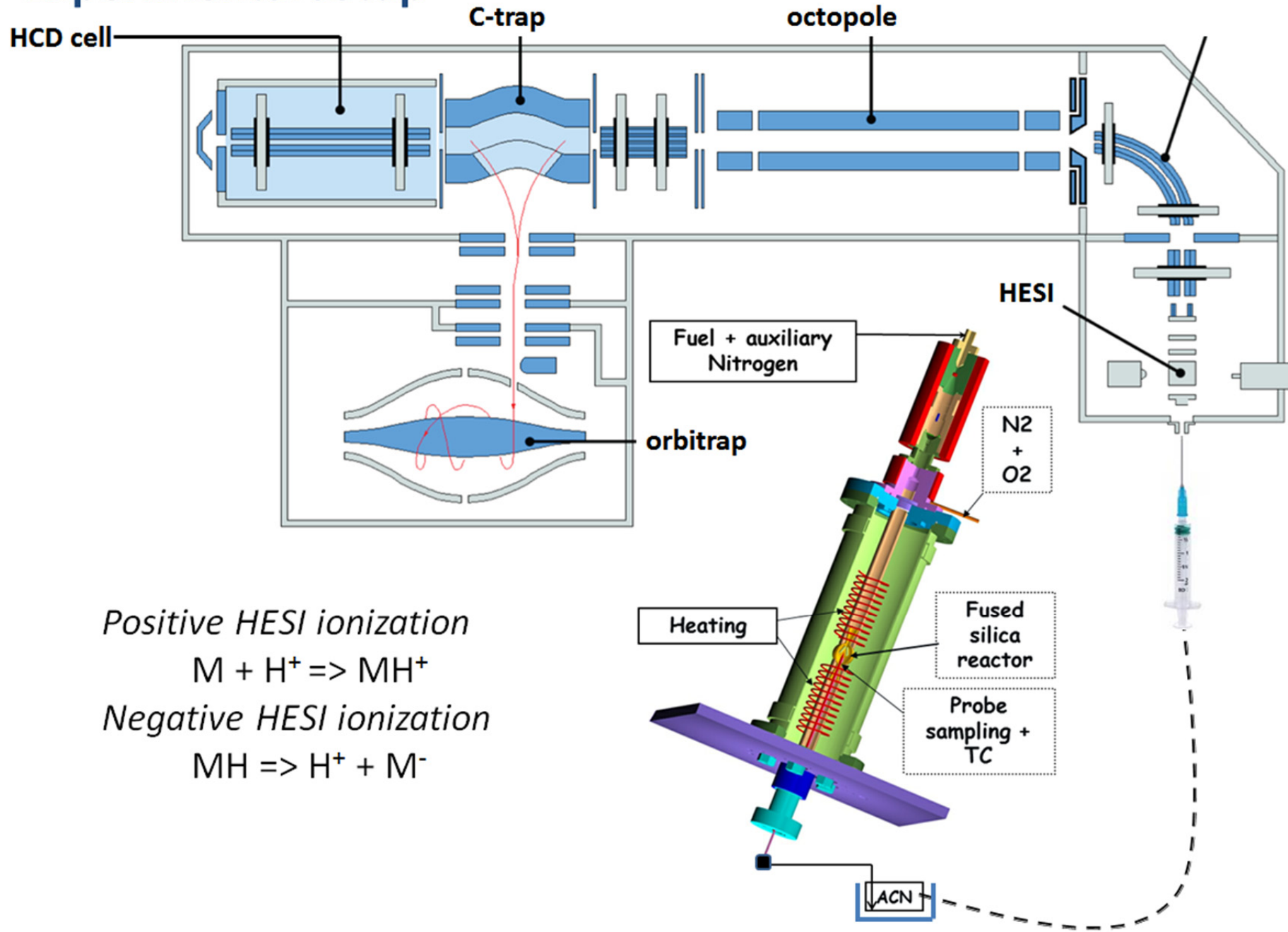
Recent results have been obtained through the combination of JSRs and high resolution mass spectrometry (Photoionization-MBMS and APCI-Orbitrap MS). They demonstrate that currently accepted reaction schemes for hydrocarbons oxidation are missing reaction pathways leading to the formation of highly oxygenated molecules.

The inclusion of such reactions and products in kinetic scheme could influence significantly model predictions (*Wang, Z. et al., PNAS, 2017. 114(50): p. 13102-13107*).

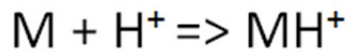


*Mass spectra of intermediates with the molecular formula of $C_7H_{10}O_x$ ($x=0-4$). (a) and (b) are for JSR-1 PI-MBMS measurements at $T=530$ K and 600 K, respectively. Photon energy is 9.6 eV. (c) is for JSR-2 APCI-OTMS measurements at 535 K. (d) is for CFR engine APCI-OTMS measurements. From Wang, Z.D. et al., *Combustion and Flame*, 187, Supporting information, p.S5, 2018.*

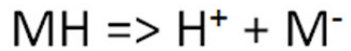
Experimental setup



Positive HESI ionization

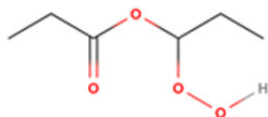


Negative HESI ionization



Results

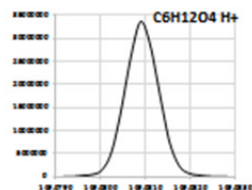
Ketohydroperoxides



$C_6H_{12}O_4 : M$

$MH^+ \quad m/z = 149.08084$

$MNa^+ \quad m/z = 171.06278$



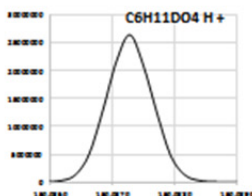
H/D exchange using D_2O : $-OH \rightarrow -OD$ to confirm the presence of $-OOH$

$MH^+ \quad m/z = 149.08084 \quad (59\%)$

$MD^+ \quad m/z = 150.08711 \quad (41\%)$

$MNa^+ \quad m/z = 171.06278 \quad (37\%)$

$MdNa^+ \quad m/z = 172.06906 \quad (63\%)$



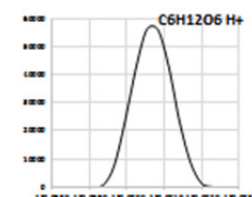
HOMs

$C_6H_{12}O_6 : M$

$MH^+ \quad m/z = 181.07066$

$MNa^+ \quad m/z = 203.05261 \quad (77\%)$

$MdNa^+ \quad m/z = 204.05889 \quad (23\%)$

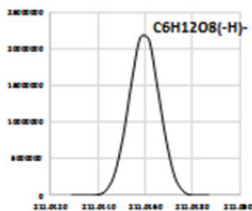


$C_6H_{12}O_8 : M$

$M(-H)^- \quad m/z = 211.04594$

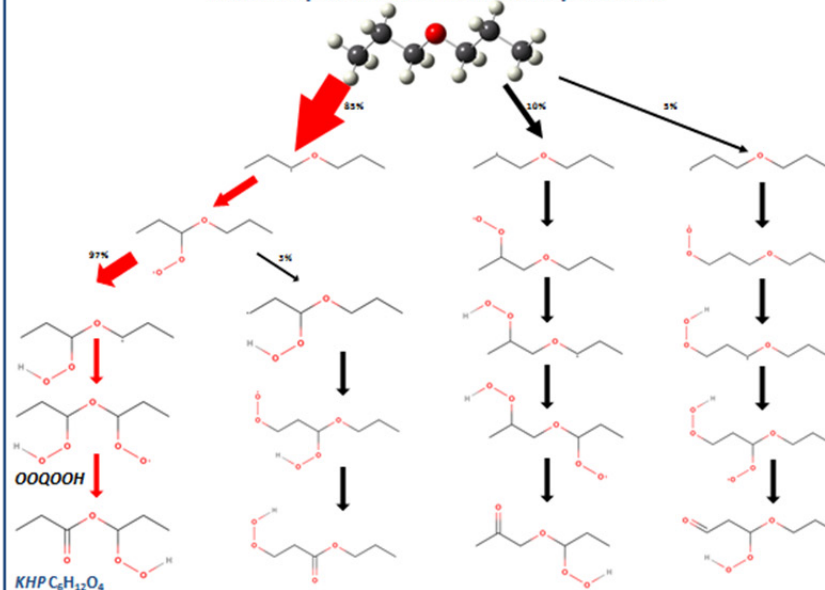
$M(-H)OH^- \quad m/z = 229.05651$

$M(-H)HCOO^- \quad m/z = 257.05142$



Dipropyl ether oxidation

Reaction pathways to ketohydroperoxides



HOMs formation mechanism

$OOQOOH \rightleftharpoons HOOPOOH$ (alternative H-transfer, not from HC-OOH)

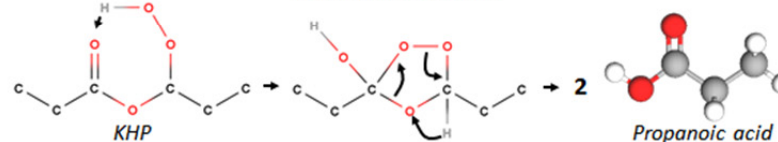
3rd O_2 addition:

$HOOPOOH + O_2 \rightleftharpoons (HOO)_2POO \rightleftharpoons (HOO)_2P'OOH \rightarrow OH + (HOO)_2P'=O \quad (C_6H_{12}O_6)$

4th O_2 addition:

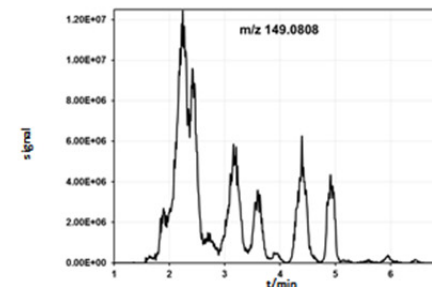
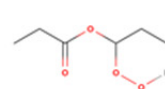
$(HOO)_2P'OOH + O_2 \rightleftharpoons (HOO)_3P''OO \rightleftharpoons (HOO)_3P''OOH \rightarrow OH + (HOO)_3P''=O \quad (C_6H_{12}O_8)$

Korcek mechanism

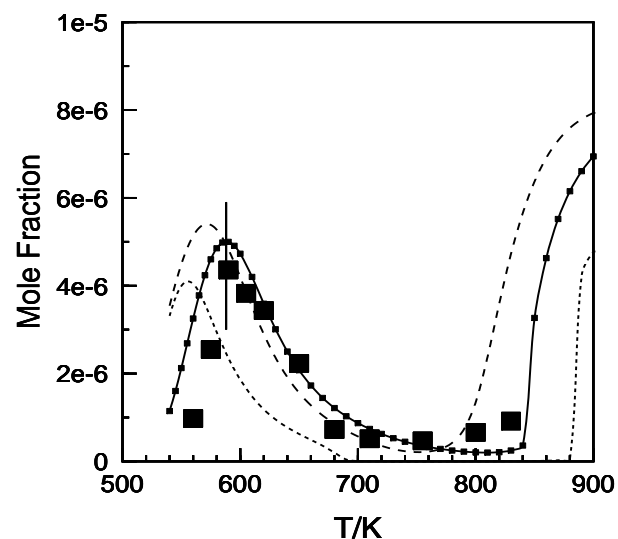


UHPLC analyses

Major KHP isomer:

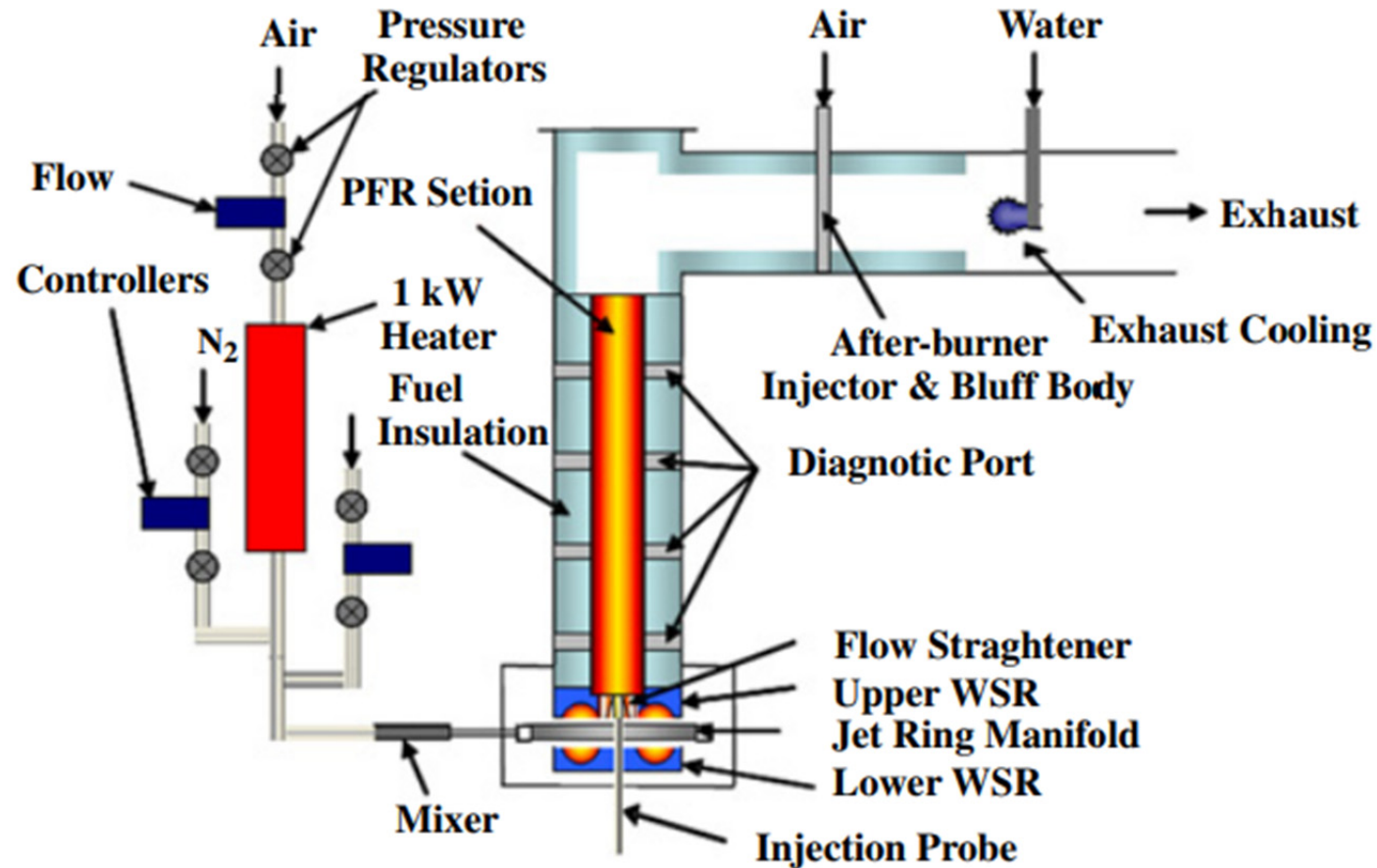


Quantitative measurements using cavity ring-down spectroscopy in the near-IR of HO₂ and H₂O₂ were reported recently (Djehiche, M. et al., JACS, 2014. 136(47): p. 16689-16694; Le Tan, N.L. et al., Fuel, 2015. 158: p. 248-252). The gas mixtures were sampled with a wide angle fused silica nozzle, the tip being located 5 mm inside the reactor. The CRDS cell was kept at low-P (0.3 to 10 mbar), while operating the JSR at 1 atm.



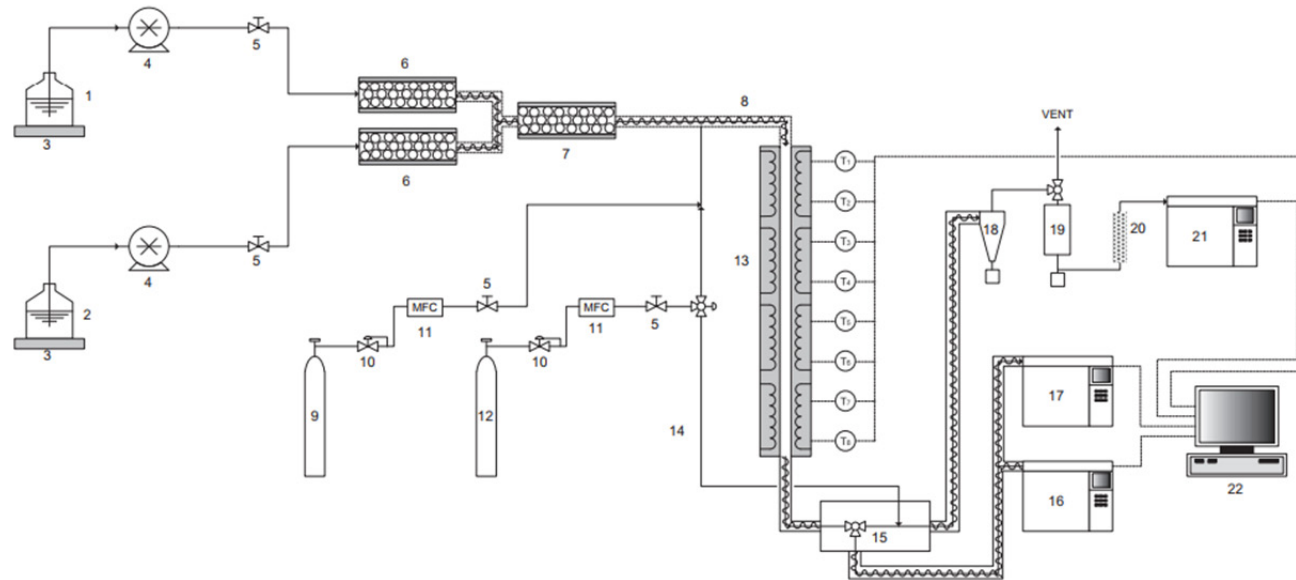
HO₂ concentration profile measured by CRDS during the oxidation of 5000ppm of dimethyl ether in a JSR at an equivalence ratio of 0.5 and a mean residence time of 1.5s. The data (symbols) are compared to simulations using three literature mechanisms. From Le Tan, N.L., M. Djehiche, C.D. Jain, P. Dagaut, and G. Dayma, Fuel, 158, p. 250, 2015.

JSR and PFR have been combined at MIT (Lam, F.W. et al., *Symp. (Int.) Combust.*, 1989. 22(1): p. 323-332) to allow probing combustion chemistry over a wider range of residence times. The original design was further modified at NIST by Lenhert and Manzello



Schematic of the NIST jet-stirred reactor/plug-flow reactor assembly inspired from an earlier MIT design (Lam, F.W. et al., *Symp. (Int.) Combust.*, 1989. 22(1): p. 323-332). From Lenhert, D.B. and S.L. Manzello, *Proc. Combust. Inst.*, 32(1), p. 658, 2009.

Both PFRs and JSRs can be pressurized (*Rasmussen, C.L. et al., IJCK, 2008. 40(8): p. 454-480; Allen, M.T. et al., IJCK, 1995. 27(9): p. 883-909; Dagaut, P. et al., J. Phys. E-Sci. Instr., 1986. 19(3): p. 207-209*). Whereas fused-silica reactors are commonly used, some were built in metal (*Lignola, P.G. and E. Reverchon, CST, 1988. 60(4-6): p. 319-333; Ciajolo, A. et al., CST, 1997. 123(n): p. 49-61; Harper, M.R. et al., CNF, 2011. 158(1): p. 16-41; Wada, T. et al., CTM, 2013. 17(5): p. 906-936*) and refractory materials (e.g., ceramic or alumina) (*Westbrook, C.K. et al., CNF, 1988. 72(1): p. 45-62; Bilbao, R. et al., Proc.. Ind. & Eng. Chem. Res., 1994. 33(11): p. 2846-2852*). Whereas **fused-silica** is generally considered chemically inert in combustion studies, other materials such as **metals** have catalytic activity that cannot be ignored.



Schematic of the Ghent University Incoloy 800HT tubular flow reactor. From Harper, M.R., K.M. Van Geem, S.P. Pyl, G.B. Marin, and W.H. Green, Comprehensive reaction mechanism for n-butanol pyrolysis and combustion. Combustion and Flame, 158(1), p. 18, 2011.

Flow reactors advantages:

Operating temperature range and the possibility to investigate pyrolysis to oxidation, whereas flame studies are much more limited.

Reactors are particularly useful for gaining insights into reaction products and intermediates through the use of advanced detection and/or quantification techniques.

Numerous analytical techniques are used after gas sampling achieved using a range of probes for stopping chemical reactions and transferring a chemical sample to the appropriate analyzers. Also, one should be aware of possible complications such as surface reactions.

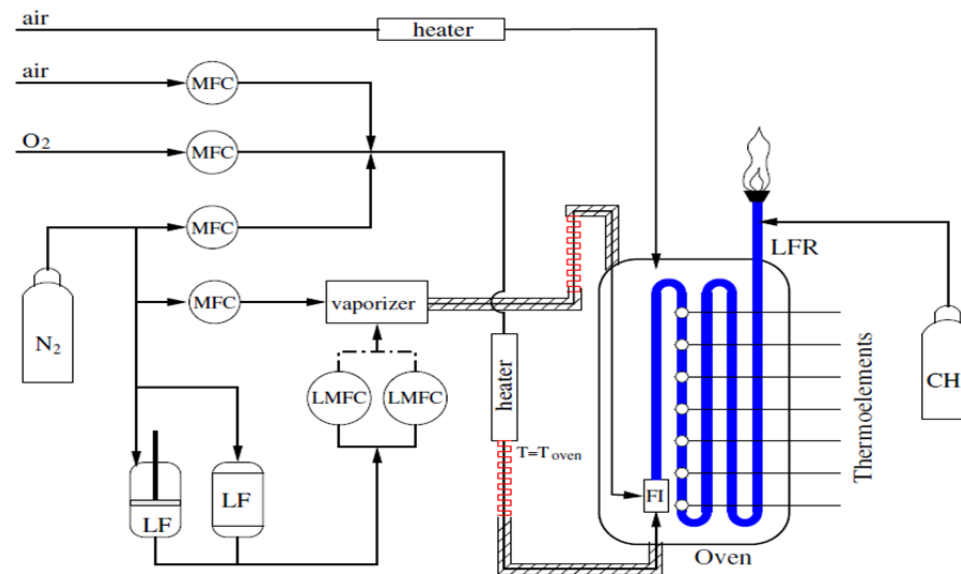
Flow reactors disadvantages:

Can operate over limited temperature, pressure, and residence time ranges. This is due to material range of use and reachable flow rates.

Experiments **need much larger fuel quantities** compared to shock-tube and RCM experiments. The quantification of intermediate species by photoionization remains limited due to unknown photoionization efficiency difficult to compute using current theoretical methods.

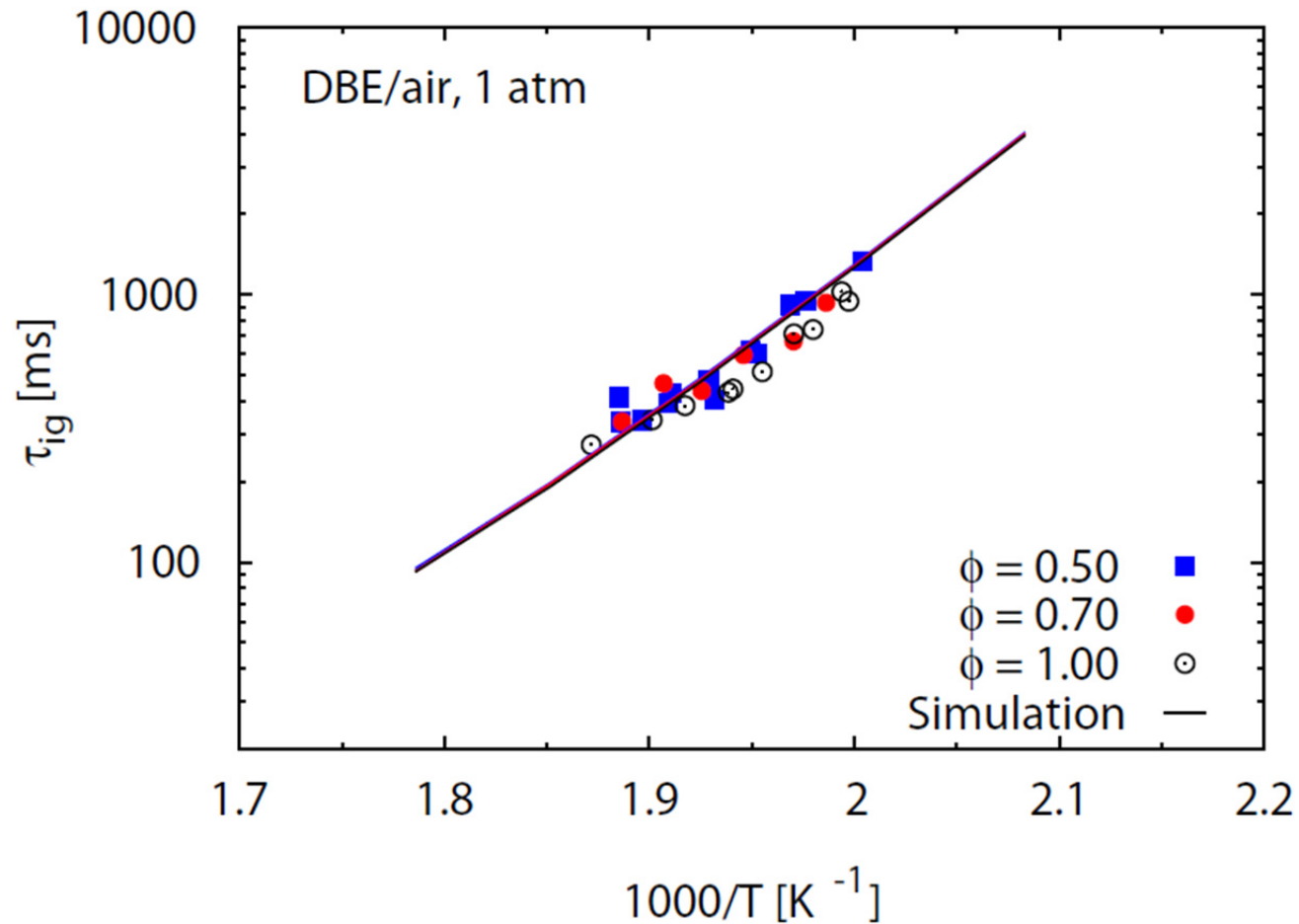
3.2 Ignition data from PFR

Ignition delays can also be determined using PFRs. Recently an experimental setup was designed for this purpose (Wada, T. et al., *CTM*, 2013. 17(5): p. 906-936). The 1st-stage ignition is observed as a temperature increase of a few degrees in the reactor. After the first-ignition, strong heat loss to the reactor wall reduces the temperature and stops chemical reactions. The 1st-stage ignition is determined based on the distance between fuel injection and the location of the first T-rise and the flow rate in the reactor.



Schematic of the Aachen University stainless steel laminar tubular flow reactor. From Cai, L.M., A. Sudholt, D.J. Lee, F.N. Egolfopoulos, H. Pitsch, C.K. Westbrook, and S.M. Sarathy, Combustion and Flame, 161(3), p. 802, 2014.

This set-up was successfully used for measuring first-stage ignition delays of biofuels:



Ignition delay times of dibutyl ether/air mixtures at 1 atm. From Cai, L.M., A. Sudholt, D.J. Lee, F.N. Egolfopoulos, H. Pitsch, C.K. Westbrook, and S.M. Sarathy. Combustion and Flame, 161(3), p. 802, 2014.

4. Flames

Laminar flames are used to obtain both global (laminar burning velocity) and detailed (spatial speciation or flame structure) data usable for validating kinetic models. Experiments are currently performed over a wide range of pressure, from ca. 0.04 to 60 bar.

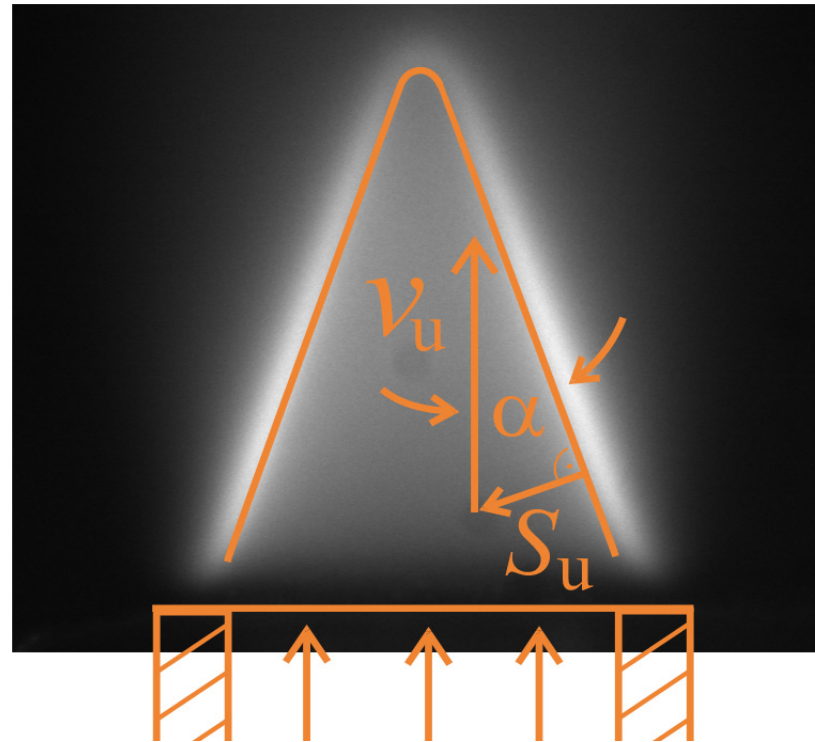
Burning velocities have been obtained from ca. 0.1 to 60 bar whereas flame structures are available up to ca. 10 bar.

Major improvements of the methods have been made over the years, allowing the acquisition of very valuable data for kinetic modelers over a very wide range of conditions and for many fuels (*Ranzi, E. et al., PECS, 2012. 38(4): p. 468-501; Egolfopoulos, F.N. et al., PECS, 2014. 43: p. 36-67*).

4.1 Burning velocities

The laminar flame speed is defined as the propagation speed of a steady, laminar, one-dimensional, planar, stretch-free, and adiabatic flame. It is an important fundamental property of a flammable mixture, being a measure of its reactivity, diffusivity, and exothermicity. It constitutes an important validation target for kinetic models and a key parameter in turbulent combustion.

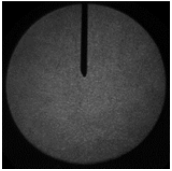
Burning velocity can be extracted from a range of experimental configurations, e.g., soap bubble method, flames in tubes, flat flame burner method, conical flames (Bunsen type), heat flux method, spherical flames in constant volume chamber, and stagnation flame/opposed-flow method:



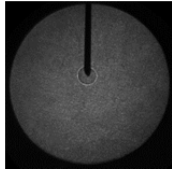
*Determination of the burning velocity S_u by applying the cone angle method ($S_u = v_u \sin \alpha$).
From Mz  Ahmed, A., P. Dagaut, K. Hadj-Ali, G. Dayma, T. Kick, J. Herbst, T. Kathrotia, M. Braun-Unkhoff, J. Herzler, C. Naumann, and U. Riedel, *The Oxidation of a Coal-to-Liquid Synthetic Jet Fuel: Experimental and Chemical Kinetic Modeling Study*. *Energy & Fuels*, 26(10), p. 6072, 2012.*

Spherical flames in constant volume chamber:

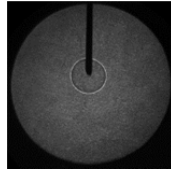
0 ms



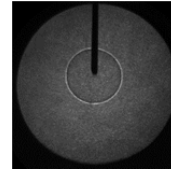
3.3 ms



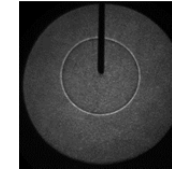
5 ms



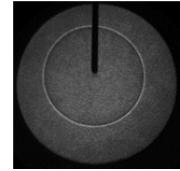
6.7 ms



8.3 ms



10 ms



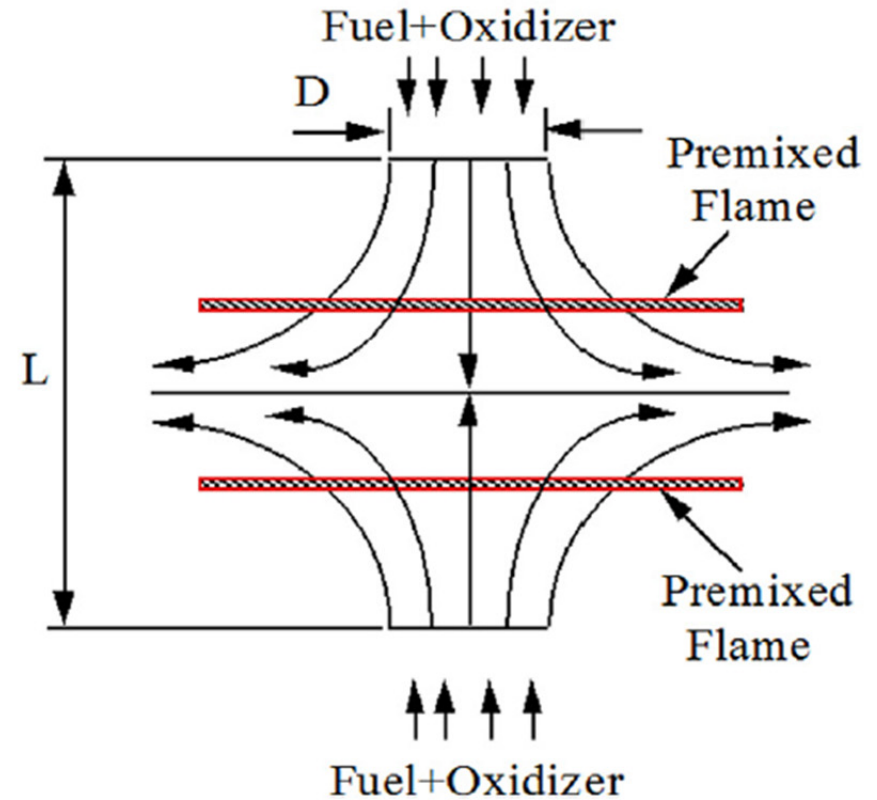
*Shadowgraphs of the temporal evolution of an ethyl propanoate/air flame front at $P = 1$ bar, $T_u = 423$ K and $\phi = 0.9$. The temporal increase of the flame radius is used to compute the stretched laminar burning velocity. The unstretched burning velocity is obtained after extrapolation to zero-stretch using proposed methods in the literature. From Dayma, G., F. Halter, F. Foucher, C. Mounaim-Rousselle, and P. Dagaut, Laminar Burning Velocities of C(4)-C(7) Ethyl Esters in a Spherical Combustion Chamber: Experimental and Detailed Kinetic Modeling. *Energy & Fuels*, 26(11), p. 6670, 2012.*

Nowadays spherical flames in constant volume chamber and stagnation flame/opposed-flow method are the most widely used.

They have been reviewed recently (*Ranzi et al. PECS, 2012. 38(4): p. 468-501 and Egolfopoulos et al. PECS, 2014. 43: p. 36-67*).

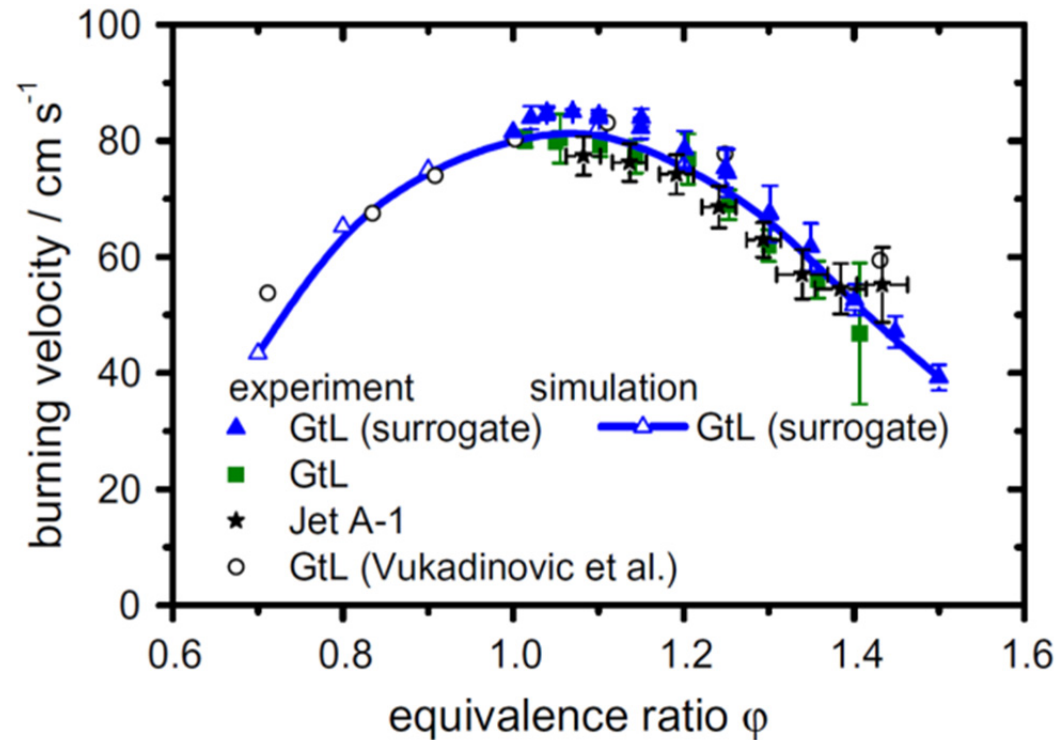
High pressure and temperature conditions are hardly reachable using Bunsen flames, counter-flow flames or heat flux burner. Most of the results reported at elevated pressures were obtained with spherical expanding flames. One limitation of this method comes from the fact that the spherical flame surface is changing during propagation inducing stretch effects which must be accounted for using extrapolation methods. Until the work of Wu and Law (*Symp. (Int.) Combust., 1985. 20(1): p. 1941-1949*), undetermined stretch effects led to lots of scatter in measurements.

Significant reduction of uncertainty on flame speed measurements has resulted from stretch correction, as outlined by Law (*AIAA Journal, 2012. 50(1): p. 19-36*) for methane-air flames for which the ± 25 cm/s scatter got reduced to ca. 2 cm/s recently by considering the non-linear nature of stretch on burning velocity (*Kelley, A.P. and C.K. Law, CNF, 2009. 156(9): p. 1844-1851; Halter, F. et al., CNF, 2010. 157(10): p. 1825-1832*). With such low uncertainties, burning velocities are very valuable for kinetic models assessment.



Picture of twin stagnation flames (left) and schematic view (right). From Egolfopoulos, F.N., N. Hansen, Y. Ju, K. Kohse-Hoinghaus, C.K. Law, and F. Qi, *Advances and challenges in laminar flame experiments and implications for combustion chemistry*. *Progress in Energy and Combustion Science*, 43, p. 49, 2014.

Burning velocities for simple to complex fuels have been published. An example of such results is given here for the combustion of synthetic jet-fuels.



*Comparison of measured (symbols) and predicted laminar burning velocities of synthetic and conventional jet-fuel-air mixtures at $T_u = 473$ K and $p = 1$. From Dagaut, P., F. Karsenty, G. Dayma, P. Diévar, K. Hadj-Ali, A. Mzé-Ahmed, M. Braun-Unkhoff, J. Herzler, T. Kathrotia, T. Kick, C. Naumann, U. Riedel, and L. Thomas, *Experimental and detailed kinetic model for the oxidation of a Gas to Liquid (GtL) jet fuel*. *Combustion and Flame*, 161(3), p. 846, 2014.*

4.2 Species measurements.

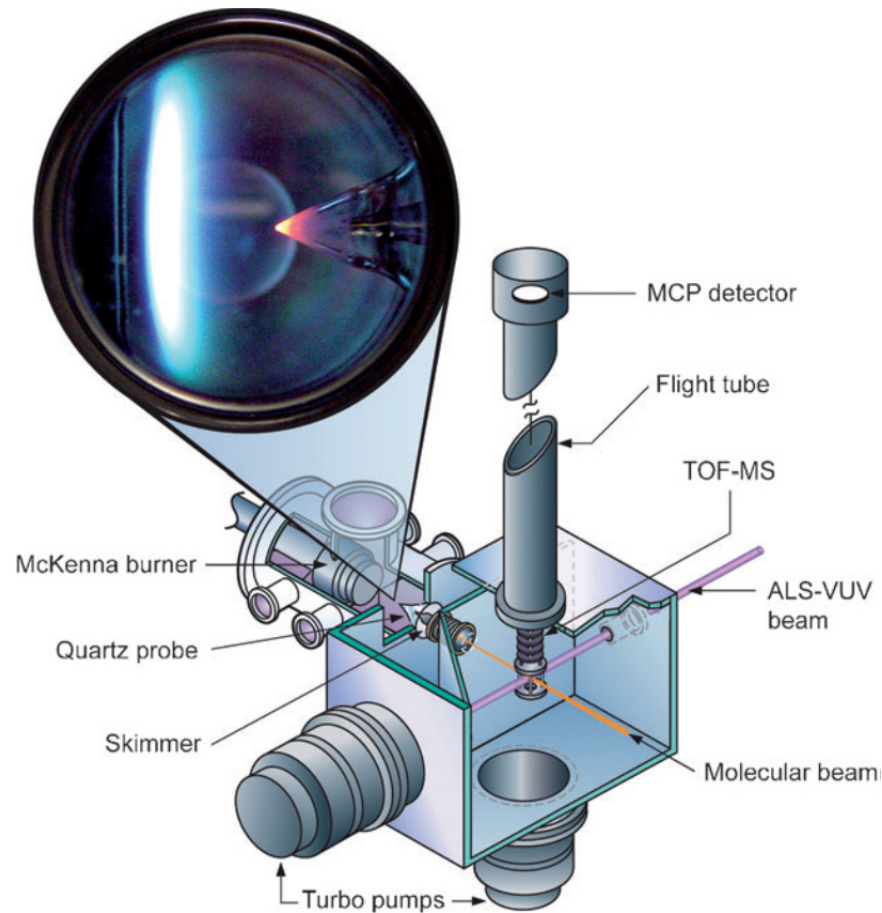
The measurement of flames structure has a long history (*Eltenton, G.C., J. Chem. Phys., 1947. 15(7): p. 455-481; Fristrom, R.M. and A.A. Westenberg, Flame Structure. 1st Ed. 1965: McGraw-Hill. 424*). Nowadays, flame structures mostly come from two methods: low-pressure premixed flat flames and stagnation flames.

These techniques have been reviewed recently (*Egolfopoulos, F.N. et al., PECS, 2014. 43: p. 36-67*).

Samples are extracted from the flame using a probe and sent to analyzers (gas chromatography, mass spectrometry).

Molecular beam-mass spectrometry has been used extensively.

More recently, photoionization by synchrotron-sourced vacuum-ultraviolet radiation was employed, generating a large body of kinetic data unreachable by other techniques (*Egolfopoulos, F.N. et al., PECS, 2014. 43: p. 36-67; Qi, F. et al., Rev. Sci. Instr., 2006. 77(8): p. 84101; Qi, F., PROCI, 2013. 34(1): p. 33-63; Hansen, N. et al., PECS, 2009. 35(2): p. 168-191; Cool, T.A. et al., J. Chem. Phys., 2003. 119(16): p. 8356-8365; Rev. Sci. Instr., 2005. 76(9); Westmoreland, P.R. et al., Comb. Expl. Shock Waves, 2006. 42(6): p. 672-677*):



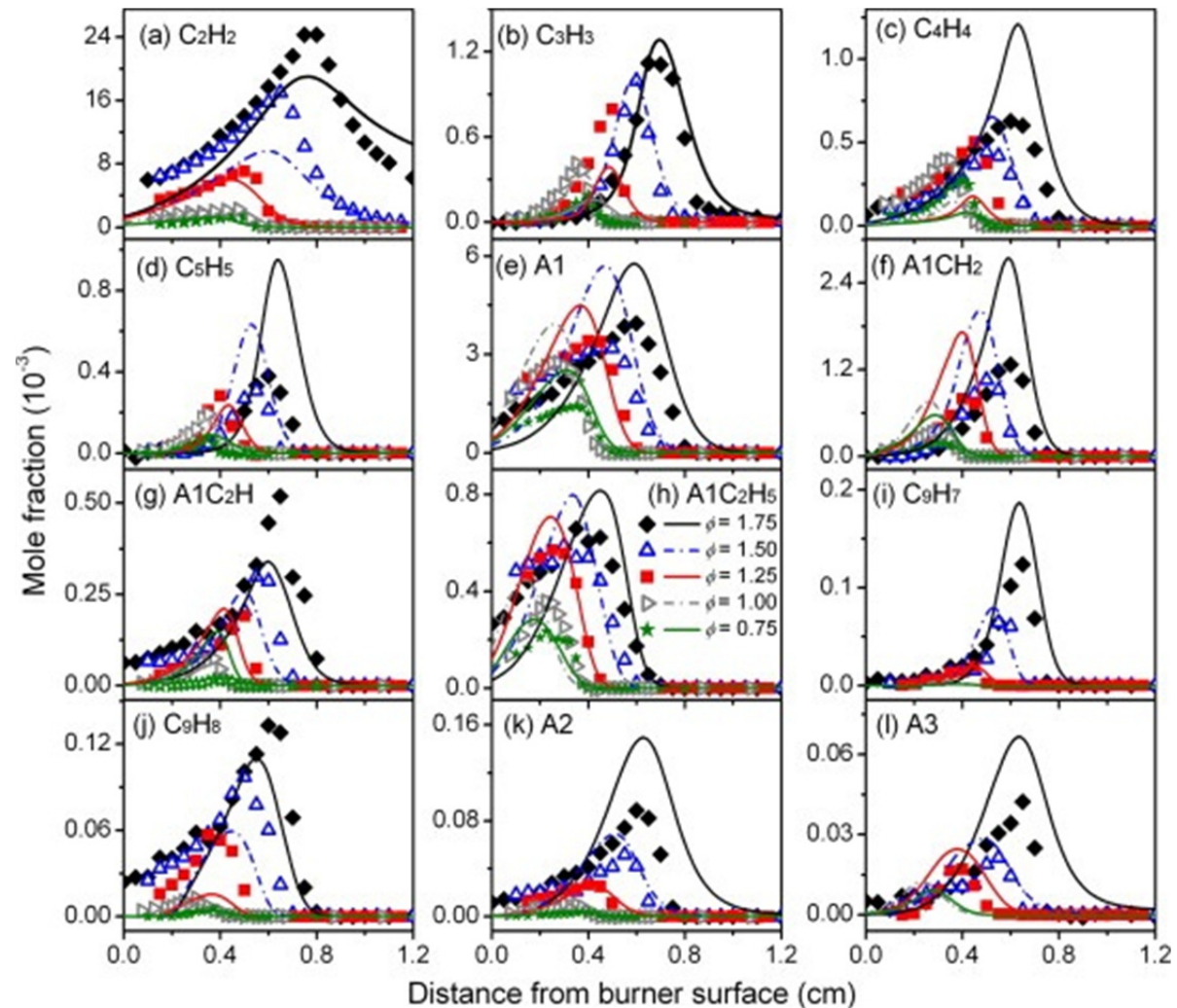
*Schematic of a low-pressure McKenna burner experimental set-up. Gases from the flame are sampled through a fused-silica probe (picture) into a time-of-flight mass spectrometer where chemicals are photo-ionized by synchrotron-generated vacuum-ultraviolet radiation. From Taatjes, C.A. et al. *Physical Chemistry Chemical Physics*, 10(1), p. 22, 2008.*

Fused-silica probe can cause significant **perturbations** to the flame, making difficult to model and interpret the experiments, as demonstrated in a recent study by Hansen et al. (*CNF*, 2017. 181: p. 214-224).

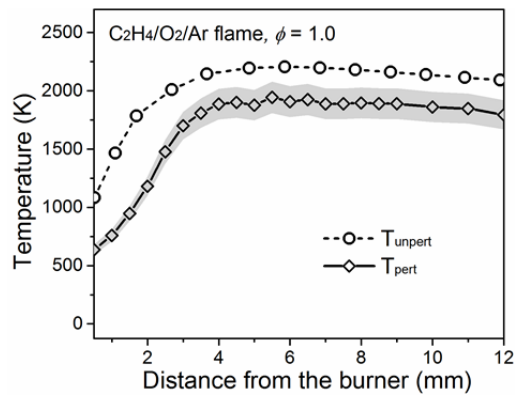
Also, the use of a thermocouple for measuring temperature profiles in the flame can alter the flow fields and temperature profiles (*Skovorodko, P.A. et al., CTM*, 2013. 17(1): p. 1-24; *CNF*, 2012. 159(3): p. 1009-1015), although these effects are small compared to sampling probe perturbations.

Nevertheless, a wide range of fuels have been studied in flames.

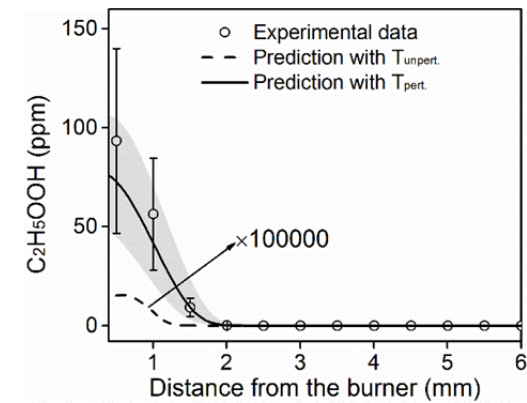
Examples of concentration profiles of C_2 – C_{14} species measured in low-pressure premixed flames of toluene next.



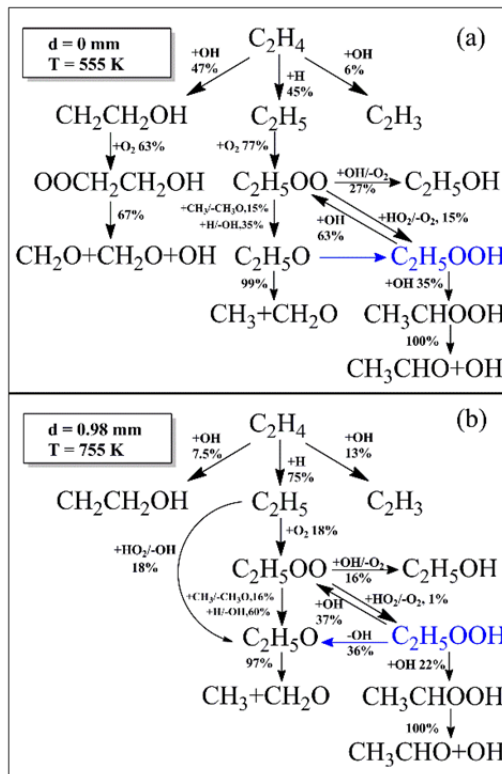
*Experimental (symbols) and simulated (lines) mole fraction profiles of acetylene (C_2H_2), propargyl (C_3H_3), vinylacetylene (C_4H_4), cyclopentadienyl (C_5H_5), benzene (A1), benzyl (A1CH₂), phenylacetylene (A1C₂H), ethylbenzene (A1C₂H₅), indenyl (C_9H_7), indene (C_9H_8), naphthalene (A2) and phenanthrene (A3) in the premixed flames of toluene at five equivalence ratios (0.75 to 1.75). The data were obtained by **MB-MS with photoionization by synchrotron-sourced vacuum-UV radiation**. From Yuan, W. et al., *CNF* 162(1), p. 36, 2015.*



Temperature profiles in the present ethylene/ O_2 /Ar flame. Open diamonds and open circles represent the T_{pert} and T_{unpert} profiles, respectively. Shadows represent the scaled T_{pert} profiles considering the uncertainties of maximum T_{pert} values.



Measured (symbol) and predicted (lines) mole fraction profiles of C_2H_5OOH in the present ethylene/ O_2 /Ar flame. The solid and dashed lines represent the predicted results with the T_{pert} and T_{unpert} profiles, respectively. Shadows represent the predicted results considering the uncertainties of T_{pert} .



ROP analysis with the Hashemi model* by using the T_{pert} profile at (a) $d = 0 \text{ mm}$ ($T = 555 \text{ K}$) and (b) $d = 0.98 \text{ mm}$ ($T = 755 \text{ K}$).

*H. Hashemi, J.G. Jacobsen, C.T. Rasmussen, J.M. Christensen, P. Glarborg, S. Gersen, M. van Essen, H.B. Levinsky, S.J. Klippenstein, High-pressure oxidation of ethane, *Combust. Flame* 182 (2017) 150-166.

From Xiaoyuan Zhang et al. *Comb. Flame* **204** (2019) 260–267

Whereas time-of-flight mass spectrometry with photoionization by synchrotron-generated vacuum-ultraviolet radiation are very useful for detecting intermediate species, the differentiation between isomers can be difficult when photoionization energies are too close.

Dias et al. (*CST*, 2004. 176(9): p. 1419-1435) have introduced a useful method consisting of a conventional EI-MBMS setup where a portion of the sample is sent to a GC-MS through a capillary, allowing separation of isomers of stable products that could not be differentiated based on their ionization energies or mass.

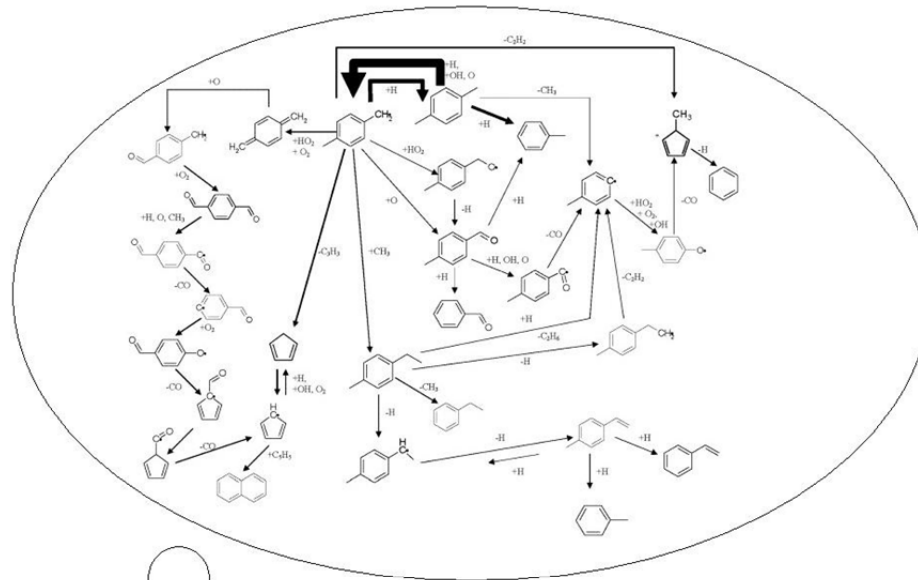
Other workers also combined EI-MBMS measurements with GC-MS measurements to get better characterization of isomers (*Bourgeois, N. et al., PROCI*, 2017. 36(1): p. 383-391).

5. Some conclusions and perspectives

The most common experiments for kinetic mechanism assessment have been presented. It was shown that shock-tube and RCM are very useful for determining fuel ignition properties but also to measure chemical products. Recent advances in CFD modeling of RCM (*Bourgeois, N. et al., PROCI, 2017. 36(1): p. 383-391; CNF, 2018. 189: p. 225-239*) are expected to facilitate the use of RCM ignition data for kinetic model validation. Tubular flow reactors and jet-stirred reactors are commonly used. Their coupling with advanced analytical techniques is able to provide unique data for kinetic models assessment. However, current limitations due to unknown photoionization efficiency for many intermediates must be addressed, possibly through the use of advanced theoretical methods. Flames can also provide valuable data in terms of burning velocities and speciation, although, limiting perturbations by conventional large sampling probes remains a major challenge for future work.

Nomenclature: APCI-OTMS: Atmospheric pressure chemical ionization-Orbitrap® mass spectrometry; CFD: Computational fluid dynamics; CFR: Cooperative Fuel Research; CRDS: Cavity ring-down spectroscopy; CtL: Coal-to-liquid; EI-MBMS: Electron ionization molecular beam-mass spectrometry; FTIR: Fourier-transform infrared; GC: Gas chromatography; GC-MS: Gas chromatography-mass spectrometry; GtL: Gas-to-liquid; IR: Infrared; JSR: Jet-stirred reactor; PFR: Plug-flow reactor; PI-MBMS: Photoionization molecular beam-mass spectrometry; PSR: Perfectly-stirred reactor; RCM: Rapid compression machine; ST: Shock-tube; T_u : temperature of fresh gas; UV: Ultraviolet; VUV: Vacuum ultraviolet; ϕ : equivalence ratio.

MODELING



Modeling: General information

Need accurate kinetics, thermochemistry, and transport data

Use inputs from **theory** and **measurements** and also **estimations** by analogy, tabulations

Need accurate data that are used to **constrain the model**

Modeling

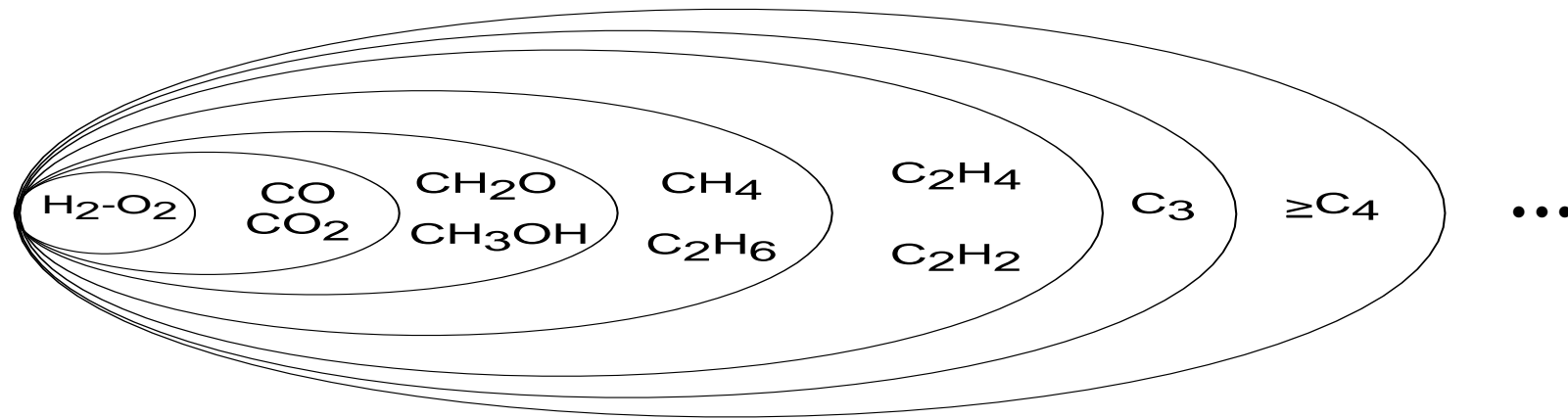
Chemkin computer package.

Kinetic reaction mechanism with modified Arrhenius equation, $k = A T^b \exp(-E/RT)$; $k(P, T)$.

Reaction mechanism with strong **hierarchical structure**.

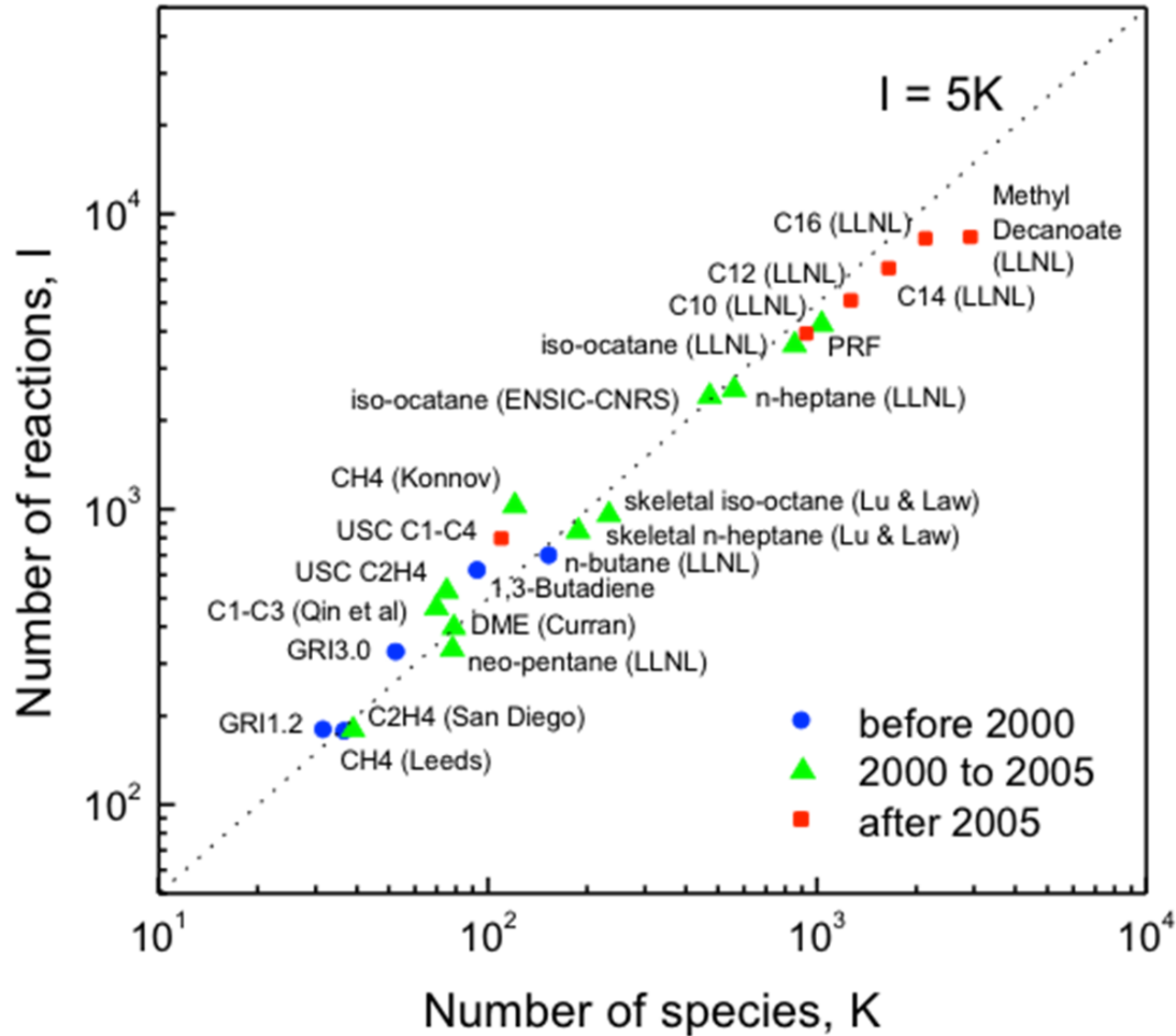
The core-mechanism is H₂/O₂ (H, O, OH, HO₂, H₂O₂, O₂, O₃, H₂).

Modeling: Hierarchical structure of chemical kinetic schemes



Structure hiérarchisée des mécanismes détaillés

Modeling: Size of chemical kinetic schemes



from T.F. Lu, C.K. Law *PECS* 35 (2009) 192–215

Modeling: reaction scheme

REACTIONS	$k=A*T^{**n}*exp(-E/RT)$	A/cc,mole,s	n	E/cal/mol	Ref
H+ H+ M = H2+ M		7.310E+17	-1.0	0.0	! (BAULCH 76)
O+ O+ M = O2+ M		1.140E+17	-1.0	0.0	! (BAULCH 76)
O+ H+ M = OH+ M		6.200E+16	-0.6	0.0	! (DIXON-LEWIS 81)
H2+ O2 = OH+ OH		1.700E+13	0.0	47780.0	! (MILLER 77)
O+ H2 = OH+ H		3.870E+04	2.7	6260.0	!GRI
H+ O2 = OH+ O		4.400E+14	-0.12	16812.0	!Nicolle 2004
H+ O2+ M = HO2+ M		8.000E+17	-0.8	0.0	! (WARNATZ 84)
H+ OH+ M = H2O+ M		8.615E+21	-2.0	0.0	! (BAULCH 76)
H2+ OH = H2O+ H		2.161E+08	1.51	3430.0	! (MICHAEL 88)
H2O+ O = OH+ OH		1.500E+10	1.14	17260.0	! (WARNATZ 84)
HO2+ OH = H2O+ O2		2.890E+13	0.0	-497.0	! (KEYSER 88)
HO2+ O = OH+ O2		1.810E+13	0.0	-400.0	! (JPL 87-41)
H+ HO2 = H2+ O2		4.280E+13	0.0	1411.0	! (94BAU/COB)
H+ HO2 = OH+ OH		1.690E+14	0.0	874.0	! (94BAU/COB)
H+ HO2 = H2O+ O		3.010E+13	0.0	1721.0	! (BAULCH 92)
HO2+ HO2 = H2O2+ O2		4.075E+02	3.321	1979.0	! (HIPPLER 90)
OH + OH (+M) = H2O2 (+M)		7.224E+13	-0.37	0.0	! (94BAU/COB)
H2O2+ OH = HO2+ H2O		5.800E+14	0.0	9557.0	! (92HIP/TRO)
H2O2+ H = HO2+ H2		1.700E+12	0.0	3750.0	! (BAULCH 72)
H2O2+ H = H2O+ OH		1.000E+13	0.0	3590.0	! (WARNATZ 84)
H2O2+ O = HO2+ OH		2.800E+13	0.0	6400.0	! (ALBERS 71)

Modeling: thermochemistry

	ELEMENT	COMPOSITION	Phase	LOWER-T	HIGHER-T	MID-T	
H	H	10 00 00	0G	300.00	5000.00	1000.00	1
		0.25000000E+01 0.00000000E+00 0.00000000E+00		0.00000000E+00	0.00000000E+00	0.00000000E+00	2
		0.25471600E+05 -0.46000000E+00		0.25000000E+01	0.00000000E+00	0.00000000E+00	3
		0.00000000E+00 0.00000000E+00		0.25471600E+05 -0.46000000E+00			4
H2	H	20 00 00	0G	300.00	5000.00	1000.00	1
		0.29914200E+01 0.70006000E-03 -0.56340000E-07 -0.92300000E-11		0.15800000E-14			2
		-0.83500000E+03 -0.13550000E+01 0.32981200E+01		0.82494000E-03 -0.81430000E-06			3
		-0.94750000E-10 0.41349000E-12 -0.10125000E+04		-0.32940000E+01			4
O	O	10 00 00	0G	300.00	5000.00	1000.00	1
		0.25420600E+01 -0.27550000E-04 -0.31000000E-08		0.45500000E-11 -0.44000000E-15			2
		0.29230800E+05 0.49200000E+01 0.29464300E+01 -0.16381700E-02		0.24210300E-05			3
		-0.16028400E-08 0.38907000E-12 0.29147600E+05		0.29640000E+01			4
O2	O	20 00 00	0G	300.00	5000.00	1000.00	1
		0.36975800E+01 0.61352000E-03 -0.12588000E-06		0.17750000E-10 -0.11400000E-14			2
		-0.12339000E+04 0.31890000E+01 0.32129400E+01		0.11274900E-02 -0.57562000E-06			3
		0.13138800E-08 -0.87686000E-12 -0.10052000E+04		0.60350000E+01			4

($a_{1,k} \dots a_{7,k}$) to calculate thermodynamics over the range 1000 - 5000 K and ($a_{8,k} \dots a_{14,k}$) over the range 300 - 1000 K.

$$\frac{C_{p,k}}{R} = a_{1,k} + a_{2,k}T + a_{3,k}T^2 + a_{4,k}T^3 + a_{5,k}T^4; \quad \frac{H_k^0}{RT} = a_{1,k} + a_{2,k}\frac{T}{2} + a_{3,k}\frac{T^2}{3} + a_{4,k}\frac{T^3}{4} + a_{5,k}\frac{T^4}{5} + a_{6,k}\frac{1}{T}$$

$$\frac{S_k^0}{R} = a_{1,k} \ln T + a_{2,k}T + a_{3,k}\frac{T^2}{2} + a_{4,k}\frac{T^3}{3} + a_{5,k}\frac{T^4}{4} + a_{7,k}$$

$$G^0 = H^0 - TS^0; \quad \Delta G^0 = G_{prod}^0 - G_{react}^0 = -RT \ln(K_p); \quad K_c = \frac{k_{for}}{k_{rev}} = K_p \left(\frac{P}{RT} \right)^{\sum \nu_{prod} - \sum \nu_{react}}$$

Modeling: transport

SPECIES	STRUCTURE	L-J POTENTIAL WELL ϵ/k	L-J COLLISION DIAM. σ	DIPOLE MOMENT μ	POLARIZABILITY α	ROTATIONAL RELAX COLL NBR Z_{rot}
O	0	80.000	2.750	0.000	0.000	0.000
O2	1	107.400	3.458	0.000	1.600	3.800
OH	1	80.000	2.750	0.000	0.000	0.000
H2O	2	572.400	2.605	1.844	0.000	4.000
H2O2	2	107.400	3.458	0.000	0.000	3.800

Structure: 0= atom; 1= linear; 2= non-linear

Very good source for the transport properties and their estimates in R. C. Reid, R. C., J. M., Prausnitz, B. E., Poling *The properties of Gases and liquids*, 4th ed, McGraw-Hill, New York, 1987.

CHEMKIN details : R. J. Kee, J. Warnatz, M. E. Coltrin, and J. A. Miller, *A FORTRAN computer code package for the evaluation of gas-phase, multicomponent transport properties*, Sandia Report 86-8246.

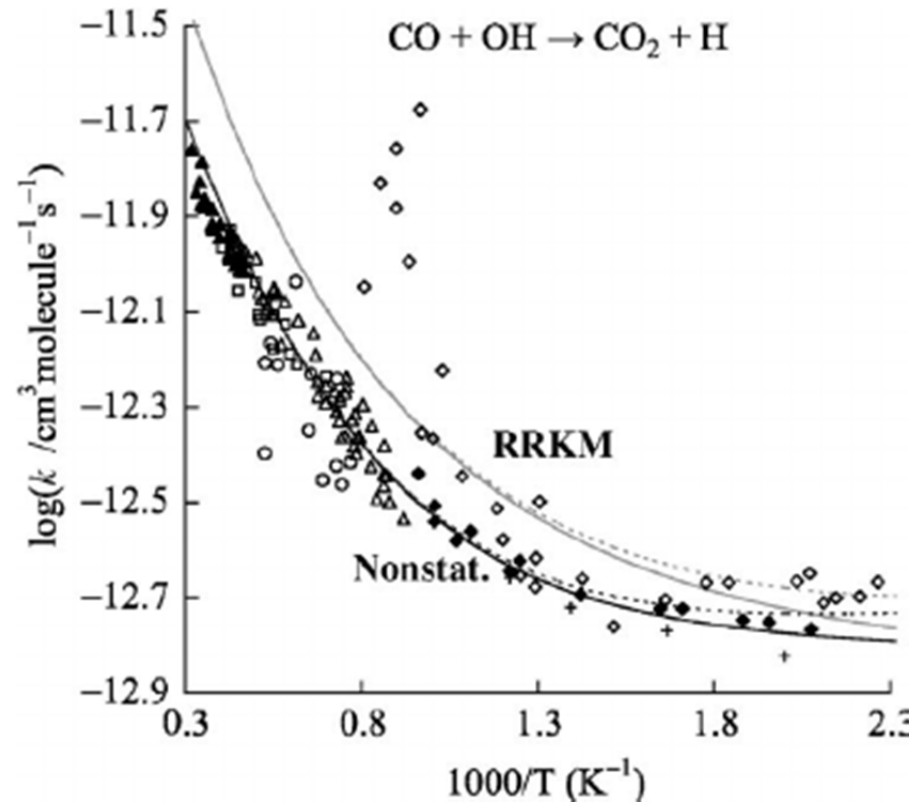
Modeling: Temperature dependencies of elementary reactions

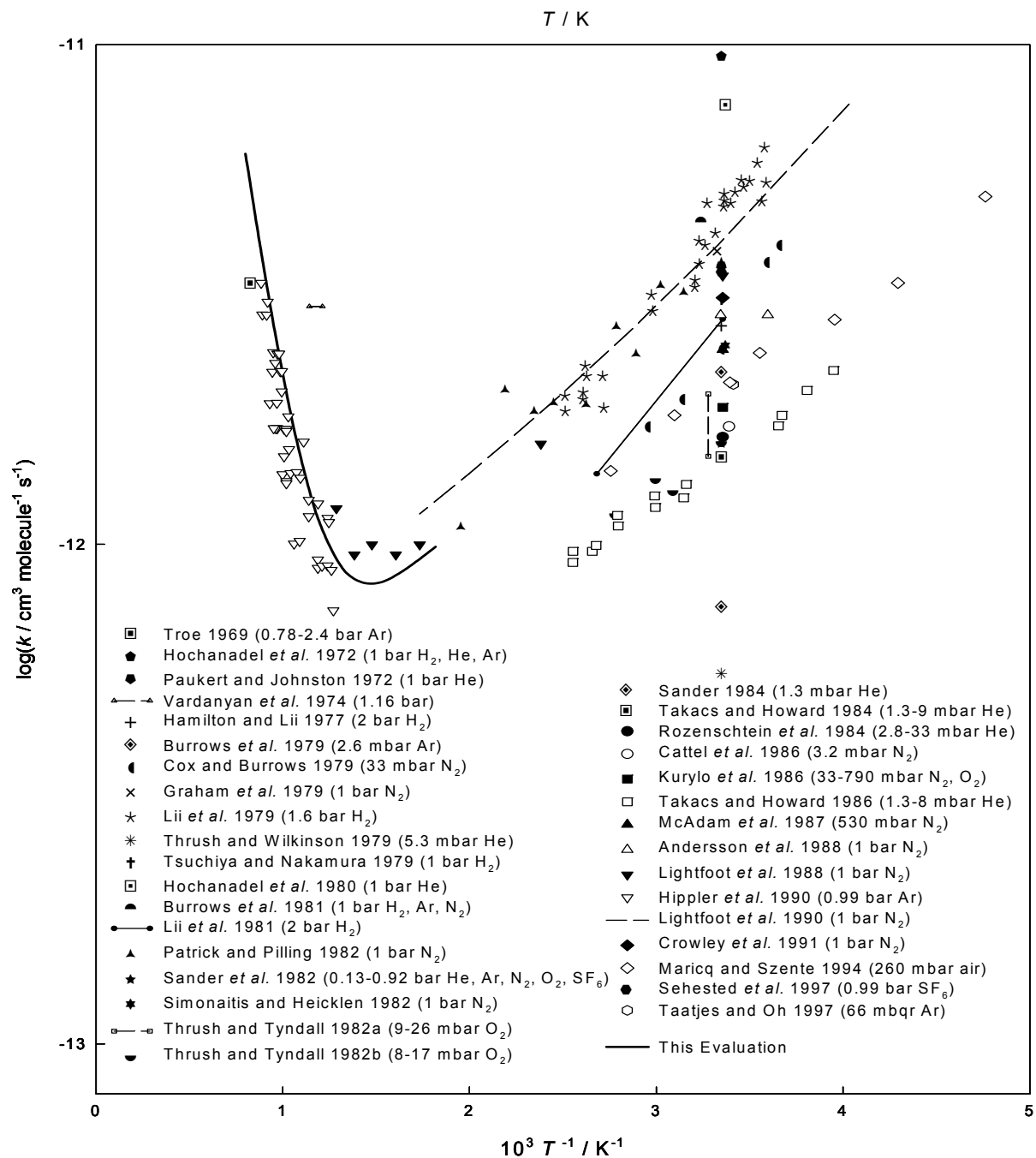
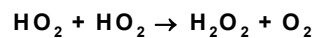
In 1889, Svante Arrhenius proposed the Arrhenius equation from direct observations of the plots of rate constants vs. temperature:

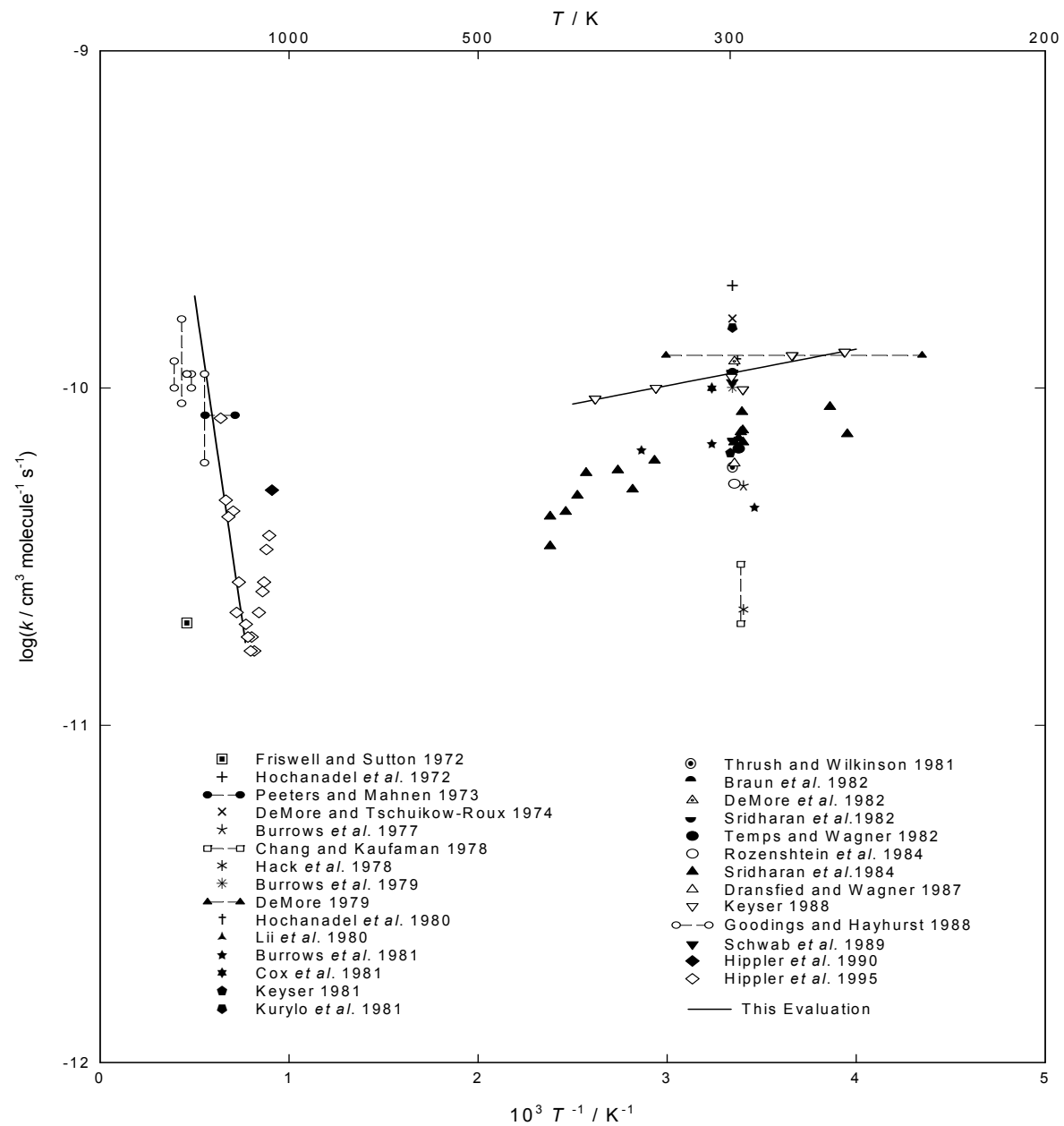
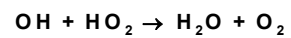
$$k = A \exp(-E_a/RT)$$

Later, modified Arrhenius expression:

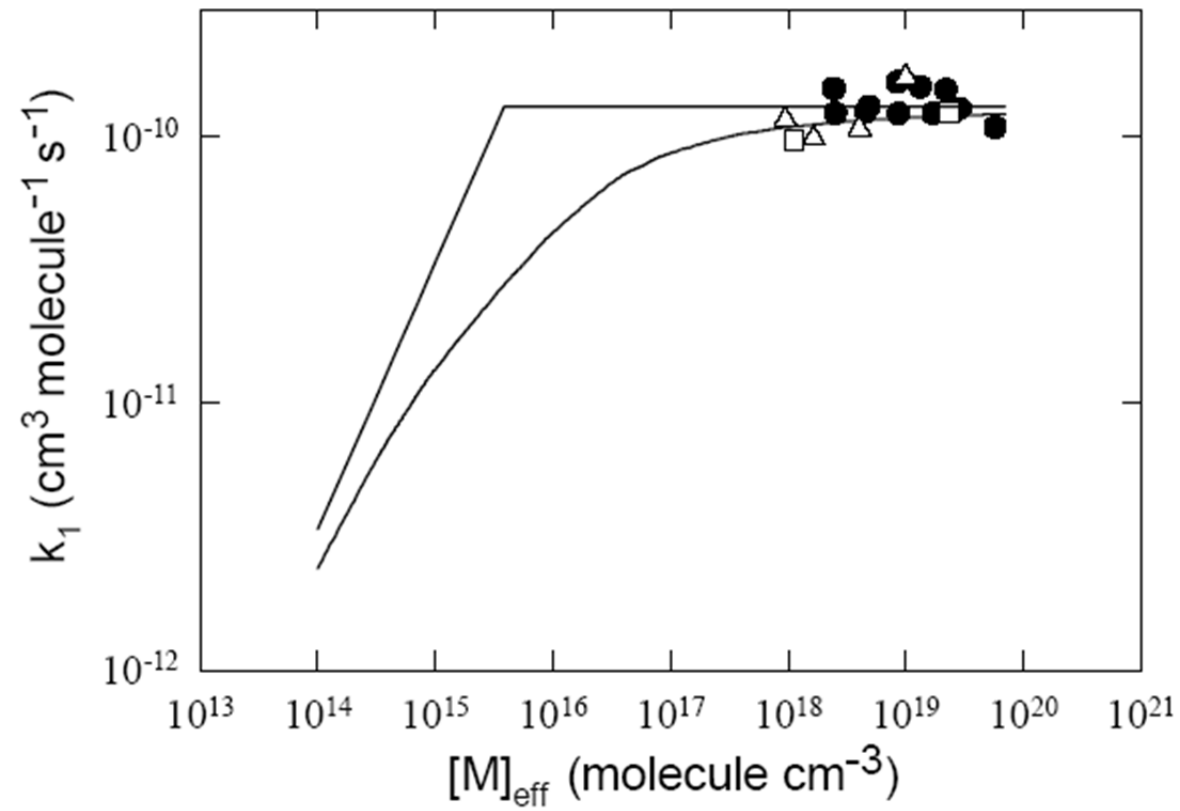
$$k = A T^n \exp(-E_a/RT)$$

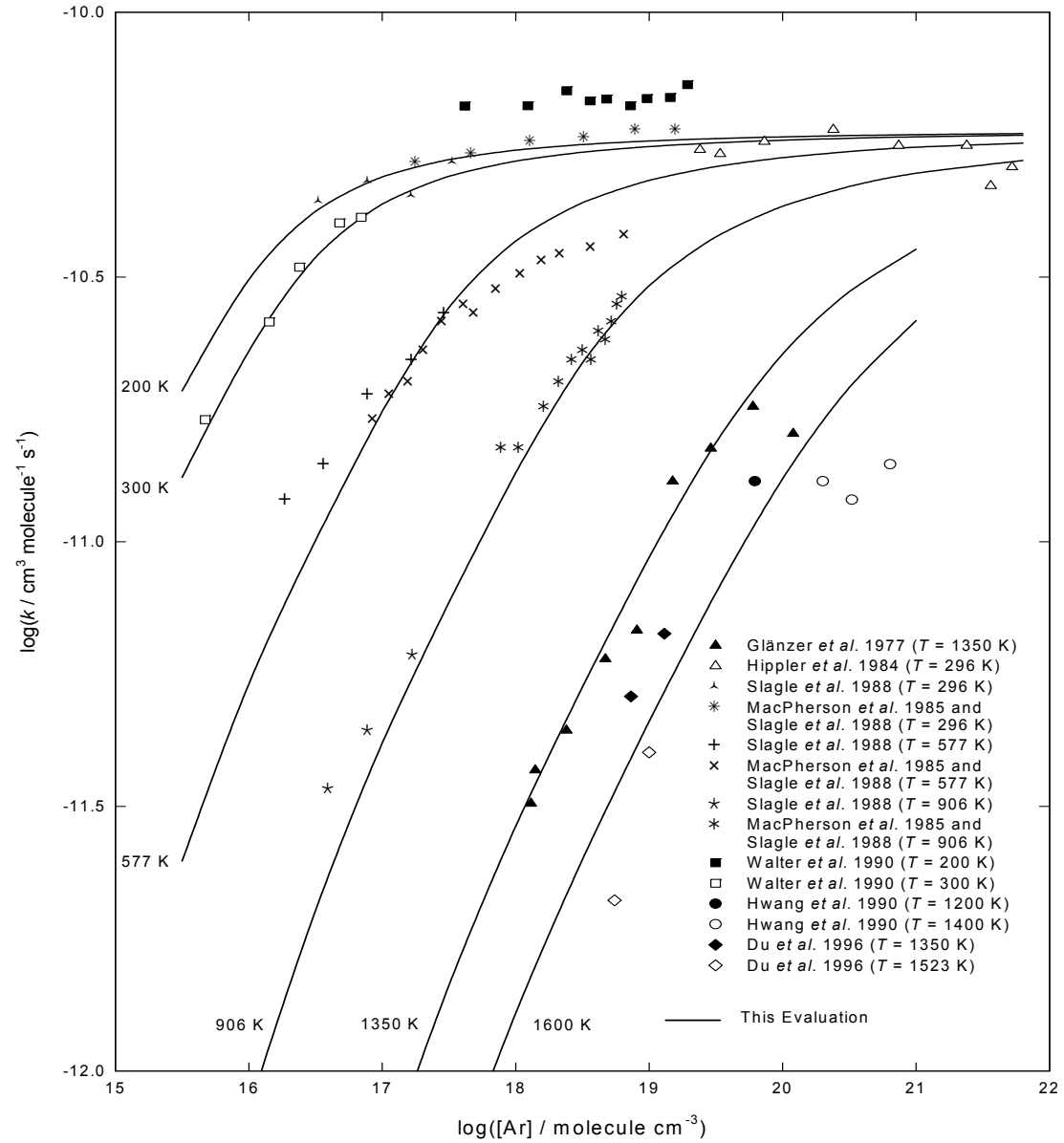
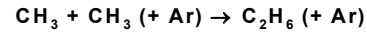






Modeling: Pressure dependencies

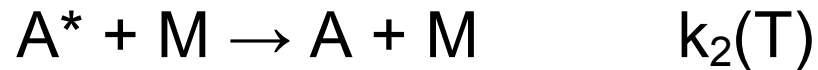




Modeling: Pressure dependencies

Lindemann-Hinshelwood

Assume every collision leads to stabilization



The quasi steady state approximation (QSSA) for A^* : $d[A^*]/dt=0$

Steady state for $[A^*] = k_1 [A] [M] / (k_2 [M] + k_3)$

Rate = $k_3 [A^*] = k_3 k_1 [A] [M] / (k_2 [M] + k_3) = k_{\text{uni}} [A]$

High Pressure limit ($[M] \rightarrow \infty, k_2 [M] \gg k_3$): rate = $k_1 k_3 [A] / k_2 = k_{\text{uni}} [A]$;

$$k_{\text{uni}} = k_1 k_3 / k_2$$

Low Pressure limit ($[M] \rightarrow 0, k_2 [M] \ll k_3$): rate = $k_1 [A] [M] = k_0 [A]$;

$$k_{\text{uni}} = k_1 [M]$$

Troe fitting

$$k(T, p) = \frac{k_0[M]k^\infty}{k^\infty + k_0[M]} F$$

$$\log_{10} F = \frac{\log_{10} F_{cent}}{1 + \left[\frac{\log_{10}(p^*) + c}{N - d(\log_{10}(p^*) + c)} \right]^2}$$

$$d = 0.14$$

$$p^* = k_0[M]/k^\infty$$

$$c = -0.4 - 0.67 \log_{10} F_{cent}$$

$$N = 0.75 - 1.27 \log_{10} F_{cent}$$

$$F_{cent} = (1 - a) \exp(-T/T^{***}) + a \exp(-T/T^*) + \exp(-T^{**}/T)$$

Modeling: Kinetic analyses

1-Reaction pathways

How reactions proceed?

How reactants and intermediates are consumed?

How products are formed?

ROP(Product1):

reaction rate (R1)/(sum of reaction rates yielding Product1)

ROC(Product1):

reaction rate (R1)/(sum of reaction rates consuming Product1)

Net rate of production = (total rate of production) – (total rate of consumption)

What are the important routes for NO-reduction?

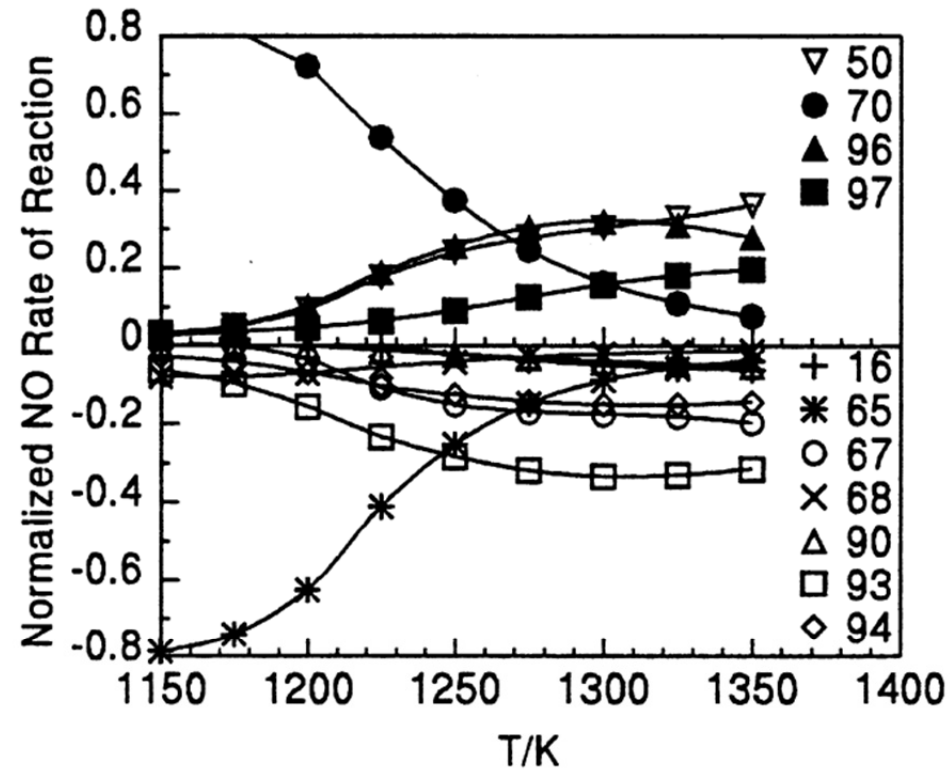
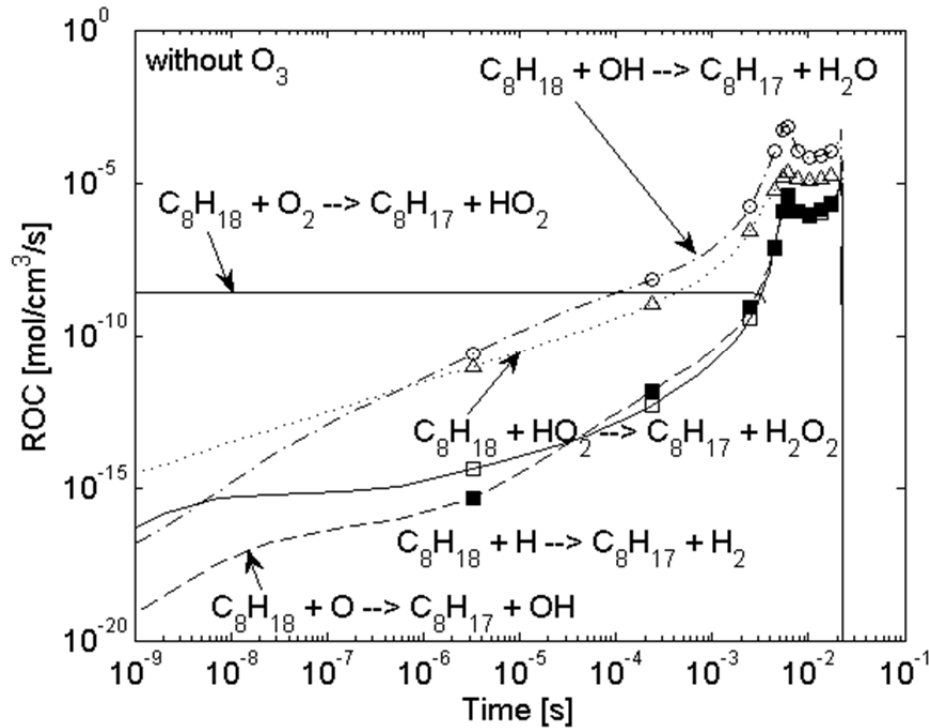


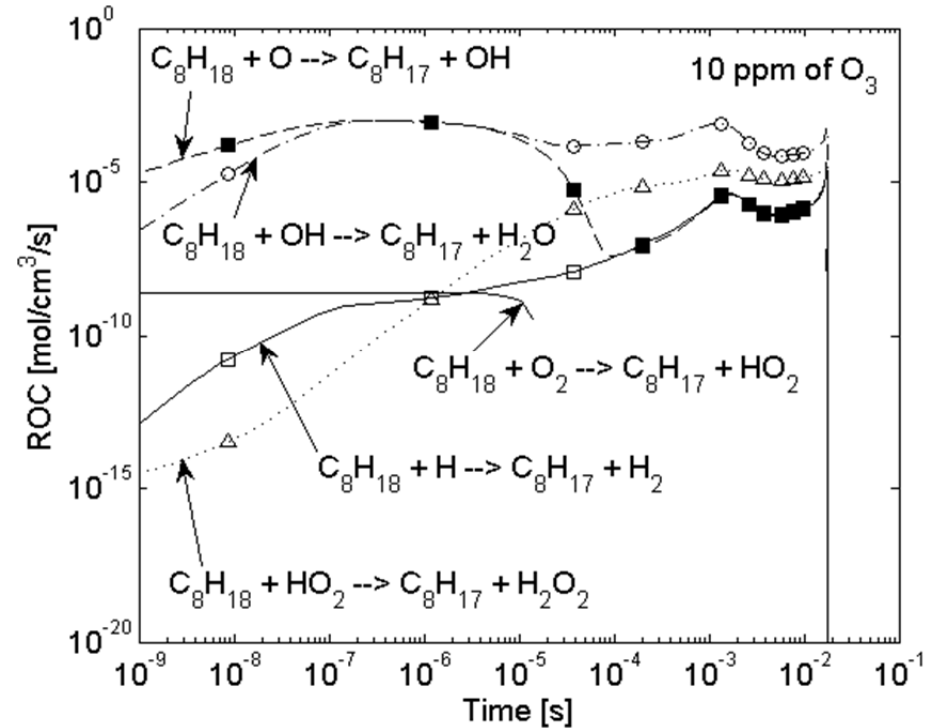
Fig. 3. The influence of temperature on the main reaction paths involved in the reduction of NO by propane at 1 atm ($\varphi = 1.25$; $\tau = 0.12$ s; 1000 ppm of NO; 2930 ppm of propane). Reactions: $\text{NH} + \text{NO} \rightleftharpoons \text{N}_2\text{O} + \text{H}$ (16); $\text{HNO} + \text{H} \rightleftharpoons \text{NO} + \text{H}_2$ (50); $\text{NO} + \text{HO}_2 \rightleftharpoons \text{NO}_2 + \text{OH}$ (65); $\text{NO} + \text{H} + \text{M} \rightleftharpoons \text{HNO} + \text{M}$ (67); $\text{NO} + \text{HCO} \rightleftharpoons \text{HNO} + \text{CO}$ (68); $\text{NO}_2 + \text{H} \rightleftharpoons \text{NO} + \text{OH}$ (70); $\text{CH}_2 + \text{NO} \rightleftharpoons \text{HCN} + \text{OH}$ (90); $\text{HCCO} + \text{NO} \rightleftharpoons \text{HCNO} + \text{CO}$ (93); $\text{HCCO} + \text{NO} \rightleftharpoons \text{HCN} + \text{CO}_2$ (94); $\text{HCNO} + \text{O} \rightleftharpoons \text{NO} + \text{HCO}$ (96); $\text{HCNO} + \text{OH} \rightleftharpoons \text{NO} + \text{CH}_2\text{O}$ (97).

How PRF100 reactions pathways are modified by ozone injection?

[O₃]=0

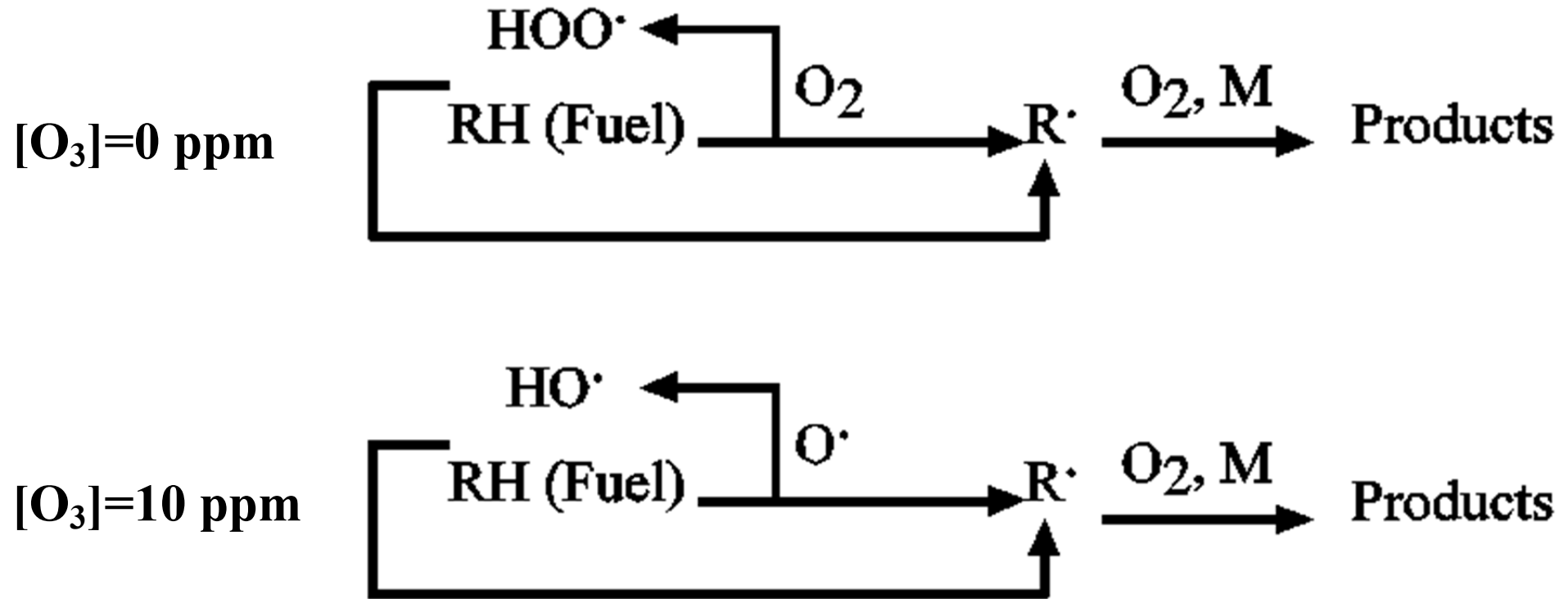


[O₃]=10 ppm



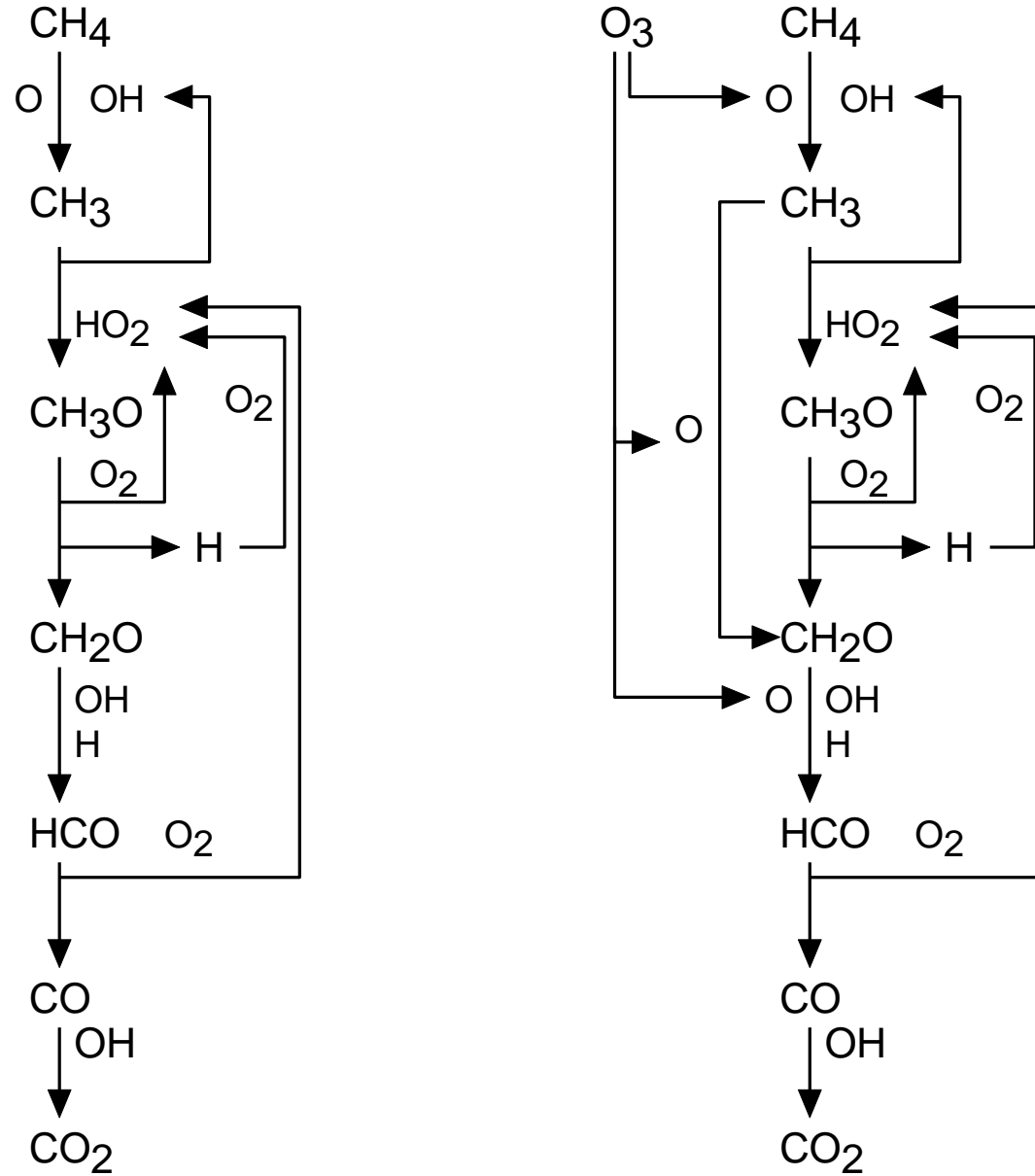
Reaction pathway analysis from rates of consumption (at the bottom) for iso-octane (PRF100) at initial temperature of 800 K, initial pressure of 50 bar and equivalence ratio of 0.3. From Masurier et al. *Energy Fuels* 2013, 27, 5495–5505.

How reactions pathways are modified by ozone injection?



Early reaction paths involved in neat and ozone seeded fuel oxidation. From Masurier et al. Energy Fuels 2013, 27, 5495–5505.

How reactions pathways are modified by ozone injection?



2-Brute force method and 1st order sensitivity analyses

What is the impact of a variation of a given parameter (e.g., A-factor, ΔH_f) on the model predictions?

What reactions influence the prediction of the formation/consumption of the product 1?

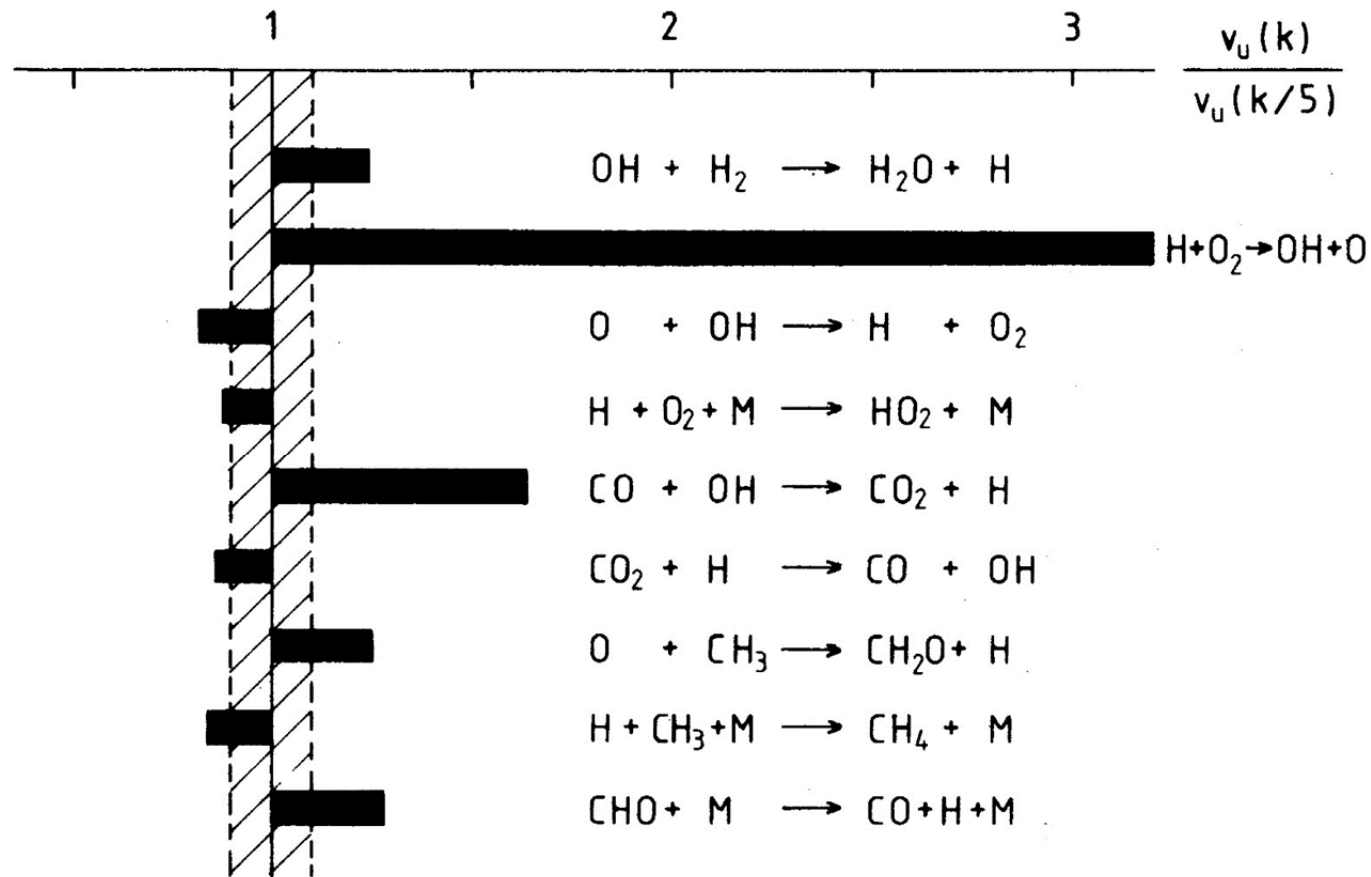
Initial $k \Rightarrow [\text{product1}]_0$

$k \cdot \varepsilon \Rightarrow [\text{product1}]_+$

$k/\varepsilon \Rightarrow [\text{product1}]_-$

$S = [\text{product1}]_{\text{ini}} / [\text{product1}]_{\text{mod}}$; e.g., $[\text{product1}]_{\text{mod}} = \text{conc. after } k_j / 5$:

Brute force method sensitivity analysis (k/5)



Sensitivity of computed laminar burning velocity of a methane-air flame at 1 bar and $T_u = 298$ K to reaction kinetics. From Warnatz, J., The structure of laminar alkane-, alkene-, and acetylene flames. Symposium (International) on Combustion, 18(1), p. 380, 1981.

2-Brute force method and 1st order sensitivity analyses

What is the impact of a variation of a given parameter (e.g., A-factor, ΔH_f) on the model predictions?

What reactions influence the prediction of the formation/consumption of the product 1?

Initial $k \Rightarrow [\text{product1}]_0$

$k \cdot \varepsilon \Rightarrow [\text{product1}]_+$

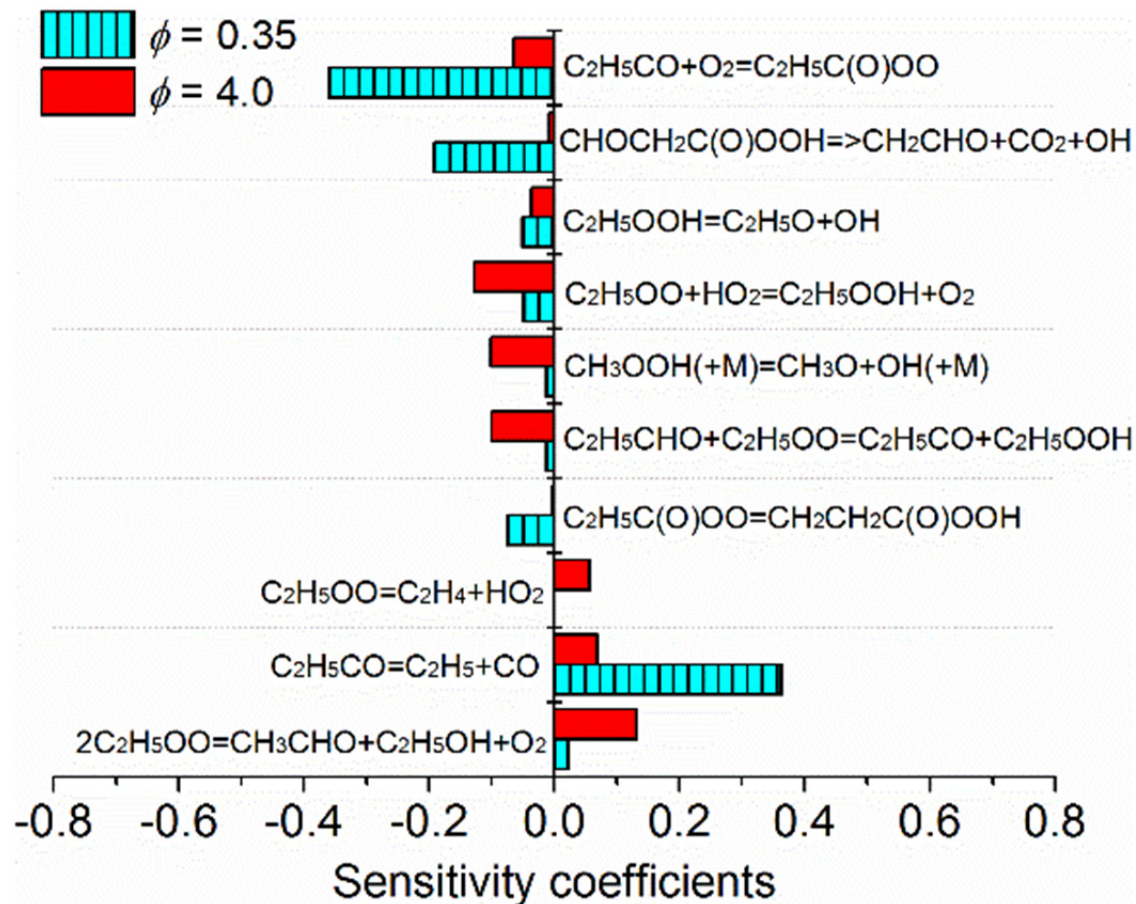
$k/\varepsilon \Rightarrow [\text{product1}]_-$

$S = [\text{product1}]_{\text{ini}} / [\text{product1}]_{\text{mod}}$; e.g., $[\text{product1}]_{\text{mod}} = \text{conc. after } k_j / 5$

$\mathbf{s} = \partial n_i / \partial \pi_i$

$\mathbf{s}' = (\partial n_i / n_i) / (\partial \pi_i / \pi_i)$ where n_i is the response of the model and π_i is a model parameter (A-factor, ΔH_f); e.g., $\mathbf{s}_{i,j} = (\partial c_i / c_i) / (\partial A_j / A_j)$ for conc. of species in reaction j:

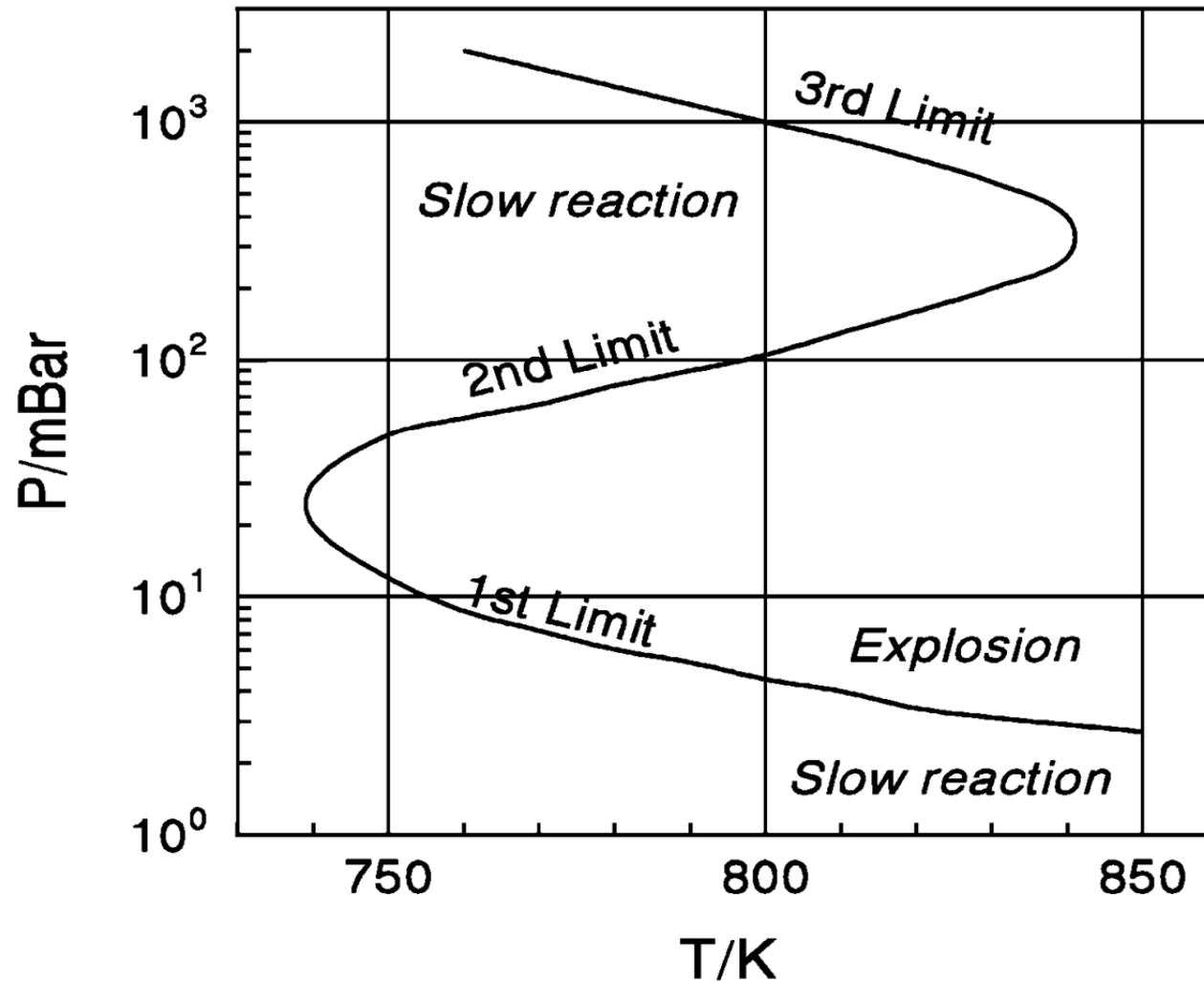
1st order sensitivity analysis



Sensitivity analysis of the present model at $\phi = 0.35$ (575 K, 1 atm) and $\phi = 4.0$ (625 K, 1 atm) in JSR oxidation of propanal. From New insights into propanal oxidation at low temperatures: Experimental and kinetic modeling study. X. Zhang et al., Proc. Combust. Inst (2019)

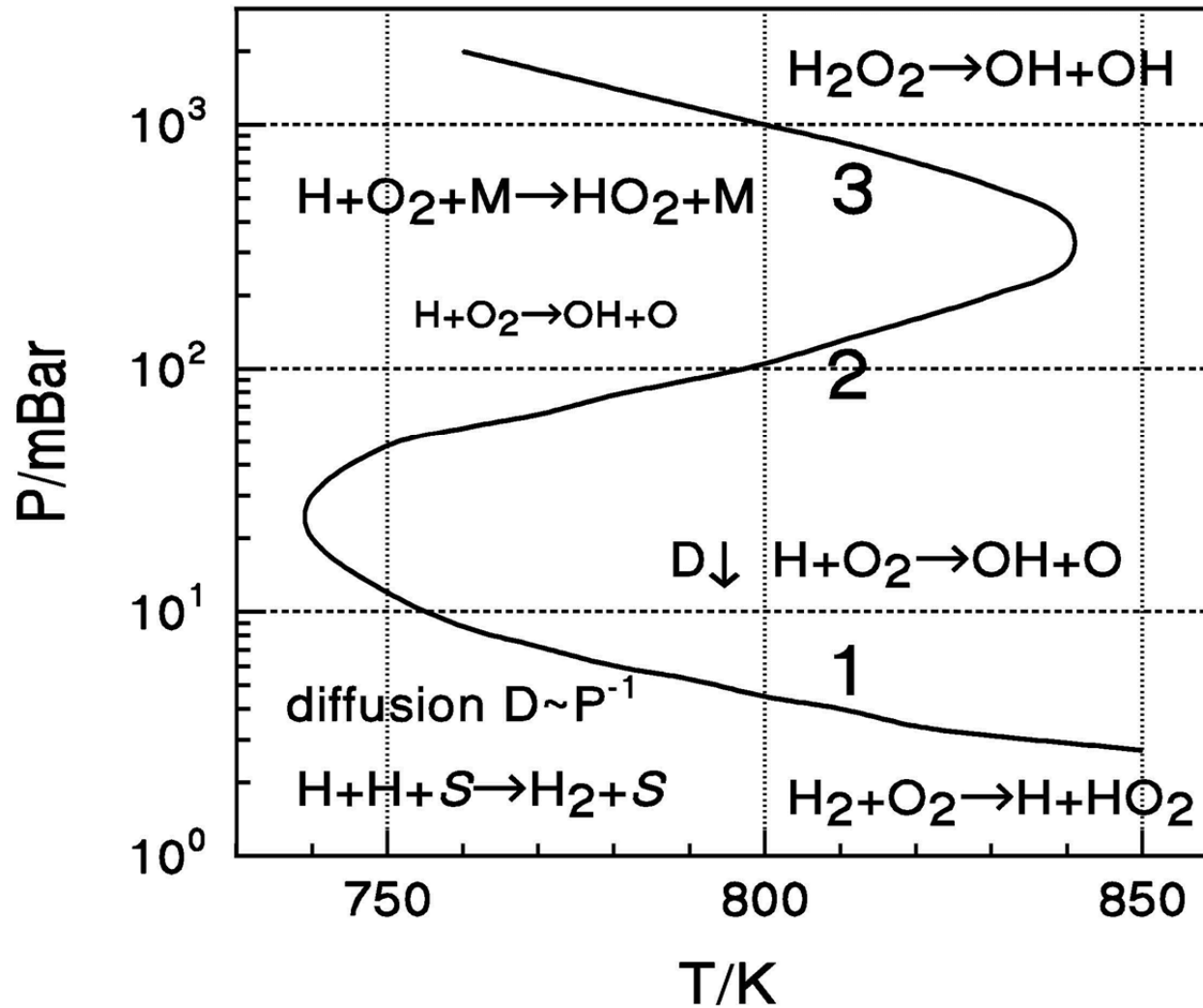
Modeling: Pressure/Temperature dependencies and reaction pathways

Explosion Limits of a $\Phi=1$ H₂-O₂ Mixture



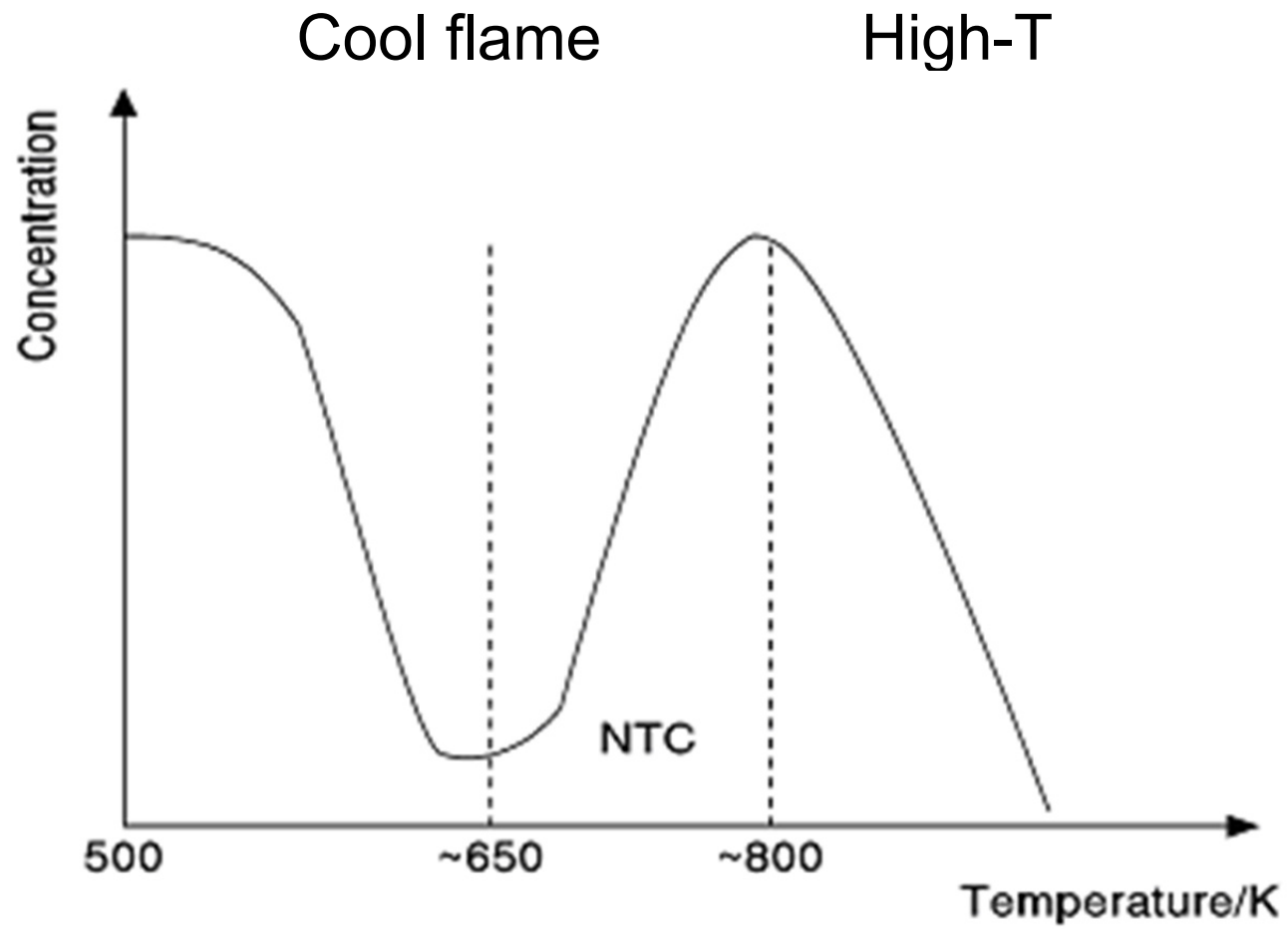
Modeling: Pressure dependencies

Explosion Limits of a $\Phi=1$ H₂-O₂ Mixture



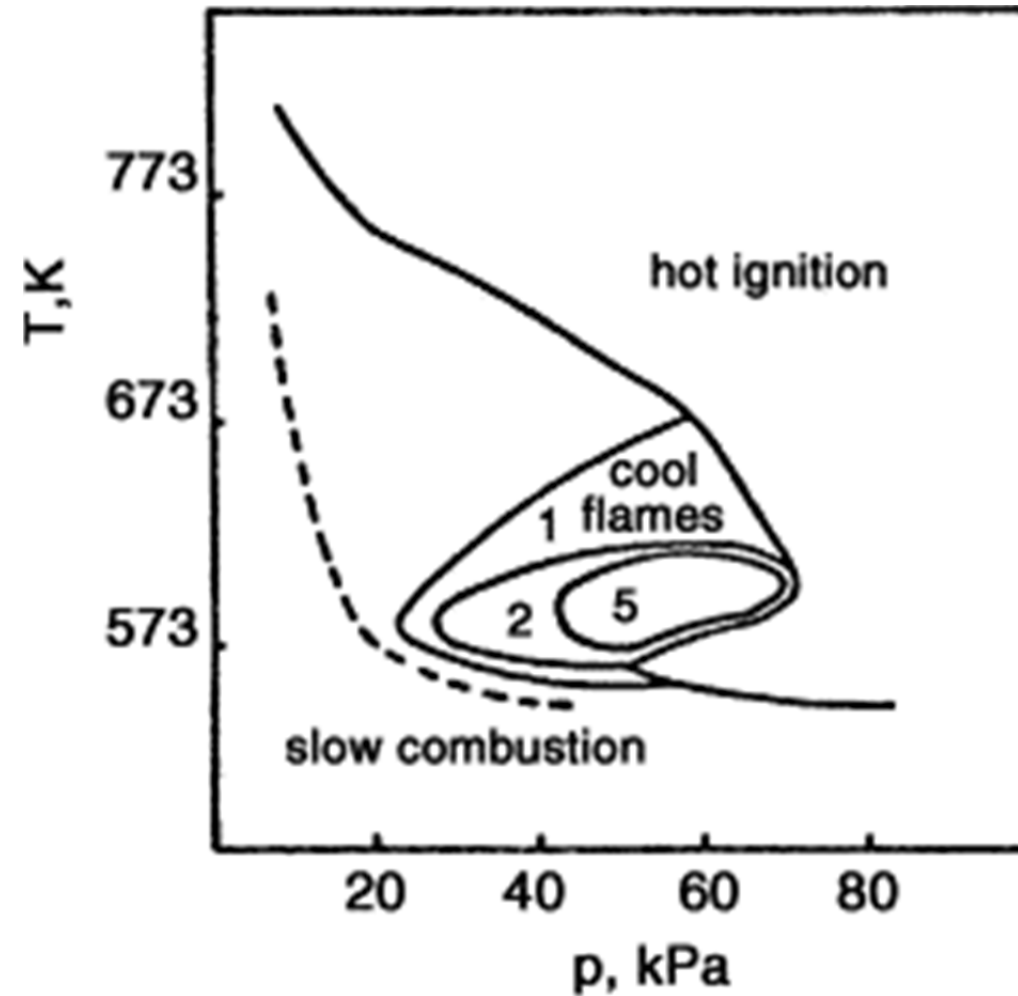
REACTIONS	$k=A*T**n*\exp(-E/RT)$	A/cc,mole,s	n	E/cal/mol	Ref
H+ + H+ = H2+	M	7.310E+17	-1.0	0.0	! (BAULCH 76)
O+ + O+ = O2+	M	1.140E+17	-1.0	0.0	! (BAULCH 76)
O+ + H+ = OH+	M	6.200E+16	-0.6	0.0	! (DIXON-LEWIS 81)
H2+ + O2 = OH+	OH	1.700E+13	0.0	47780.0	! (MILLER 77)
O+ + H2 = OH+	H	3.870E+04	2.7	6260.0	!GRI
H+ + O2 = OH+	O	4.400E+14	-0.12	16812.0	!Nicolle 2004
H+ + O2+ = HO2+	M	8.000E+17	-0.8	0.0	! (WARNATZ 84)
H+ + OH+ = H2O+	M	8.615E+21	-2.0	0.0	! (BAULCH 76)
H2+ + OH = H2O+	H	2.161E+08	1.51	3430.0	! (MICHAEL 88)
H2O+ + O = OH+	OH	1.500E+10	1.14	17260.0	! (WARNATZ 84)
HO2+ + OH = H2O+	O2	2.890E+13	0.0	-497.0	! (KEYSER 88)
HO2+ + O = OH+	O2	1.810E+13	0.0	-400.0	! (JPL 87-41)
H+ + HO2 = H2+	O2	4.280E+13	0.0	1411.0	! (94BAU/COB)
H+ + HO2 = OH+	OH	1.690E+14	0.0	874.0	! (94BAU/COB)
H+ + HO2 = H2O+	O	3.010E+13	0.0	1721.0	! (BAULCH 92)
HO2+ + HO2 = H2O2+	O2	4.075E+02	3.321	1979.0	! (HIPPLER 90)
OH + OH (+M) = H2O2 (+M)		7.224E+13	-0.37	0.0	! (94BAU/COB)
H2O2+ + OH = HO2+	H2O	5.800E+14	0.0	9557.0	! (92HIP/TRO)
H2O2+ + H = HO2+	H2	1.700E+12	0.0	3750.0	! (BAULCH 72)
H2O2+ + H = H2O+	OH	1.000E+13	0.0	3590.0	! (WARNATZ 84)
H2O2+ + O = HO2+	OH	2.800E+13	0.0	6400.0	! (ALBERS 71)

Modeling: Hydrocarbons oxidation



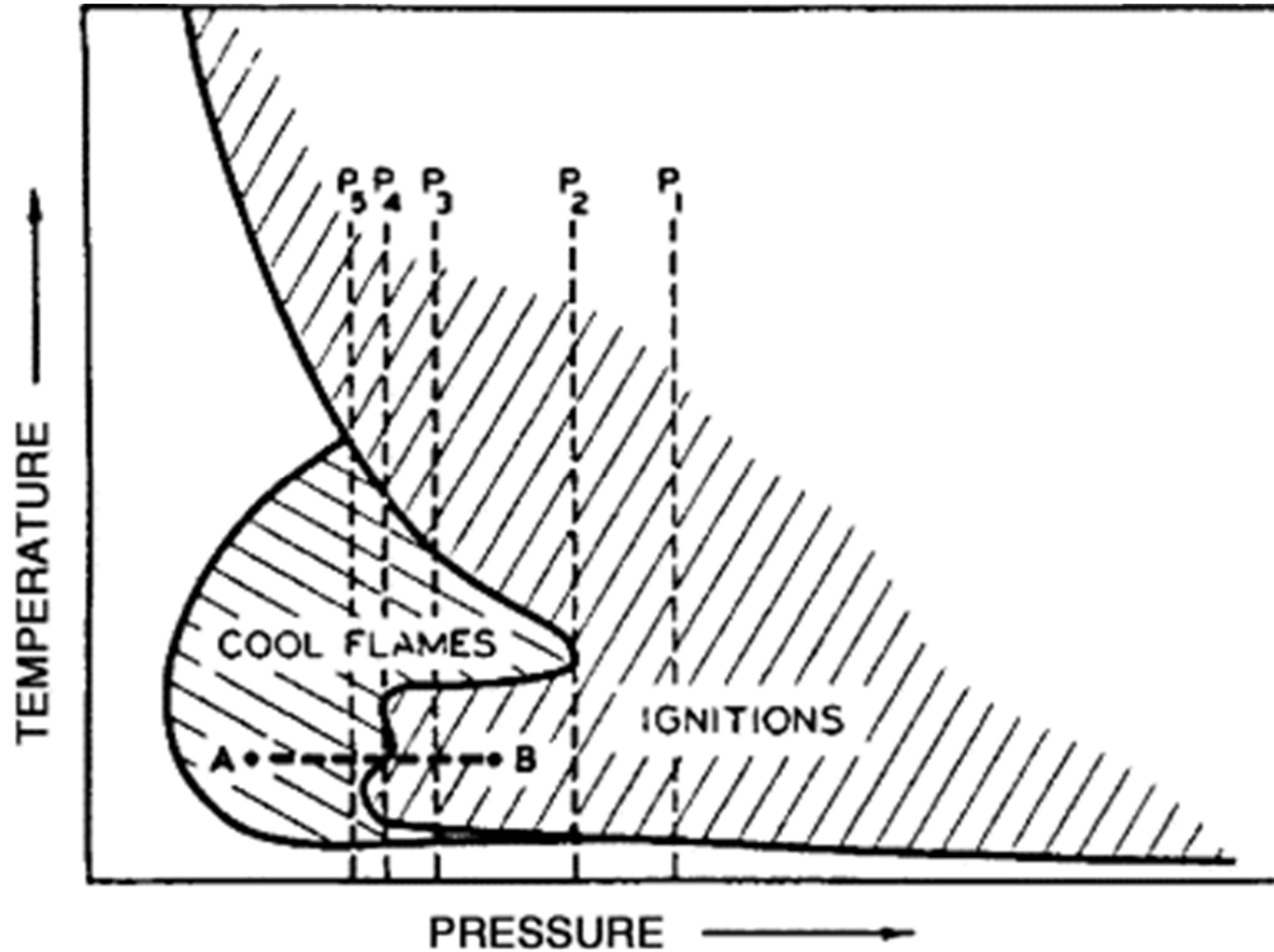
Fuel concentration vs. temperature

Modeling: Multiple cool flames



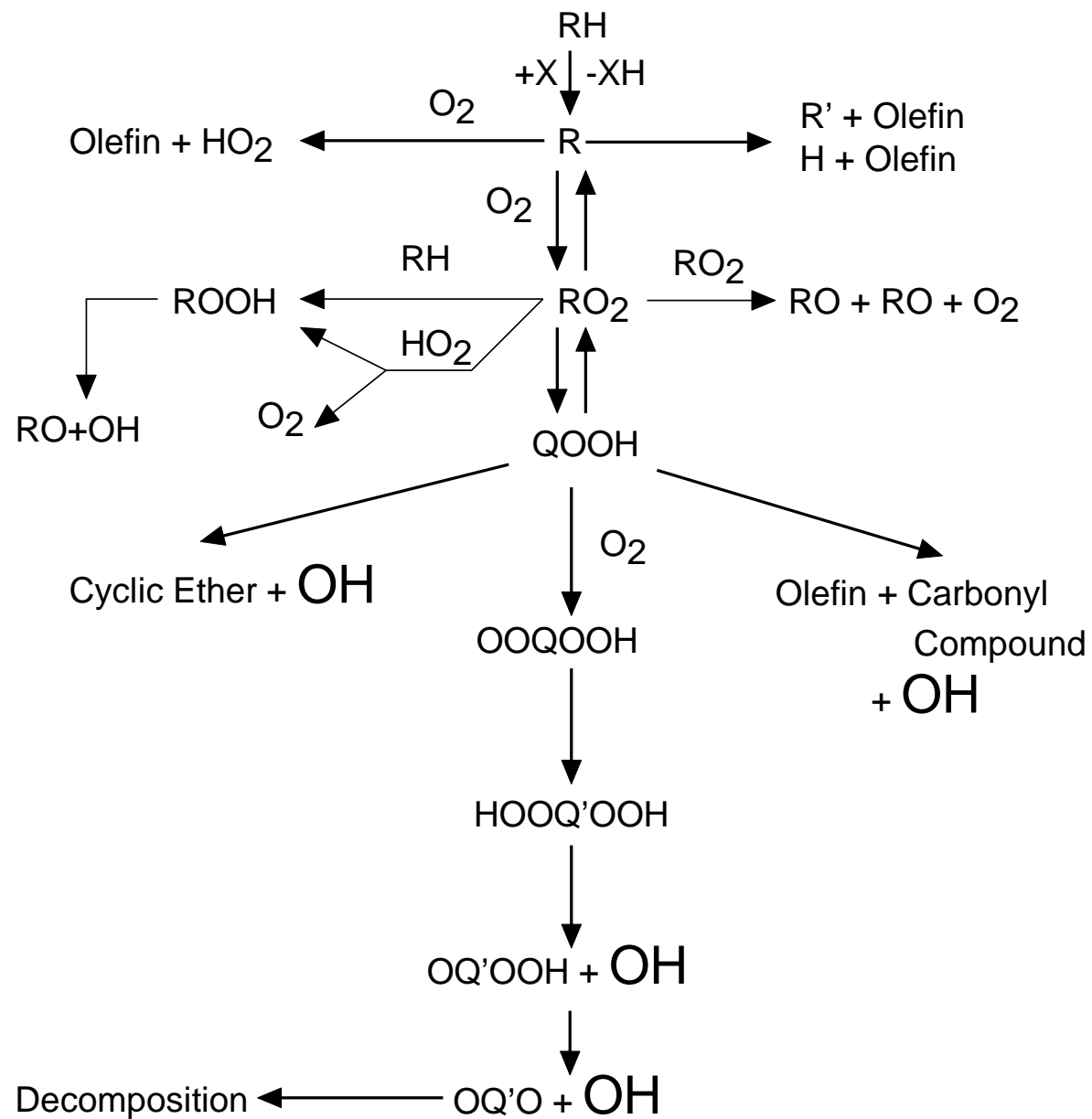
Ignition diagram of a propane/oxygen (1:1) mixture. The numbers refer, to the number of cool flames occurring in the respective region. From P.G. Lignola, E. Reverchon, Prog. Energy Combust. Sci., 13 (1987), p. 75

Modeling

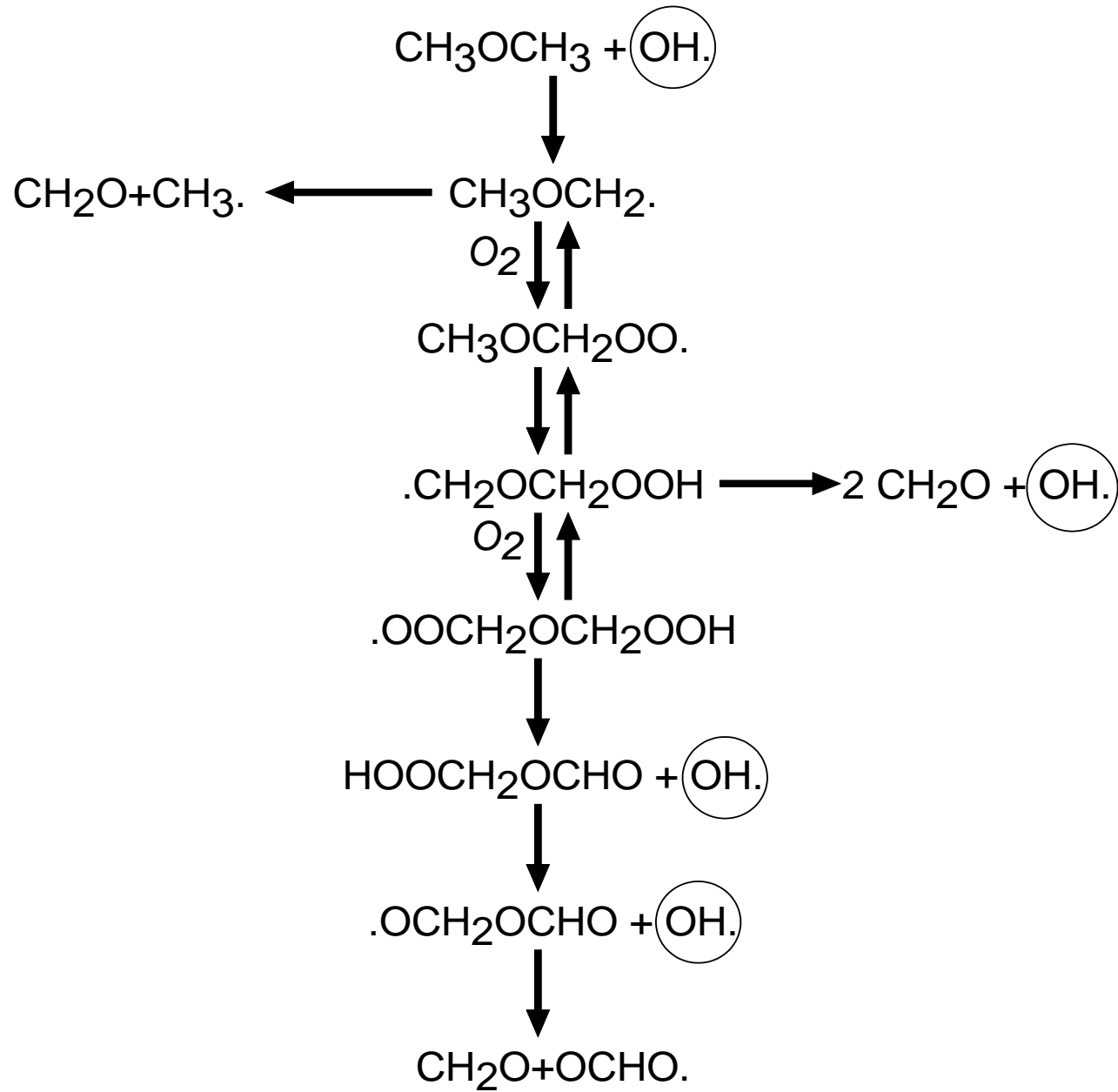


Ignition diagram for fuel concentration within the flammable range. Moving from A to B can yield to strong ignition

Modeling



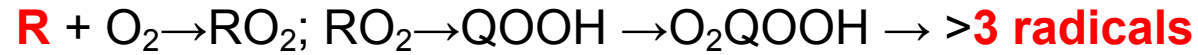
Modeling



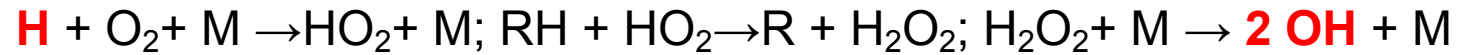
Modeling

Branching reactions: multiplication of the number of active species

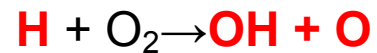
Low-T



Medium-T

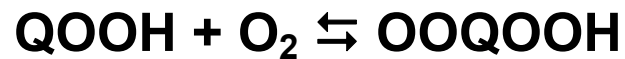


High-T

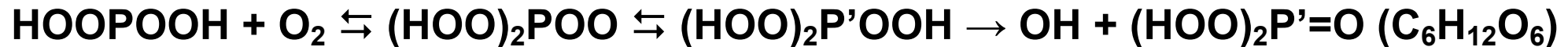


More reaction pathways at low-T

Example: di-n-propyl ether oxidation



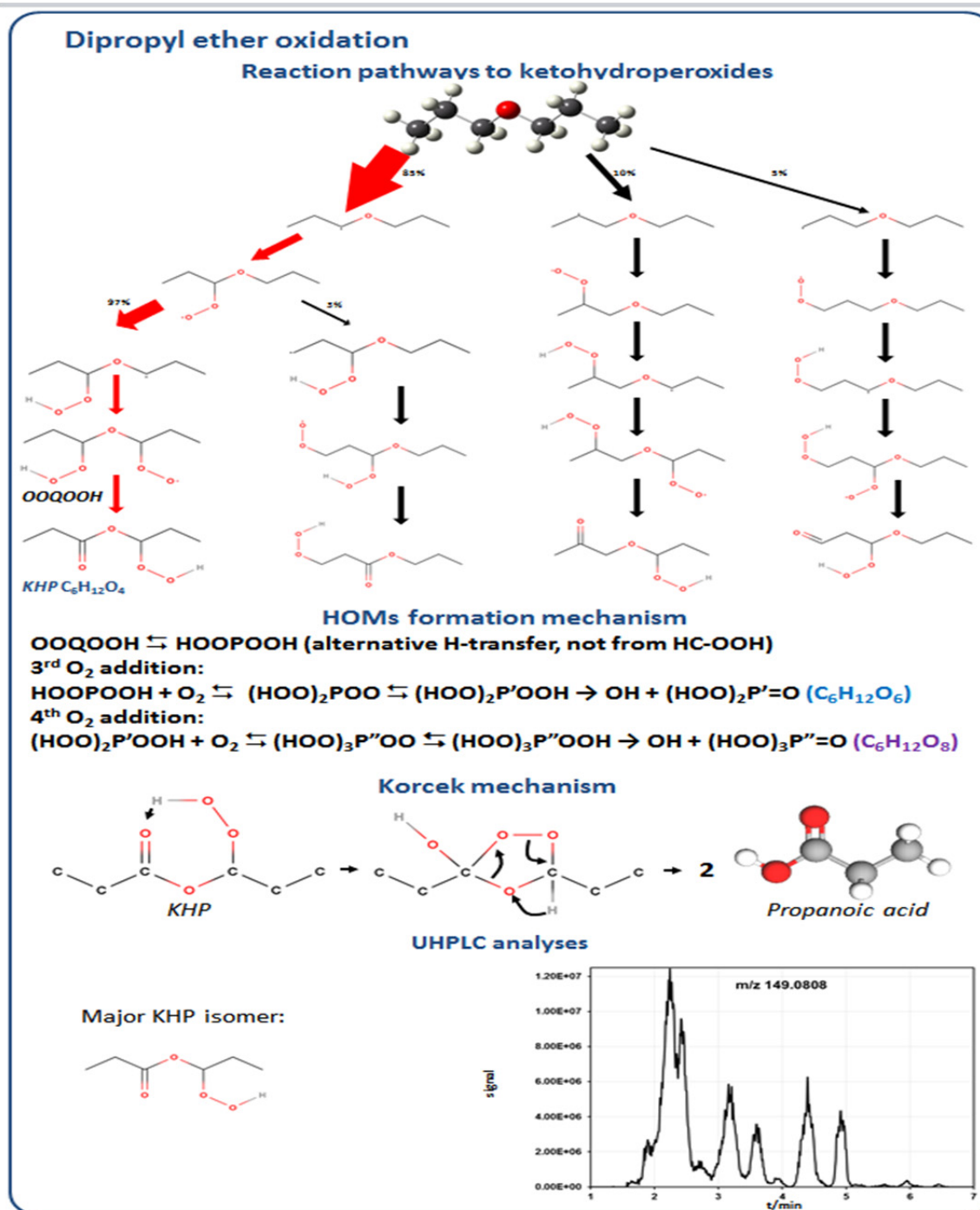
3rd O₂ addition:



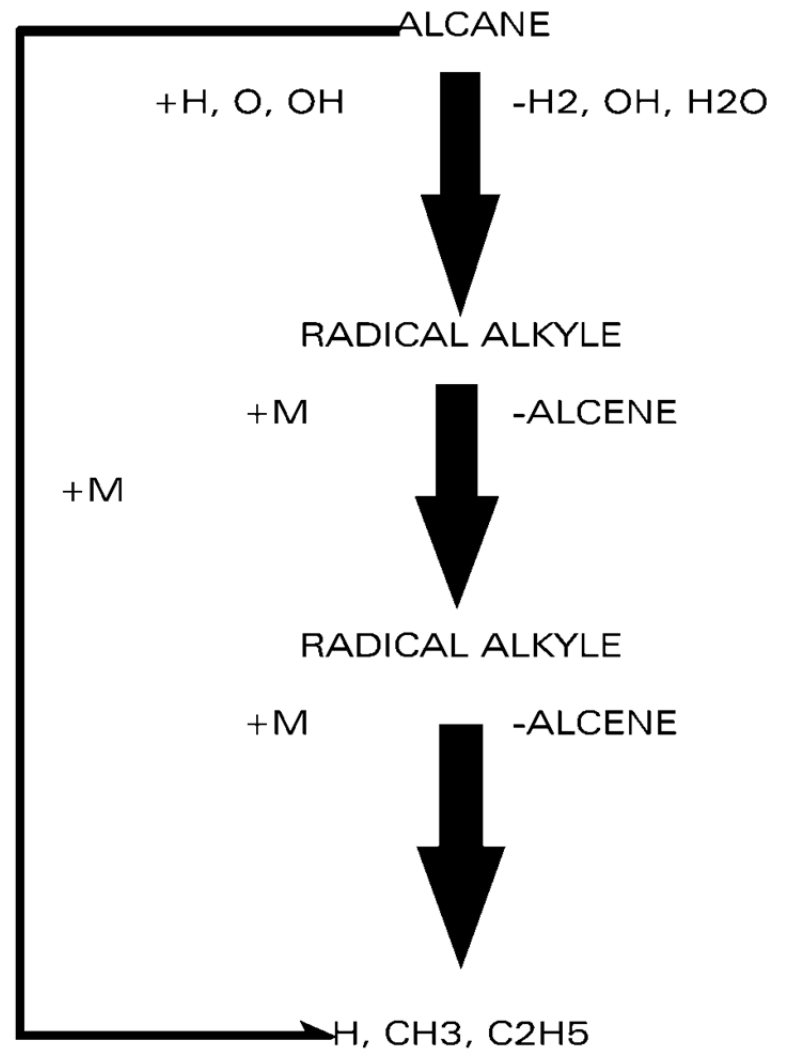
4th O₂ addition:



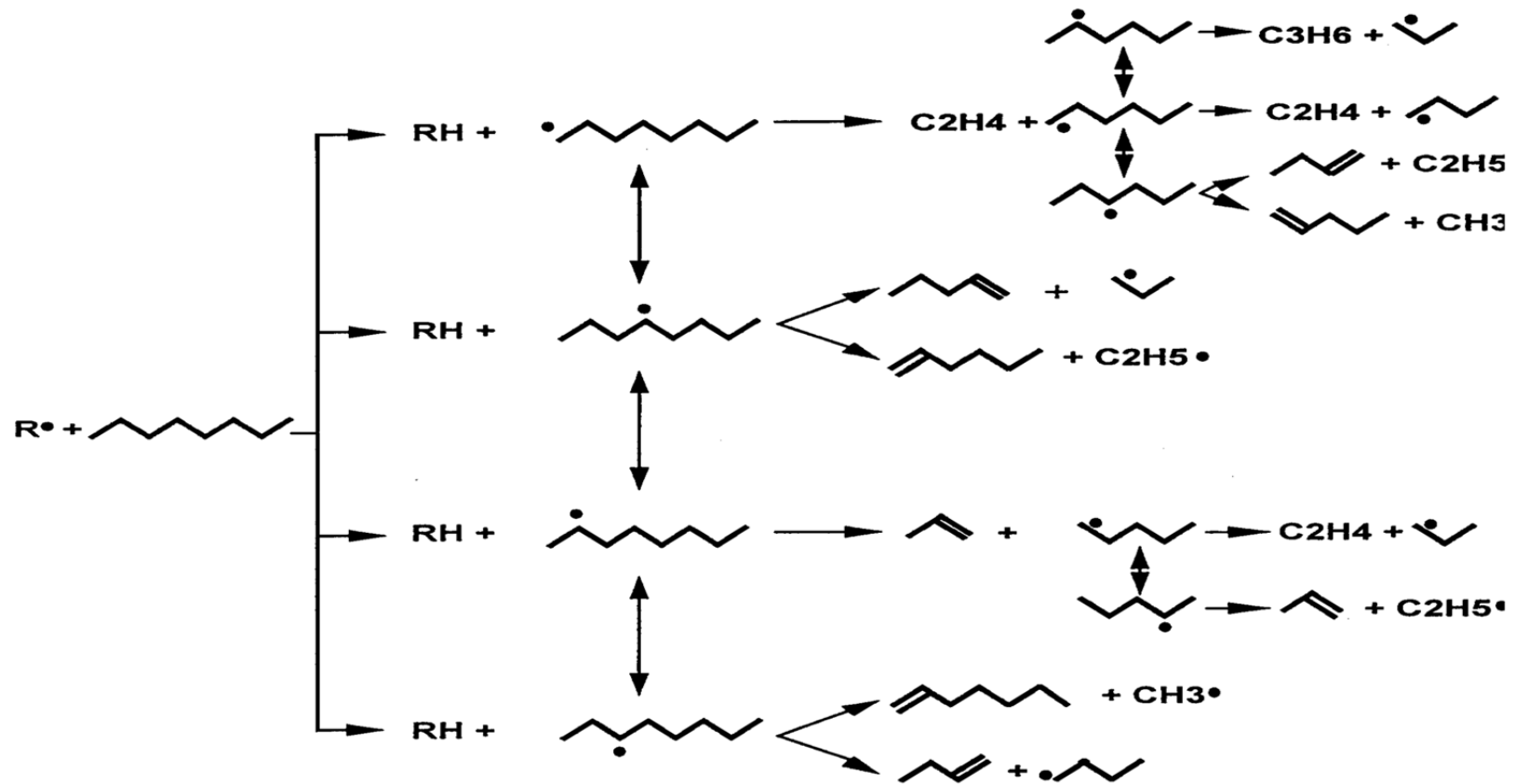
5th addition ...



Pyrolysis and high-T oxidation



n-OCTANE



Bonds dissociation energies

Bond ⇄	Bond ⇄	Bond-dissociation energy at 298 K		
		(kcal/mol) ⇄	(kJ/mol) ⇄	(eV/Bond) ⇄
I-I	Iodine	36	151	1.57
Br-Br	Bromine	46	192	1.99
Cl-Cl	Chlorine	58	242	2.51
O=CH ₂	Formaldehyde	179	748	7.75
N≡N	Nitrogen	226	945	9.79
O-H	in α-tocopherol (an antioxidant)	77	323	3.35
O-H	in methanol	105	440	4.56
O=CO	Carbon dioxide	127	532	5.51
C-Cl	in CH ₃ Cl	83.7	350	3.63
C-C	in typical alkane	83-90	347-377	3.60-3.90
H-H	Hydrogen	104	436	4.52
O=O	Oxygen	119	498	5.15
C≡O	Carbon monoxide	257	1077	11.16
H-F	Hydrogen fluoride	136	569	5.90
O-H	in water	119	497	5.15

Bonds dissociation energies

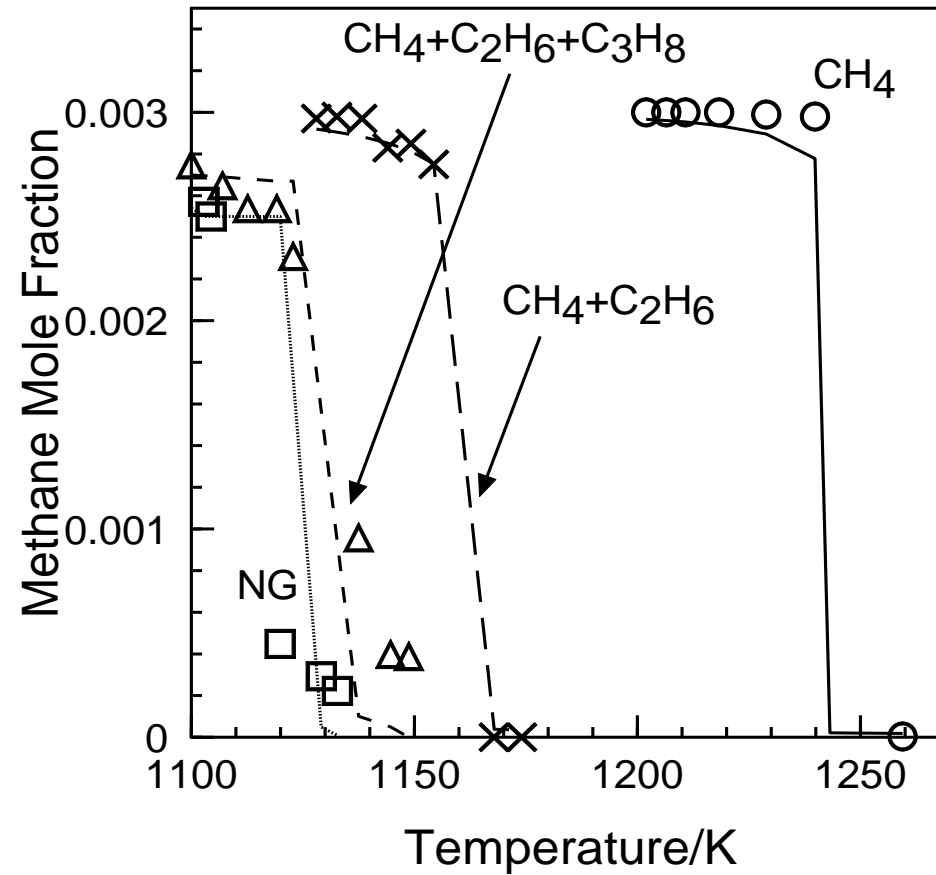
Bond ⇄	Bond ⇄	Bond-dissociation energy at 298 K		
		(kcal/mol) ⇄	(kJ/mol) ⇄	(eV/Bond) ⇄
H ₃ C–H	Methyl C–H bond	105	439	4.550
C ₂ H ₅ –H	Ethyl C–H bond	101	423	4.384
(CH ₃) ₂ CH–H	Isopropyl C–H bond	99	414	4.293
(CH ₃) ₃ C–H	<i>t</i> -Butyl C–H bond	96.5	404	4.187
(CH ₃) ₂ NCH ₂ –H	C–H bond α to amine	91	381	3.949
(CH ₂) ₃ OCH–H	C–H bond α to ether	92	385	3.990
CH ₃ C(=O)CH ₂ –H	C–H bond α to ketone	96	402	4.163
CH ₂ CH–H	Vinyl C–H bond	111	464	4.809
HCC–H	Acetylenic C–H bond	133	556	5.763
C ₆ H ₅ –H	Phenyl C–H bond	113	473	4.902
CH ₂ CHCH ₂ –H	Allylic C–H bond	89	372	3.856
C ₆ H ₅ CH ₂ –H	Benzylic C–H bond	90	377	3.907
H ₃ C–CH ₃	Alkane C–C bond	83–90	347–377	3.60–3.90
H ₂ C=CH ₂	Alkene C=C bond	~170	~710	~7.4
HC≡CH	Alkyne C≡C triple bond	~230	~960	~10.0

Bonds dissociation energies vs. kinetic parameters

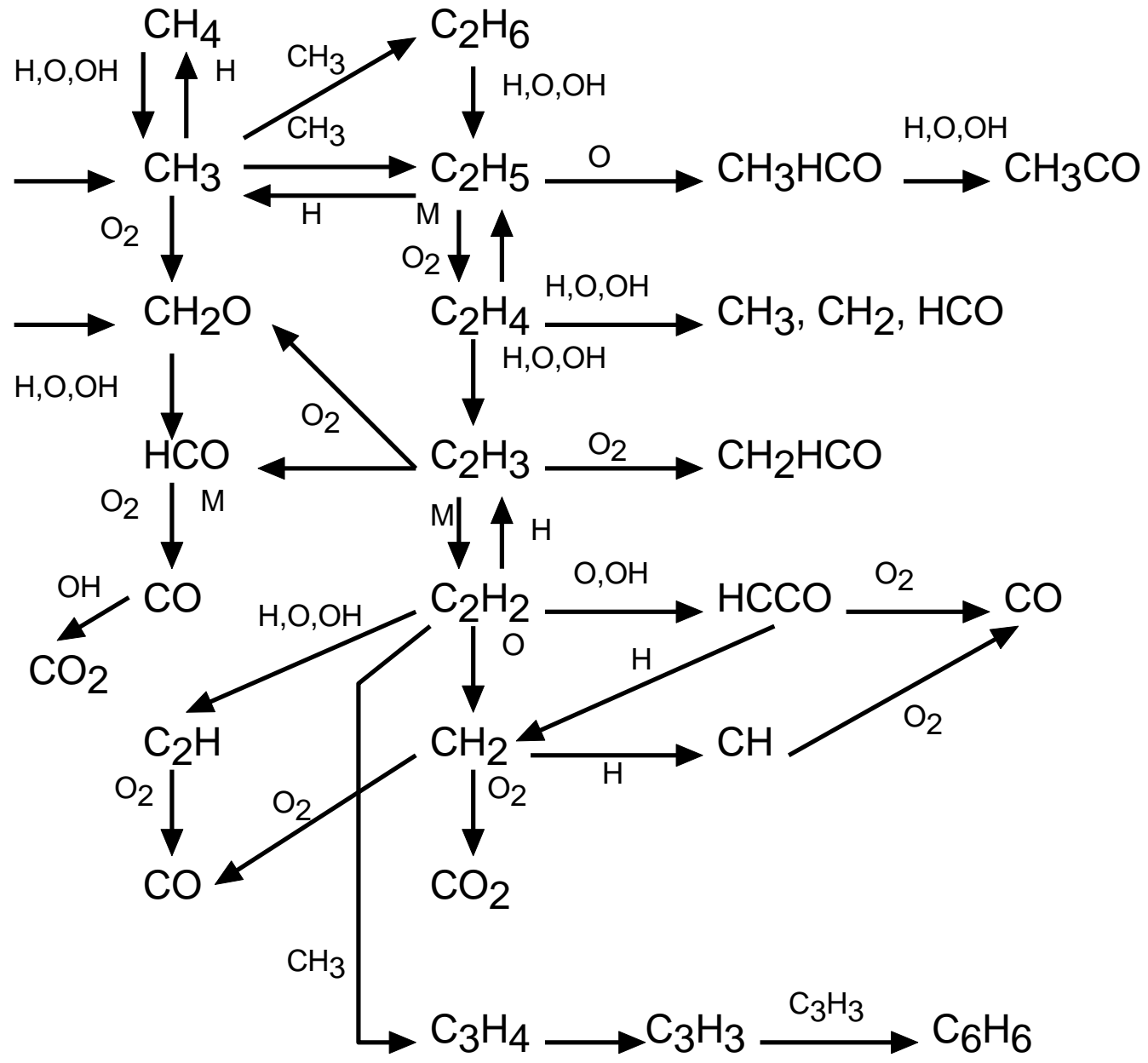
Reaction	A	n	E/cal/mol	bond
$\text{CH}_4 = \text{CH}_3 + \text{H}$	1.168E+33	-5.43	108732.0	C-H
$\text{C}_2\text{H}_6 = \text{C}_2\text{H}_5 + \text{H}$	6.684E+33	-5.48	105330.0	C-H
$\text{C}_3\text{H}_8 = \text{C}_2\text{H}_5 + \text{CH}_3$	1.698E+44	-1.77	103004.0	C-C

Single-fuel vs. multi-fuel components





Oxidation of methane and NG-mixtures in a JSR at 1 atm and 140ms.

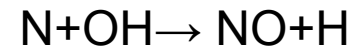
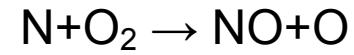
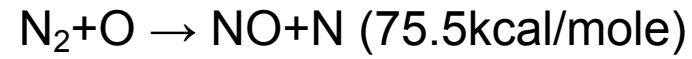


POLLUTANTS



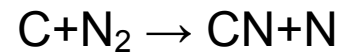
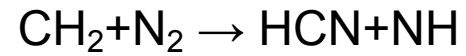
1-NOx formation

1-1-Thermal-NO (Zel'dovich, 1946)

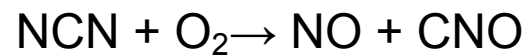
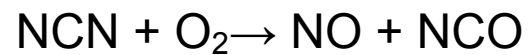
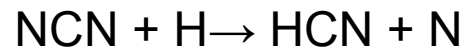
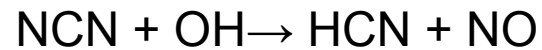
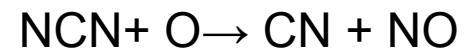
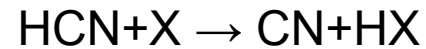


Global rate (NO formation) = $[\text{N}_2][\text{O}_2] \exp(-133000/RT)$

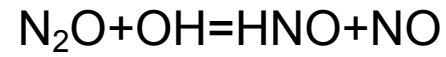
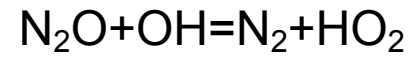
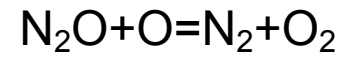
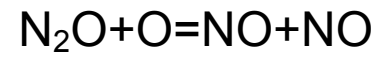
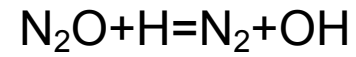
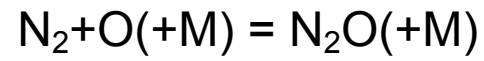
1-2-Prompt-NO (Fenimore, 1979)



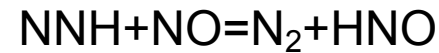
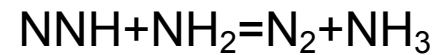
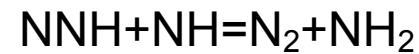
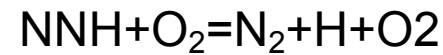
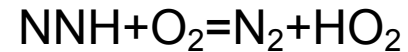
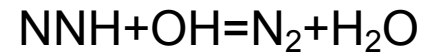
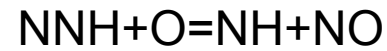
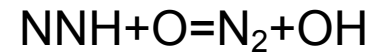
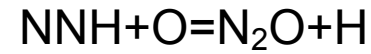
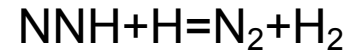
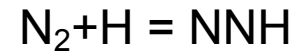
Followed by:



1-3-N₂O (Malte and Pratt, 1974)

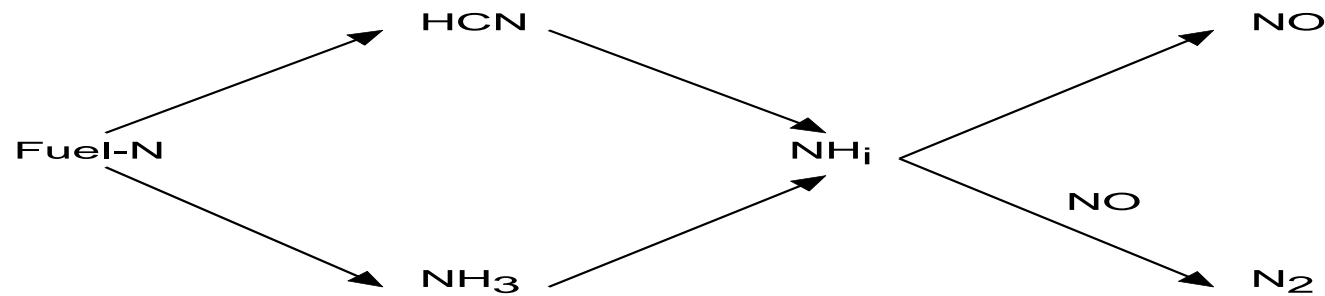


1-4-NNH (Bozzelli, Dean, IJCK 1995)



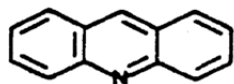
1-5-Fuel-NO

Formation of HCN and NH_3 by pyrolysis of amines, pyridinic compounds or pyrroles followed by oxidation of HCN or NH_3 to NO and N_2O

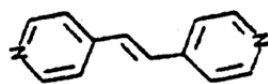


($i=1, 2$)

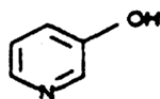
Pyridinic-type



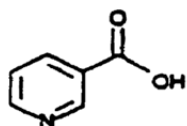
acridine or
2,3,5,6-dibenzo-
pyridine



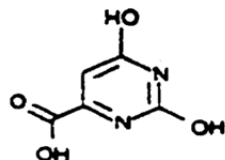
1,2-bis (4-pyridyl)-
ethane



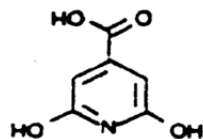
3-pyridol or
3-hydroxypyridine



nicotinic acid or
3-pyridinecarboxylic
acid

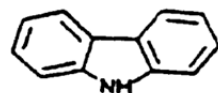


orotic acid or
6-uracilcarboxylic
acid

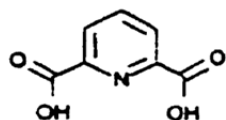


citrazinic acid or
2,6-dihydroxy-4-pyridine-
carboxylic acid

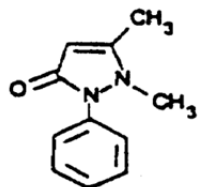
Pyrrole-type



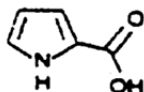
carbazole or
dibenzopyrrole



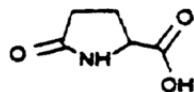
dipicolinic acid or 2,6-
pyridinedicarboxylic acid



antipyrine or 2,3-
dimethyl-1-phenyl-
5-pyrazolone

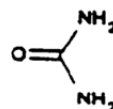


2-pyrrolecarboxylic
acid

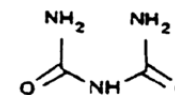


DL-pyrroglutamic
acid or DL-5-pyrrolidone-
2-carboxylic acid

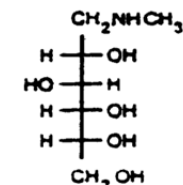
Amino-type



urea

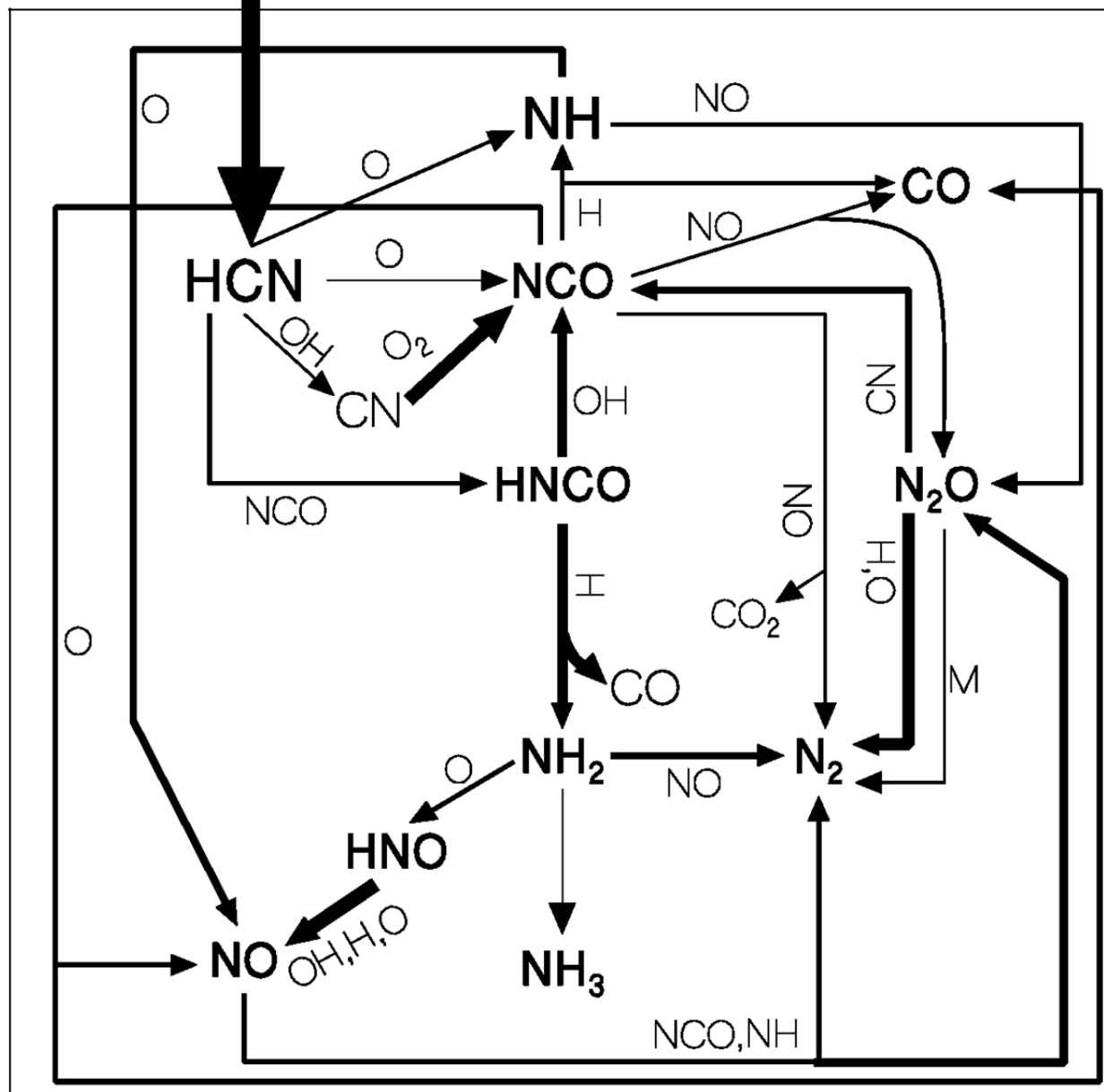


biuret or
N-carbamoyurea



meglumine or
N-methyl-D-glucamine

Coal-N → Tar-N



2-NOx reduction

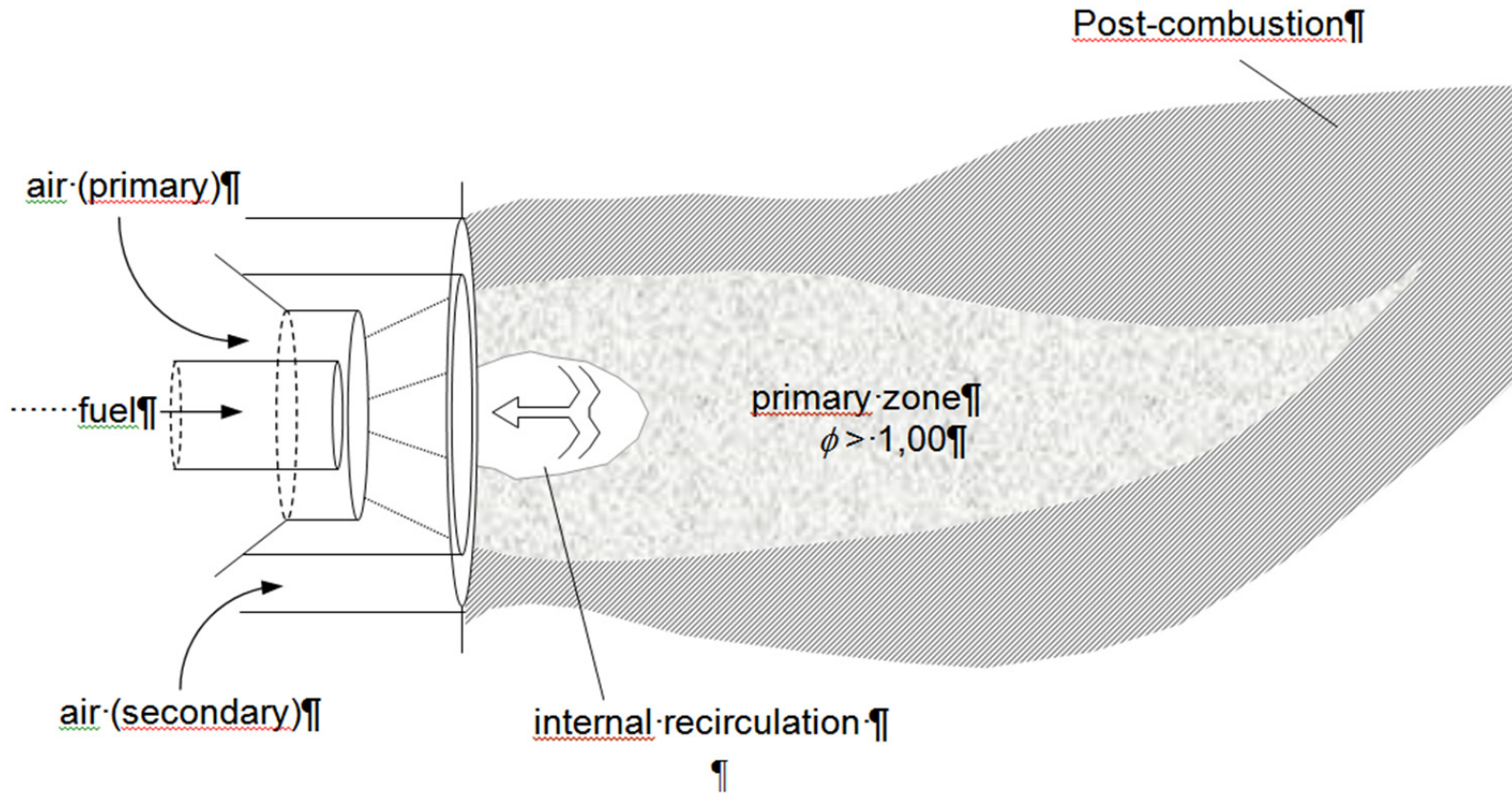
2-1-Reduction through combustion modifications

2-1-1-Optimization of burner parameters - BasNOx burners

Burner parameter optimization techniques and lowNOx burners are used to limit NO production during combustion. These burners are specially designed to control the mixing of air and fuel to create more or less turbulent flames stabilized by internal recirculation zones. The temperature of the flame is lowered, thus limiting the production of thermal-NO. This type of burner works as a dual internal staging of fuel and combustion air:

The fuel burns with primary air (70-90%) under fuel-rich conditions. Secondary air (10-30%) is injected over the main combustion zone and completes the oxidation of the fuel. This increases the volume of the flame which decreases the flame temperature and thus the production of thermal-NO.

Low-NOx burner



2-1-2-Flue gas recirculation (FGR, EGR)

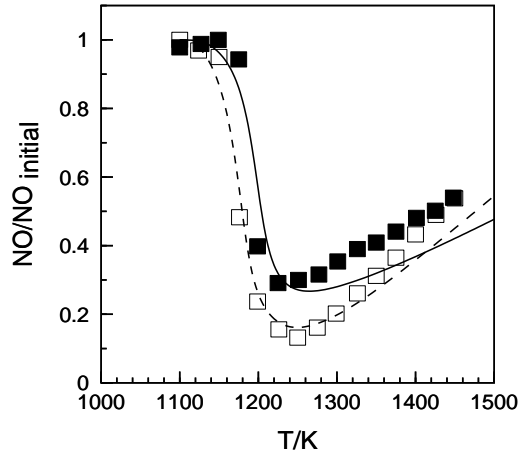
The recirculation of the fumes inside the oven or burner allows a dilution of the flame and therefore a sharp decrease in temperature. Generally, 20 to 30% of the flue gases recirculate and are mixed with the combustion air. The stoichiometry is not modified since the concentration of oxygen in the fumes is negligible. The efficiency is relatively low (<20%) because the contribution of thermal NO does not dominate in installations burning coal.

2-1-3-Fuel staging

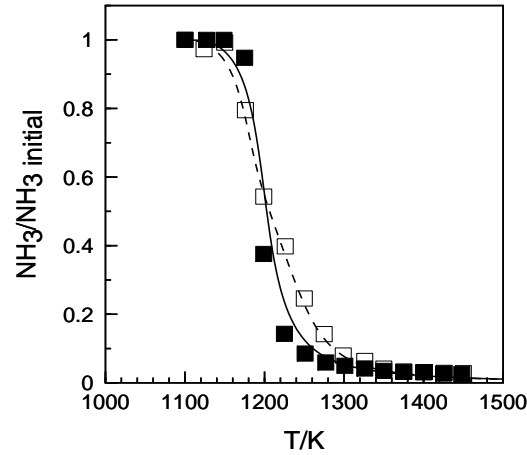
Staging of the fuel allows alternation between a fuel-rich zone and a fuel-lean zone which limits the temperature of the flame, improves the distribution of oxygen, and limits NO_x formation.

2-2-Chemical reduction of NOx

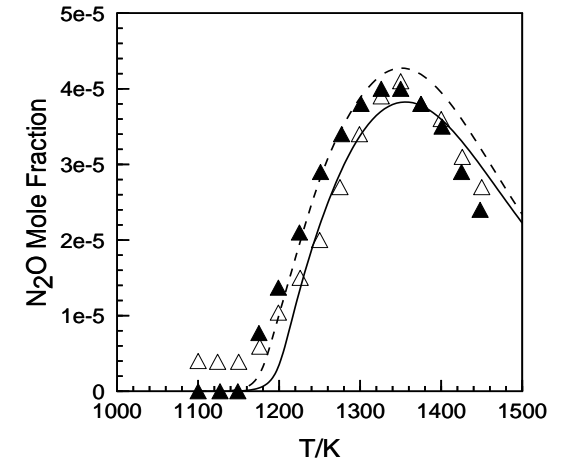
2-2-1-NOx reduction by SNCR (Lyon, 1974)



a

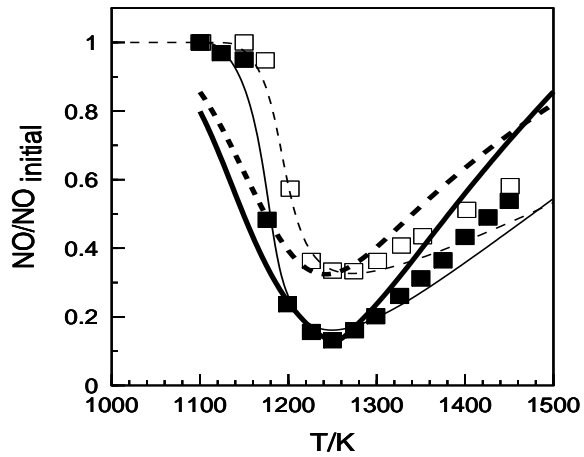


b

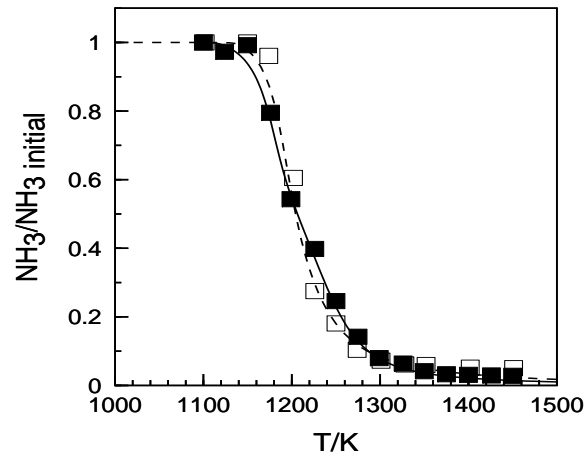


c

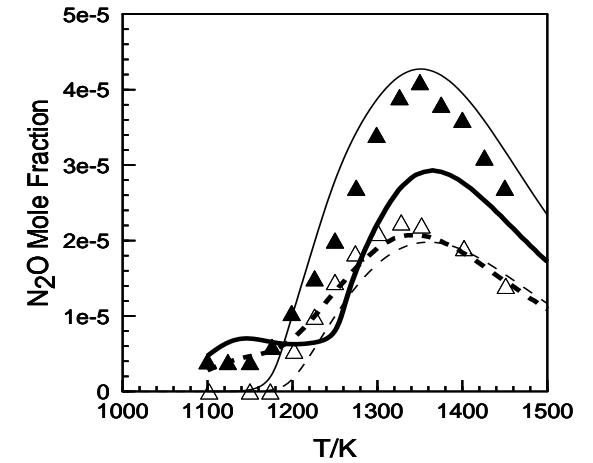
Effect of NO initial concentration on its removal by ammonia in lean conditions ($\Phi=0.1$). The initial conditions were: 1000 ppm of NH_3 , 12500 ppm of O_2 , residence time=100 ms, 500 ppm of NO (open symbols and dashed lines) or 1000 ppm of NO (closed symbols and solid line). The data (symbols) are compared to the modeling results (lines).



a

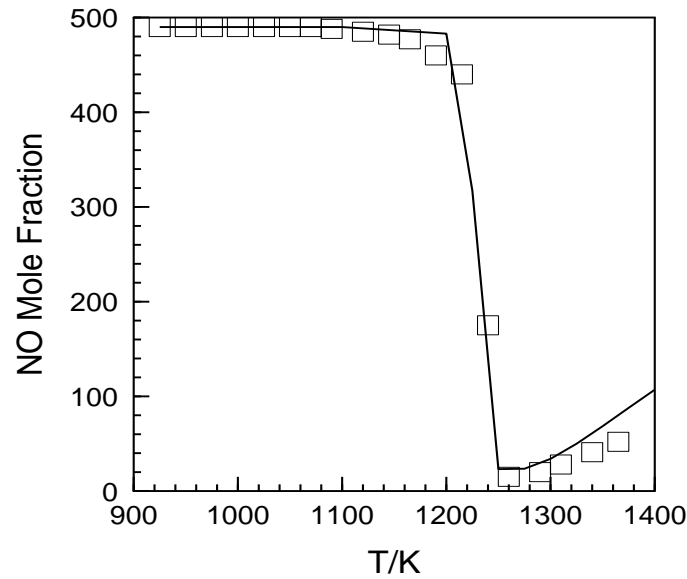


b



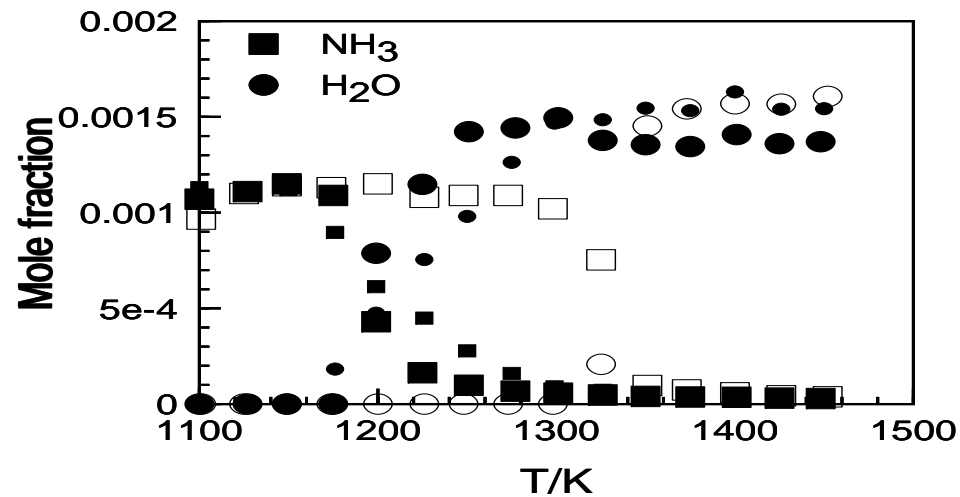
c

Effect of NH_3 initial concentration on NO reduction and N_2O formation in lean conditions ($\Phi=0.1$). The initial conditions were: residence time=100 ms, 500 ppm of NO, (i) 500 ppm of NH_3 and 6250 ppm of O_2 (open symbols and dashed lines), (ii) 1000 ppm of NH_3 and 12500ppm of O_2 (closed symbols and solid line). The data (symbols) are compared to the modeling results using the present kinetic reaction mechanism (thin lines) and that of ref. [14] (thick lines).

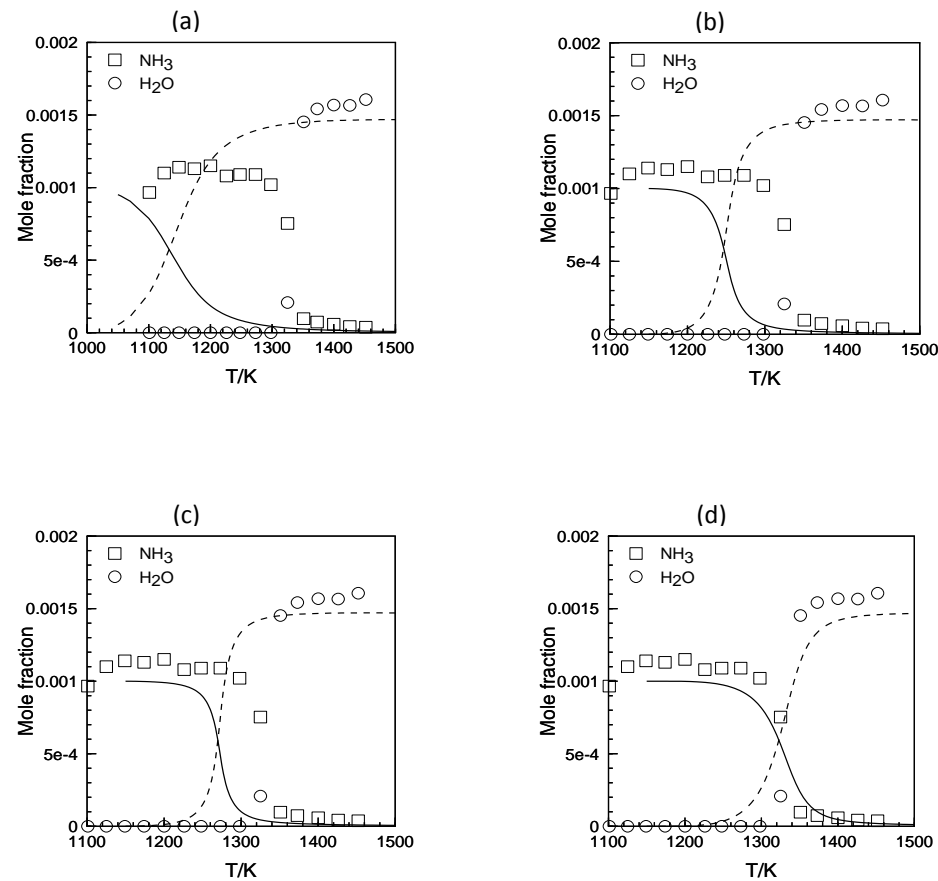


The reduction of NO by ammonia in a plug flow reactor: comparison between the experimental results of Kasuya et al. [F. Kasuya, P. Glarborg, J.E. Johnsson, K. Dam-Johansen, Chem. Eng. Sci. 50 (1995) 1455.] (symbols) and this modeling (line). The initial conditions were: 1000 ppm of NH_3 , residence time= $(88 \text{ K/T}) \text{ s}$, 500 ppm of NO, 4% O_2 , 5% H_2O , balance N_2 .

Ammonia oxidation boosted by NO :



Impact of the initial concentration of NO on NH₃ conversion. Experimental results obtained in a JSR at 1 bar, 1000 ppm NH₃, $\tau=100$ ms, $\phi=0.1$, 0 ppm (open symbols), 500 ppm (small black symbols), and 1000 ppm (large black symbols) of NO.



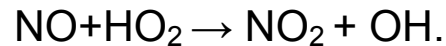
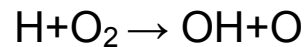
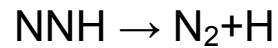
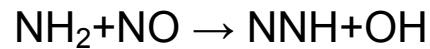
Data (symbols) and computed (lines) results for NH_3 oxidation in a JSR: 1000 ppm of NH_3 , $\tau=100\text{ms}$; $\phi=0.1$. Models: (a), (b), (c), and (d).

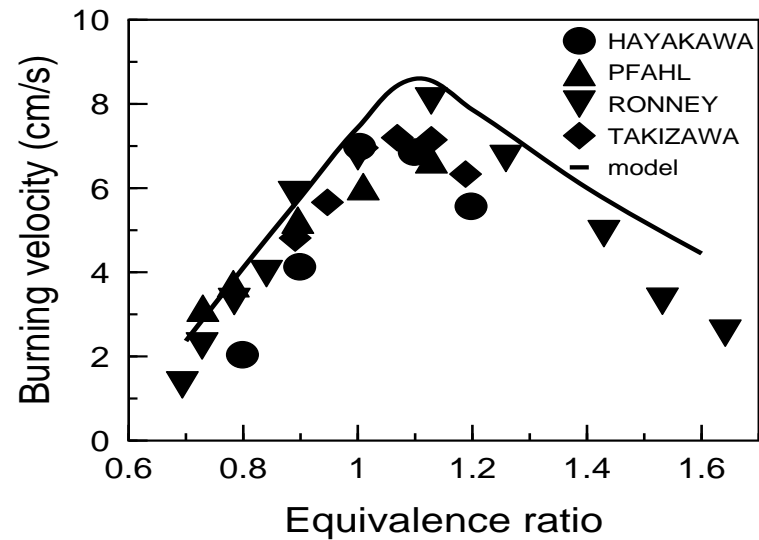
- [a] A.A. Konnov, *Combust. Flame* 156 (11) (2009) 2093-2105.
- [b] Y. Song, H. Hashemi, J.M. Christensen, C. Zou, P. Marshall, P. Glarborg, *Fuel* 181 (2016) 358-365.
- [c] J. Otomo, M. Koshi, T. Mitsumori, H. Iwasaki, K. Yamada, *Int. J. Hydrogen Energy* 43 (5) (2018) 3004-3014.
- [d] P. Dagaut, P. Glarborg, M.U. Alzueta, *Prog. Energy Combust. Sci.* 34 (1) (2008) 1-46.

Ammonia oxidation boosted by NO :

Reaction pathway analyses were performed to delineate the mechanism responsible for the mutual sensitization of ammonia and nitric oxide. The computations shows that it occurs via several reaction pathways leading to OH production, which is the main species involved in ammonia oxidation. In the present conditions HO₂ is mainly produced via: $\text{NNH} + \text{O}_2 \rightarrow \text{N}_2 + \text{HO}_2$ and $\text{H} + \text{O}_2 + \text{M} \rightarrow \text{HO}_2 + \text{M}$.

The production of OH results from a sequence of reaction including

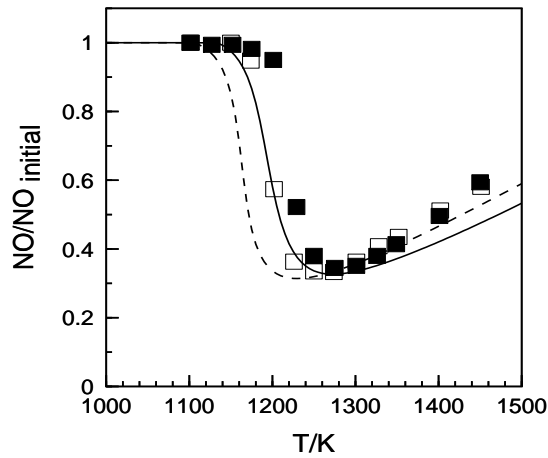




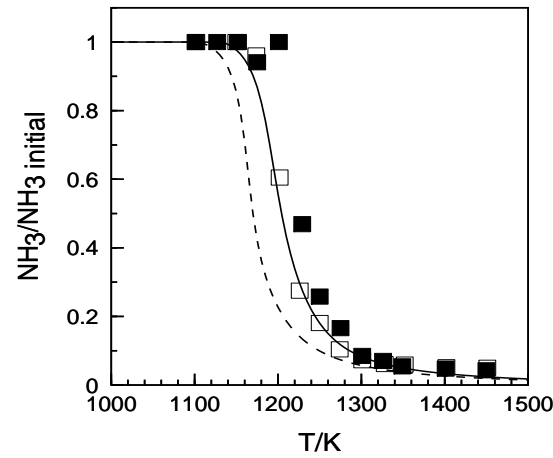
Computed (lines) and experimental (symbols) results [16-19] for NH₃-air flames at 1 atm.

The kinetics of the reactions $\text{NH}_2 + \text{H} \rightarrow \text{NH} + \text{H}_2$ and $\text{HNO} + \text{H} \rightarrow \text{NO} + \text{H}_2$ were updated (Otomo et al.) to better simulate burning velocities of ammonia in air.

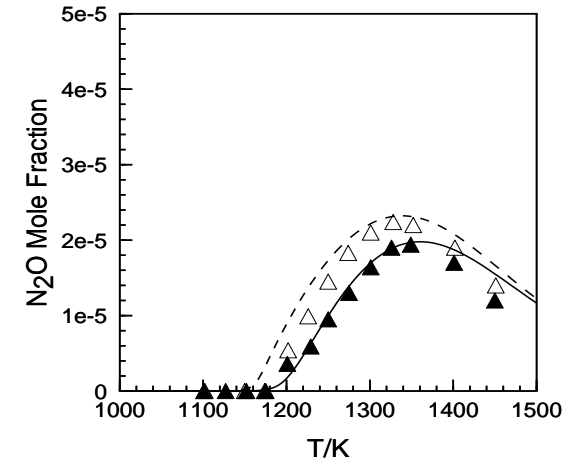
Perturbation by sulfur dioxide



a

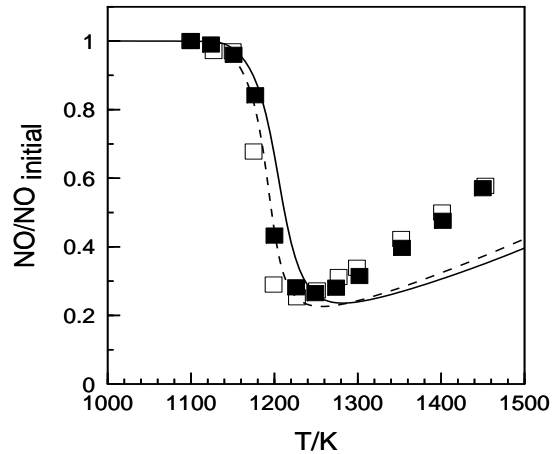


b

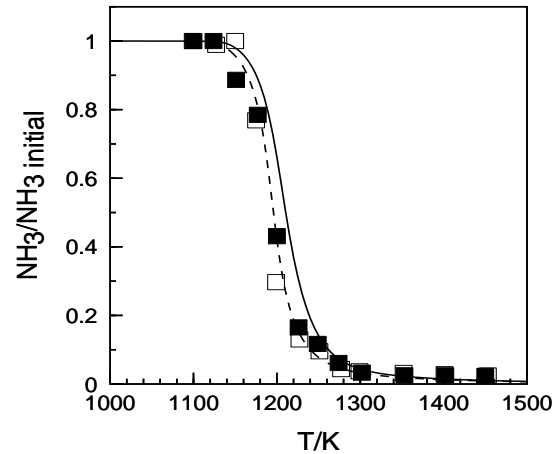


c

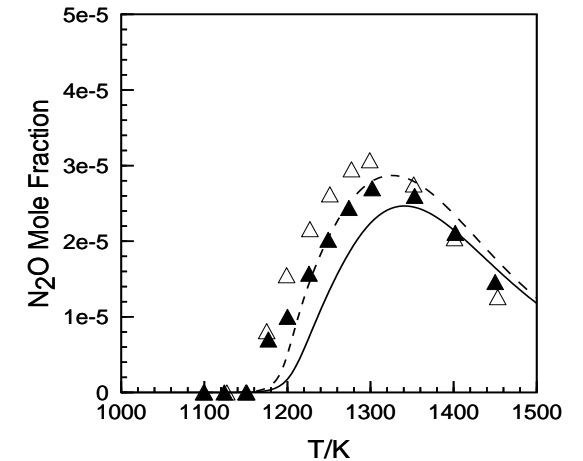
Effect of SO₂ initial concentration on NO removal by ammonia in lean conditions ($\Phi=0.1$). The initial conditions were: 500 ppm of NH₃, 6250 ppm of O₂, residence time=100 ms, 500 ppm of NO (open symbols and dashed lines) and 1000 ppm of SO₂ (closed symbols and solid line). The data (symbols) are compared to the modeling results (lines).



a

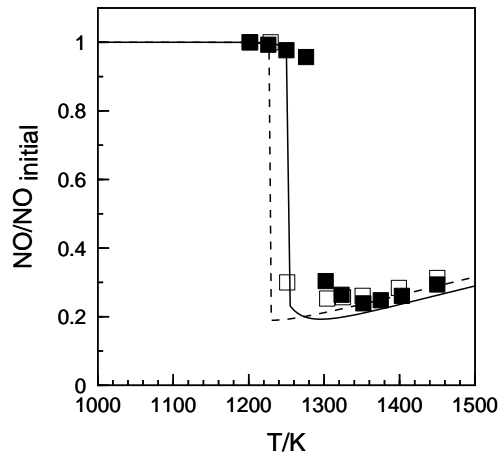


b

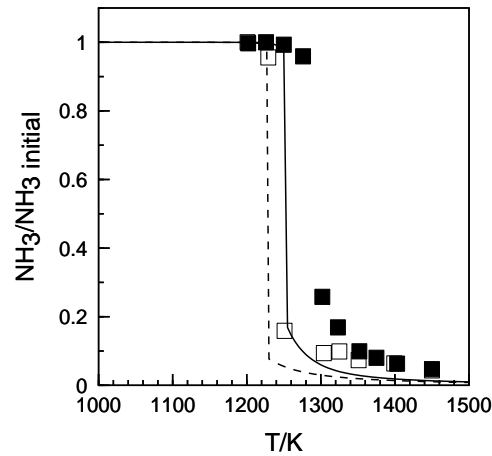


c

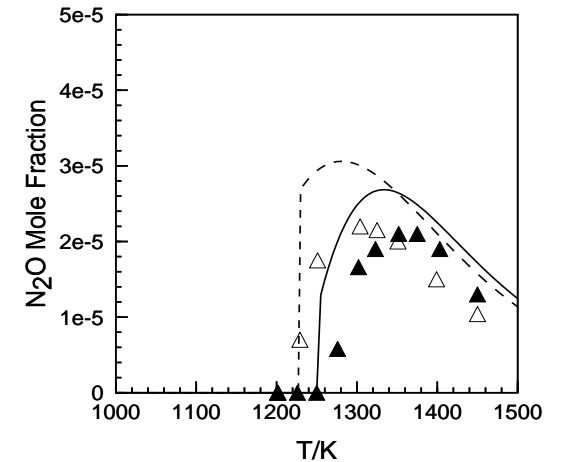
Effect of SO_2 initial concentration on NO removal by ammonia in lean conditions ($\Phi=0.1$). The initial conditions were: 1000 ppm of NH_3 , 12500 ppm of O_2 , residence time=200 ms, 1000 ppm of NO (open symbols and dashed lines) and 1000 ppm of SO_2 (closed symbols and solid line). The data (symbols) are compared to the modeling results (lines).



a



b



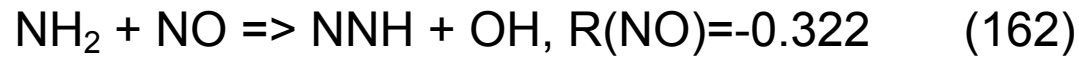
c

Effect of SO_2 initial concentration on NO removal by ammonia in fuel-rich conditions ($\Phi=2$). The initial conditions were: 1000 ppm of NH_3 , 625 ppm of O_2 , 200 ms, 1000 ppm of NO (open symbols and dashed lines) and 1000 ppm of SO_2 (closed symbols and solid line). The data (symbols) are compared to the modeling results (lines).

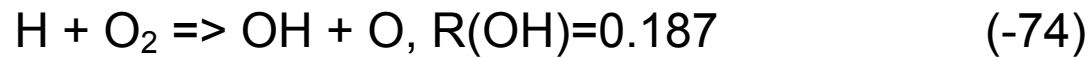
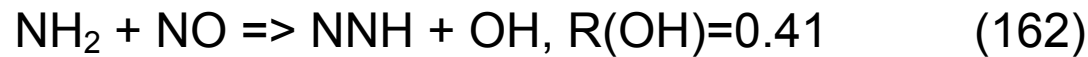
NH₂ production:



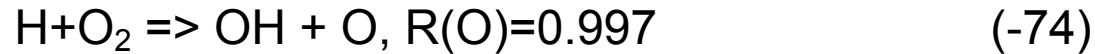
NH₂ reacts with NO via (161) and (162),



Under conditions, **OH** radicals are produced via



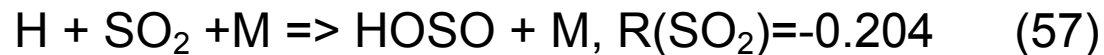
O-atoms are produced by reaction (-74),



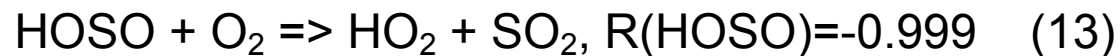
SO₂ contributes moderately to the removal of O-atoms through reaction (7):



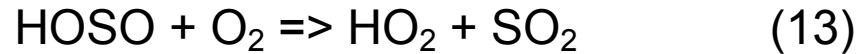
The model indicates that SO₂ reacts mostly through 3 reactions:



HOSO formed in reaction (57) recycles SO₂ via reaction (13):



The sequence of reactions (13) + (57)



is equivalent to $\text{H} + \text{O}_2 + \text{M} = \text{HO}_2 + \text{M} \Rightarrow$ reduction of the radical pool since the fraction of H atoms reacting in (57) will not produce OH and O via reaction (-74) and OH via reaction (100), $\text{NO}_2 + \text{H} \Rightarrow \text{NO} + \text{OH}$.

Thus, under such conditions, introducing 1000 ppm of SO_2 reduces the rate of production of O by a factor of 1.8 and that of OH by a factor of 1.75. Since O and OH are the major agents of oxidation of NH_3 , via reactions (149) and (150), the rate of ammonia oxidation is reduced by a factor of 1.7, resulting in the reduction of the rate of NH_2 production by a factor of 1.7 and in a reduction of 42% of NO-consumption rate.

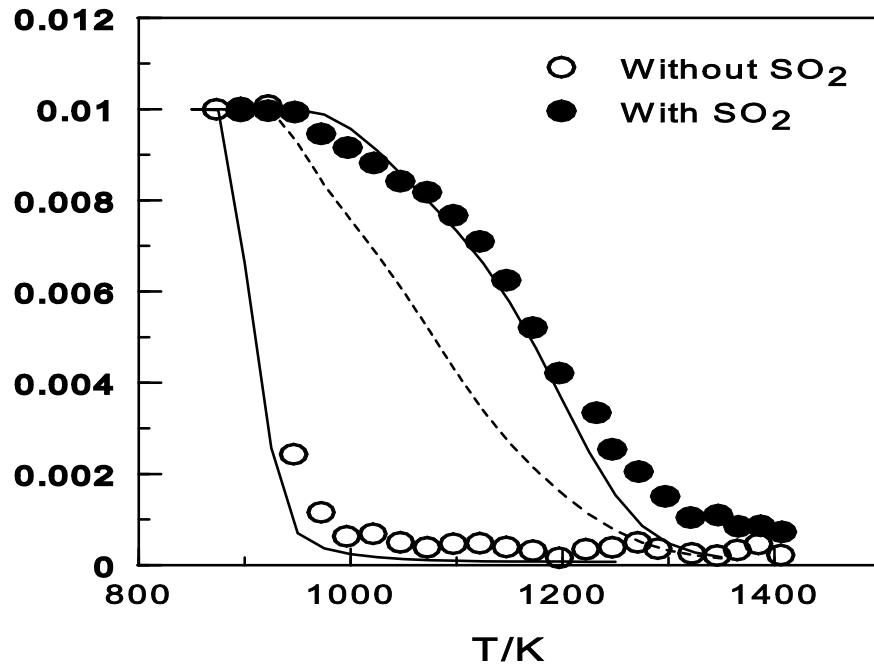
Summary

Under fuel-lean conditions, the addition of SO_2 inhibits the process via $\text{H} + \text{SO}_2 + \text{M} = \text{HOSO} + \text{M}$ followed by $\text{HOSO} + \text{O}_2 = \text{HO}_2 + \text{SO}_2$ equivalent to the equation $\text{H} + \text{O}_2 + \text{M} = \text{HO}_2 + \text{M}$.

Under fuel rich conditions, the addition of SO_2 inhibits the process via $\text{H} + \text{SO}_2 + \text{M} = \text{HOSO} + \text{M}$ followed $\text{HOSO} + \text{H} = \text{H}_2 + \text{SO}_2$ and via $\text{H} + \text{SO}_2 + \text{M} = \text{HOSO} + \text{M}$ followed by $\text{HOSO} + \text{O}_2 = \text{HO}_2 + \text{SO}_2$.

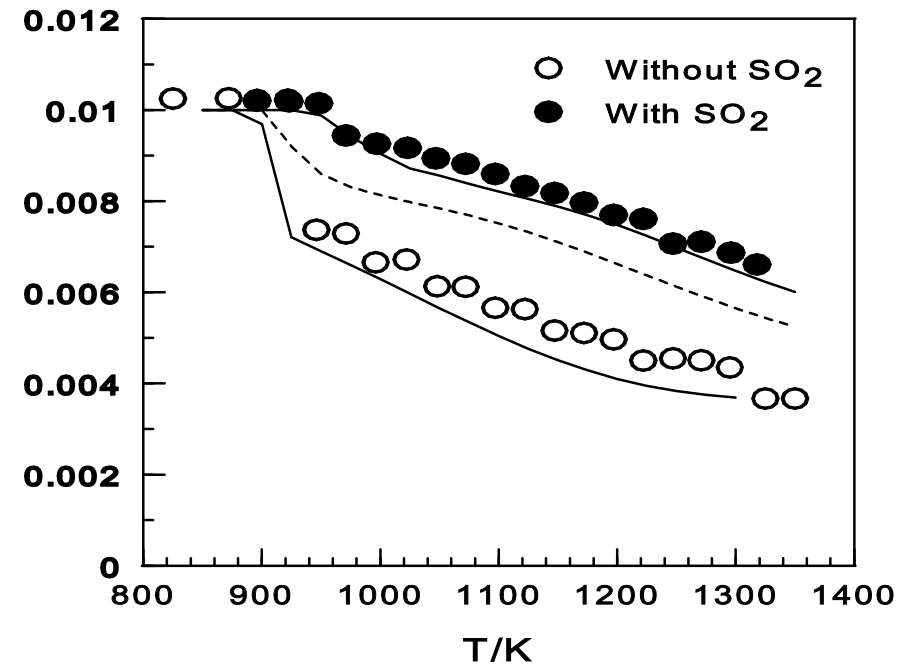
SO_2 does not reduce the efficiency of the thermal de- NO_x process but shifts the optimal temperature to higher values.

Further inhibiting effects of SO₂



CO Mole Fraction

a

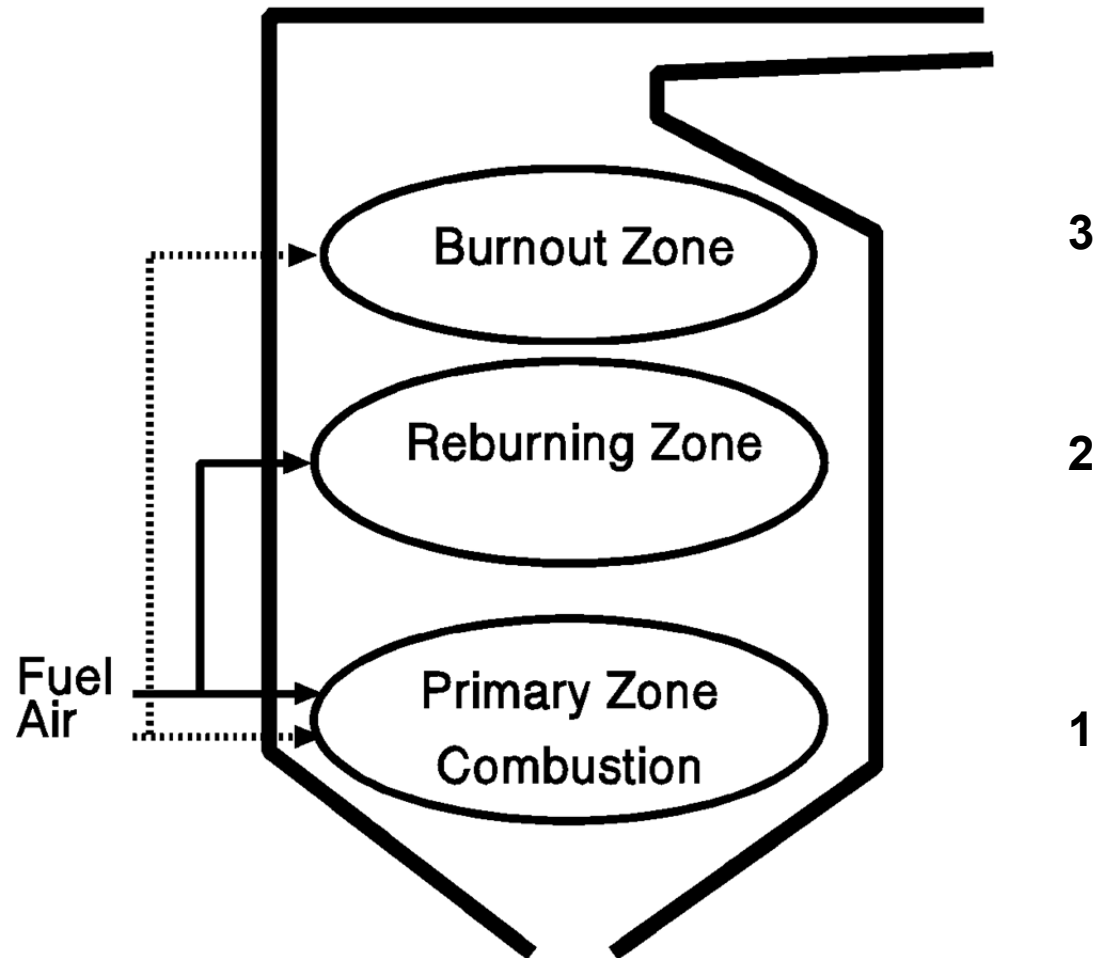


CO Mole Fraction

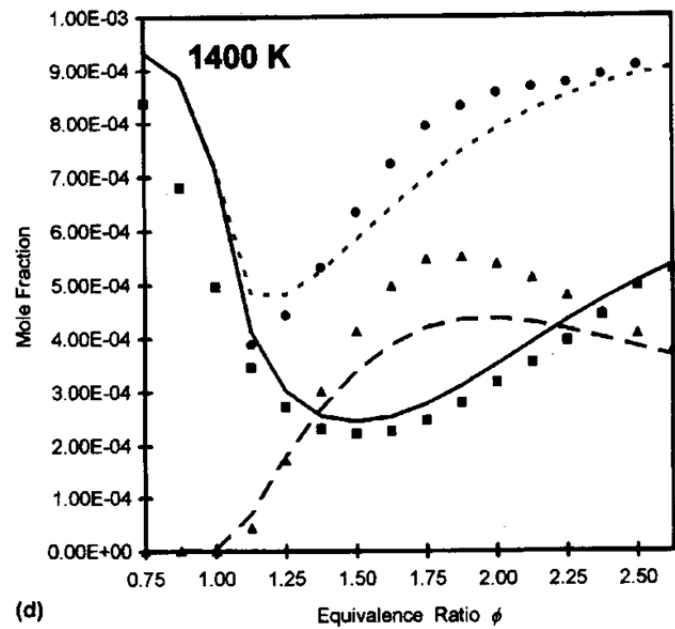
b

The effect of SO₂ on the oxidation of a CO/H₂ mixture in a plug-flow reactor. Initial conditions: (a) CO = 1.0%, H₂ = 1.0%, O₂ = 1.0%, H₂O = 2.0%, balance N₂, without and with SO₂ = 1.2%, residence time is 192.7/T or 192.3/T; (b) CO = 1.0%, H₂ = 1.0%, O₂ = 0.5%, H₂O = 2.0%, balance N₂, without and with SO₂ = 0.3%, residence time is 192.7/T or 192.3/T. Inhibition is due to H+SO₂+M=HOSO+M followed by HOSO+H=H₂+SO₂. From Dagaut et al., *Int J Chem Kinet* 35: 564–575, 2003.

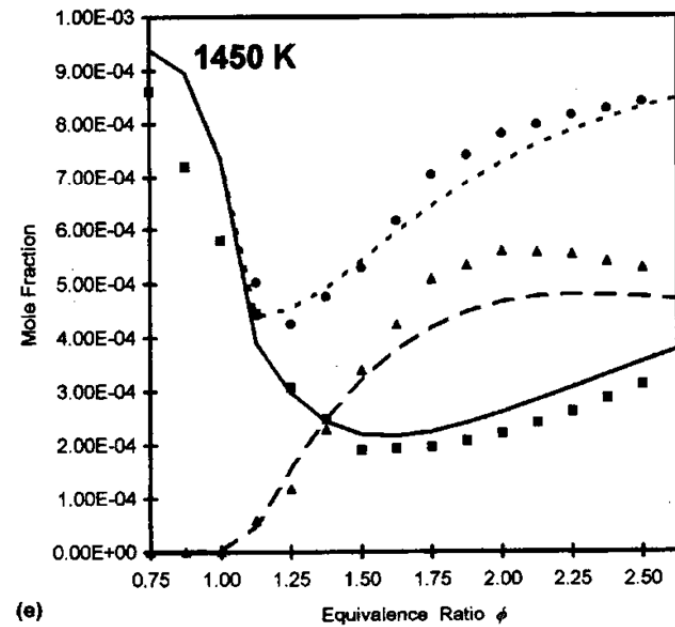
2-2-2-NOx reduction by reburning)



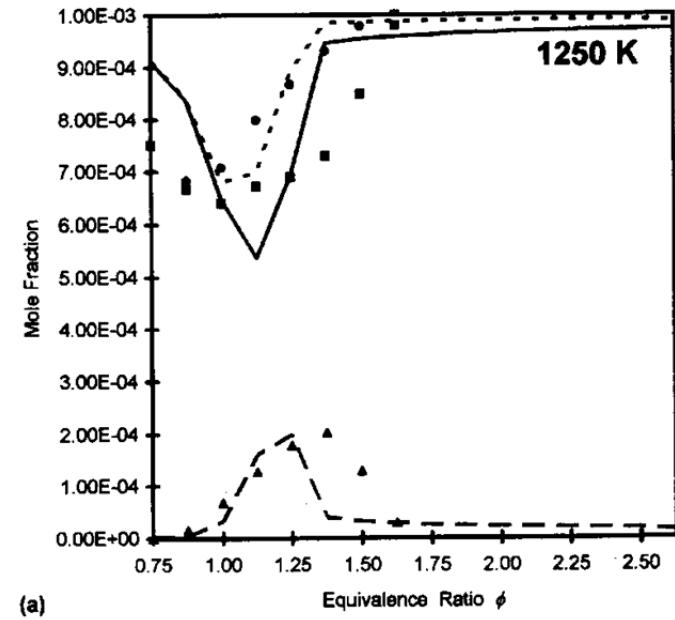
(1) Thermal-NO production in near-stoichiometric conditions; (2) fuel-rich zone, $\text{NO} + \text{HC} \rightarrow \text{N}_2, \text{HCNO}_x$; (3) excess-air, $\text{HCNO}_x \text{ oxidation} \rightarrow \text{NO}$



(d)

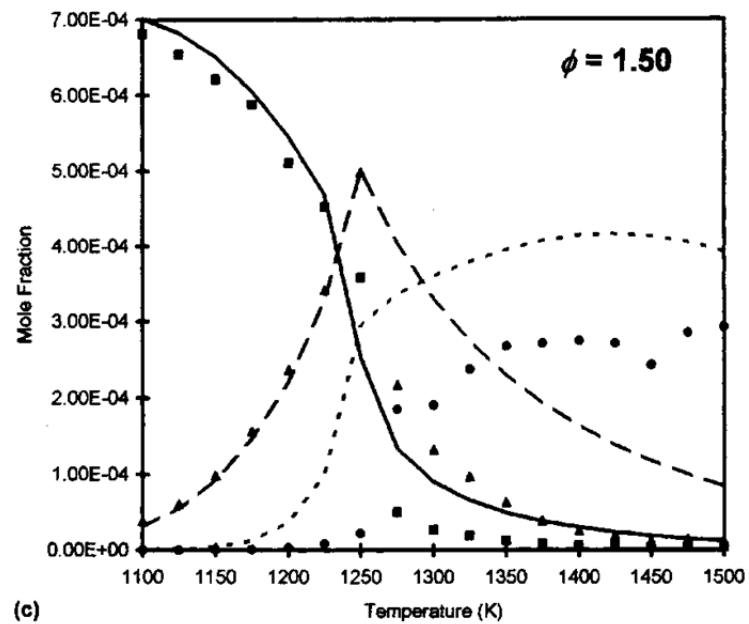


(e)



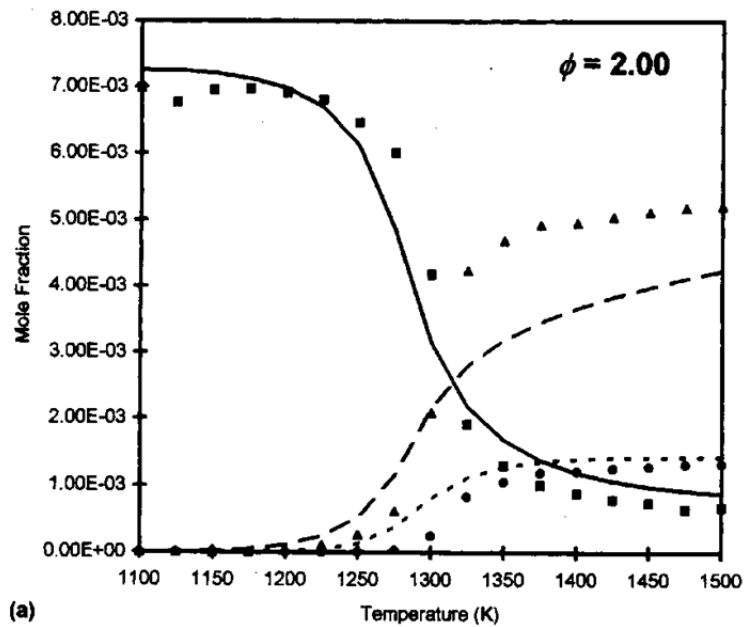
(a)

FIGURE 11 The effect of equivalence ratio on the reburning of NO by a CH₄/C₂H₆ (10:1) mix at 1 atm ($\tau = 0.12$ s; 1000 ppm of NO; 7272 ppm of CH₄; 728 ppm of C₂H₆). Comparison between experimental data (symbols) and modeling (lines): NO, ■—; HCN, ▲---; TFN, ●...; (a) 1250 K; (b) 1300 K; (c) 1350 K; (d) 1400 K; (e) 1450 K.



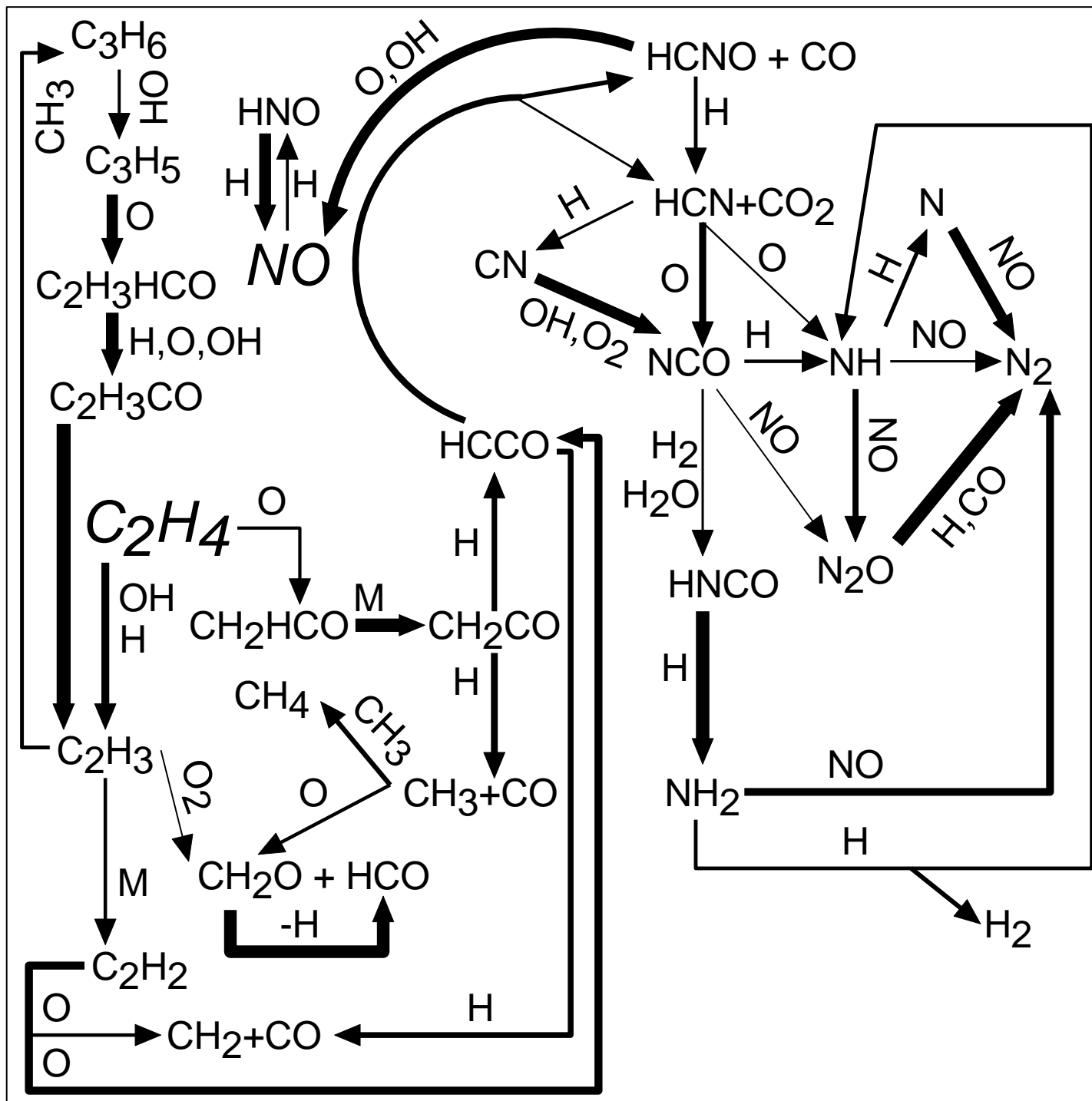
(c)

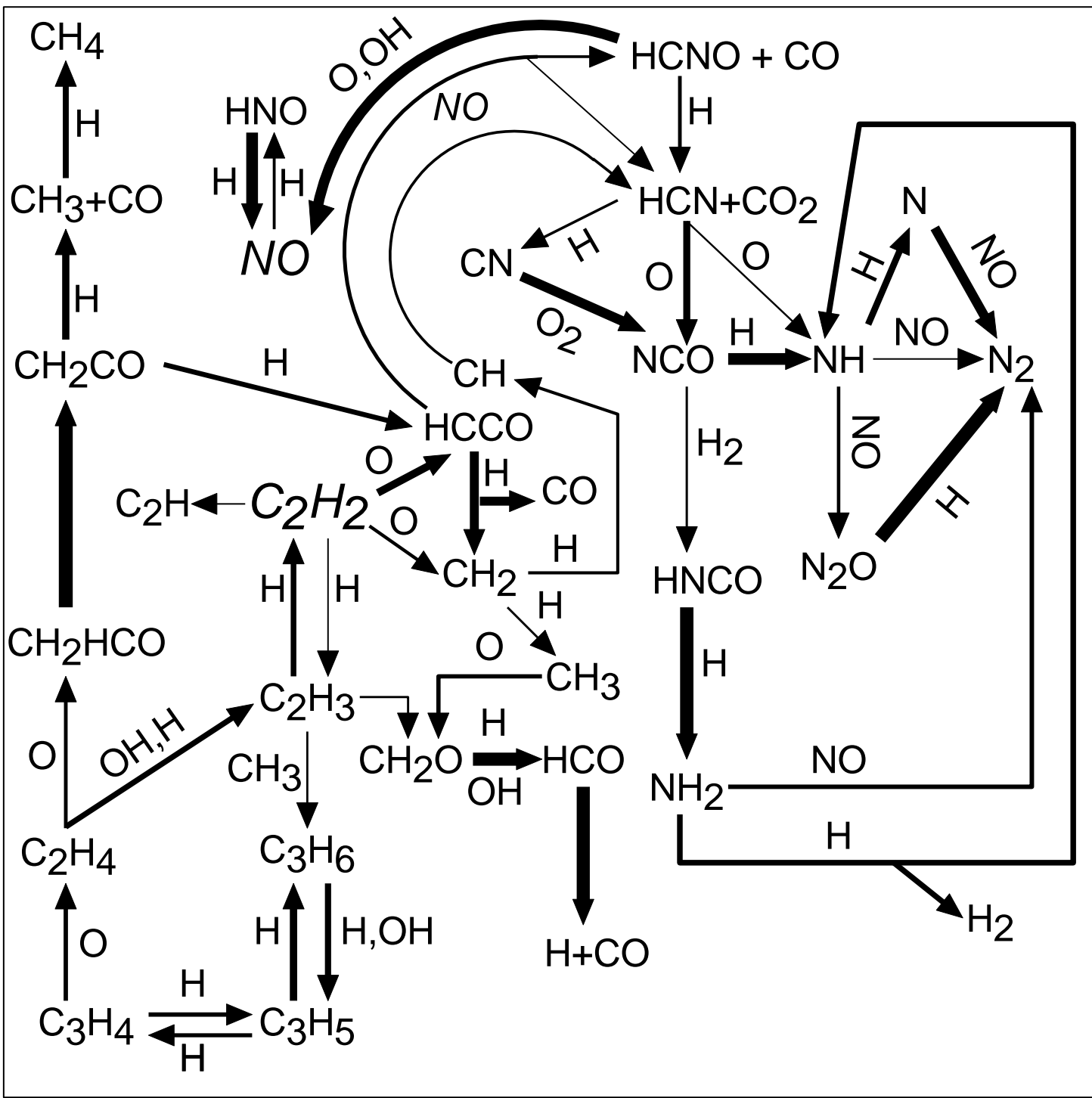
FIGURE 9 (Continued).

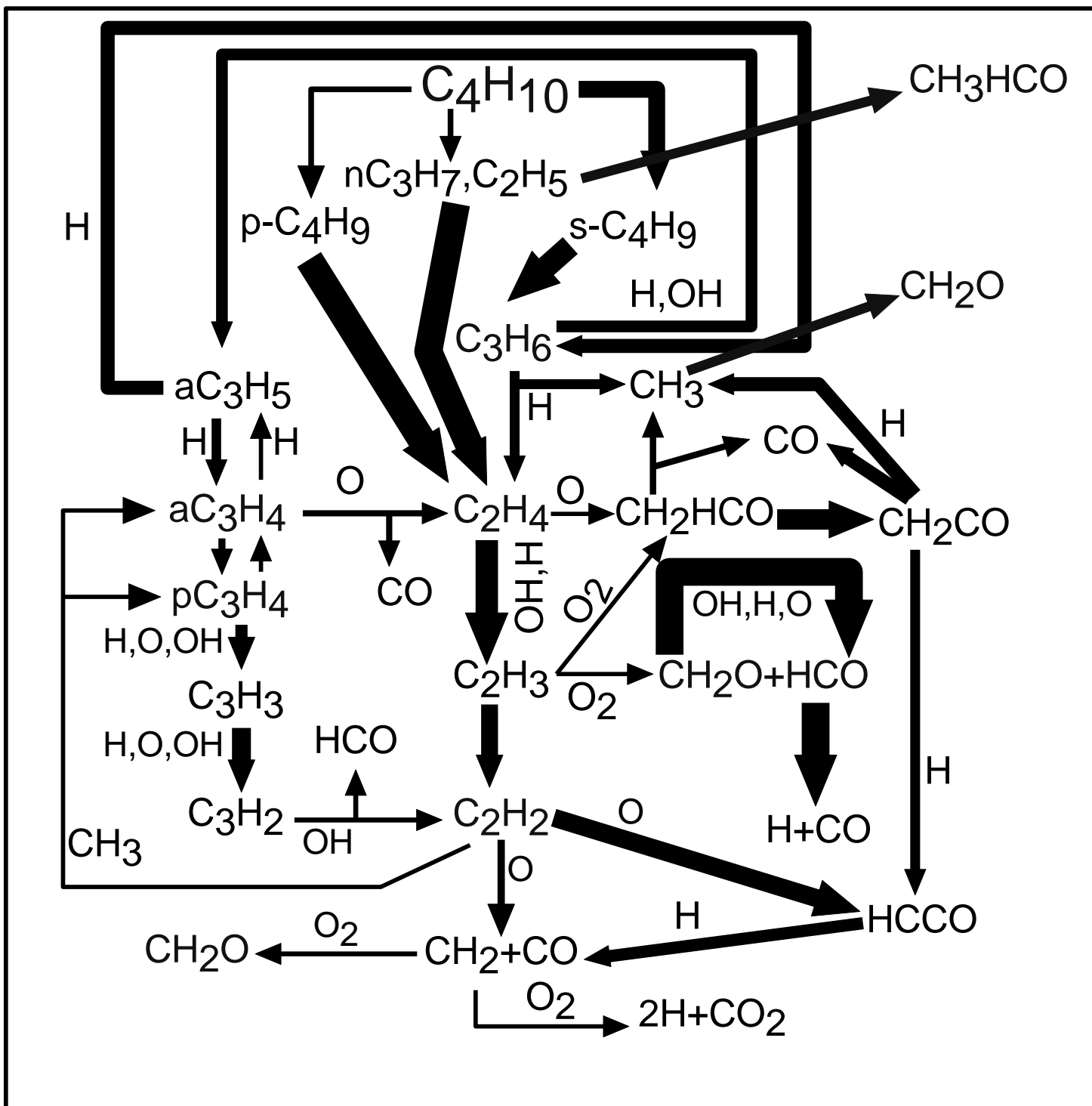


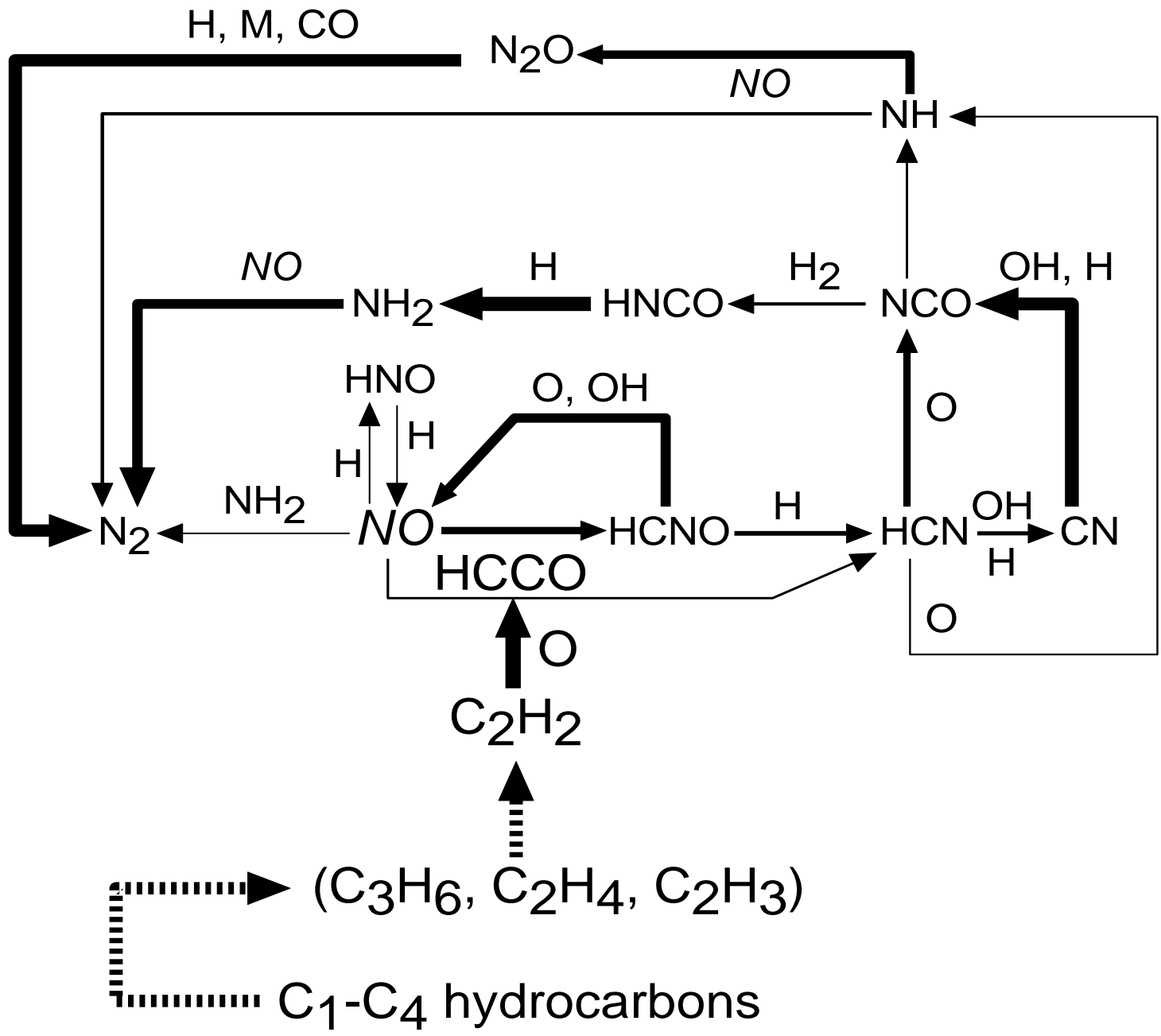
(a)

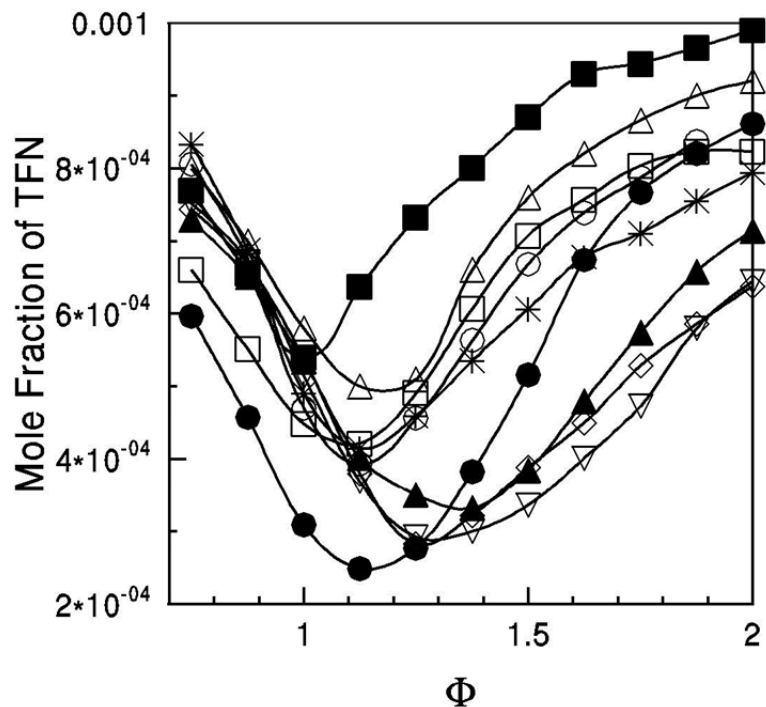
FIGURE 10 The oxidation of a $\text{CH}_4/\text{C}_2\text{H}_6$ (10:1) mix in a JSR at 1atm ($\tau = 0.12$ s; 7272 ppm of CH_4 ; 728 ppm of C_2H_6 ; 8546 ppm of O_2 ; $\phi = 2$). Comparison between experimental data (symbols) and modeling (lines); (a) CH_4 , \blacksquare ; CO , \blacktriangle ; CO_2 , \bullet ; (b) O_2 , \blacksquare ; H_2 , \blacktriangle ; (c) C_2H_6 , \blacksquare ; C_2H_4 , \blacktriangle ; C_2H_2 , \bullet .



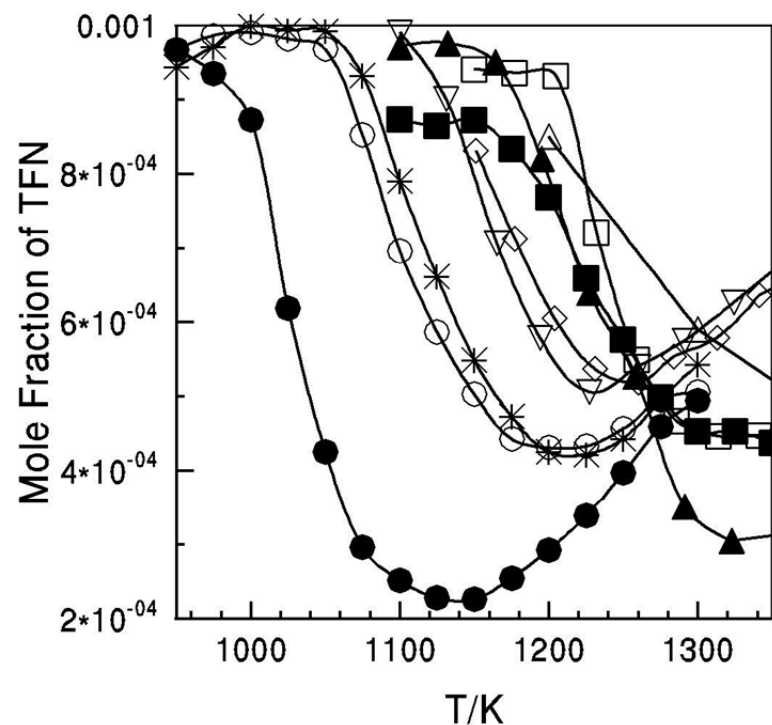






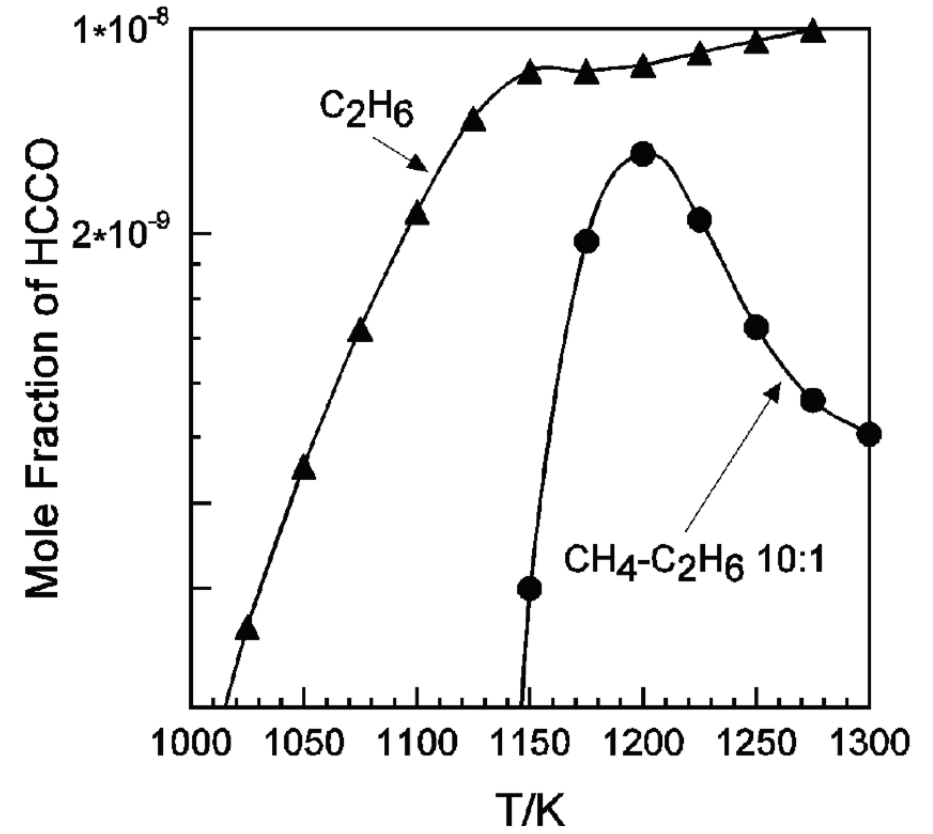
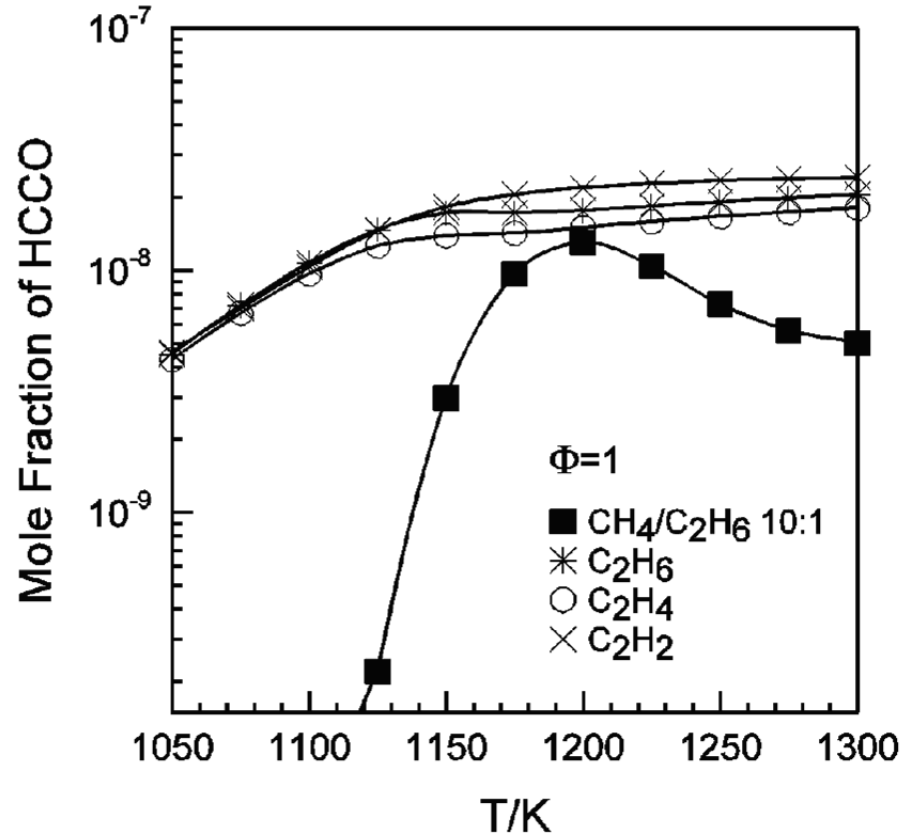


TFN (NO+HCN) vs eq. ratio; 1300 K, 1000ppm NO, 8800 ppm C, 0.12s. Reburn fuels: NG-blend ■; ethane *; ethylene ○, acetylene ●; NG △; propene □; propane ◇; n-butane △; i-butane ▲.

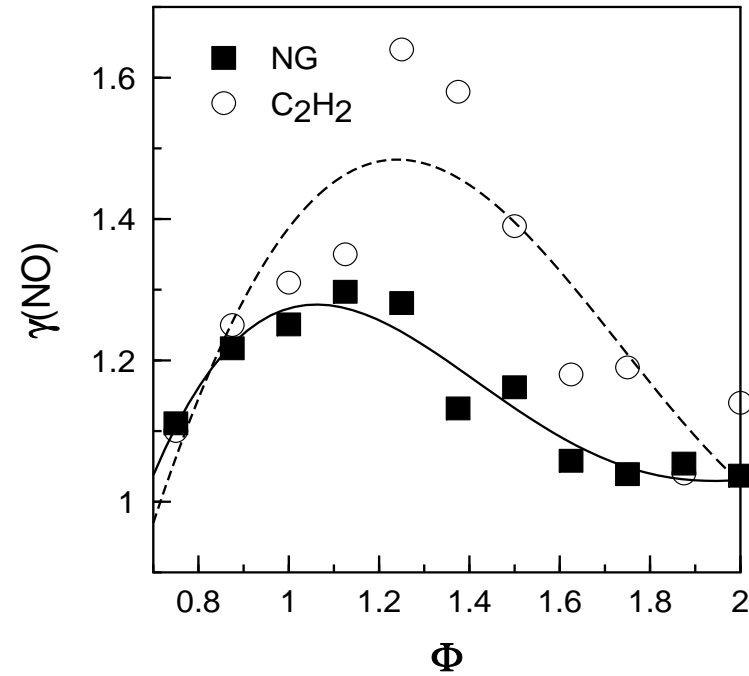


TFN (NO+HCN) vs. T for 8 reburn fuels: NG-blend ■; ethane *; ethylene ○, acetylene ●; NG △; propene □; propane ◇; n-butane △; i-butane ▲. Stoichiometric mix, 1000ppm NO, 8800 ppm C, 0.12-0.16s

HCCO production



Inhibiting effect of SO₂ on NO-reburning using 2 reburn fuels at 1300K



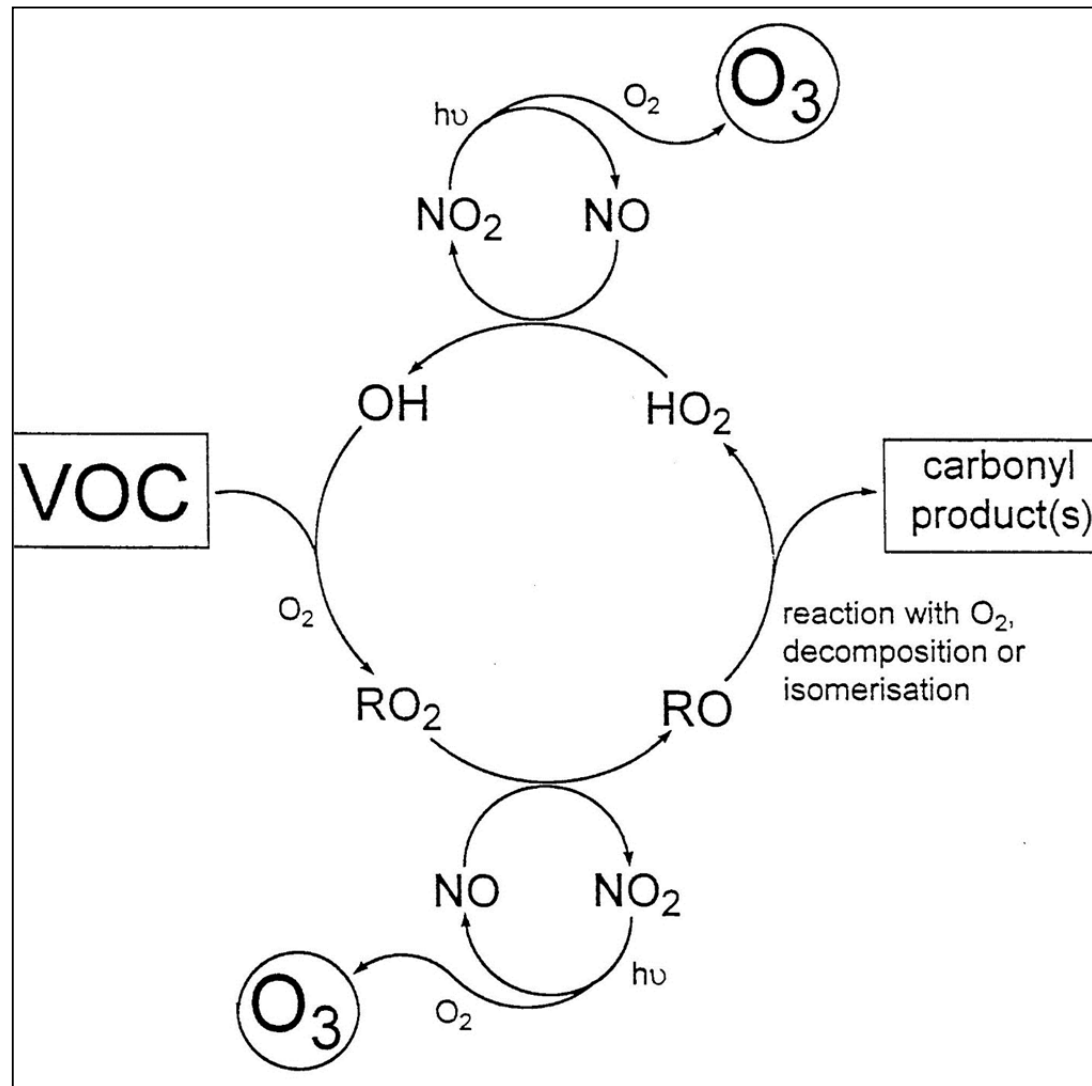
No residual increased in presence of sulfur dioxide

3-UHC and Soot

Organic compounds in the troposphere

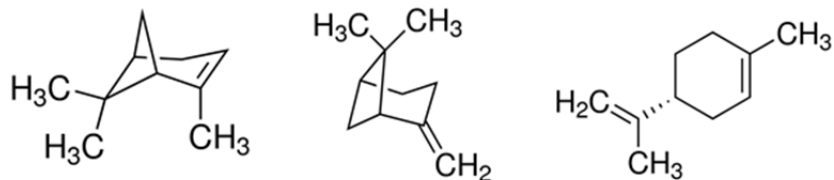
Class	Compound	Formula	Typical Source	Sink	Concentration Range
Alkanes	Methane	CH ₄	Microbial processes, natural gas	OH	1.7 ppm
	Ethane	C ₂ H ₆	Motor vehicles	OH	0–100 ppb
	Hexane	C ₆ H ₁₄	Motor vehicles	OH	0–30 ppb
Alkenes	Ethene	C ₂ H ₄	Motor vehicles, microbial processes	OH, O ₃	0–100 ppb
	Propene	C ₃ H ₆	Motor vehicles	OH, O ₃	0–50 ppb
	Isoprene	C ₅ H ₈	Vegetation	OH, O ₃	0.2–30 ppb
Alkynes	Acetylene	C ₂ H ₂	Motor vehicles	OH	0–100 ppb
Aromatics	Benzene	C ₆ H ₆	Motor vehicles	OH	
	Toluene	C ₇ H ₈	Motor vehicles	OH	
Aldehydes	Formaldehyde	HCHO	Motor vehicles	<i>hν</i> , OH	
	Acetaldehyde	CH ₃ CHO	Motor vehicles	<i>hν</i> , OH	
	Acrolein	CH ₂ CHCHO			
Ketones	Acetone	CH ₃ C(O)CH ₃		<i>hν</i> , OH	0–10 ppb
Acids	Formic acid	HCOOH		Rain	
	Acetic acid	CH ₃ COOH		Rain	
Alcohols	Methanol	CH ₃ OH		OH	

Oxidation of organic compounds in the troposphere

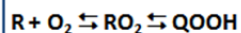


Terpenes to HOMs and Secondary Organic Aerosols (SOAs)

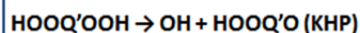
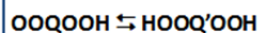
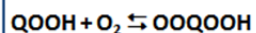
Terpenes oxidation



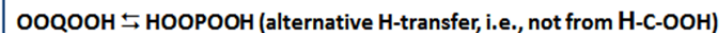
Reaction pathways to ketohydroperoxides



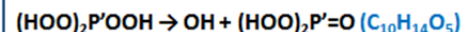
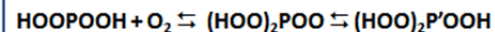
2nd O₂ addition:



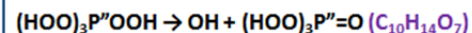
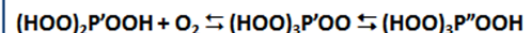
HOMs formation mechanism



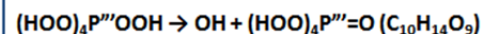
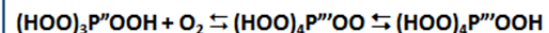
3rd O₂ addition:



4th O₂ addition:



5th O₂ addition:



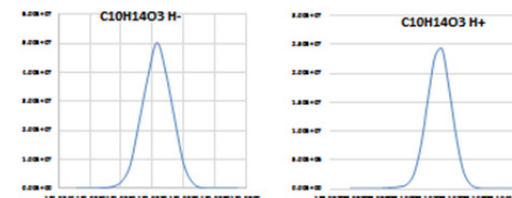
Results

Ketohydroperoxides

C₁₀H₁₄O₃ : M

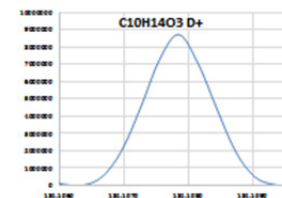
MH⁺ m/z= 183.10167

M(-H)⁻ m/z= 181.08715



H/D exchange using D₂O: -OH → -OD to confirm the presence of -OOH

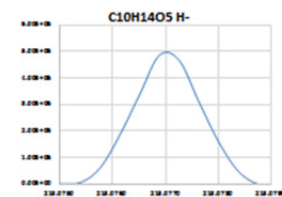
MD⁺ m/z= 184.10785



HOMs

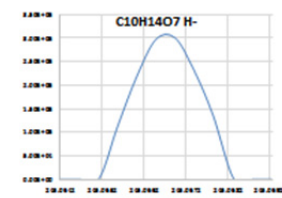
C₁₀H₁₄O₅ : M

M(-H)⁻ m/z= 213.07688

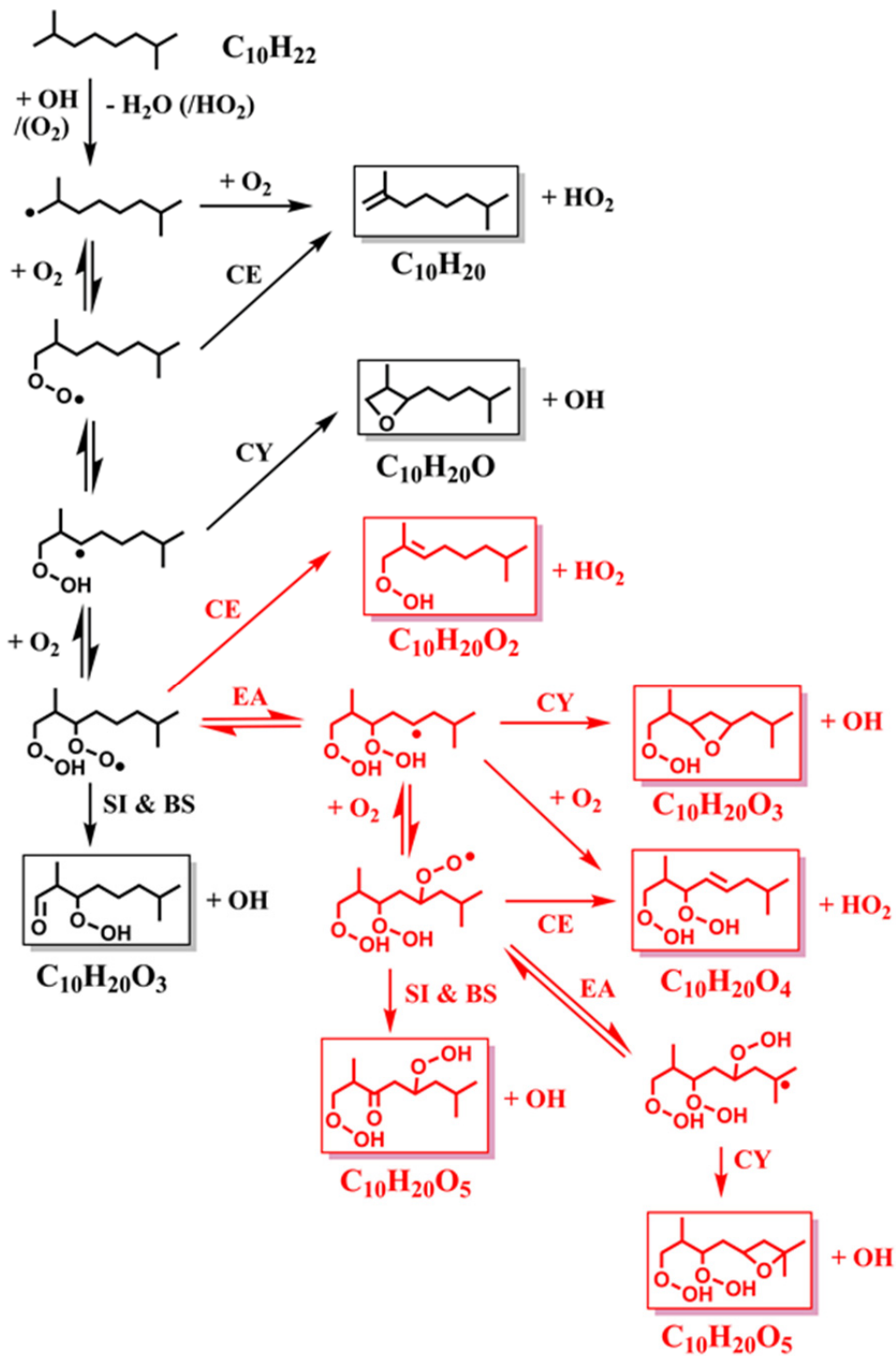


C₁₀H₁₄O₇ : M

M(-H)⁻ m/z= 245.06694

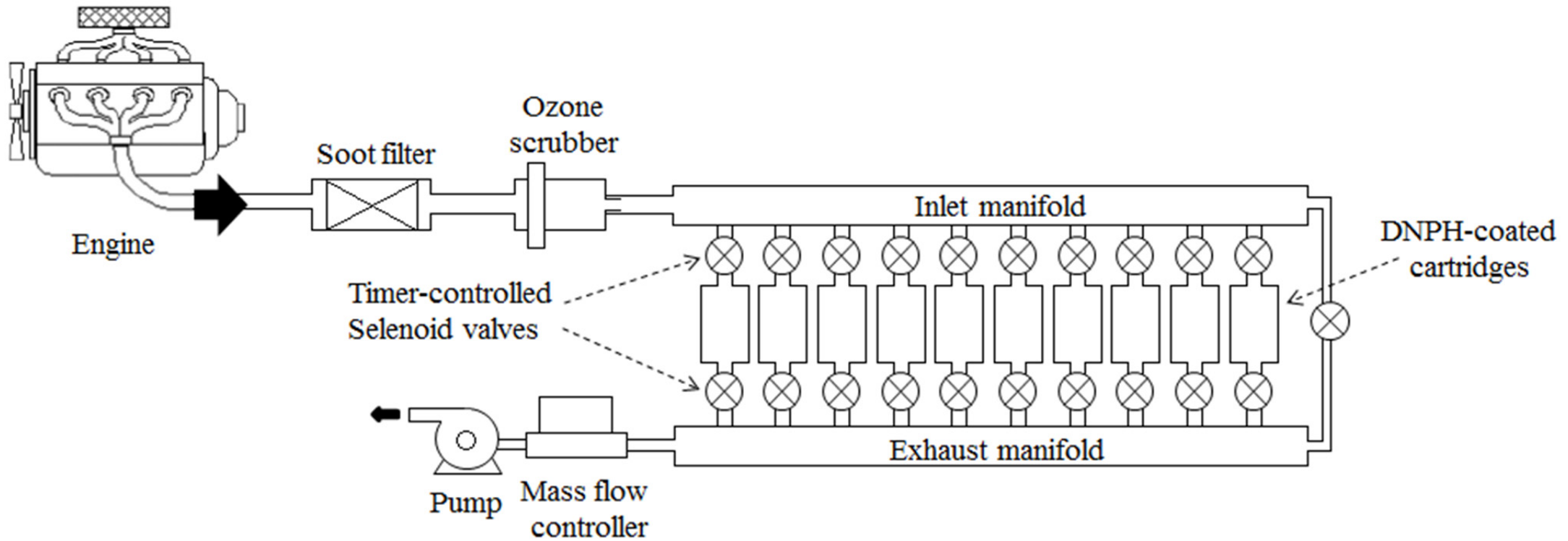


From Belhadj et al. ICCK, 2019



Additional pathways to HOMs by *Wang et al. PNAS (2017)*

Pollutants from Diesel/biofuels combustion in I.C. engine



Engine and gas sampling system. DNPH+carbonyl; HPLC with UV detection @360nm.

From Dagaut et al., J. Eng. Gas Turbines Power 141, 031028-1 (2019)

Diesel engine conditions

Nbr of cylinders	4
Cycle	4
Cylinder (cm³)	1460.74
Vol. Ratio	15.21
injector	Continental SA.
Type of injection	Direct Common Rail
Nbr of injectors	4
Nbr of injection	3 per cycle
Post-treatment	no

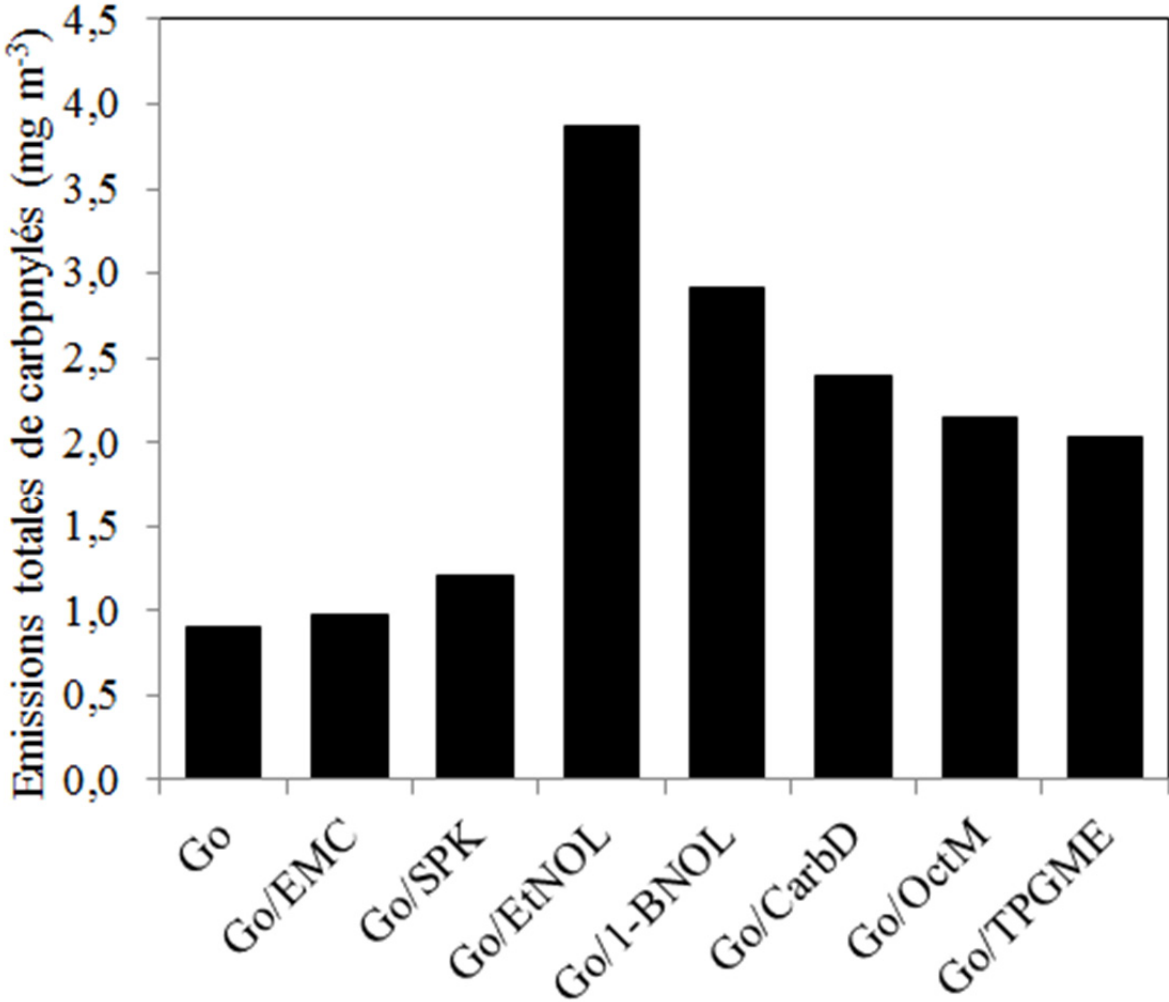
Pollutants from Diesel/biofuels combustion in I.C. engine

Additives used (mix Diesel/additive 90/10 vol.)

<i>Mix DCN</i>	Additive	Chemical class	Formula	Density	M.W.
				(g/mL @ 25°C)	(g/mol)
55,34	none				
46.32	EtNOL	Alcool	C₂H₆O	0.789	46.07
49.71	1-BNOL	Alcool	C₄H₁₀O	0.810	74.12
48.96	CarbD*	ester of carbonate	C₅H₁₀O₃	0.975	118.13
54.22	OctM	methyl ester	C₉H₁₈O₂	0.877	158.24
55.56	EMHC	Mixed methylesters	C_{17.92}H₃₃O₂	0.883[#]	280
54.75	TPGME	ether	C₁₀H₂₂O₄	0.963	206.28
52.74	SPK	Mixed paraffins[‡]	C_{11.03}H_{23.37}	0.761[#]	156

[#] @ 15°C; [‡] 0,21% vol. aromatics; * DEC

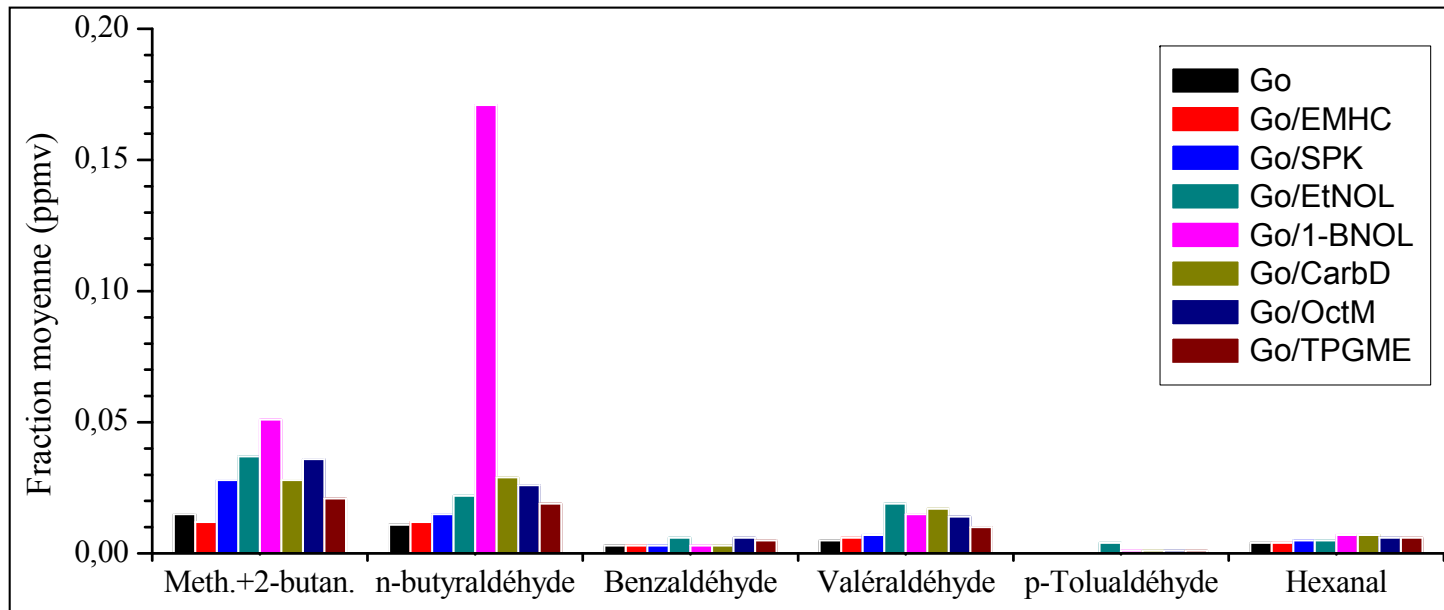
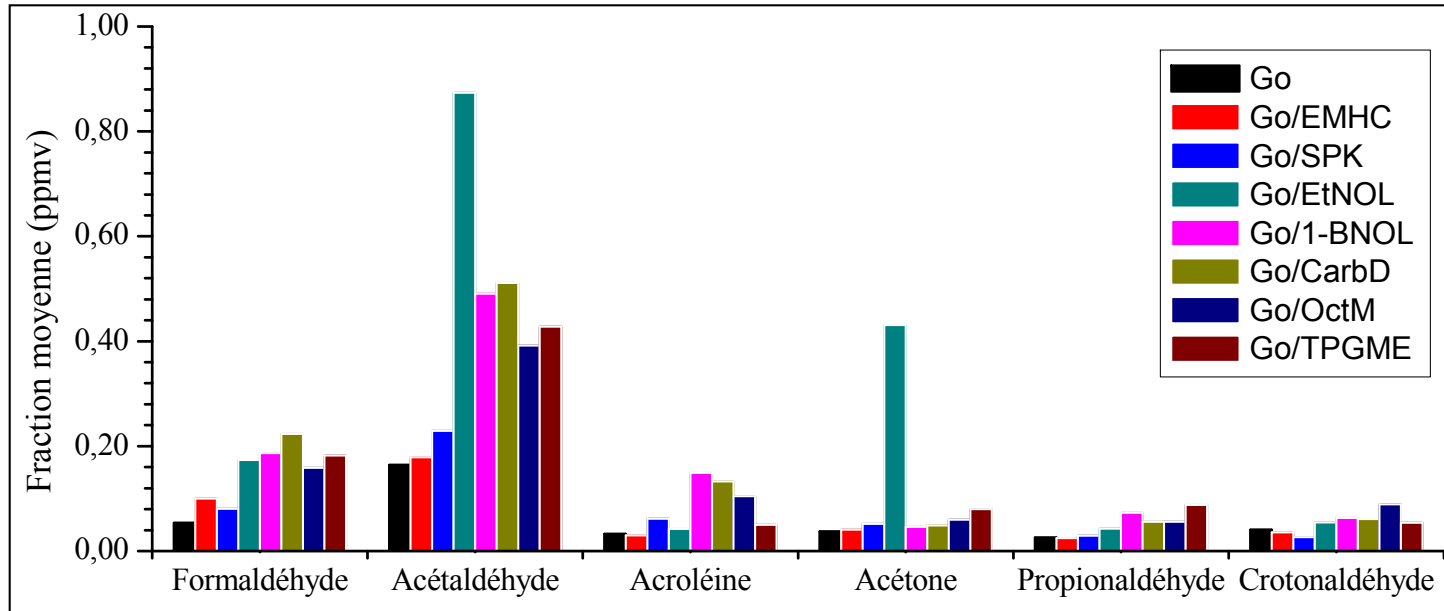
Pollutants from Diesel/biofuels combustion in I.C. engine



Global emission of carbonyl compounds at I.C.E. exhaust



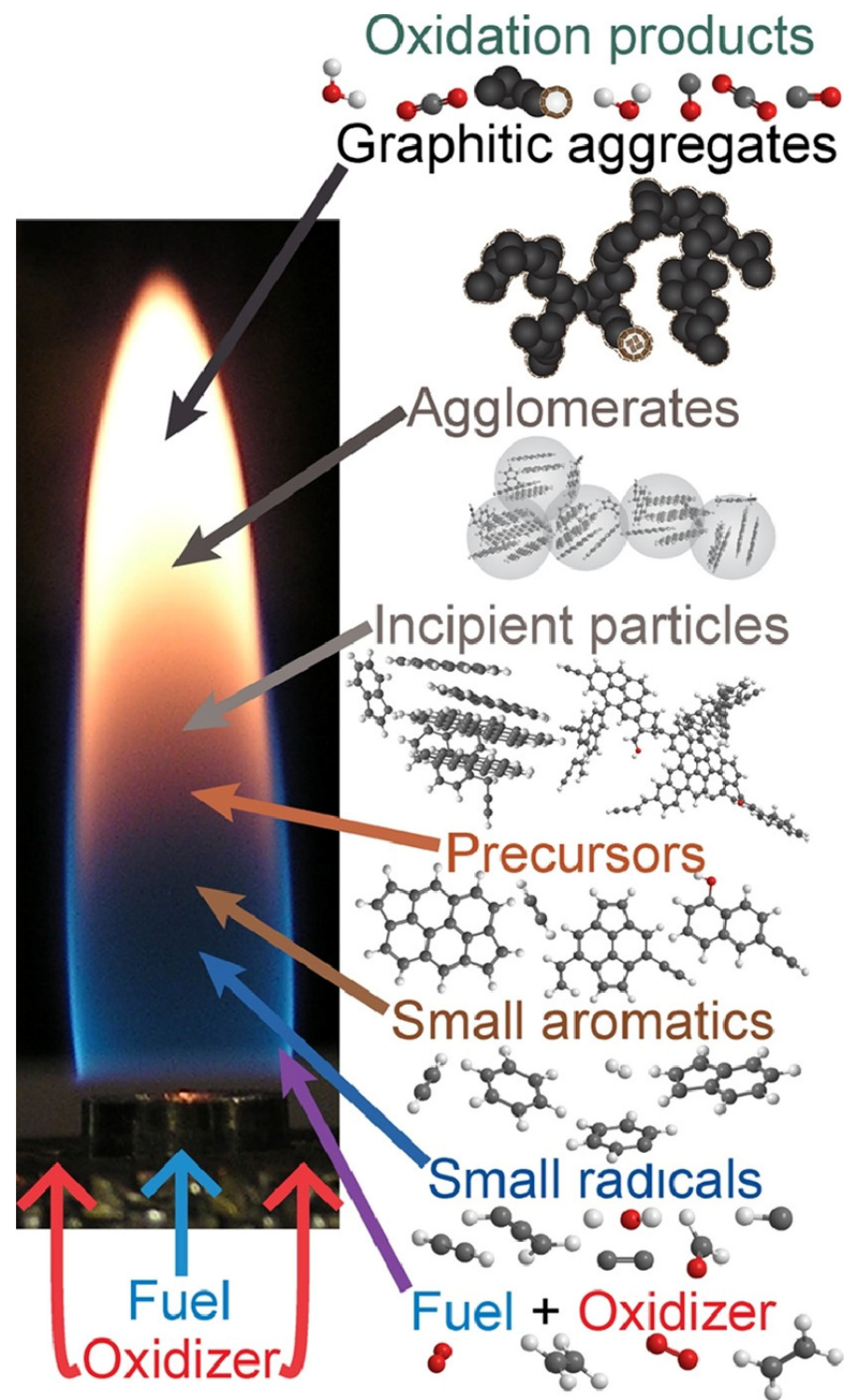
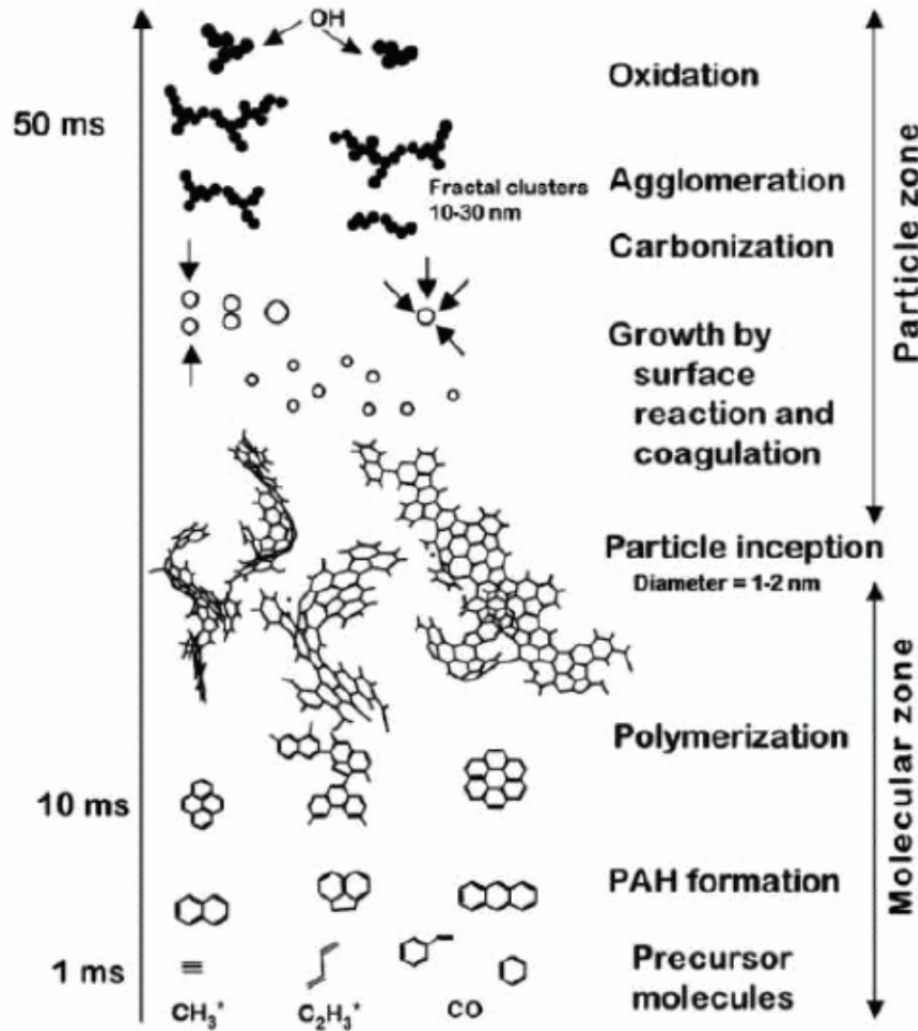
Pollutants from Diesel/biofuels combustion in I.C. engine



Shahla, Ph.D., 2015

Soot and PAHs

H.A. Michelsen, *Proc. Combust. Inst.* 36, 717-735 (2016)



PAHs formation via the HACA mechanism (Frenklach and Wang)

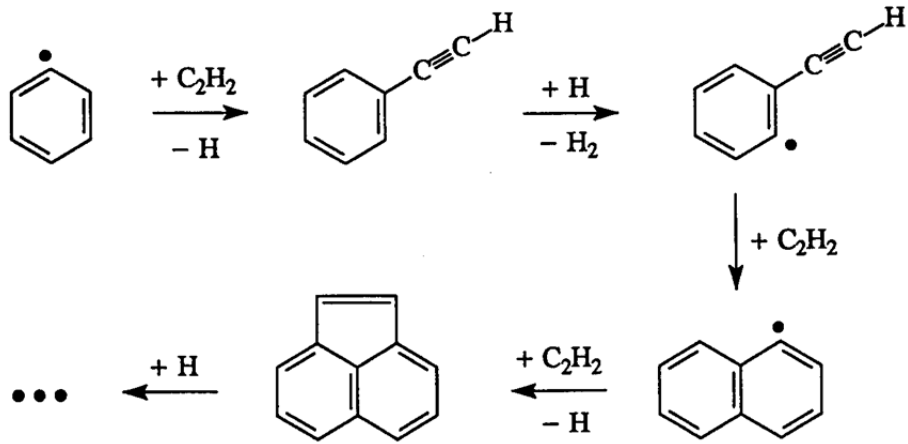


Fig. 10.2. H-abstraction-C₂H₂-addition reaction pathway of PAH growth

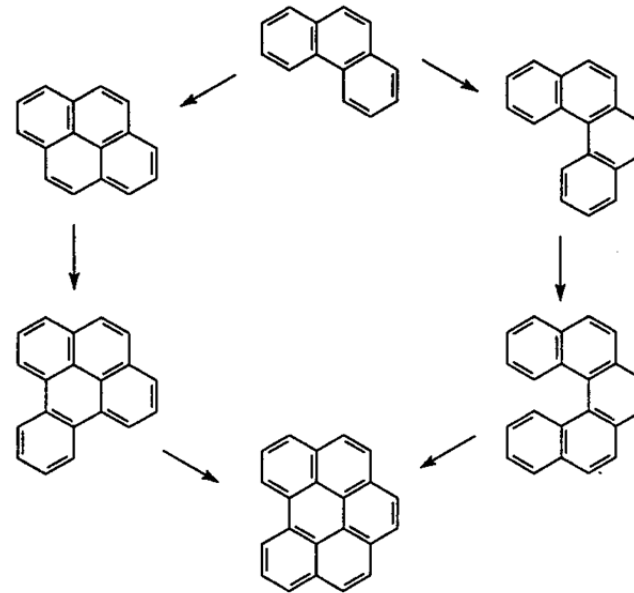


Fig. 10.4. Comparison of two pathways of PAH growth

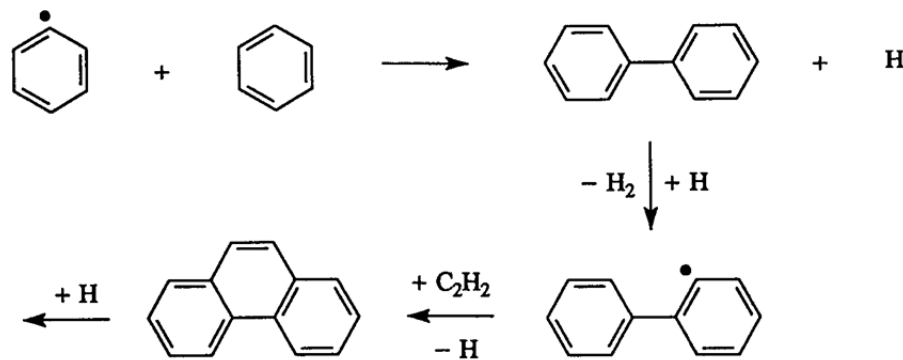
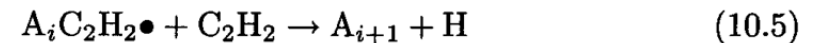
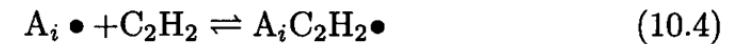
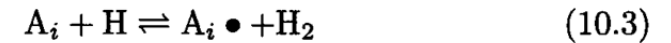


Fig. 10.3. PAH growth initiated by aromatic "combination"

The main kinetic features of PAH growth after a certain PAH size, i_0 , are revealed by considering an analytical solution with the smallest set of reactions that represent the principal elements of the HACA sequence [10.24]. This minimal reaction set is given as



Benzene formation

Fuels: acetylene ($\text{HC}\equiv\text{CH}$)

propene ($\text{CH}_3\text{-CH}=\text{CH}_2$), propyne ($\text{HC}\equiv\text{C-CH}_3$), allene ($\text{H}_2\text{C}=\text{C}=\text{CH}_2$)

1,3-butadiene ($\text{H}_2\text{C}=\text{CH-CH}=\text{CH}_2$)

Conditions: JSR, 1 atm, 900-1300 K

Benzene formation from acetylene, allene and propyne proceeds through a **C₃ channel** involving the recombination of propargyl radicals:



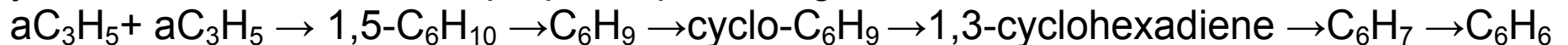
In the case of 1,3-butadiene, the formation of benzene is driven by 2 competitive routes, a (**C₂+C₄**) **route** and the **C₃ route** (1):



According to our computations, the formation of 1,3-C₄H₅ results from the intermediate formation of 1,3-cyclopentadiene (1,3-CPD):

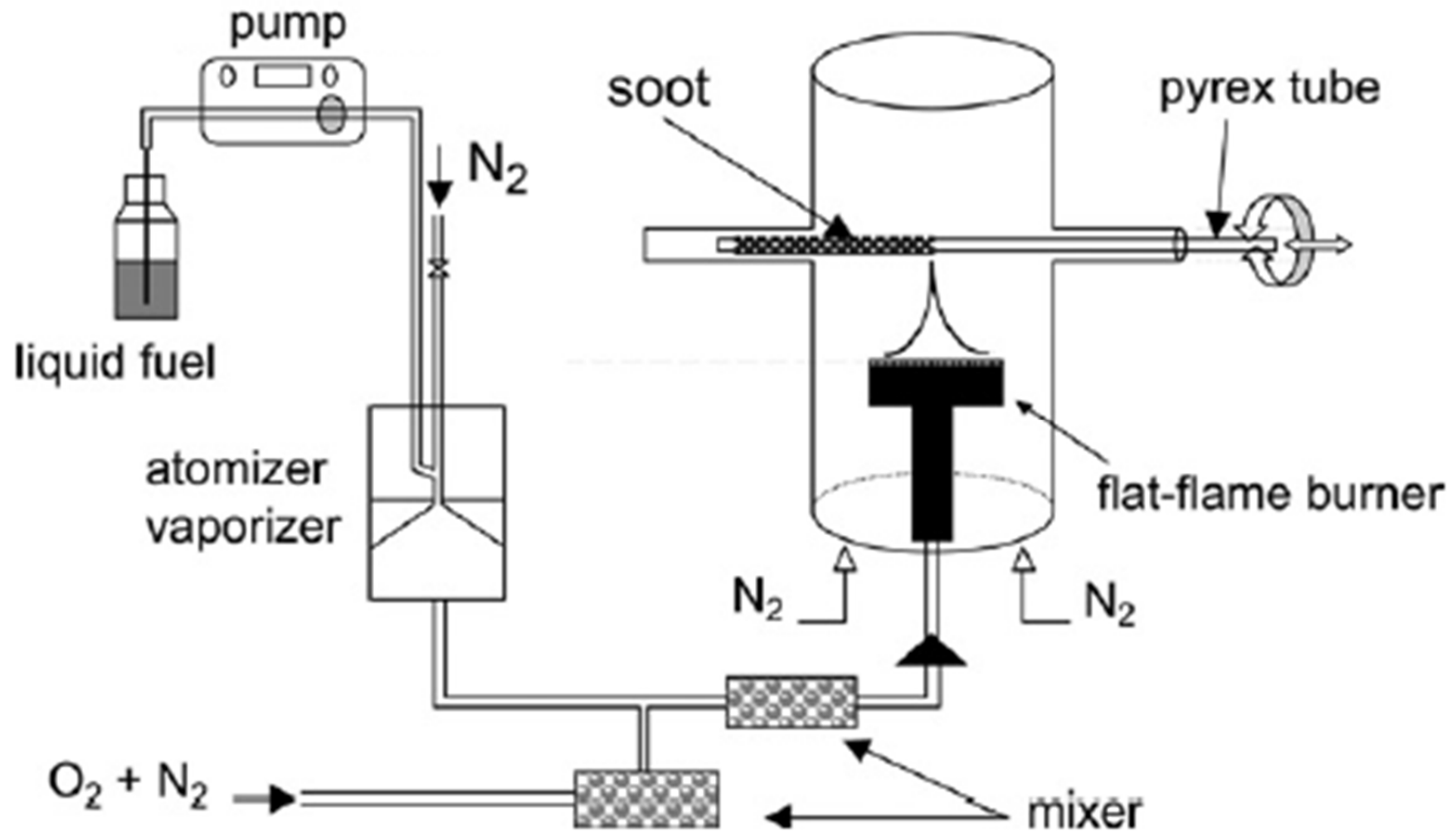


For propene, the early formation of benzene involves a **C₃ route**: the recombination of allyl radicals, formed by H-atom abstraction from propene, producing 1,5-hexadiene



From P. Dagaut and M. Cathonnet. A comparative study of the kinetics of benzene formation from unsaturated C₂ to C₄ hydrocarbons, Combust. Flame, 113, 620 (1998).

Pollutants from Jet A-1/biofuels combustion



Experimental set-up, premixed sooting flame.

From Dagaut et al., J. Eng. Gas Turbines Power 141, 031028-1 (2019)

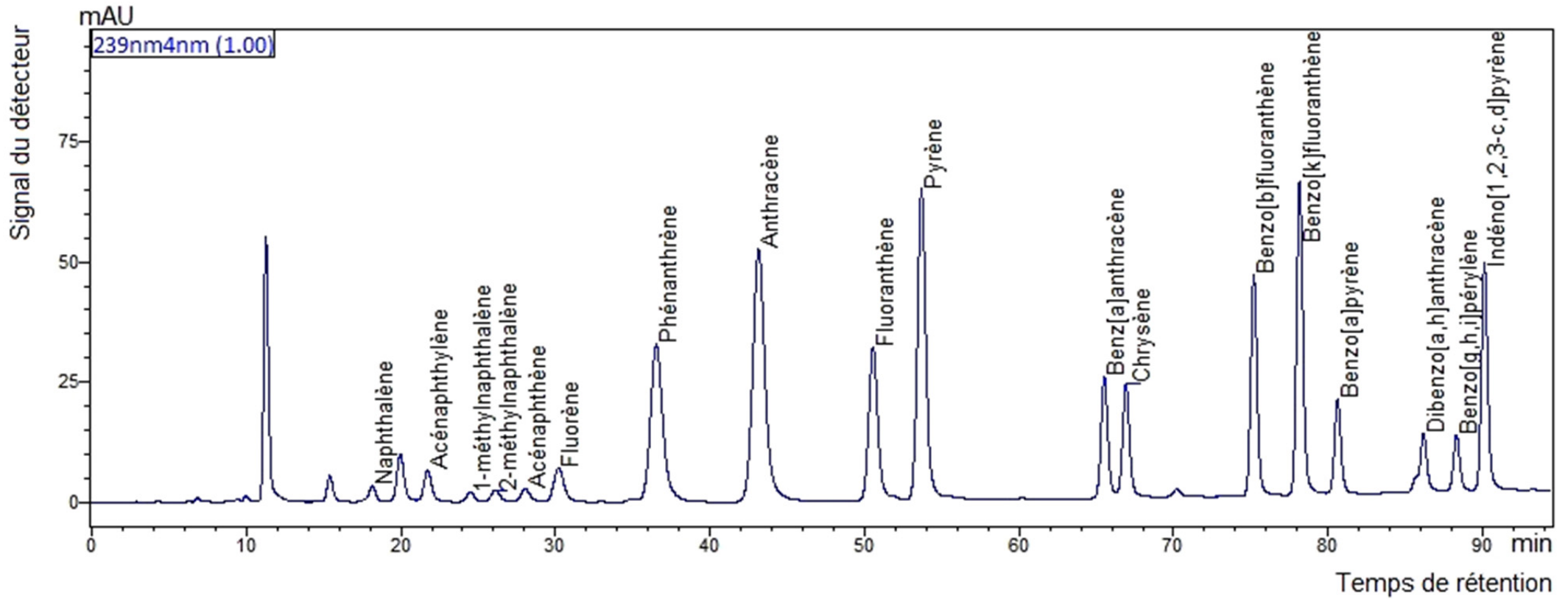
Pollutants from Jet A-1/biofuels combustion

Experimental conditions

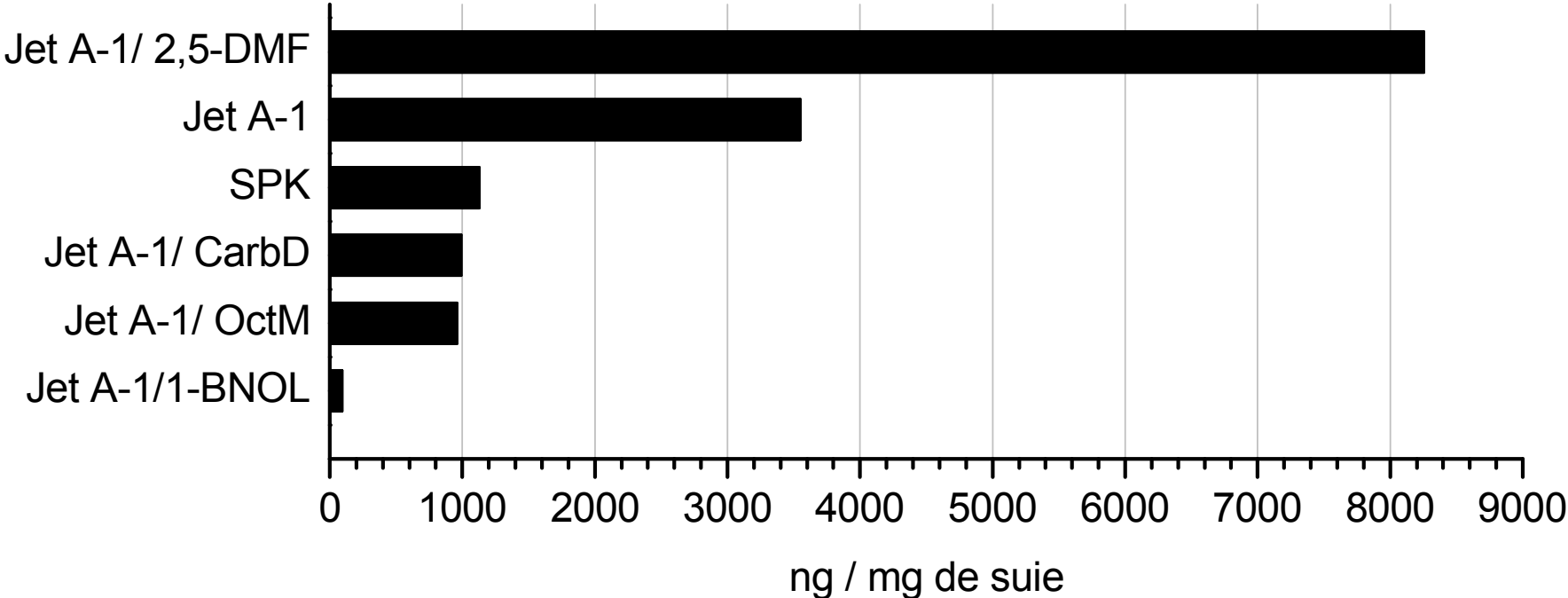
Fuel	Formula	Fuel flow rate (cm ³ . s ⁻¹)	Air flow rate (cm ³ . s ⁻¹)		E.R.
			N ₂	O ₂	
Jet A-1	C ₁₁ H ₂₂	1.58	35	11.7	2.23
Jet A-1/1-BNOL*	C _{9.6} H _{19.6} O _{0.2}	1.87	35	12.0	2.24
Jet A-1/CarbD*	C _{9.8} H _{19.6} O _{0.6}	1.80	35	11.7	2.28
Jet A-1/OctM*	C _{10.6} H _{21.2} O _{0.4}	1.68	35	11.3	2.28
Jet A-1/2,5-DMF*	C ₁₀ H _{19.2} O _{0.2}	1.70	35	11.2	2.23

* Jet A-1/additif 80:20 v/v

HPLC Chromatogram showing 18 HAPs after extraction



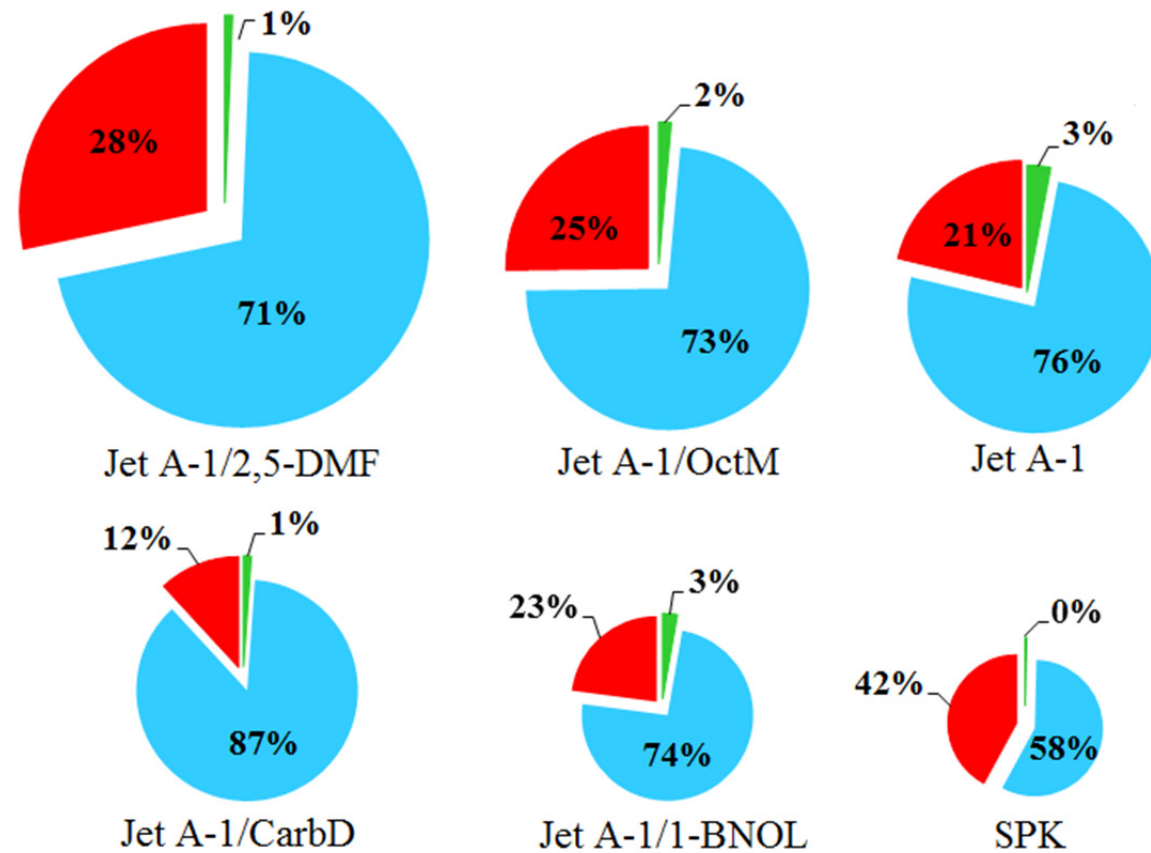
Pollutants from Jet A-1/biofuels combustion



Concentration of 18 HAPs on soot particles



Pollutants from Jet A-1/biofuels combustion



- Fraction massique des HAPs de petite taille
- Fraction massique des HAPs de taille moyenne
- Fraction massique des HAPs de grande taille

Contribution of ≠ classes of PAHs to total amount of PAHs on soot (Shahla, 2015)

Pollutants from Jet A-1/biofuels combustion

Global toxicity of soot samples*

Fuel	Equivalent toxicity(TEQ)	Variation to Jet A-1 %
Jet A-1/1-BNOL	1,294	-99
Jet A-1/CarbD	10,834	-94
Jet A-1/OctM	83,976	-57
SPK	115,904	-40
Jet A-1	193,574	0
Jet A-1/2,5-DMF	574,136	+197

From Shahla (2015)

*Nisbet et Lagoy (*Regulatory Toxicology and Pharmacology*, vol. 16, pp. 290-300, 1992) defined a global equivalent toxicity:

$$TEQ = \left(\sum_{i=HAP} C_i \times TEF_i \right) \cdot f$$

Effect of trace species on ignition: NO_x, ozone

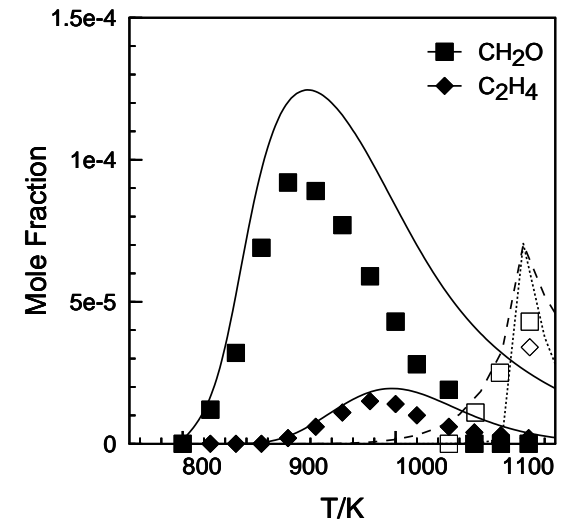
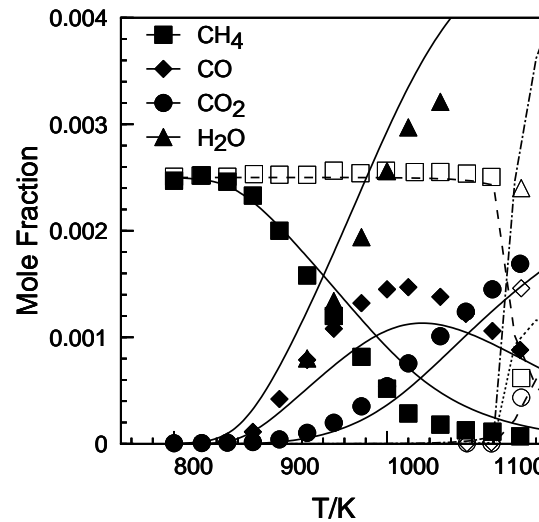
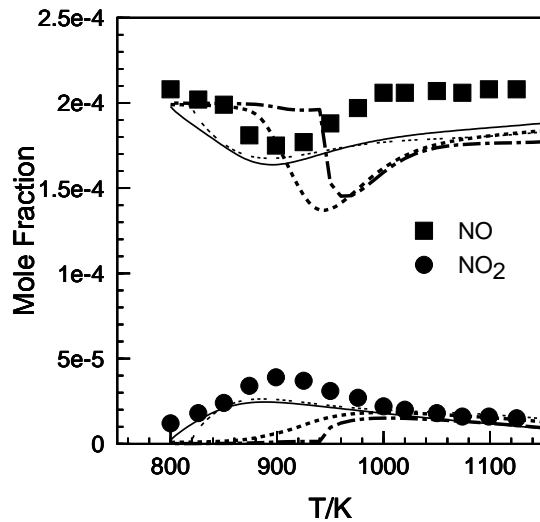
1-NO_x-HC interactions

The mutual sensitization of the oxidation of methane and NO proceeds through the NO to NO₂ conversion by HO₂ and CH₃O₂.

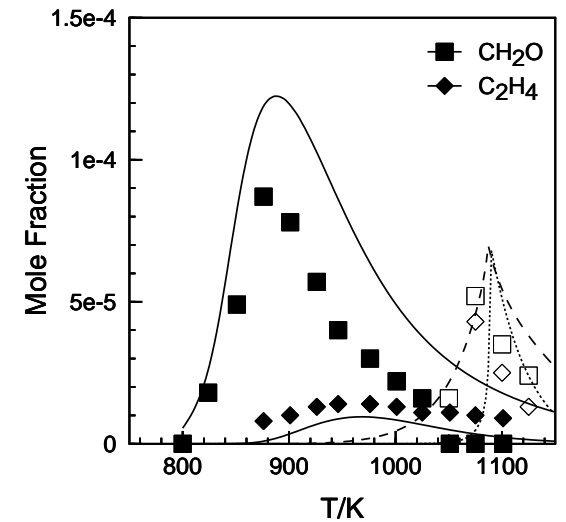
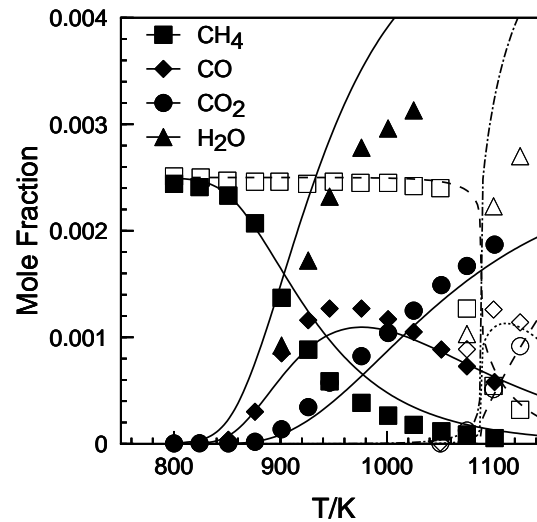
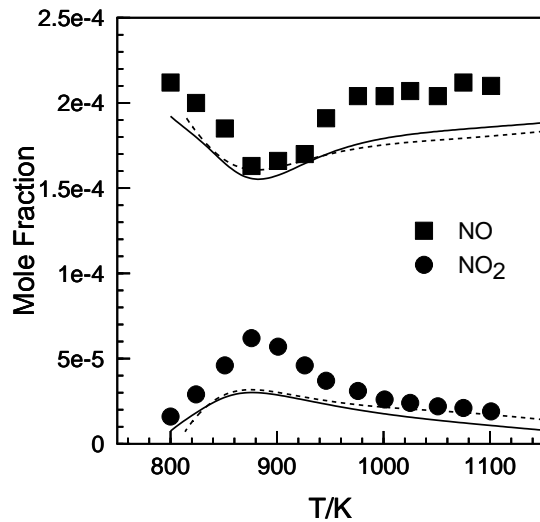
At 1-10 atm, the conversion of NO to NO₂ by CH₃O₂ is more important at low temperatures (800 K) than at higher temperatures (850-900 K) where the reaction of NO with HO₂ dominates the production of NO₂.

The NO to NO₂ conversion is enhanced by the production of HO₂ and CH₃O₂ radicals from the oxidation of the fuel. The production of OH resulting from the oxidation of NO promotes the oxidation of the fuel : NO + HO₂ => OH+ NO₂ is followed by OH + CH₄ => CH₃. At low temperature, the reaction further proceeds via CH₃ + O₂ => CH₃O₂; CH₃O₂ + NO => CH₃O + NO₂. At higher temperature, the production of CH₃O involves NO₂ : CH₃ + NO₂ => CH₃O.

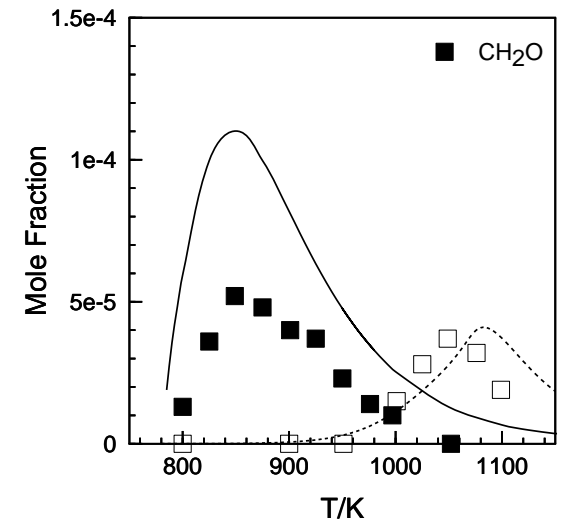
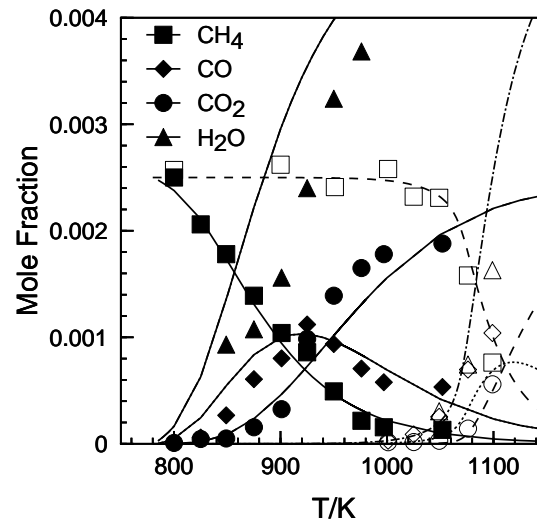
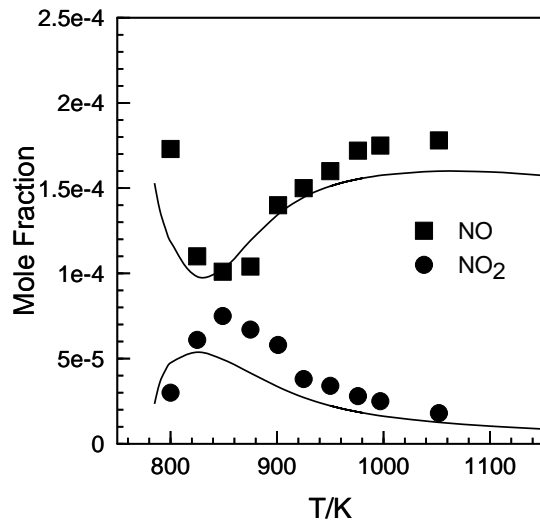
The sequence of reactions: CH₃O => CH₂O + H; CH₂O +OH => HCO; HCO + O₂ => HO₂ and H + O₂ => HO₂. => CH₂O + H; CH₂O +OH => HCO; HCO + O₂ => HO₂ and H + O₂ => HO₂.



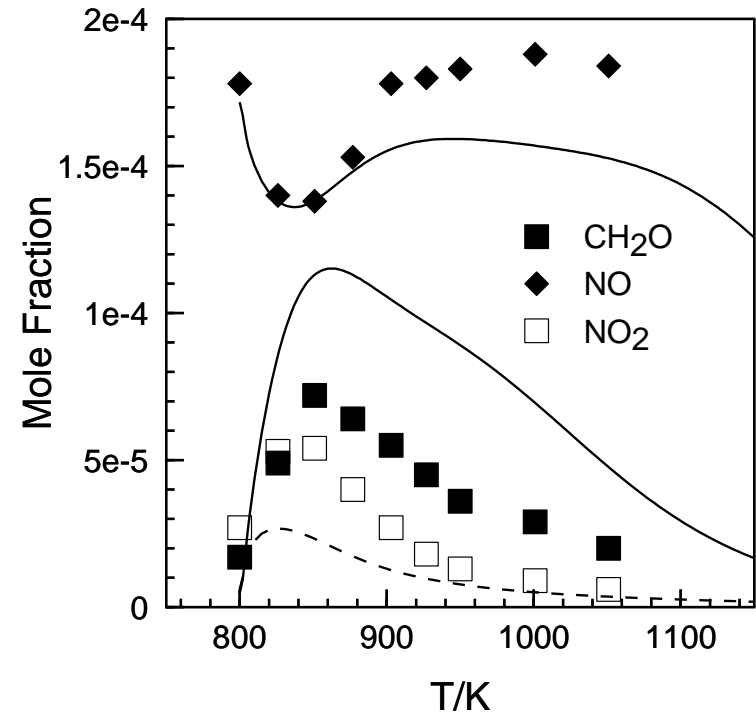
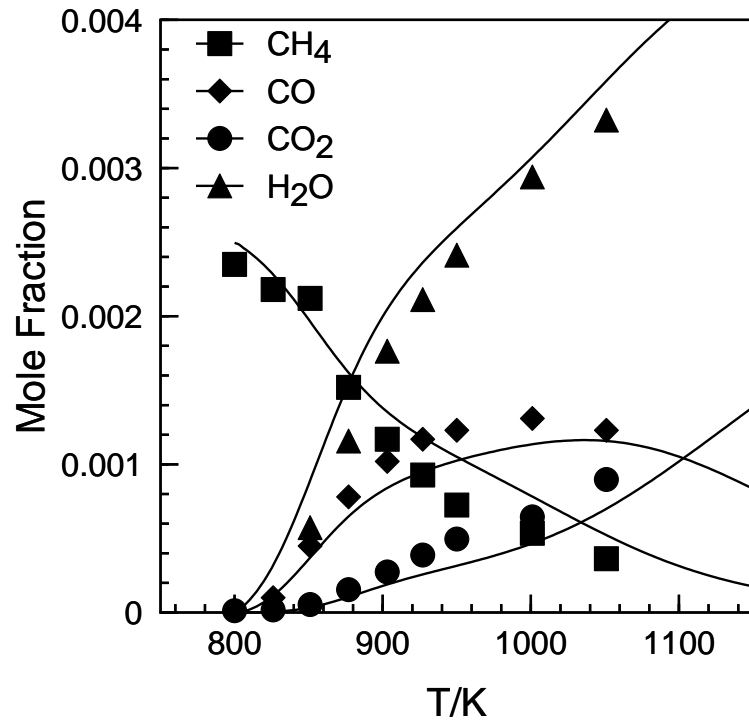
The mutual sensitization of the oxidation of methane and NO in a JSR at 1 atm: Effect of the introduction of 200ppm of NO on the oxidation of methane in fuel-lean conditions ($\phi=0.1$, 2500 ppm of CH_4 , 50000 ppm of O_2 , $t=120$ ms). (a): The dashed-dotted line represents the results obtained with the mechanism and thermochemical data of [Hori 2002]. The results obtained with the mechanism and thermochemical data of [Hori 1998] are presented as dashed lines, those using [Faravelli 2003] as a dotted line (... ..), the results of the proposed model are presented as full lines. In (b) and (c): The filled symbols and the continuous lines refer respectively to the data and the simulations (proposed scheme) with NO added; the open symbols and dotted lines refer respectively to the data and simulations (proposed scheme) without NO.



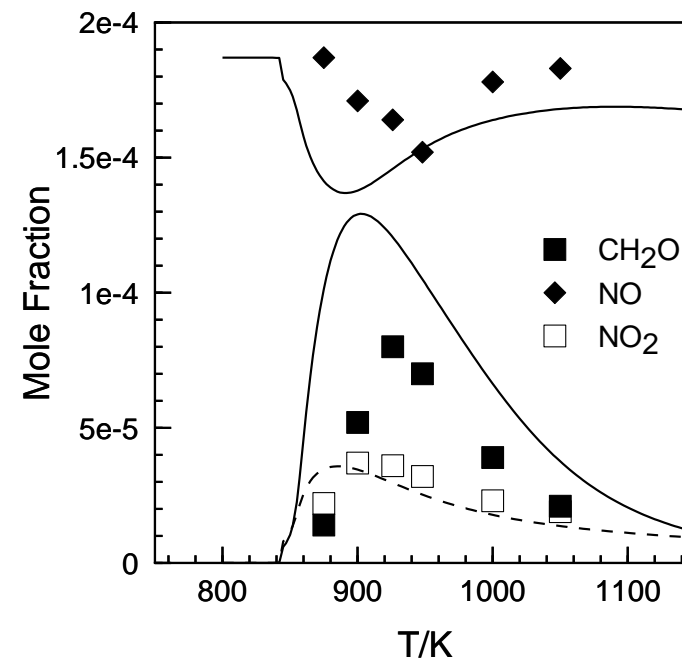
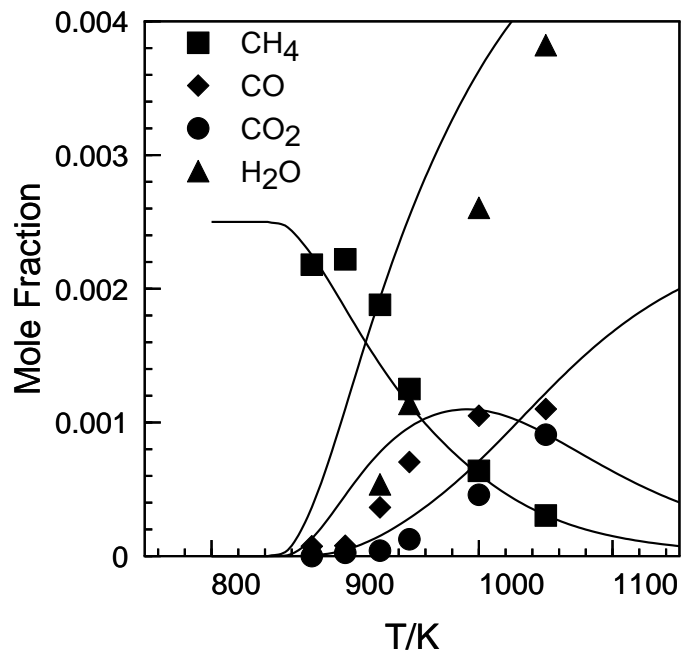
The mutual sensitization of the oxidation of methane and NO in a JSR at 1 atm: Effect of the introduction of 200ppm of NO on the oxidation of methane in fuel-lean conditions ($\phi=0.1$, 2500 ppm of CH_4 , 50000 ppm of O_2 , $t=240$ ms). (a) The experimental results (symbols) are compared to the computations (dashed lines using the model of [Faravelli 2003], continuous line for this work). In (b) and (c): The filled symbols and the continuous lines refer respectively to the data and simulations with NO added; the open symbols and dotted lines refer respectively to the data and simulations without NO.



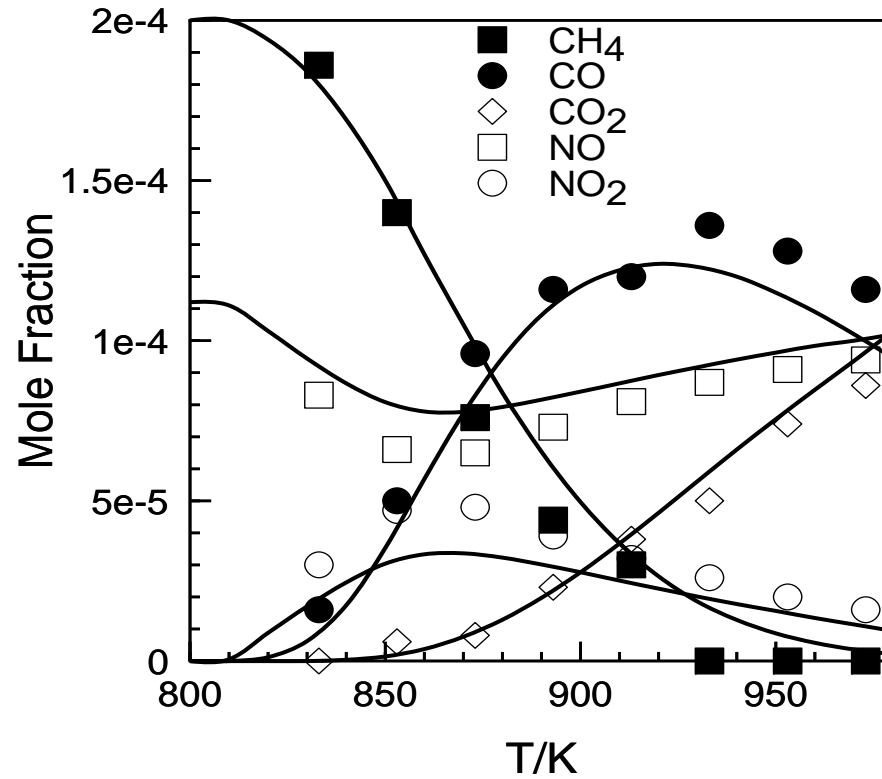
The mutual sensitization of the oxidation of methane and NO in a JSR at 10 atm: Effect of the introduction of 200ppm of NO on the oxidation of methane in fuel-lean conditions ($\phi=0.5$, 2500 ppm of CH_4 , 10000 ppm of O_2 , $t=1000$ ms). (a) The NO_x experimental results are compared to the computations. (b) and (c): The filled symbols and the continuous lines refer respectively to the data and simulations with NO added; the open symbols and dotted lines refer respectively to the data and simulations without NO.



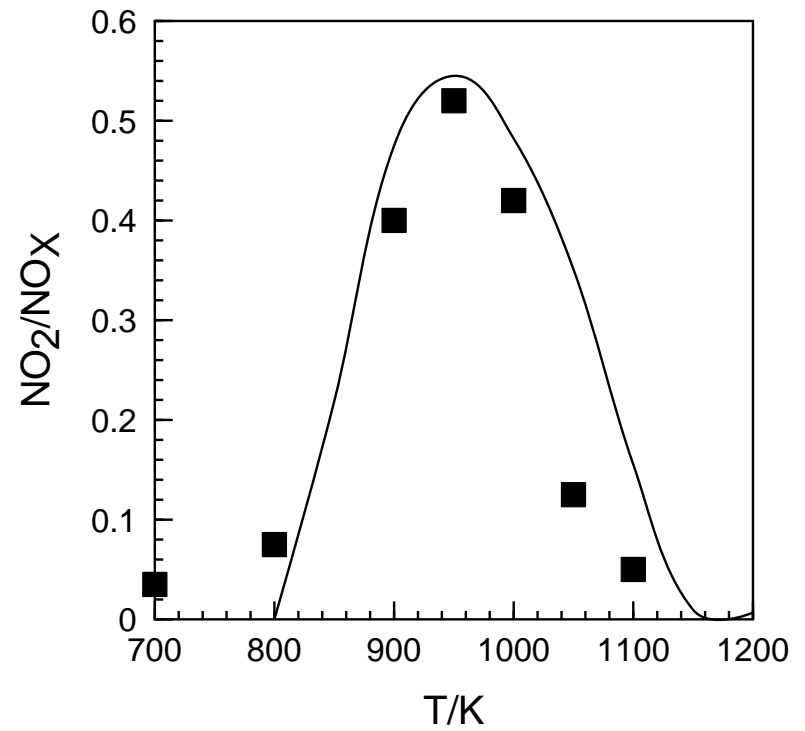
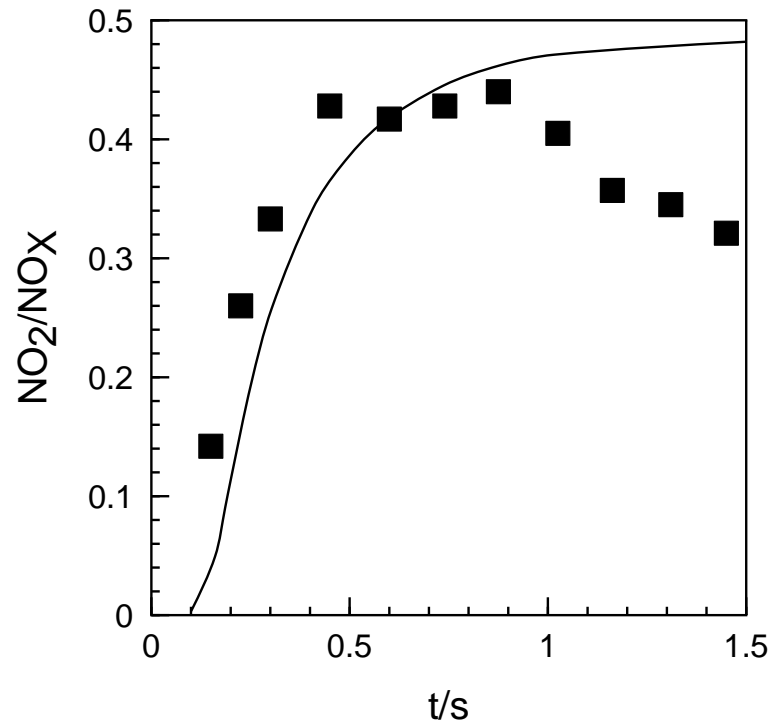
The mutual sensitization of the oxidation of methane and NO in a JSR at 10 atm (200 ppm of NO, $\phi=1$, 2500 ppm of CH₄, 5000 ppm of O₂, $t=1000$ ms). Comparison between modeling (lines) and experiments (symbols).



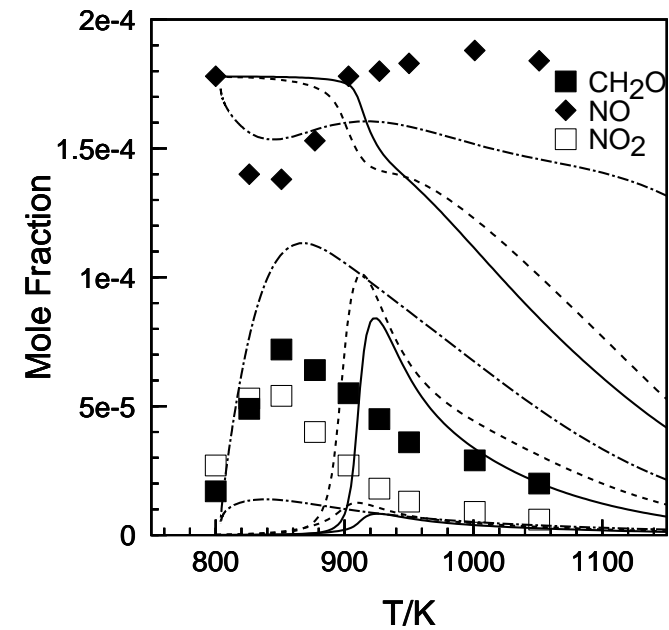
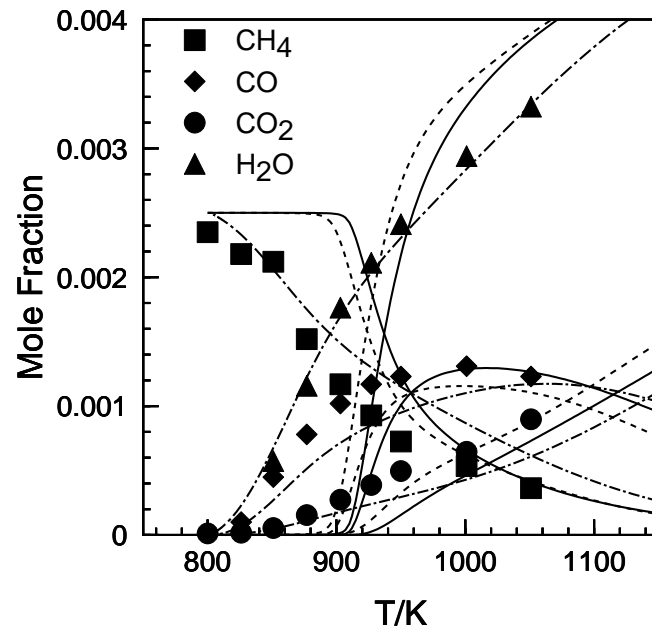
The mutual sensitization of the oxidation of methane and NO in a JSR at 10 atm (200 ppm of NO, $\phi=0.5$, 2500 ppm of CH₄, 10000 ppm of O₂, $t=240$ ms). Comparison between modeling (lines) and experiments (symbols).



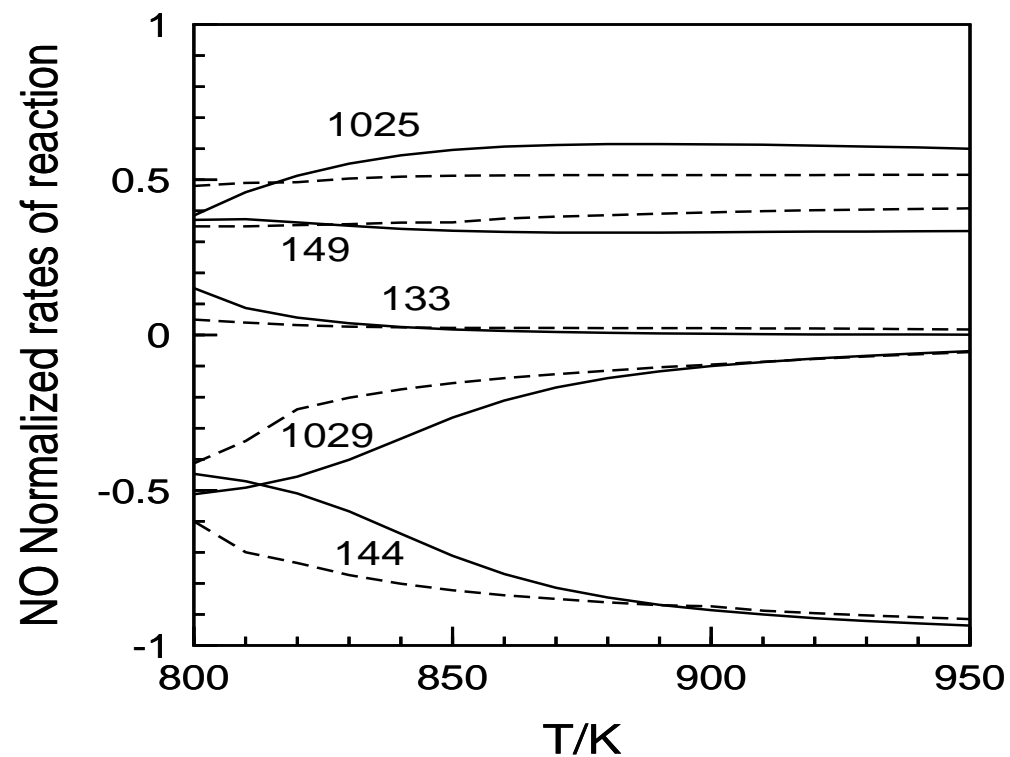
The mutual sensitization of the oxidation of methane and NO in a tubular flow reactor at 1 atm (112 ppm of NO, 200 ppm of CH₄, 5% of O₂, t=2.8 s). Comparison between modeling (lines) and experiments (symbols).



Comparison between this modeling (lines) and experimental data (symbols) obtained in a tubular flow reactor at 1000 K [Hori 1998] (initial conditions: 20 ppm of NO and 50 ppm of methane in air).

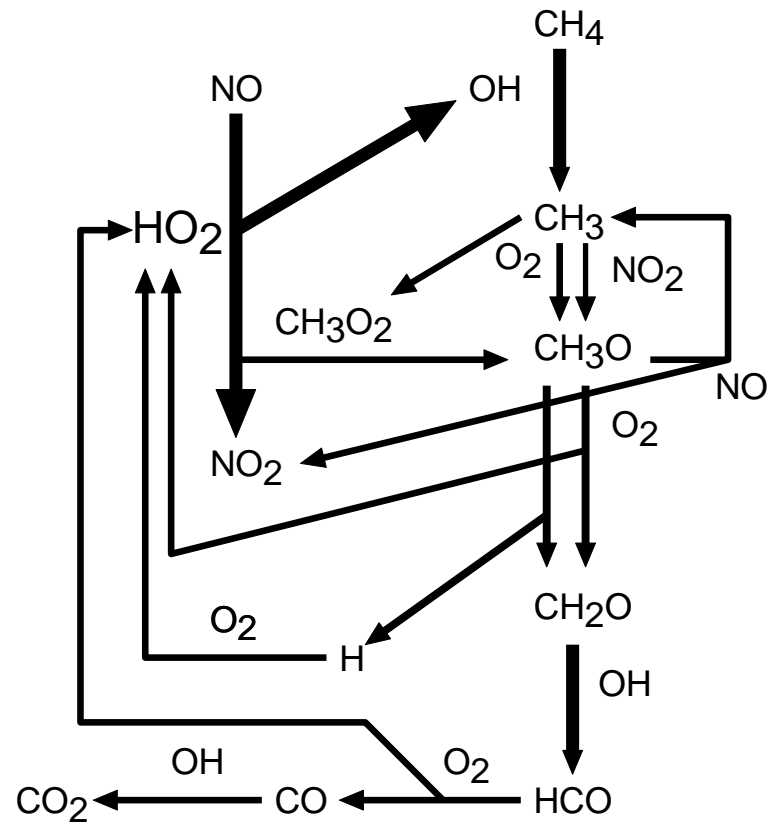


The mutual sensitization of the oxidation of methane and NO in a JSR at 10 atm (200ppm of NO, $\phi=1$, 2500 ppm of CH₄, 5000 ppm of O₂, t=1000 ms). Comparison between modeling results using the mechanism and thermochemical data of [Hori 1998] (continuous line), [Hori 2002] (dashed lines), [Faravelli 2003] (dash-dot line) and experiments (symbols).

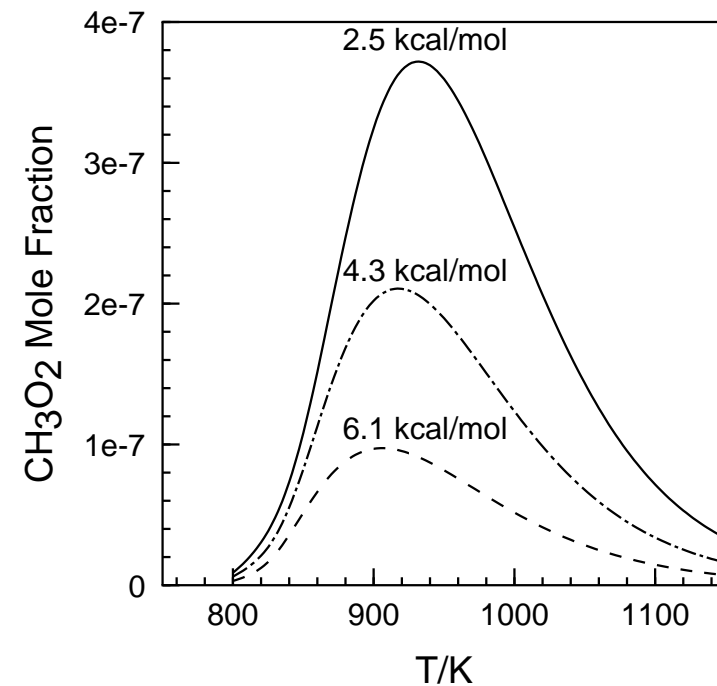
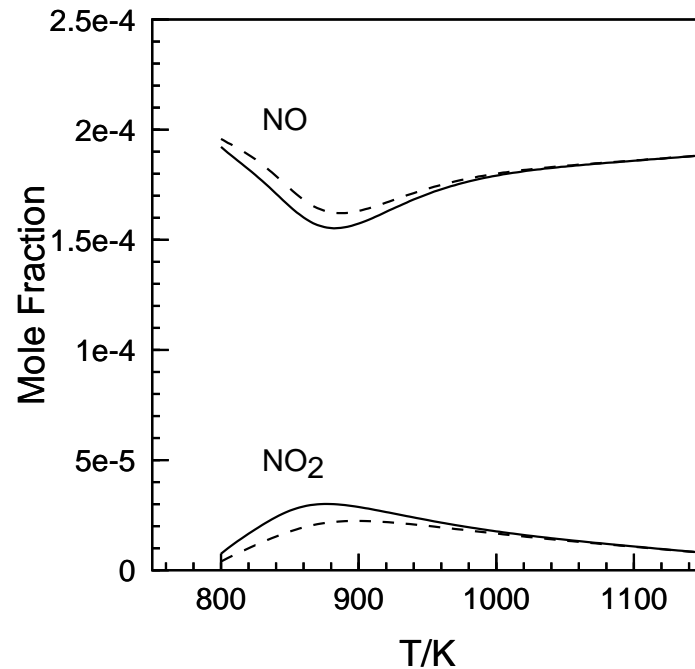


Normalized rates of reaction of NO at 1 atm (continuous lines) and 10 atm (dotted lines).

$\text{HNO} + \text{NO}_2 = \text{NO} + \text{HONO}$ (133); $\text{NO} + \text{HO}_2 = \text{NO}_2 + \text{OH}$ (144); $\text{NO}_2 + \text{H} = \text{NO} + \text{OH}$ (149);
 $\text{CH}_3 + \text{NO}_2 = \text{CH}_3\text{O} + \text{NO}$ (1025); $\text{CH}_3\text{O}_2 + \text{NO} = \text{CH}_3\text{O} + \text{NO}_2$ (1029)



Schematic representation of the reaction paths involved in the mutual sensitization of the oxidation of methane and NO.



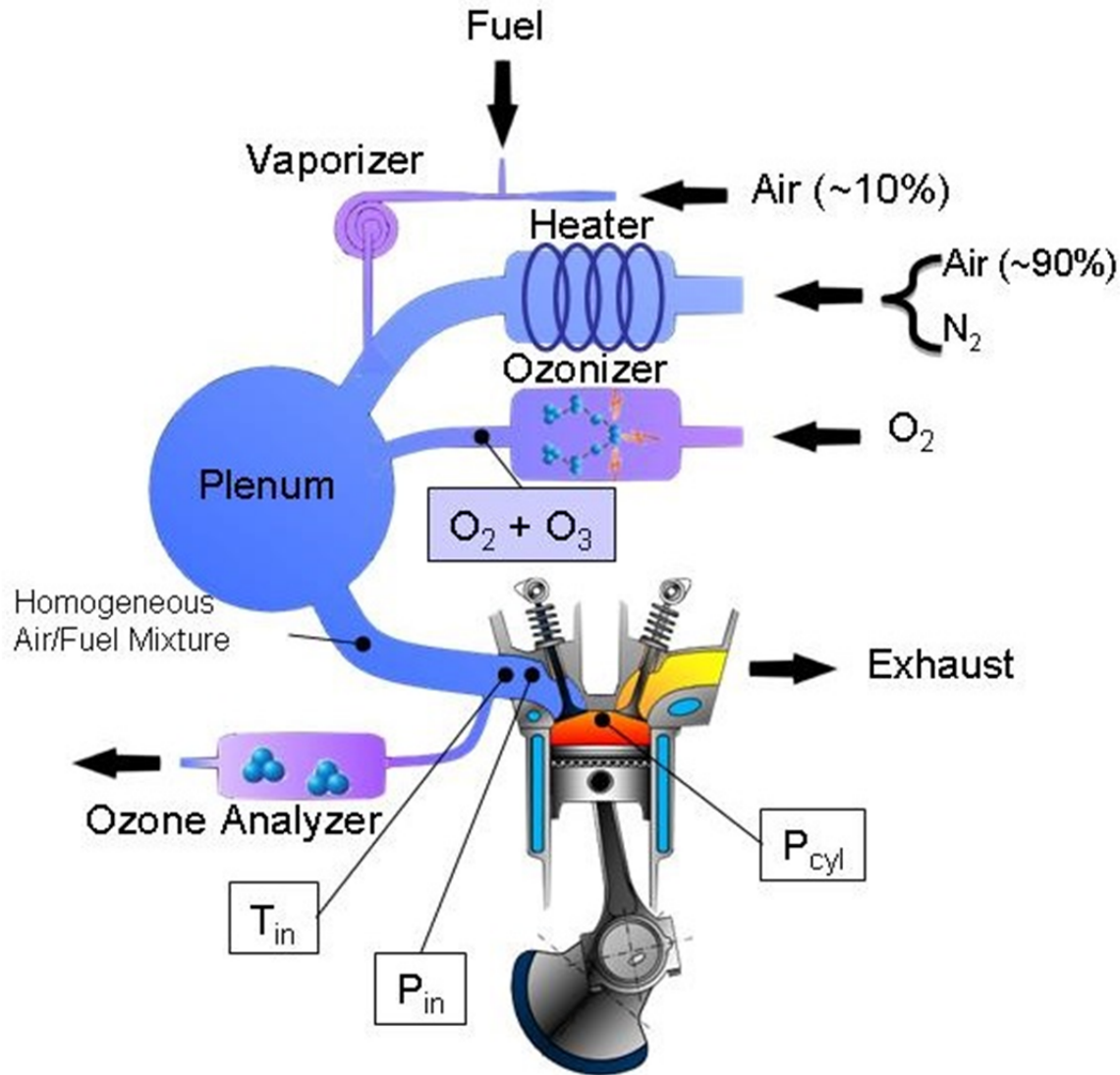
Sensitivity of the computations to the heat of formation of the methylperoxy radical (initial conditions: 2500 ppm of methane, 50000 ppm of oxygen, 200 ppm of nitric oxide, $\phi=0.1$, 240 ms). The upper value of ΔH°_{298} (CH_3O_2) used was 6.1 kcal/mole (dashed lines) and the lower value was 2.5 kcal/mole (continuous lines).

M. Hori, N. Matsunaga, N.M. Marinov, J.W. Pitz, C.K. Westbrook, Proc. Combust. Inst. 27 (1998) 389-396.

M. Hori, Y. Koshiishi, N. Matsunaga, P. Glaude, N. Marinov, Proc. Combust. Inst. 29 (2002) 2219-2226.

T. Faravelli, A. Frassoldati, E. Ranzi, Combust. Flame 132 (2003) 188-207.

HCCI control via Sensitization by ozone ($O_3 \rightarrow O_2 + O$)



Engine Characteristics

Bore	85 mm
Stroke	88 mm
Displaced Volume	499 cc
Connecting Rod	145 mm
Compression Ratio	16:1

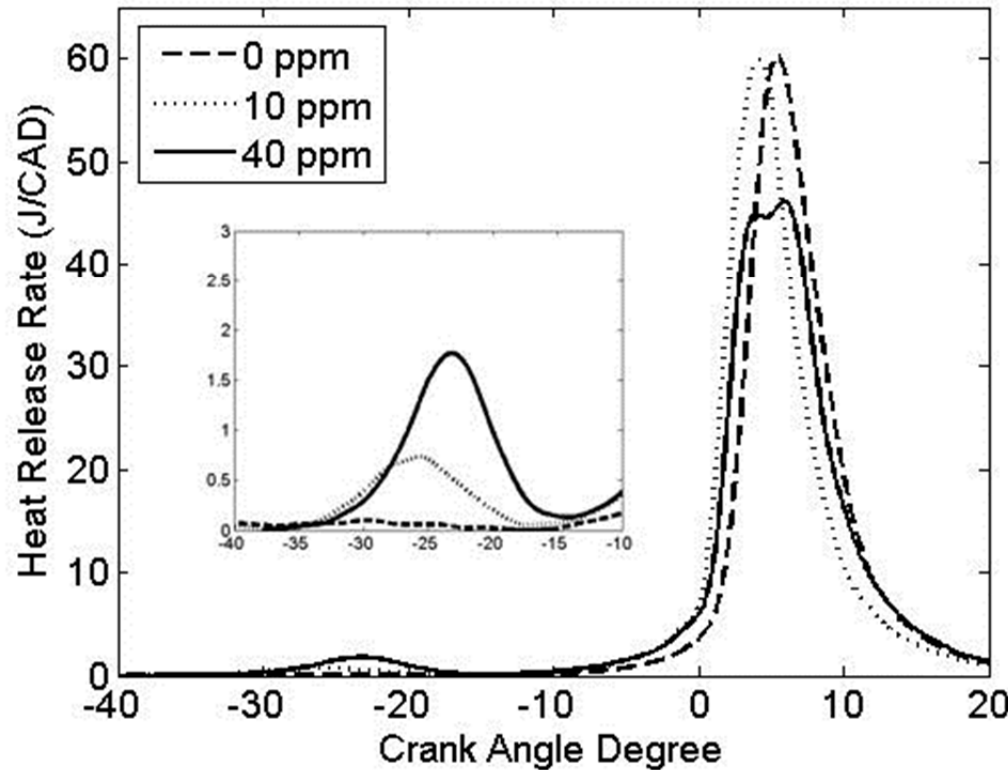
All the results presented were conducted for :

- Constant rotation speed : 1500 rpm
- Constant equivalence ratio 0.3

Masurier et al., ICE2013

Results: HCCI control via Sensitization by ozone ($O_3 \rightarrow O_2 + O$)

Heat release rates analysis at low temperature with ozone seeding



Experimental conditions :

- Intake pressure : 1.3 bar
- CA50 : ~5 CAD
- Ozone : 0, 10 and 40 ppm

Observations :

- A cool flame occurs with a low HRR.
- Ozone mainly acts on early fuel oxidation

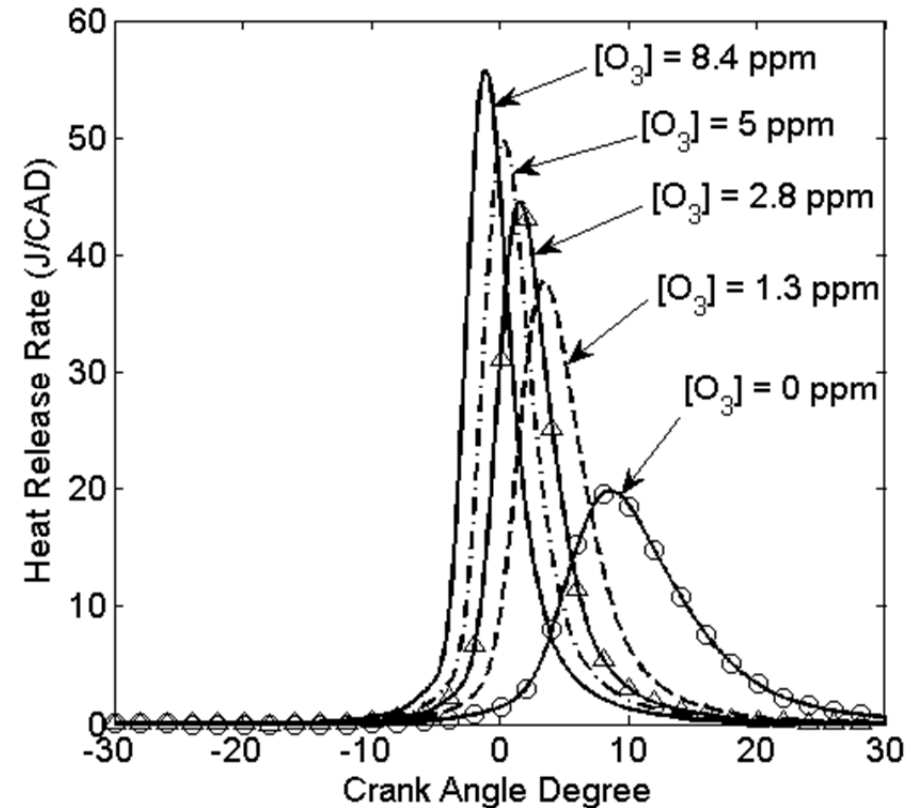
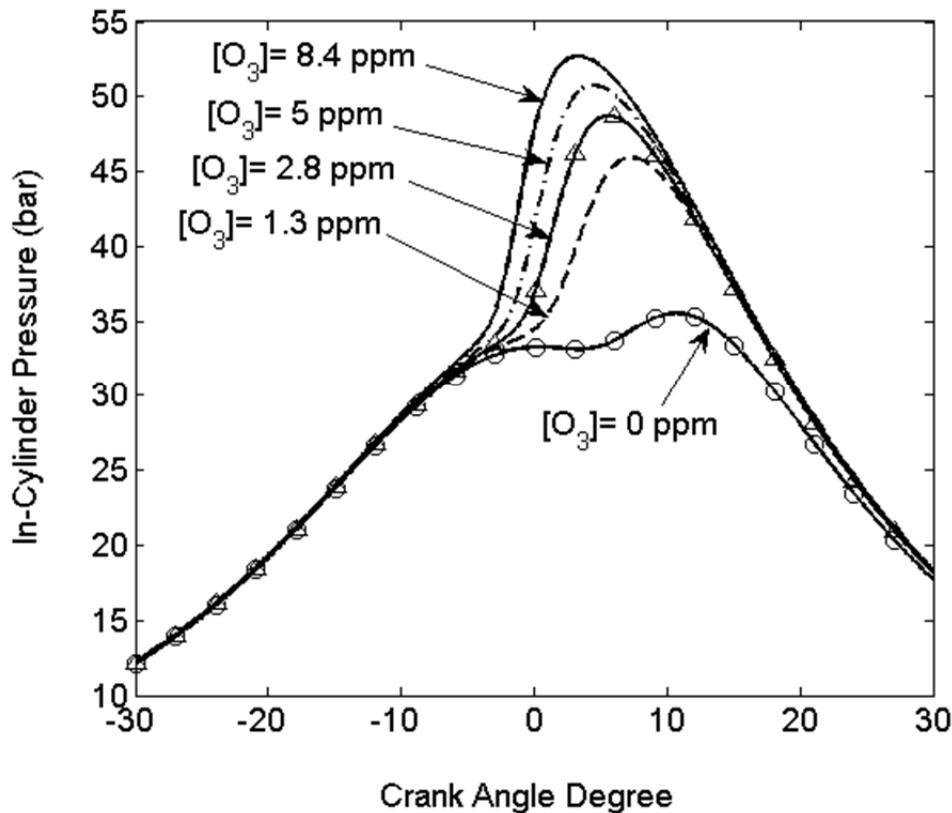
Masurier et al., ICE2013

w/o O_3 : $O_2 + \text{fuel} \rightarrow HO_2 + R$ followed by $HO_2 + \text{fuel} \rightarrow H_2O_2 + R$ (slow)

with O_3 : $O + \text{fuel} \rightarrow OH + R$ followed by $OH + \text{fuel} \rightarrow H_2O + R$ (FAST)

Results: HCCI control via Sensitization by ozone ($O_3 \rightarrow O_2 + O$)

In-cylinder pressures and Heat release rates

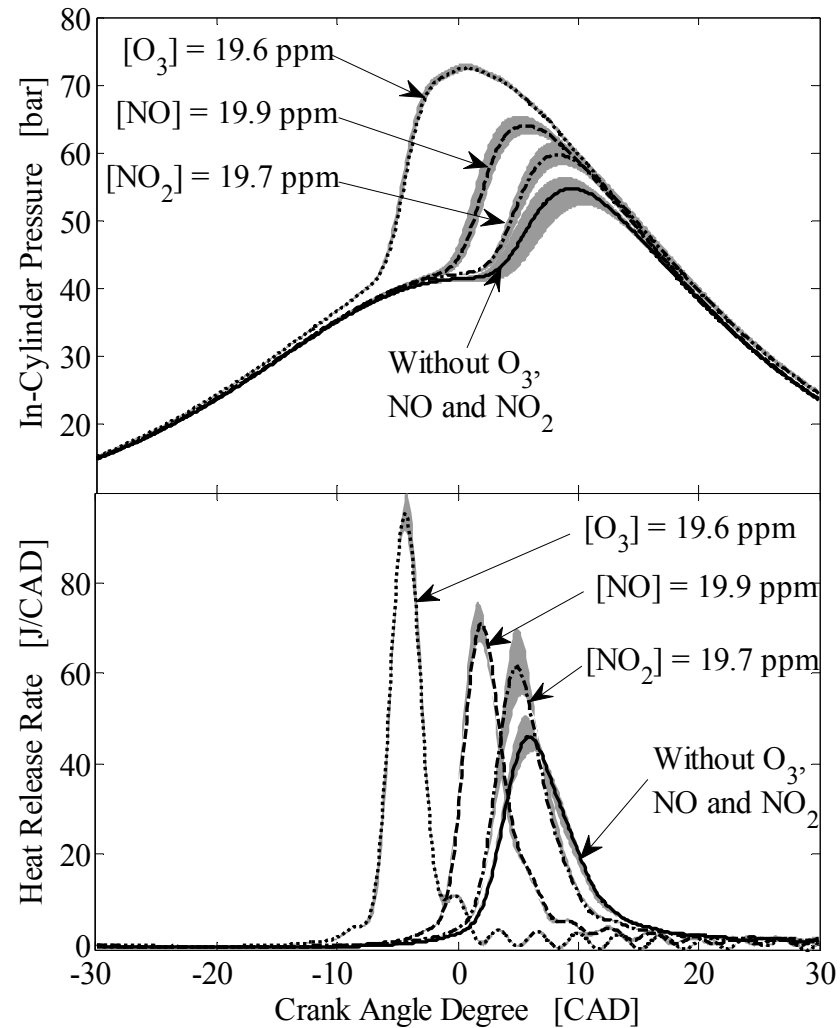


Masurier et al., ICE2013

w/o O₃: $O_2 + \text{fuel} \rightarrow HO_2 + R$ followed by $HO_2 + \text{fuel} \rightarrow H_2O_2 + R$ (slow)

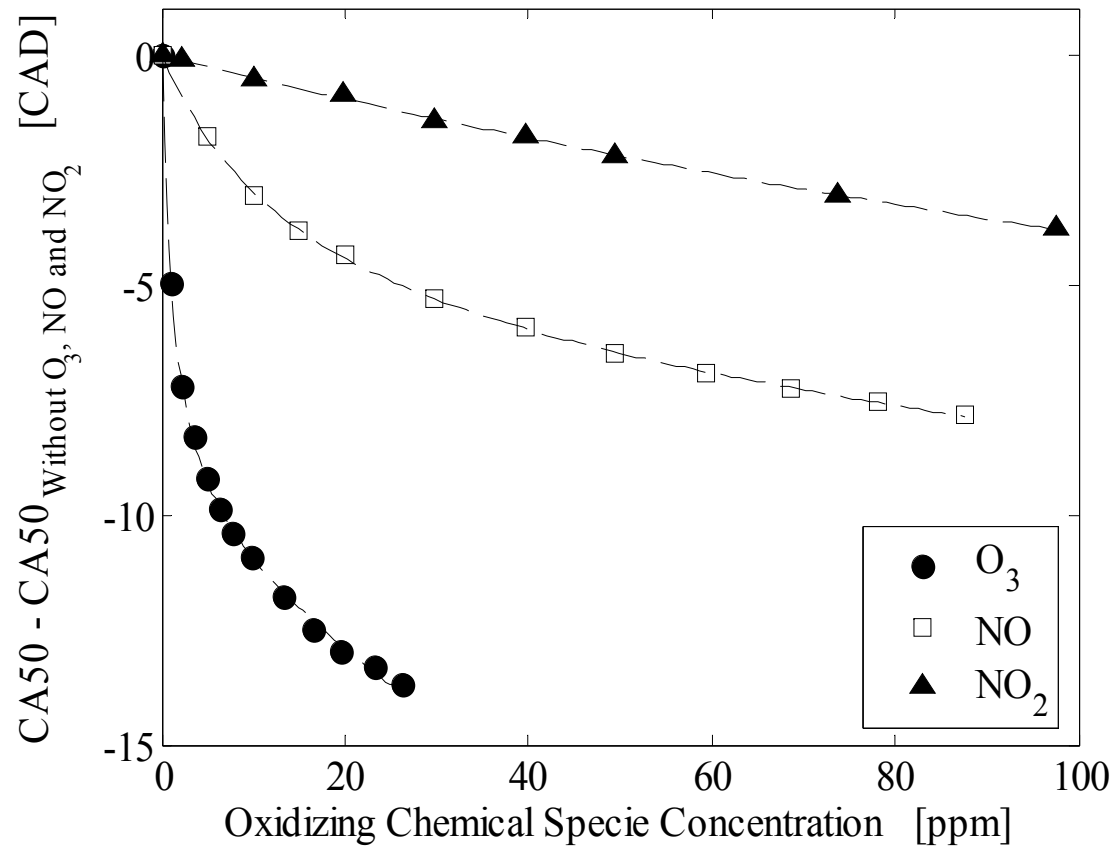
with O₃: $O + \text{fuel} \rightarrow OH + R$ followed by $OH + \text{fuel} \rightarrow H_2O + R$ (FAST)

Results: HC/CI control via Sensitization by Ozone, NO, and NO₂



In-cylinder pressure and heat release rate traces without any species and with 20 ppm of each species separately injected. *Masurier et al., SIC 35/ PROCI 2015*

HCCI control via Sensitization by Ozone, NO, and NO₂



Shift of the CA50 as a function of the three species when they are separately injected. (**CA50** is the crank angle where **50 % of the fuel has burned**) *Masurier et al., SIC 35/ PROCI 2015*

Effect on CA50: O₃>>NO>NO₂

HCCI control via Sensitization by Ozone, NO, and NO₂

Simple computations to understand the process

- **Ozone** mainly decomposes into oxygen molecules (O₂) and **O**-atoms, **FAST**. Then, the fuel reacts directly with **O**-atoms to yield **OH** radicals and rapid oxidation of the fuel ensues: $C_8H_{18}+O \rightarrow C_8H_{17}+OH$ (a) followed by $C_8H_{18}+OH \rightarrow C_8H_{17}+H_2O$ (b).



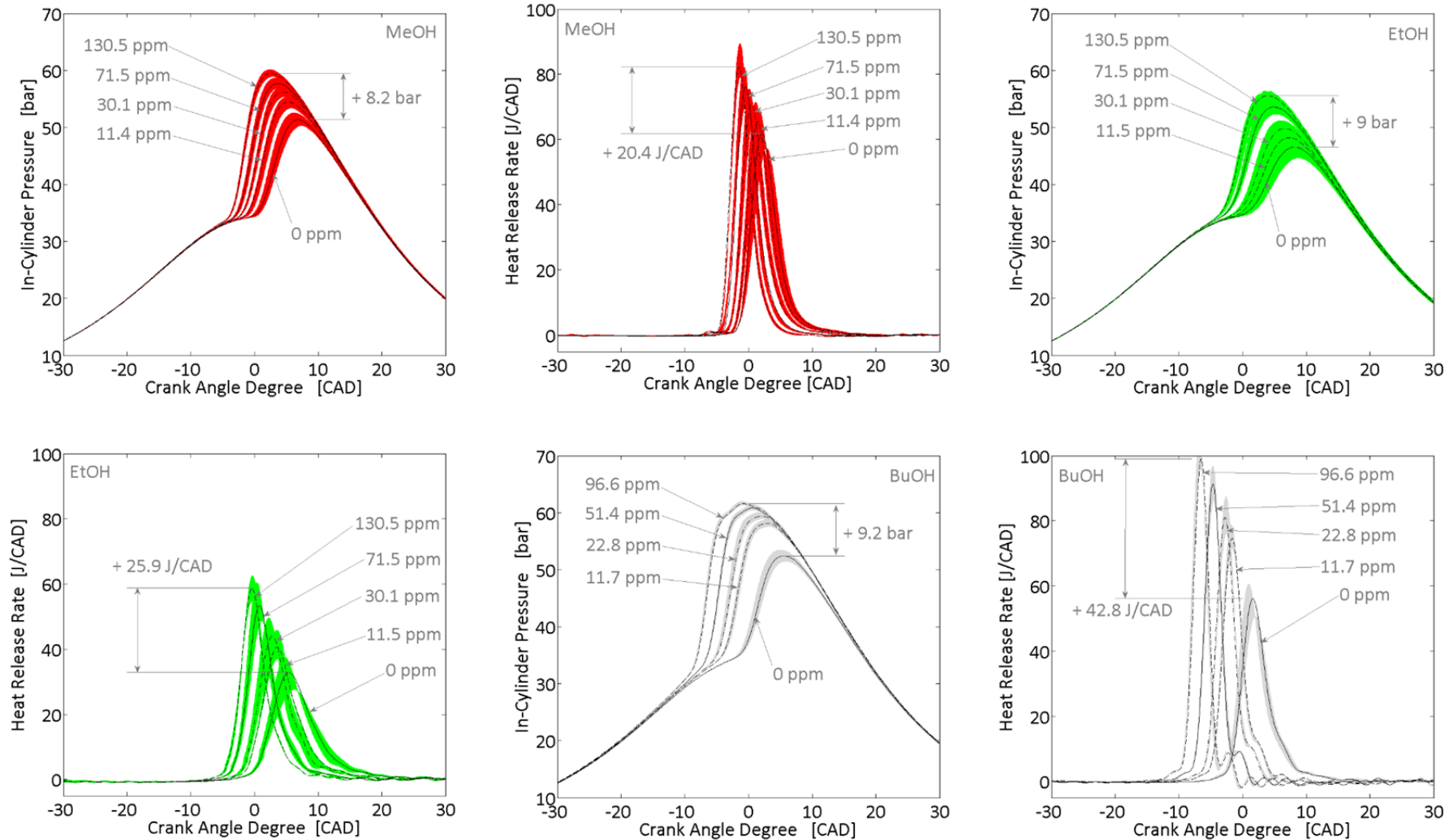
- **NO** is mostly consumed by reaction with HO₂, resulting in the initial oxidation of the fuel via $C_8H_{18}+O_2 \rightarrow C_8H_{17}+HO_2$, **SLOW**, **OH** radicals are produced via $NO+HO_2 \rightarrow NO_2+OH$, **FAST**. Subsequently, rapid fuel consumption can take place via (b) due to **OH** production. Consequently, as nitric oxide requires an HO₂ radical to yield an **OH** radical, this explains the **lower effect of NO** on ignition delays compared to ozone.



- **Nitrogen dioxide** addition: OH production results from the following reaction system: $CH_3+NO_2 \rightarrow CH_3O+NO$; $NO_2+HO_2 \rightarrow HONO+O_2$; $HONO+M \rightarrow NO+OH+M$; and $NO+HO_2 \rightarrow NO_2+OH$. As nitrogen dioxide presents intermediate reactions before OH production, its **effect on ignition delays is the lowest** of the 3 additives considered.

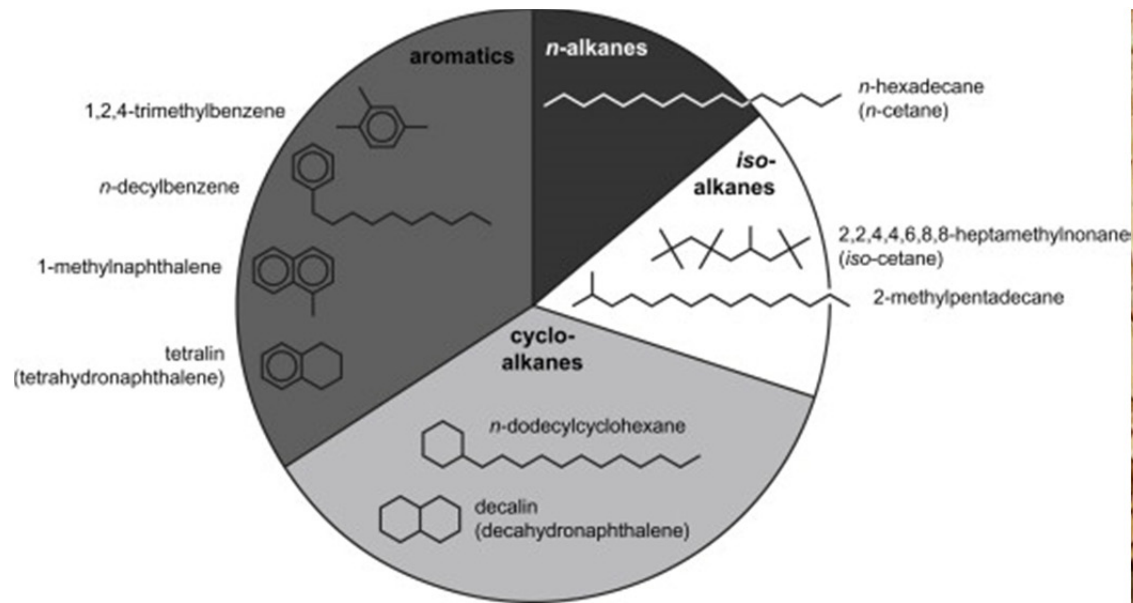


HCCI control via Sensitization by Ozone and NOx



In-cylinder pressure traces and heat release rate traces for **alcohols** as a function of the ozone input. Black curves correspond to the average of 100 cycles recorded and areas represent the variation over 100 cycles. *Masurier et al., Appl. Energ. 2016*

COMMERCIAL FUELS, SURROGATES, BIOFUELS



(from W.J.Pitz and C.J.Mueller)

MODELING USING SURROGATES/MODEL-FUELS

Surrogate model fuels* are used for the kinetic modeling to simplify the problem

DCN, fuel composition in terms of **chemical classes** and hydrocarbons concentrations, **H/C ratio**, and the **availability of valid chemical kinetic oxidation sub-models** are used to select the components of the model fuels.

DCN is a parameter related to fuel ignition

- * S. Dooley et al., *Combust. Flame* 157 (12) (2010) 2333-2339.
- F.L. Dryer, *Proc. Combust. Inst.* 35 (2015) 117-144.
- A. Agosta et al., *Exp. Thermal Fluid Sci.* 28 (7) (2004) 701-708.

Modeling using surrogates/model-fuels

The **fuel composition** impacts the relative formation of products and intermediates.

The **fuel composition** impacts radical pool and cross-reactions

The **H/C ratio** is a parameter influencing soot formation.

Threshold sooting index (TSI) is a parameter related to soot tendency

Molecular weight is a parameter related to fuel diffusivity

Validation of this approach needs extensive testing

5.1 Gasoline

Gasoline is constituted by several hundreds of components: it is not feasible to incorporate of all them in a kinetic model.

Therefore, surrogate model fuels are used to describe gasoline behavior.

In this example, 4 hydrocarbons of dominant gasoline chemical classes were chosen to represent a commercial gasoline:

iso-octane for iso-paraffins,

toluene for aromatics,

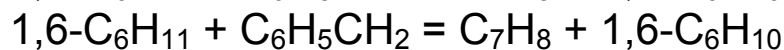
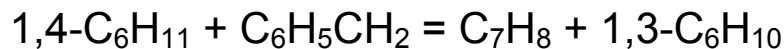
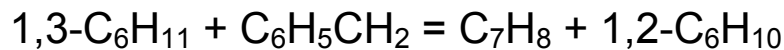
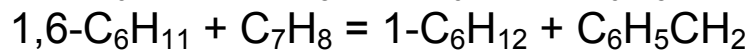
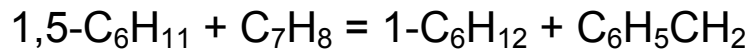
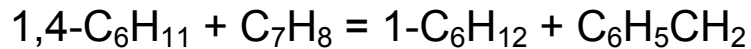
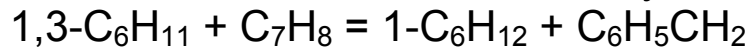
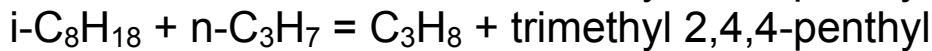
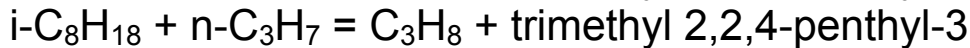
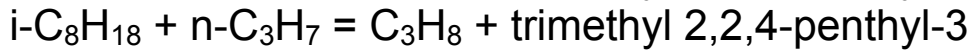
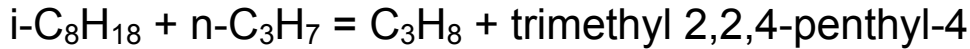
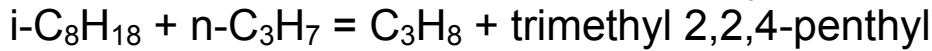
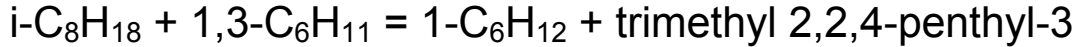
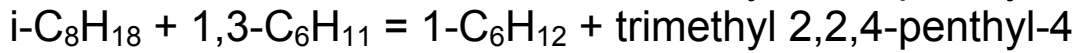
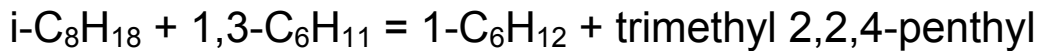
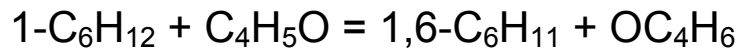
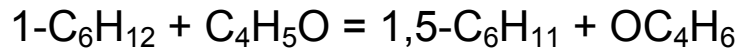
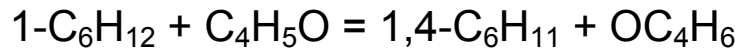
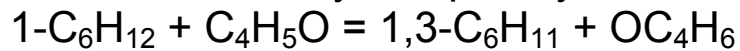
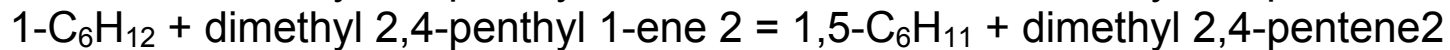
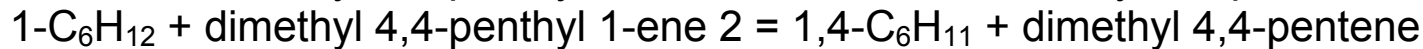
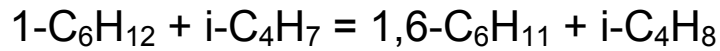
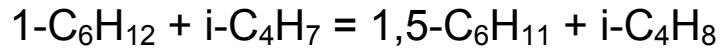
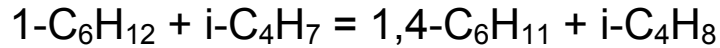
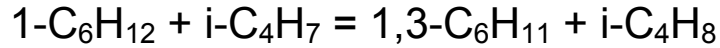
1-hexene for olefins,

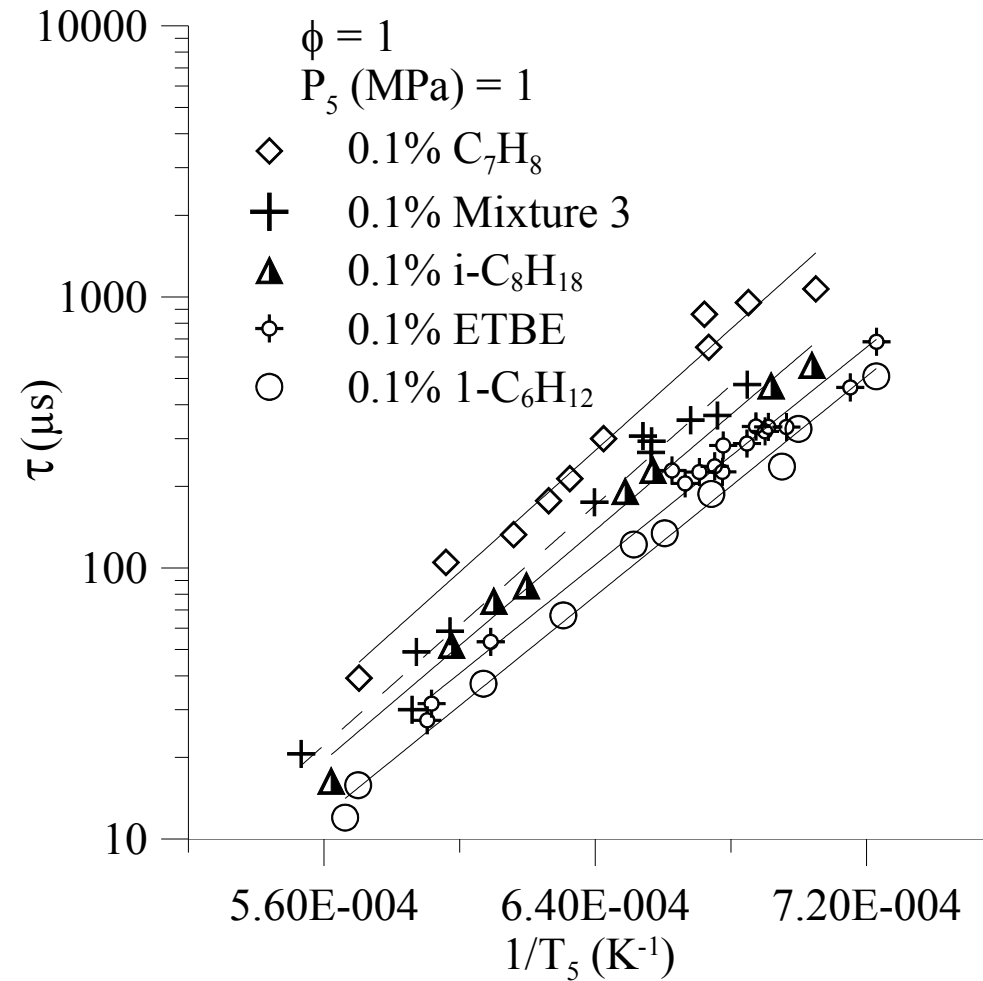
ETBE for oxygenated additives.

Mole fraction composition of the different surrogate gasoline mixtures

	Iso-octane	Toluene	1-hexene	ETBE
Mixture 1	50	35	15	0
Mixture 2	47.5	33.25	14.25	5
Mixture 3	45	31.5	13.5	10

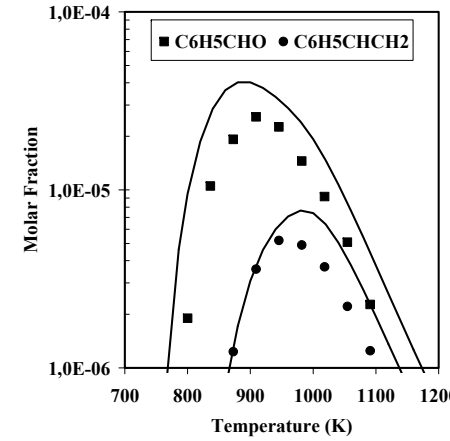
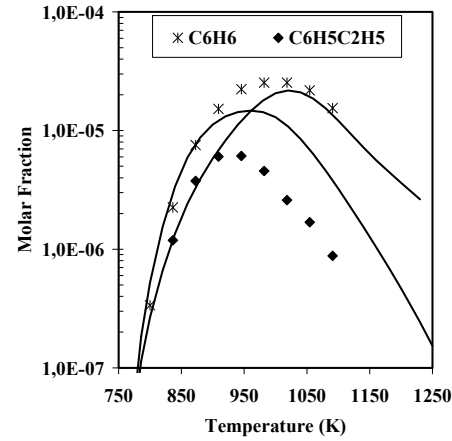
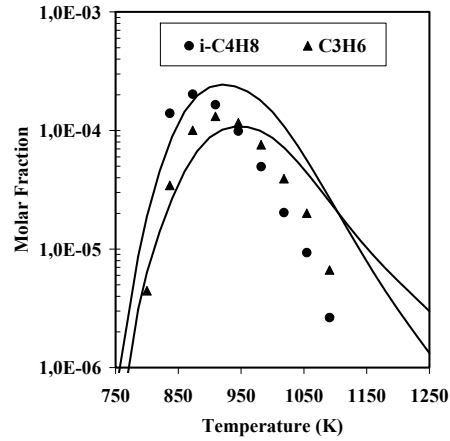
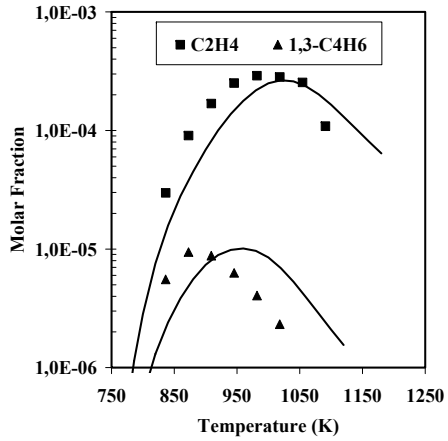
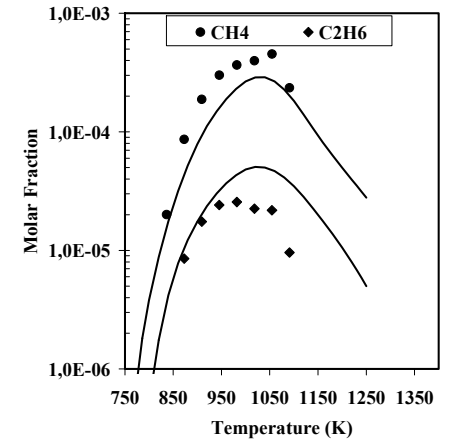
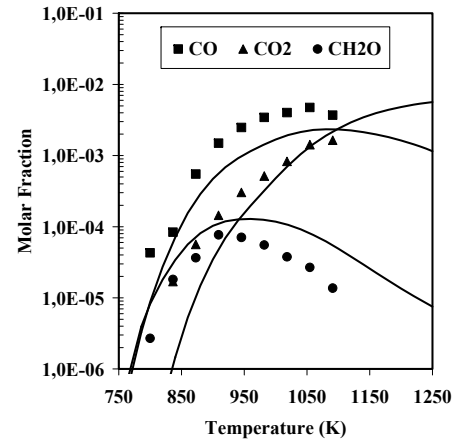
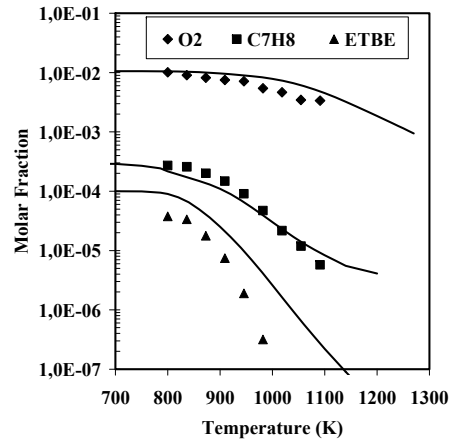
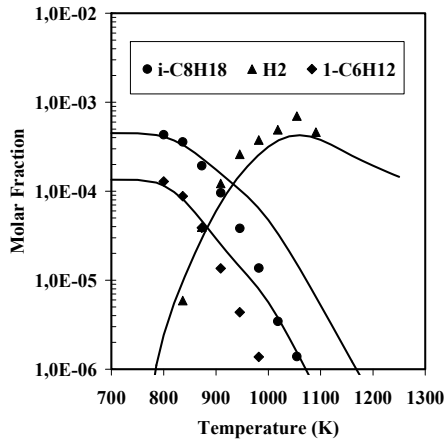
Reactions of interaction between different fuel fragments during the oxidation of surrogate mixtures.





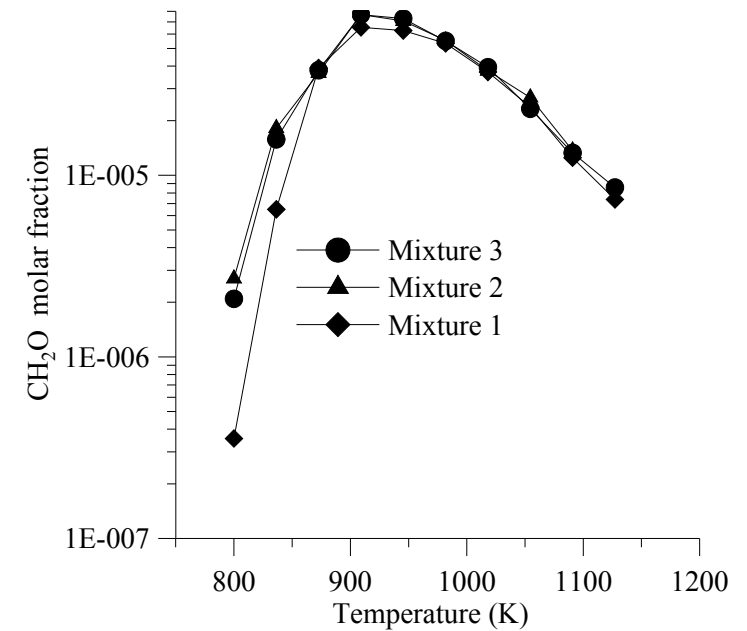
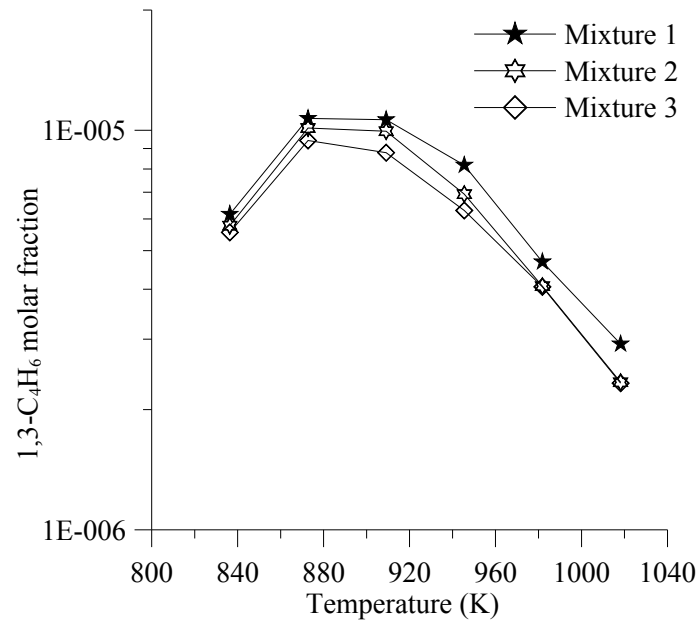
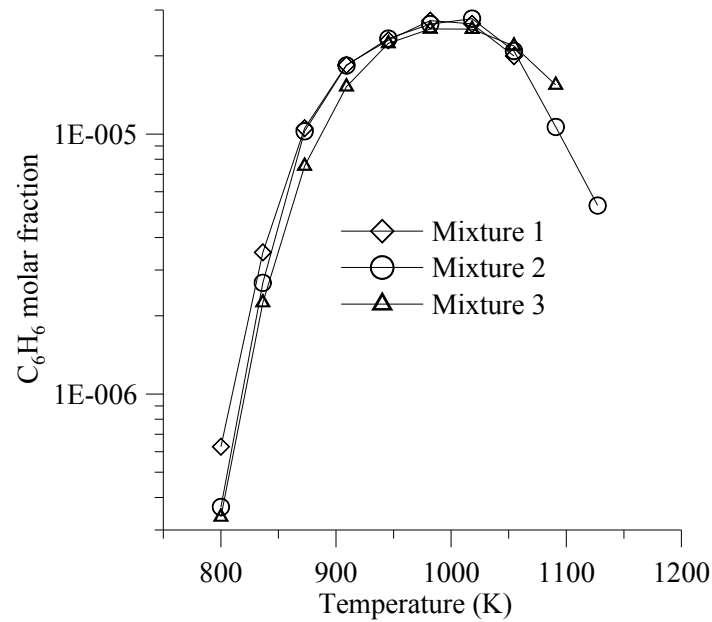
Comparison between neat hydrocarbons ignition delay times and mixture 3 (45% iso-octane, 31.5% toluene, 13.5% 1-hexene, 10% ETBE).

M. Yahyaoui et al., Proc. Combust. Inst. 31, 385–391 (2007)



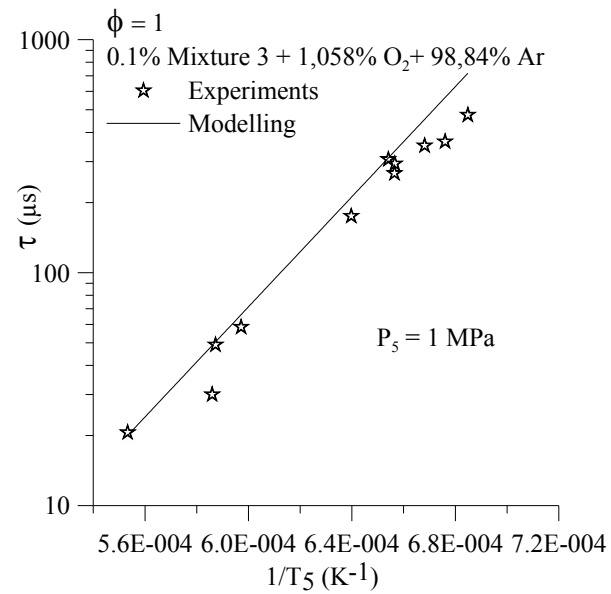
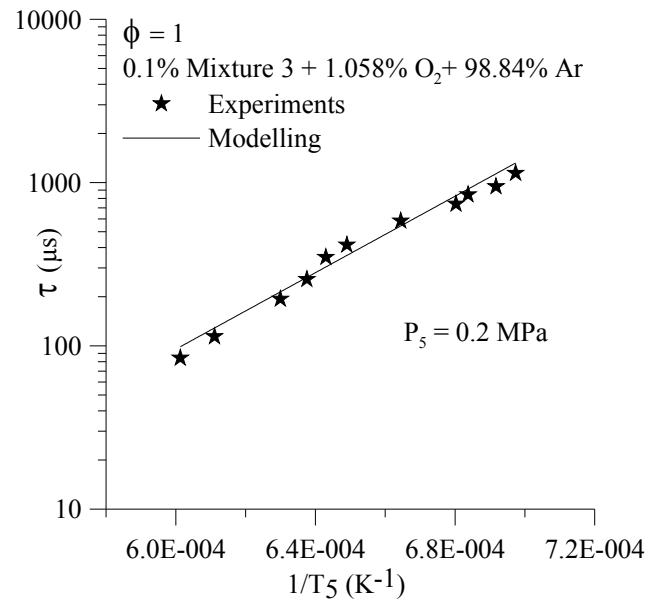
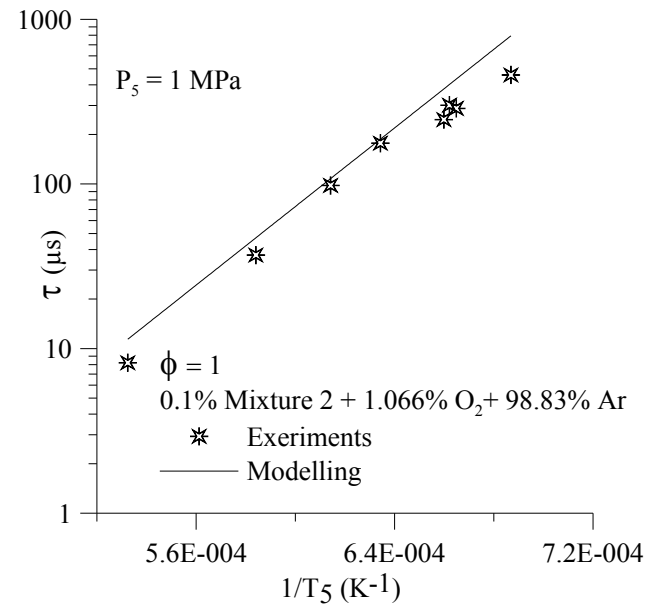
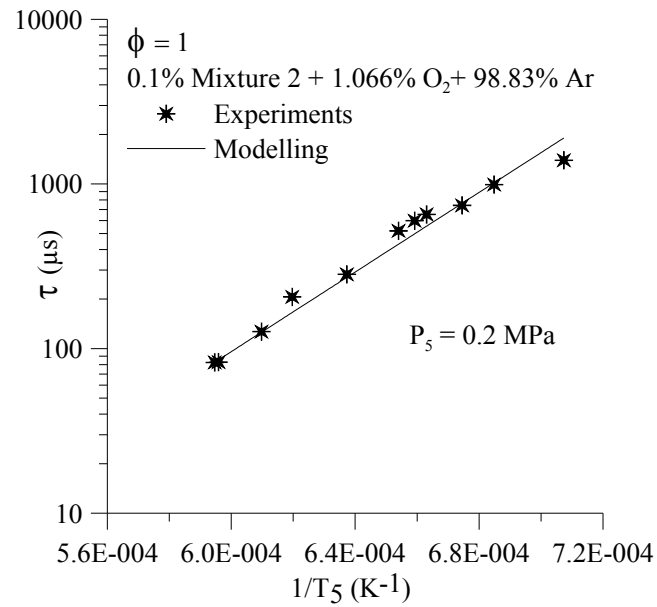
Comparison between experimental and computed concentration profiles in JSR for the oxidation of the Mixture 3 (45% iso-octane, 31.5 toluene, 13.5% 1-hexene, 10% ETBE)

M. Yahyaouiet al., Proc. Combust. Inst. 31, 385–391 (2007)



Experimental mole fractions of benzene, 1,3-butadiene and formaldehyde obtained from the oxidation of different initial fuel composition versus temperature in a JSR. (45% iso-octane, 31.5 toluene, 13.5% 1-hexene, 10% ETBE)

M. Yahyaoui et al., Proc. Combust. Inst. 31, 385–391 (2007)

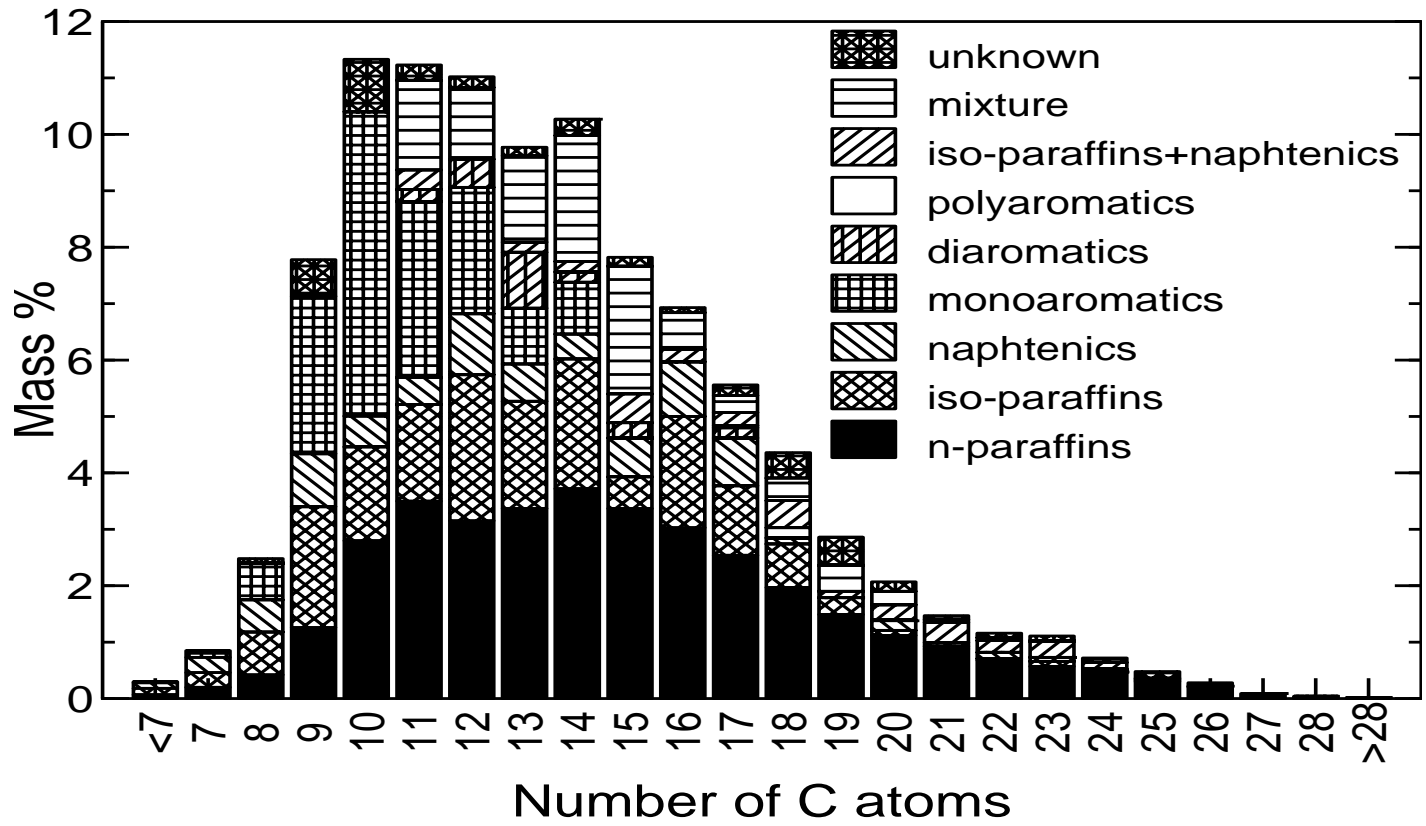


Comparison between experimental (symbols) and computed (lines) ignition delays of the Mixture 2 and 3 in a shock tube M. Yahyaoui et al., Proc. Combust. Inst. 31, 385–391 (2007)

5.2 Diesel

Example of Diesel oxidation study: The major components of the diesel fuel studied were n-paraffins (36.6% by weight), i-paraffins (14.8% w), cycloalkanes (31.4% w) and aromatic hydrocarbons (17.3% w) including mono- and poly-aromatic hydrocarbons.

The global formula for this diesel fuel was determined to be $C_{15.5}H_{30}$.



The reaction mechanism consisted of 2755 reversible reactions involving 377 species.

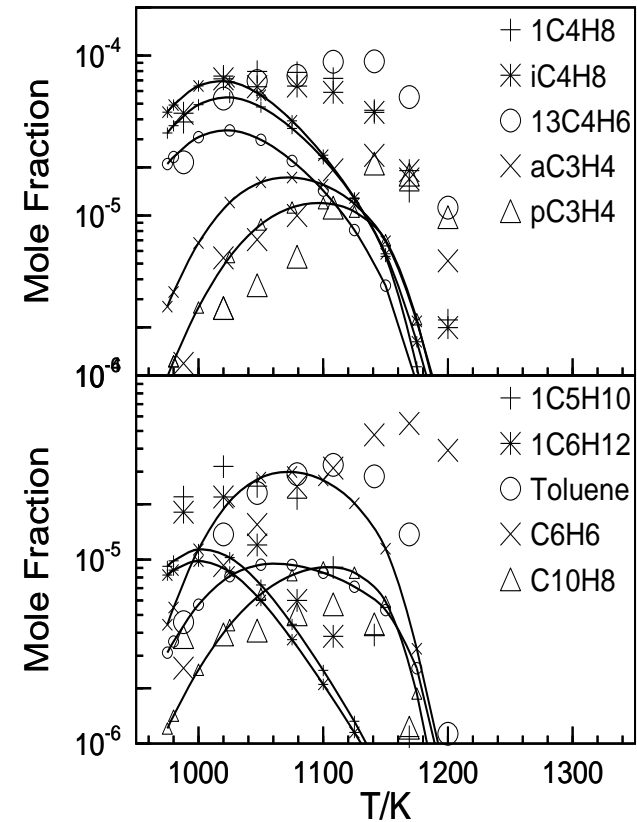
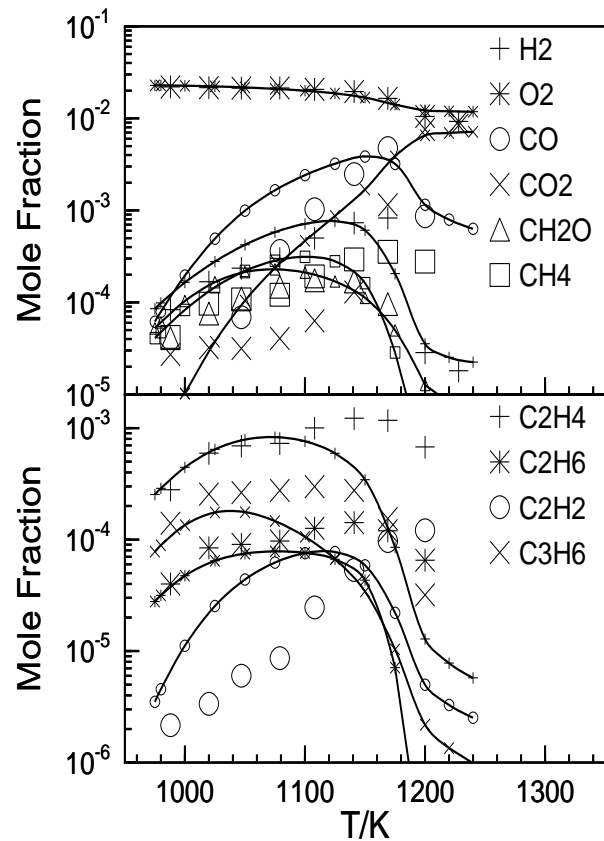
The rates of reaction were computed from the kinetic reaction mechanism and the rate constants calculated at the experimental temperature. The rate constants for the reverse reactions were computed from the forward rate constants and the appropriate equilibrium constants.

The pressure dependencies of P-dependent reactions were taken into account and updated.

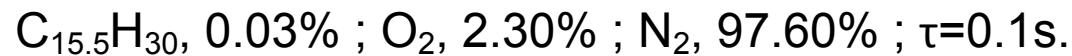
The oxidation mechanism for the diesel fuel was obtained by merging the individual oxidation mechanisms previously validated for the oxidation of n-hexadecane, iso-octane, n-propylcyclohexane, n-propylbenzene, and 1-methylnaphthalene.

Few 'coupling reactions' were included whereas no specific kinetic adjustments were made to better fit pressure dependences. As in previous work from this group, the proposed kinetic mechanism has a strong hierarchical structure.

The model-fuel had 4 constituents: n-hexadecane (36.1% by weight, 23.5% vol.), n-propylcyclohexane (23.1%w, 26.9% vol.), n-propylbenzene (18.7% w, 22.9% vol.), iso-octane (14.7% w, 19% vol.), and 1-methylnaphthalene (7.4%w, 7.7% vol.).

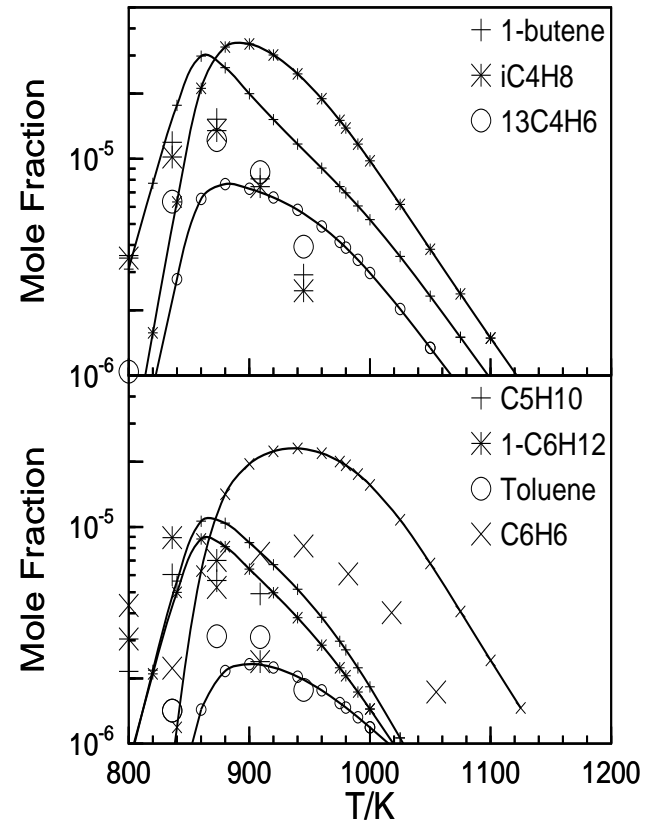
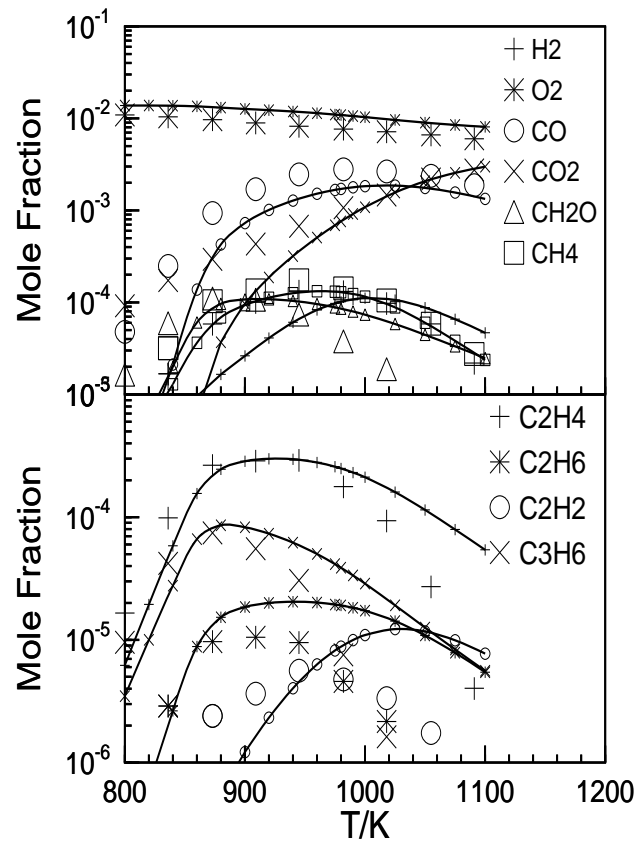


Synthetic diesel fuel oxidation in a JSR at 1 atm and $\phi = 0.5$. The initial conditions were:



The experimental data (symbols) are compared to the computations (lines and small symbols).

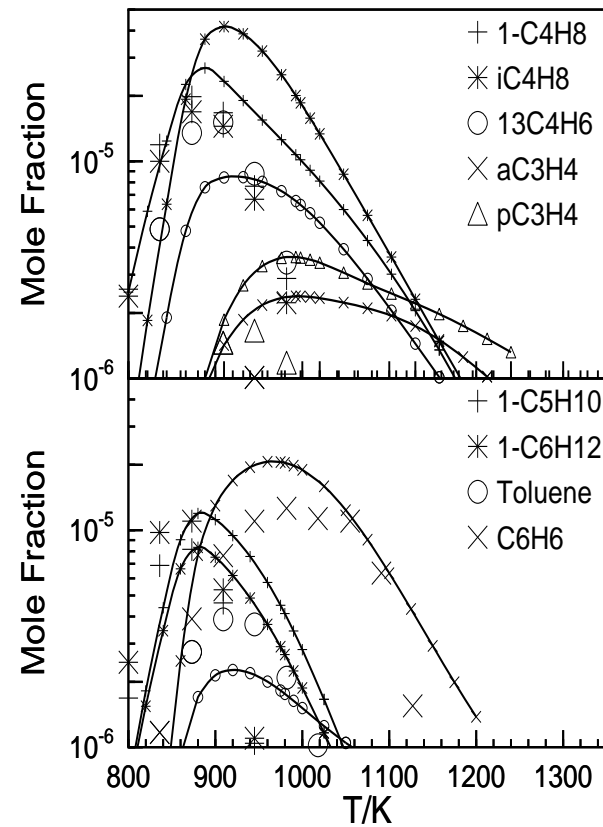
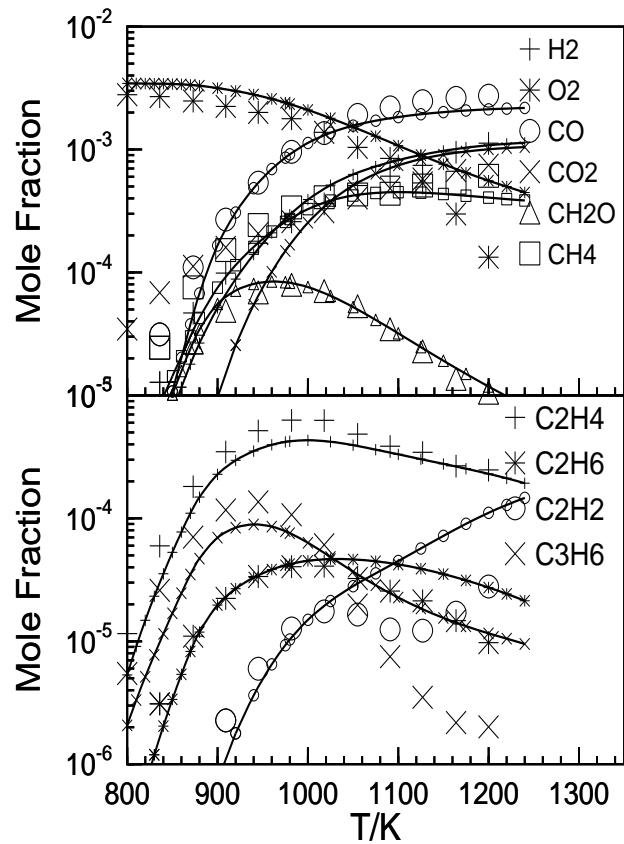
K. Mati et al., Proc. Combust. Inst. 31, 2939–2946 (2007)



Synthetic diesel fuel oxidation in a JSR at 10 atm and $\phi = 0.5$.

The initial conditions were: C_{15.5}H₃₀, 0.05% ; O₂, 1.38% ; N₂, 98.57% ; $\tau = 0.5$ s.

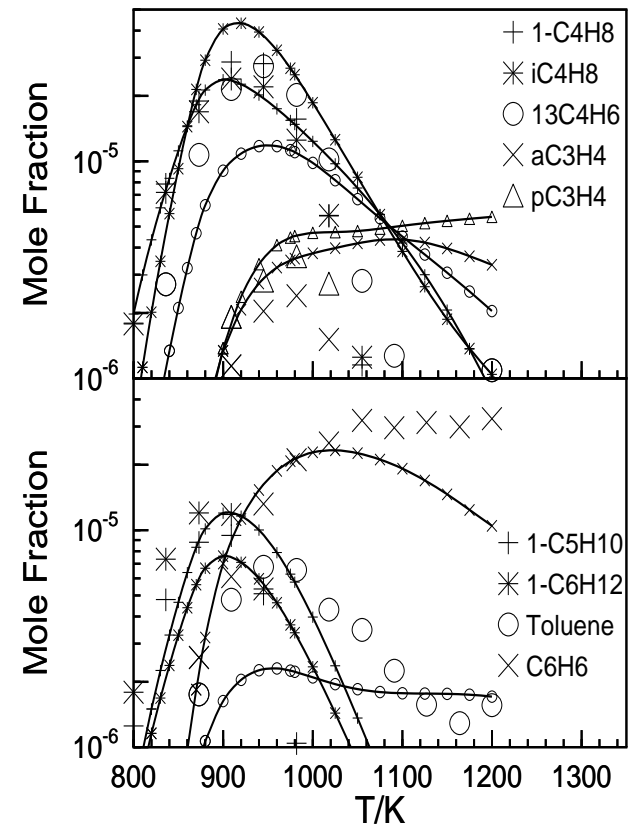
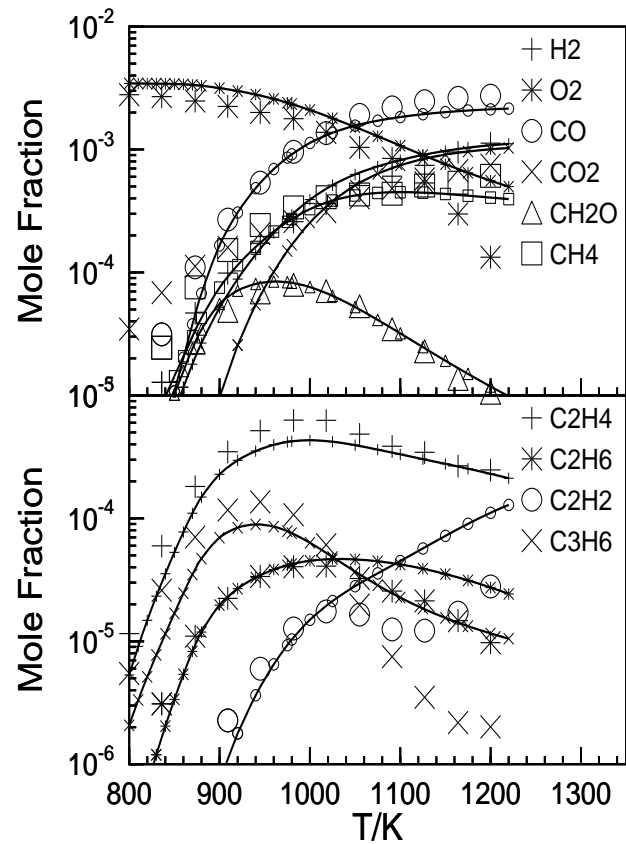
K. Mati et al., Proc. Combust. Inst. 31, 2939–2946 (2007)



Synthetic diesel fuel oxidation in a JSR at 10 atm and $\phi = 1.0$.

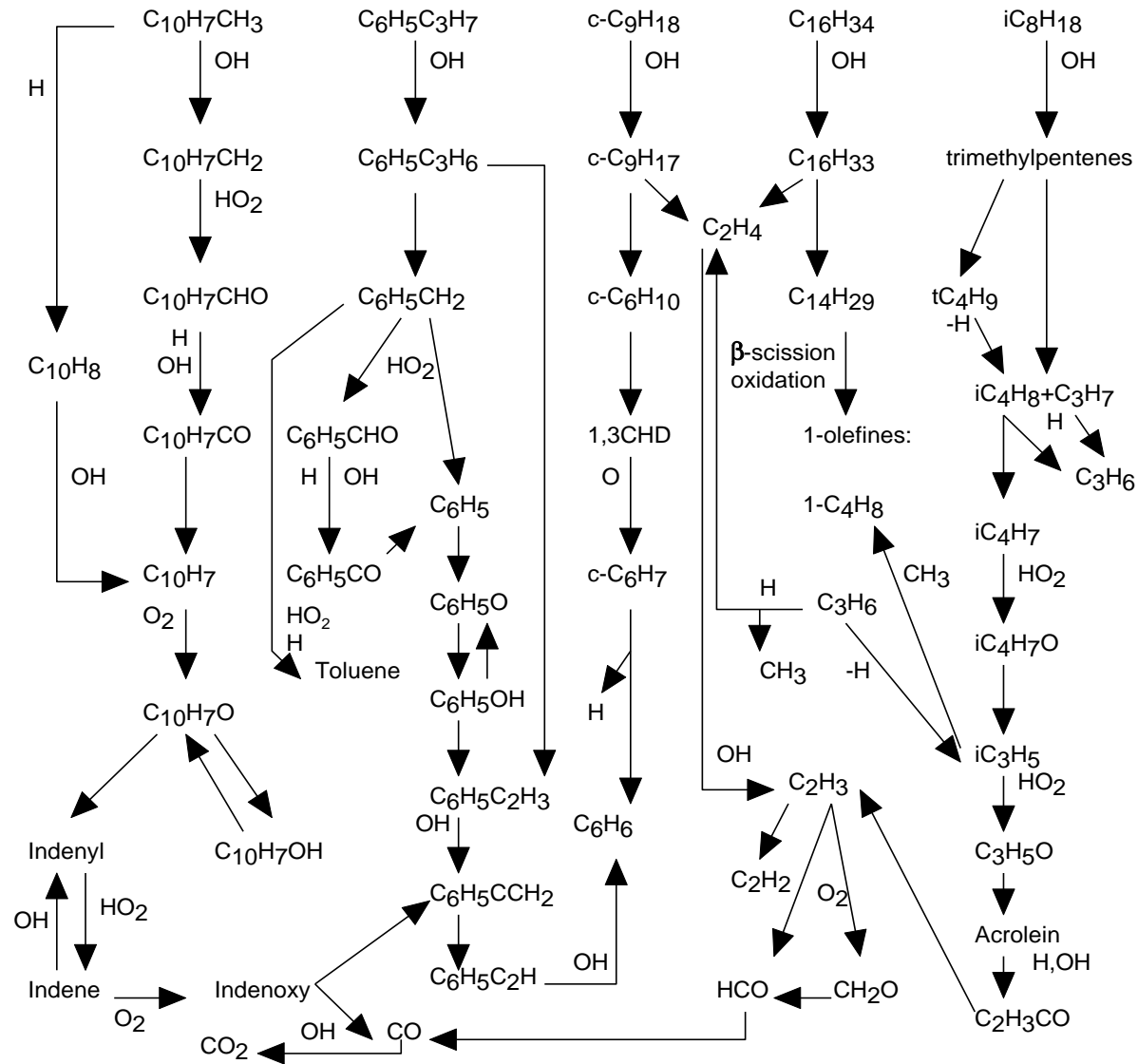
The initial conditions were: C_{15.5}H₃₀, 0.05% ; O₂, 0.69% ; N₂, 99.26% ; $\tau=0.5$ s.

K. Mati et al., Proc. Combust. Inst. 31, 2939–2946 (2007)



Synthetic diesel fuel oxidation in a JSR at 10 atm and $\phi = 2$. The initial conditions were: C_{15.5}H₃₀, 0.05% ; O₂, 0.345% ; N₂, 99.6% ; $\tau=0.5$ s.

K. Mati et al., Proc. Combust. Inst. 31, 2939–2946 (2007)



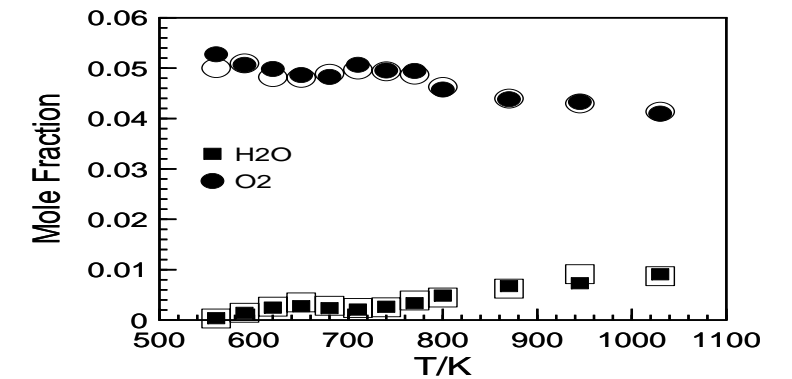
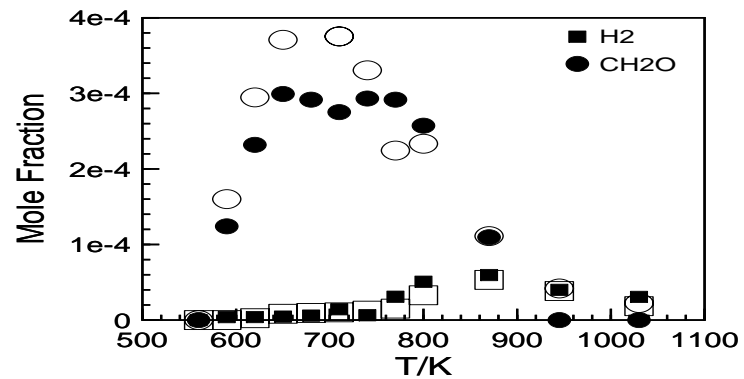
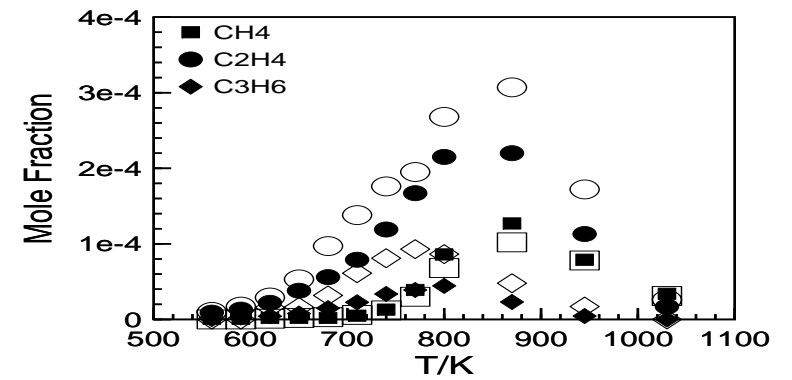
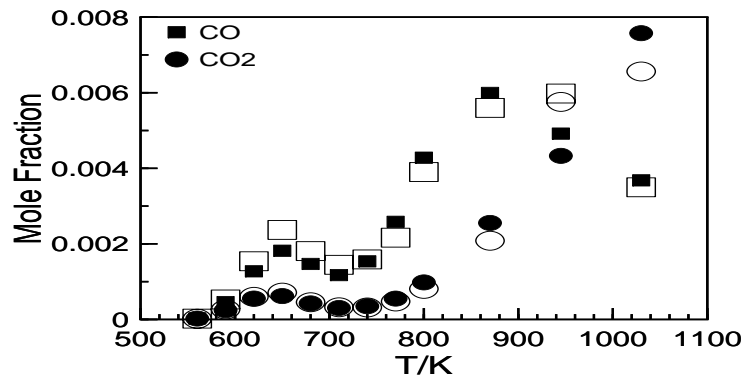
Main reaction paths during the oxidation of the model fuel in a JSR at 10 atm, 1000 K, and $\phi=1.0$.
 Initial conditions: $C_{15.5}H_{30}$, 0.05%; O_2 , 0.69%; N_2 , 99.26%; $\tau=0.5s$.

K. Mati et al., Proc. Combust. Inst. 31, 2939–2946 (2007)

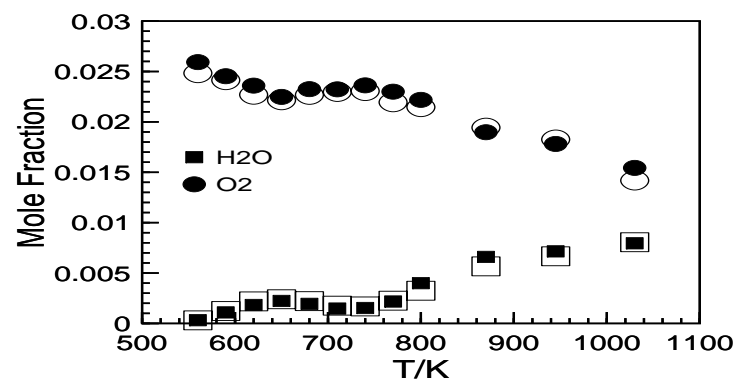
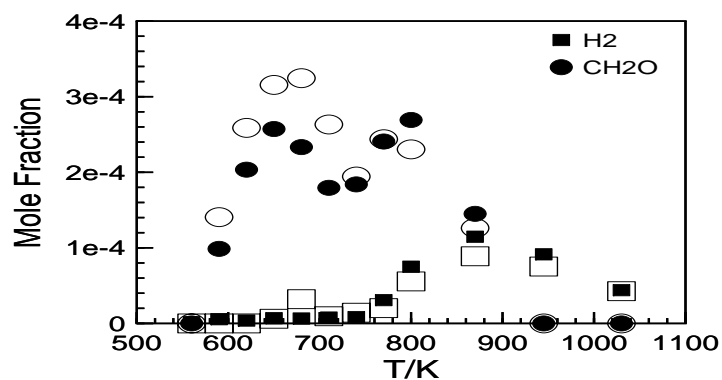
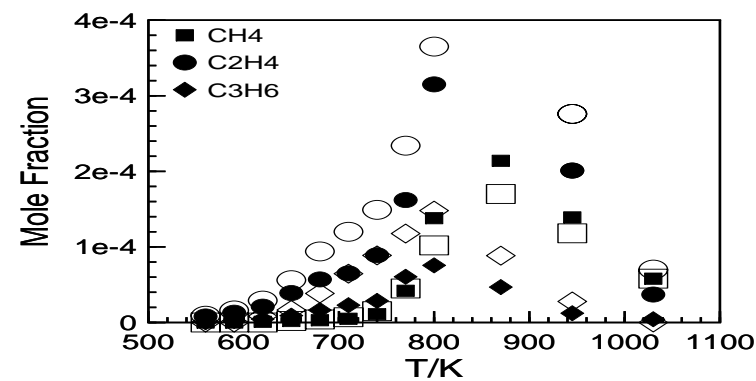
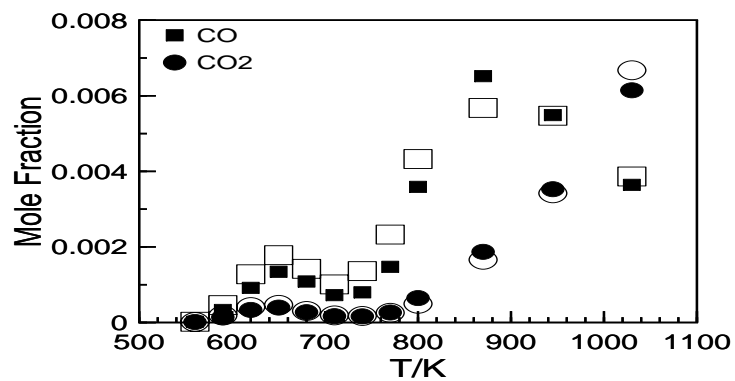
2nd example of Diesel oxidation study:

A surrogate Diesel fuel called the IDEA fuel, consisting of 70% n-decane and 30% 1-methyl naphthalene was formulated previously as part of the Integrated Development on Engine Action (IDEA) program. This fuel mixture matches both the physicochemical properties and combustion behavior of a conventional Diesel fuel. The IDEA fuel has properties similar to those of a conventional Diesel fuel, i.e. it has a normal density of 798 kg/m³ at 20°C, a CN of ca. 53, and hydrogen-to-carbon ratio of 1.8.

The kinetic oxidation mechanisms of large n-paraffins and aromatics have been developed separately in several fundamental studies and merged to simulate the oxidation of surrogate gasoline, kerosene, and Diesel fuels. A long carbon chain n-paraffin compound is highly suitable for representing the paraffinic fraction of a Diesel fuel because of the high concentration of these chemicals in this kind of fuel. On the other hand, aromatic hydrocarbons play an important role in soot formation reactions and must be used in Diesel surrogate mixtures. They also contribute to the reduction of the cool-flame oxidation of long chain n-alkanes.

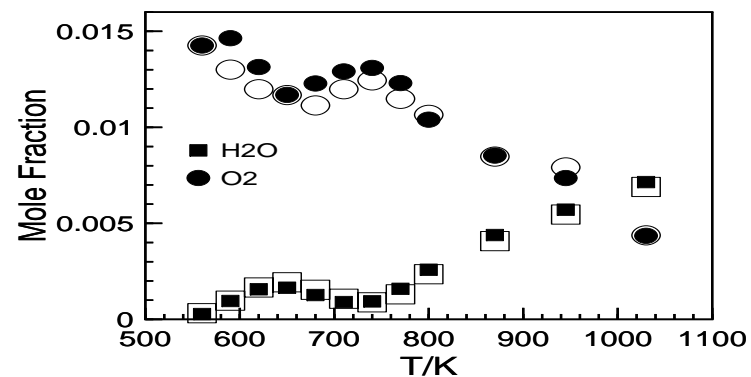
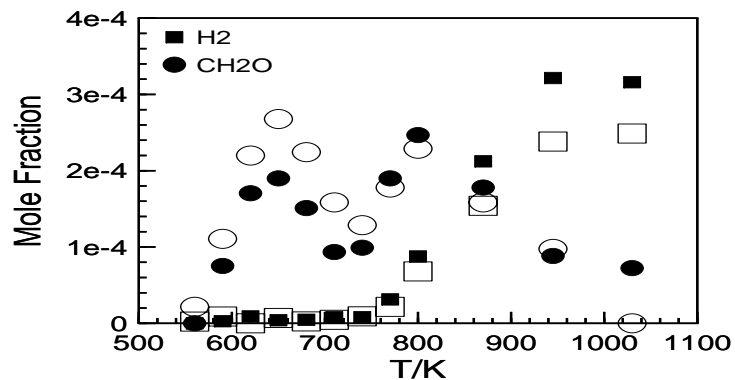
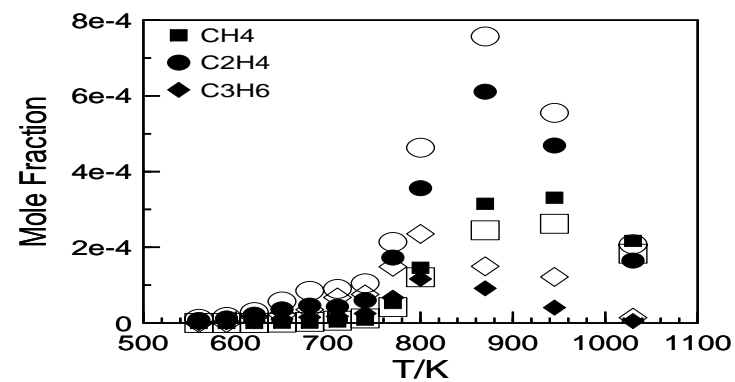
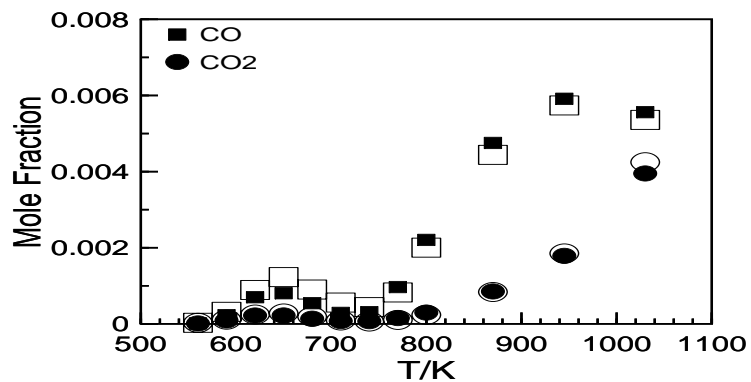


Experimental species concentration profiles from the oxidation of the conventional (filled symbols) and IDEA surrogate (empty symbols) Diesel fuels in a JSR at 10 atm, $\phi=0.25$ and $\tau=1$ s.



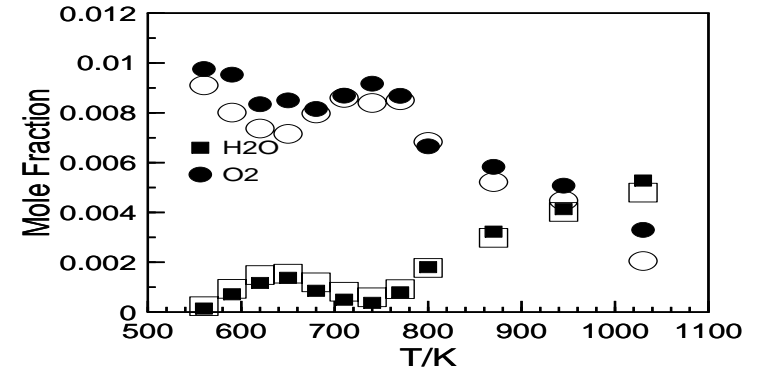
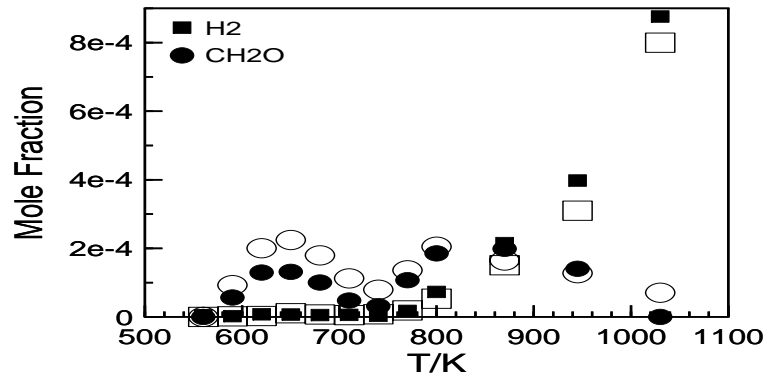
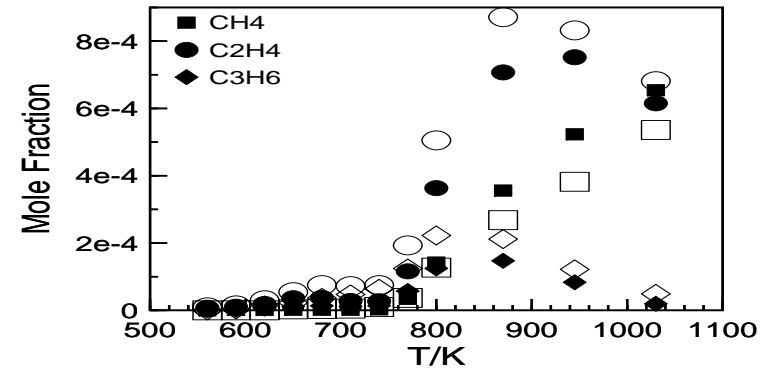
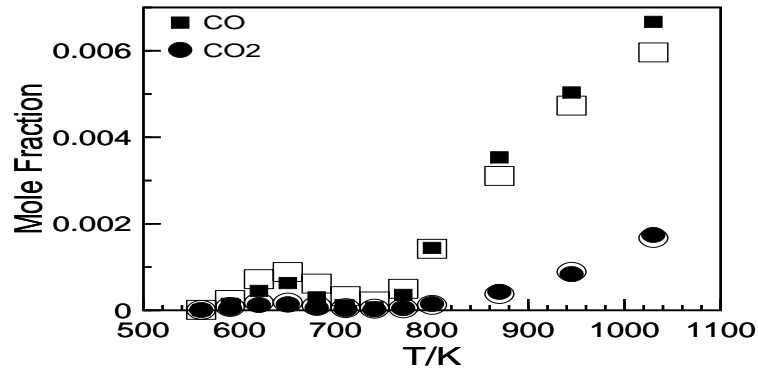
Experimental species concentration profiles from the oxidation of the conventional (filled symbols) and IDEA surrogate (empty symbols) Diesel fuels in a JSR at 10 atm, $\phi = 0.5$ and $\tau = 1$ s.

H. P. Ramirez L et al. , Energy & Fuels **24**(3) 1668–1676 (2010)



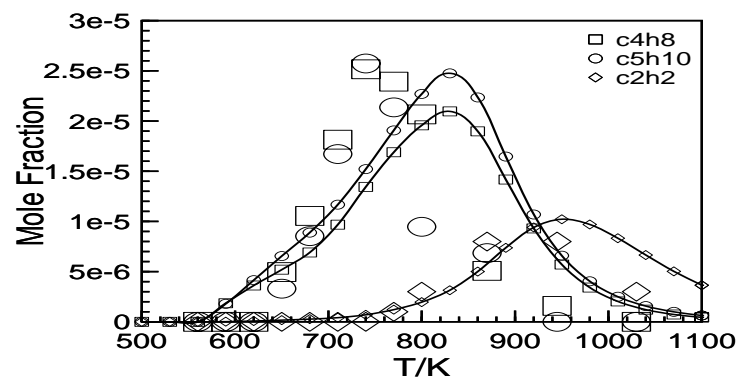
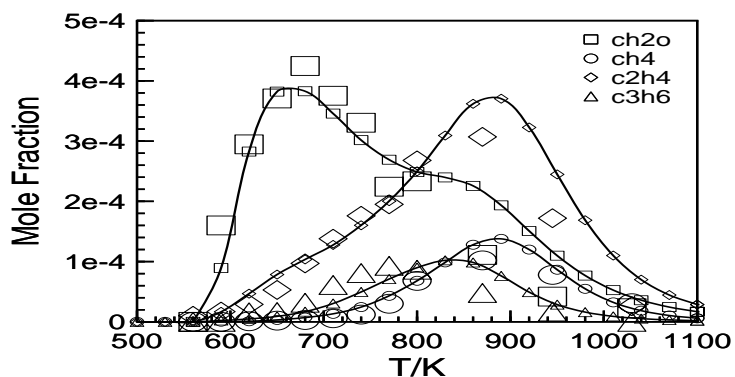
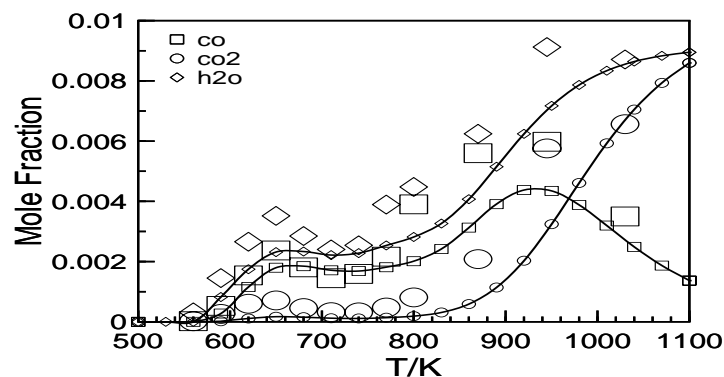
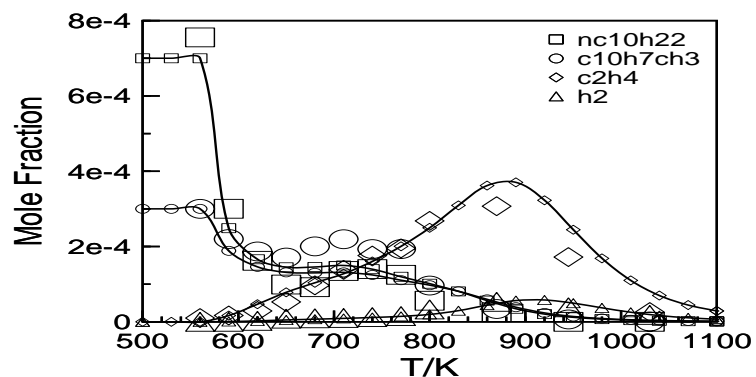
Experimental species concentration profiles from the oxidation of the conventional (filled symbols) and IDEA surrogate (empty symbols) Diesel fuels in a JSR at 10 atm, $\phi = 1$ and $\tau = 1$ s.

H. P. Ramirez L et al. , Energy & Fuels **24**(3) 1668–1676 (2010)

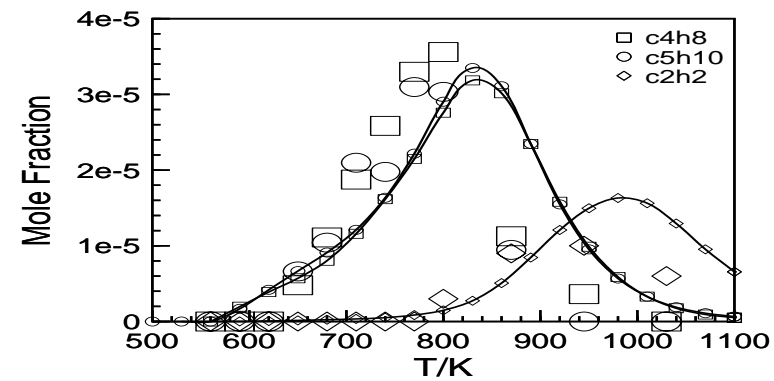
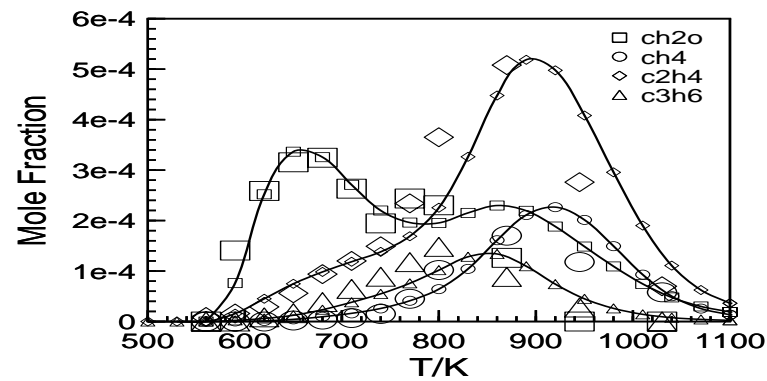
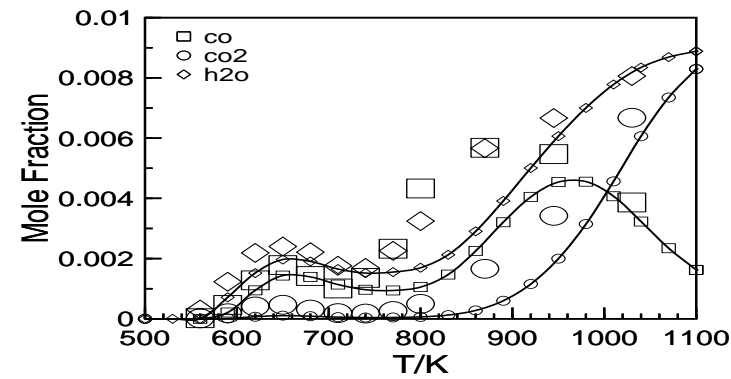
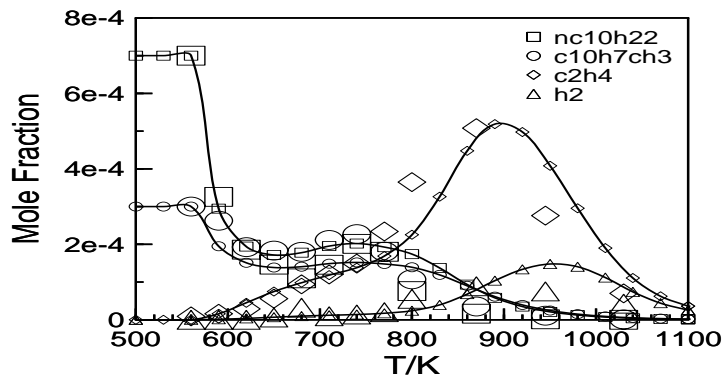


Experimental species concentration profiles from the oxidation of the conventional (filled symbols) and IDEA surrogate (empty symbols) Diesel fuels in a JSR at 10 atm, $\phi = 1.5$ and $\tau = 1$ s.

H. P. Ramirez L et al. , Energy & Fuels **24**(3) 1668–1676 (2010)

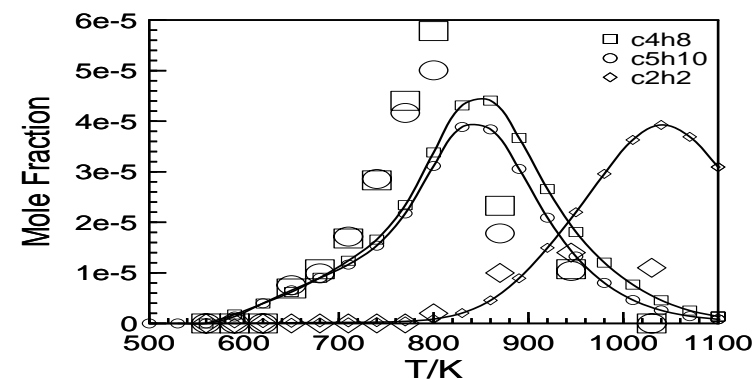
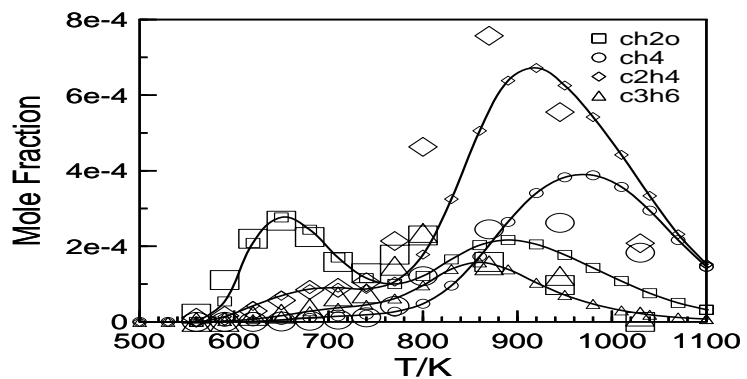
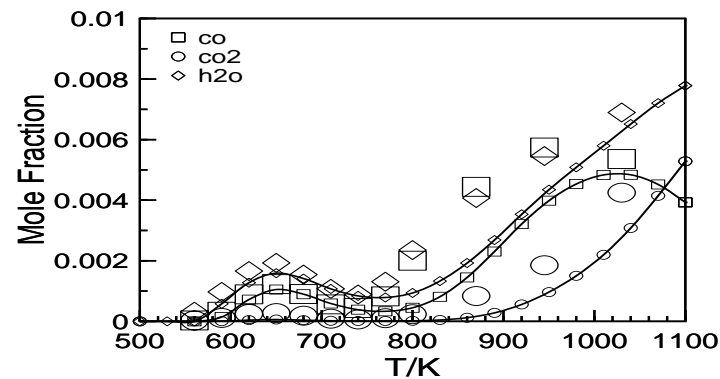
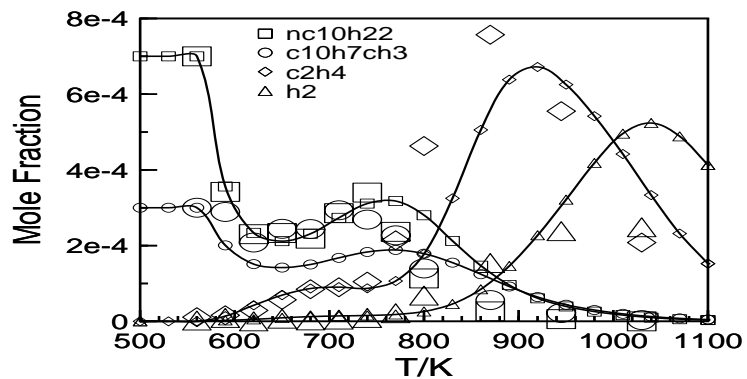


The IDEA surrogate Diesel fuel oxidation in a JSR at 10 atm, $\tau = 1$ s and $\phi = 0.25$. The initial mole fractions were: 1-Methylnaphthalene, 0.03%; n-Decane, 0.07%; O₂, 5.96%; N₂, 93.94%. The experimental data (filled symbols) are compared to the computations (lines with empty symbols).
 H. P. Ramirez L et al. , Energy & Fuels **24**(3) 1668–1676 (2010)



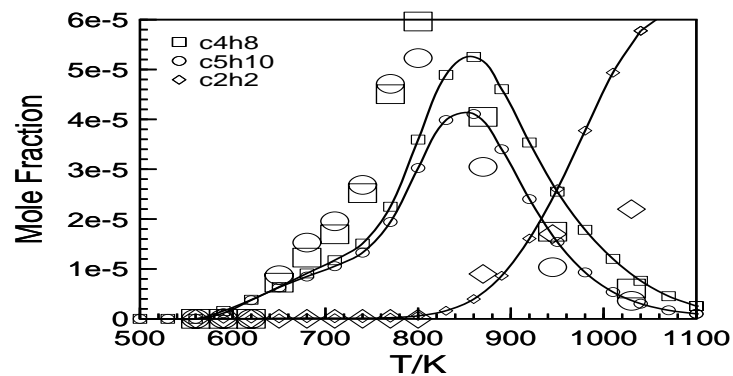
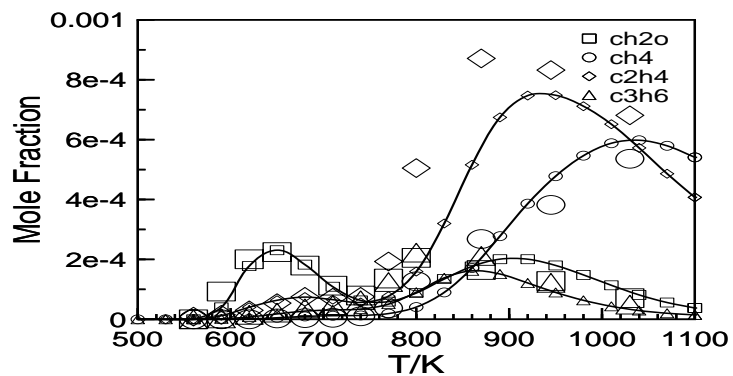
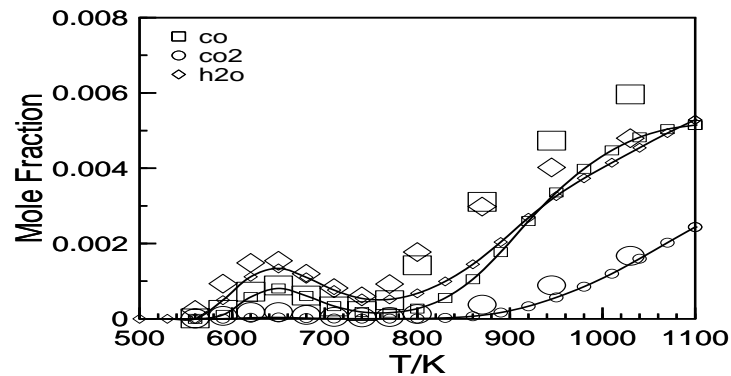
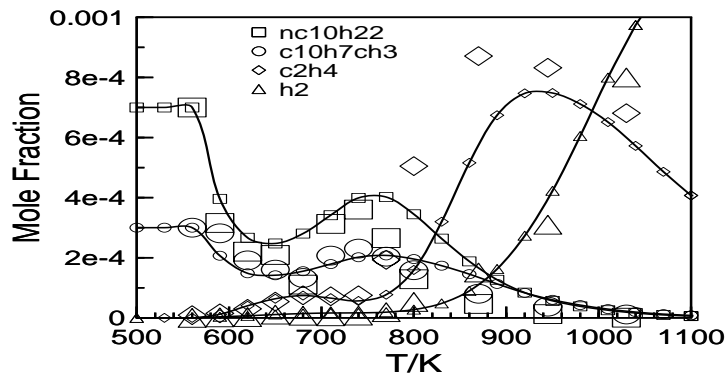
The IDEA surrogate Diesel fuel oxidation in a JSR at 10 atm, $\tau = 1$ s and $\phi = 0.5$. The experimental data (filled symbols) are compared to the computations (lines with empty symbols).

H. P. Ramirez L et al. , Energy & Fuels **24**(3) 1668–1676 (2010)



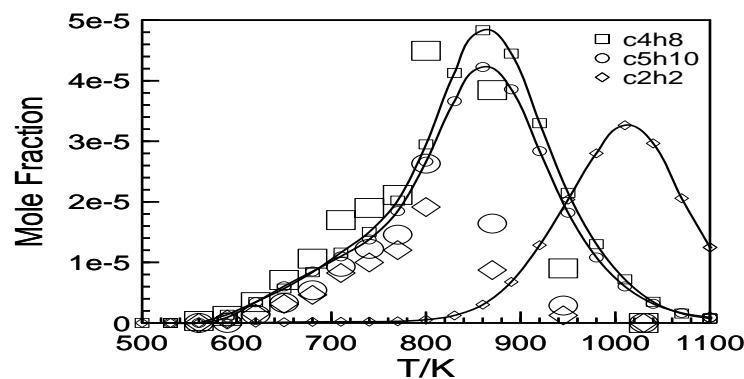
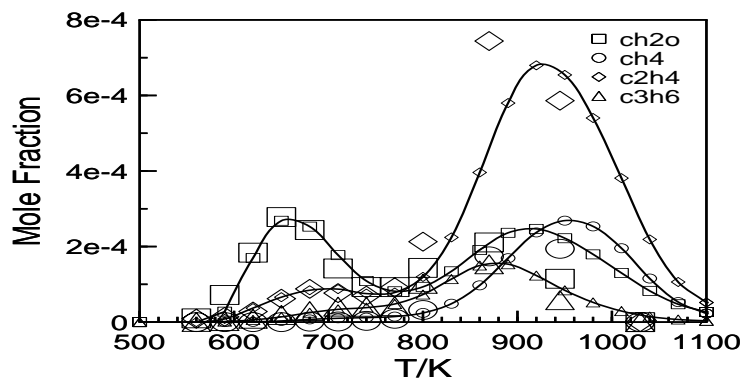
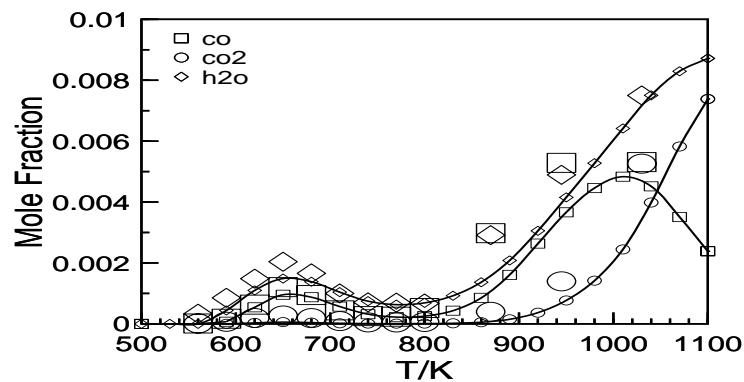
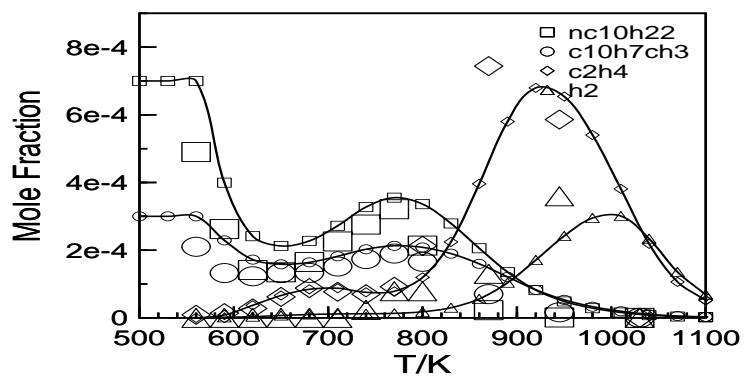
The IDEA surrogate Diesel fuel oxidation in a JSR at 10 atm, $\tau = 1$ s and $\phi = 1.0$. The experimental data (filled symbols) are compared to the computations (lines with empty symbols).

H. P. Ramirez L et al. , Energy & Fuels **24**(3) 1668–1676 (2010)



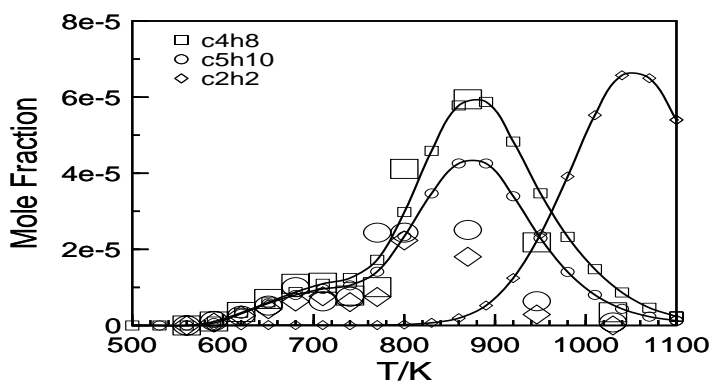
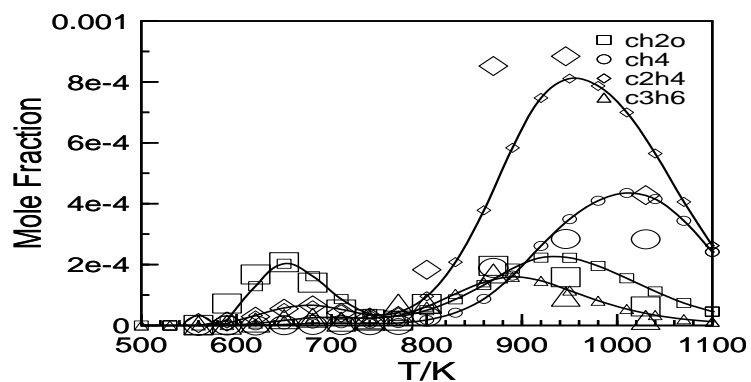
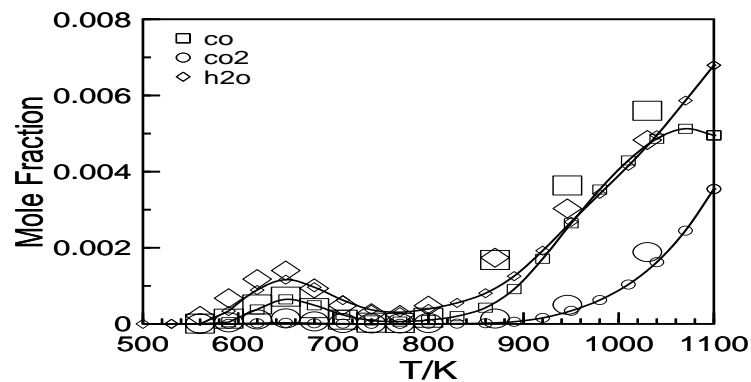
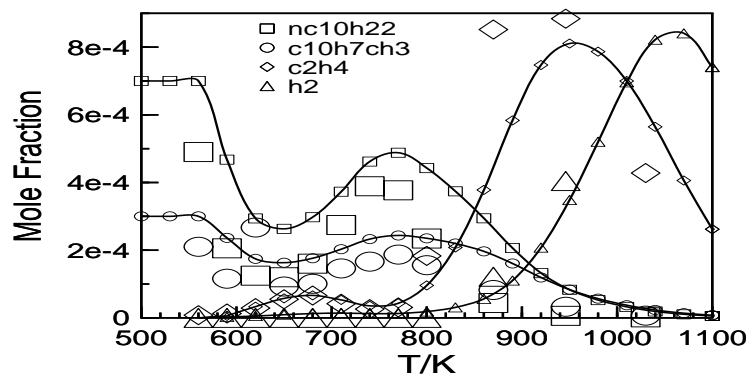
The IDEA surrogate Diesel fuel oxidation in a JSR at 10 atm, $\tau = 1$ s and $\phi = 1.5$. The experimental data (filled symbols) are compared to the computations (lines with empty symbols).

H. P. Ramirez L et al. , Energy & Fuels **24**(3) 1668–1676 (2010)



The IDEA surrogate Diesel fuel oxidation in a JSR at 6 atm, $\tau = 0.6$ s and $\phi = 0.5$. The experimental data (filled symbols) are compared to the computations (lines with empty symbols).

H. P. Ramirez L et al. , Energy & Fuels **24**(3) 1668–1676 (2010)

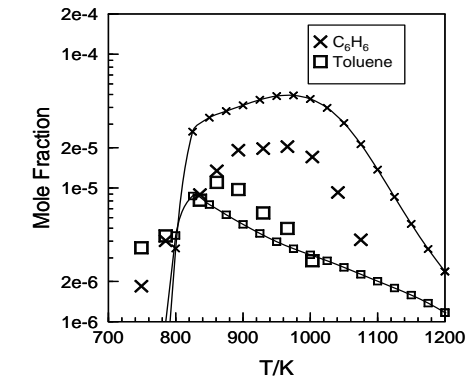
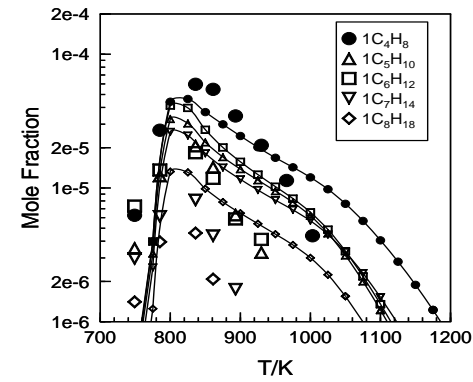
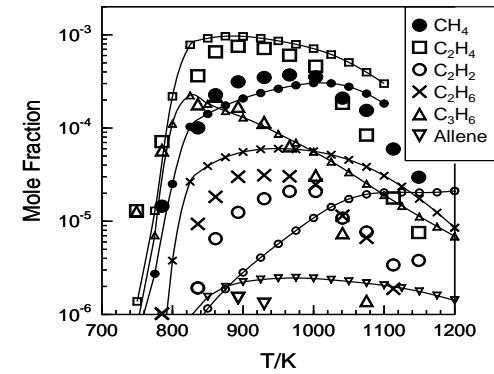
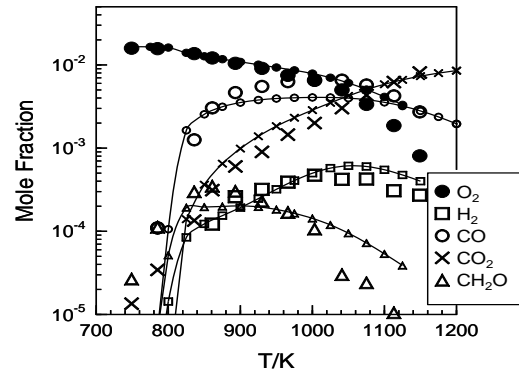


The IDEA surrogate Diesel fuel oxidation in a JSR at 6 atm, $\tau = 0.6$ s and $\phi = 1.0$. The experimental data (filled symbols) are compared to the computations (lines with empty symbols).

H. P. Ramirez L et al. , Energy & Fuels **24**(3) 1668–1676 (2010)

5.3 Jet fuels

Example of early jet fuel oxidation study:

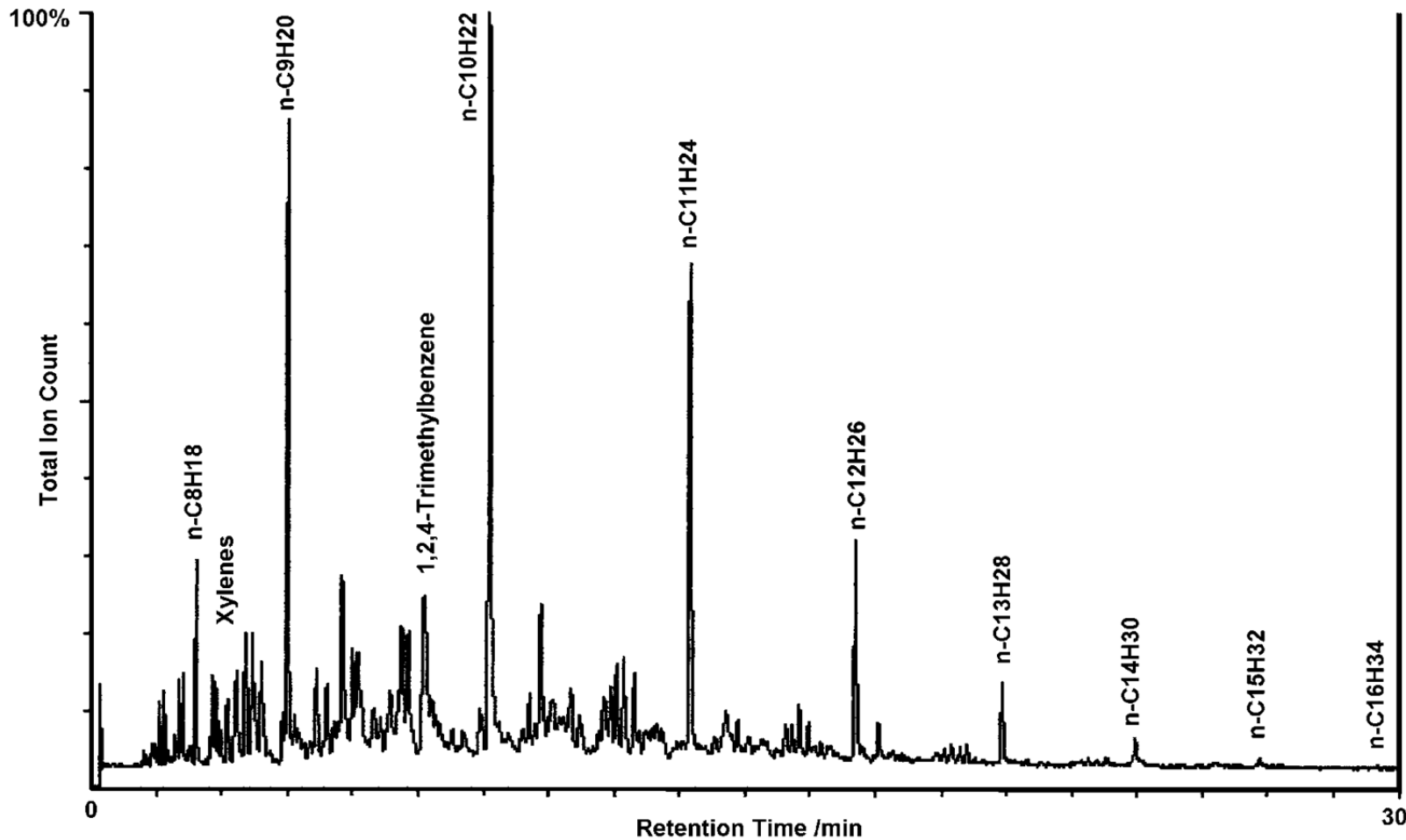


Oxidation of kerosene in a JSR at **10 atm** and $t=0.5$ s (initial conditions: 1000 ppmv of kerosene TR0, 16500 ppmv of O_2 , diluent nitrogen). Model fuel: n-decane/ n-propylbenzene/ n-propyl-cyclohexane (74% / 14% / 11% mole).

Dagaut & Cathonnet, *PECS* **32**, 48-92, 2006

Introduction

Kerosene (Jet A, Jet A1, JP-8, TR0) is a complex mixture of alkanes (50-65% vol.), mono- and polyaromatics (10-20% vol.) and cycloalkanes or naphthenes (mono- and polycyclic, 20-30% vol.) widely used in aircraft engines.



GC/MS analysis of a kerosene TR0 sample showing the importance of n-alkanes.

The compounds identified in kerosene at the highest levels of concentration are n-alkanes.

The average chemical formula for kerosene (Jet A, Jet A-1, TR0, JP-8) differs from one source to another:

$C_{12}H_{23}$ in Gracia-Salcedo, C.M., Brabbs, T.A., and McBride, B.J., 1988, NASA Tech. Memorandum 101475,

$C_{11}H_{21}$ in Edwards, T., and Maurice, L.Q., 2001, J. Propulsion and Power, **17**, 461-466,

$C_{11.6}H_{22}$ in Martel, C.R., 1988, AFWAL/POSF Report, July 15, 1988

$C_{11}H_{22}$ in Guéret, C., 1989, Thesis, University of Orléans (in French).

$C_{11}H_{23}$ in Nguyen, H.L., and Ying, S.J., 1990, AIAA-90-2439.

For this study, the adopted formula was $C_{11}H_{22}$.

Due to the complexity of the composition of this fuel, it is necessary to use a surrogate model fuel for simulating its oxidation.

Under high-pressure JSR conditions, the detailed kinetic modeling of kerosene oxidation was initially performed using n-decane as a model-fuel, since n-decane and kerosene showed very similar oxidation rates under JSR and premixed flame conditions as reported in:

Dagaut et al., *Proc. Combust. Inst.*, **25**, pp 919-926, 1994.

Dagaut et al., *J. Chim. Phys. Phys.-Chim. Biol.* **92**, pp 47-76, 1995.

Cathonnet et al. *RTO Meeting Proc.* 14, pp 1-9, 1999.

Douté et al. *Combust. Sci. and Technol.* **106**, pp 327-344, 1995.

n-Decane is an acceptable model-fuel for kerosene oxidation as far as modeling the formation of aromatics is not a major issue since the oxidation of n-decane yields much less aromatics than kerosene.

Therefore, more complex model fuels are necessary to model the formation of aromatics from the oxidation of kerosene as demonstrated in the literature:

Mawid et al., 2002, AIAA 2002-3876.

Dagaut 2002, *Phys. Chem. Chem. Phys.*, **4**, 2079-2094.

Mawid et al. 2003, AIAA 2003-4938.

Mawid et al. 2004, AIAA 2004-4207.

Surrogate model fuels consisting of n-decane and mixtures of n-decane with simple aromatic hydrocarbons and cycloalkanes are tested here, mainly under JSR conditions.

The detailed kinetic reaction mechanisms for the pure components of the surrogate model fuel had first to be validated before merging the sub-schemes (Ristori et al. 2001, *Combust. Sci. and Technol.*, **65**, pp 197-228; Dagaut et al. 2002, *Fuel*, **81**, pp 173-184) to yield a kerosene kinetic reaction mechanism

The study includes:

New experimental results obtained for the oxidation of kerosene in a JSR, over a wide range of equivalence ratio (0.5 to 2), and temperatures in the range 900-1300 K.

The oxidation of n-decane
under JSR conditions
shock-tube conditions
premixed flame conditions,

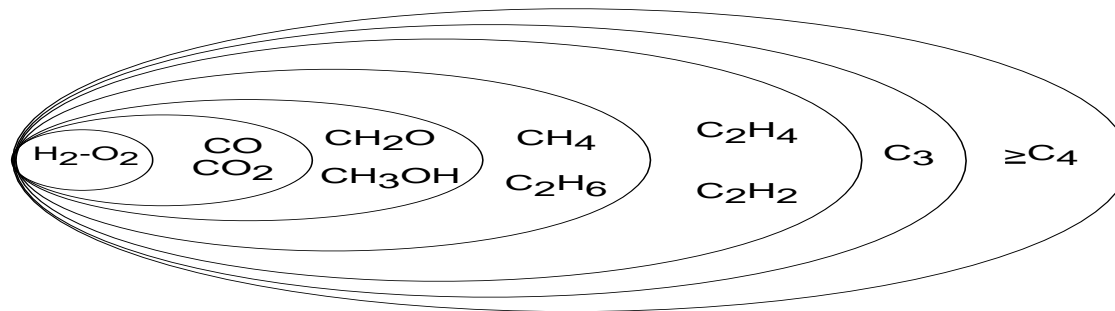
Modeling

For simulating the oxidation of n-decane and kerosene in premixed flames, we used the Premix computer code.

For simulating the ignition delays of kerosene-air mixtures, we used the SENKIN code.

For the JSR computations, we used the PSR computer code.

The reaction rates are computed from the kinetic reaction mechanism and the rate constants of the elementary reactions calculated at the experimental temperature, using the modified Arrhenius equation.



Structure hiérarchisée des mécanismes détaillés

The reaction mechanism used in this study has a strong hierarchical structure.

The reaction mechanism is based on the comprehensive commercial fuel oxidation mechanism developed earlier (Dagaut 2002, Phys. Chem. Chem. Phys., **4**, 2079-2094) where the rate expressions of pressure dependent reactions have been updated.

The reaction mechanism used here consisted of 209 species and 1673 reversible reactions.

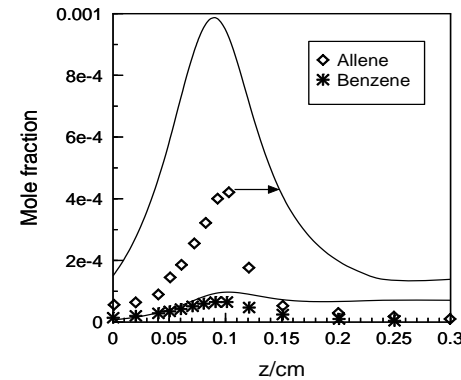
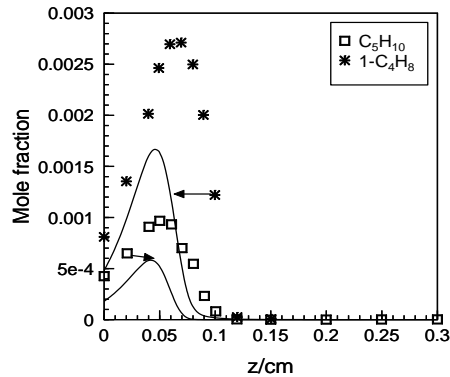
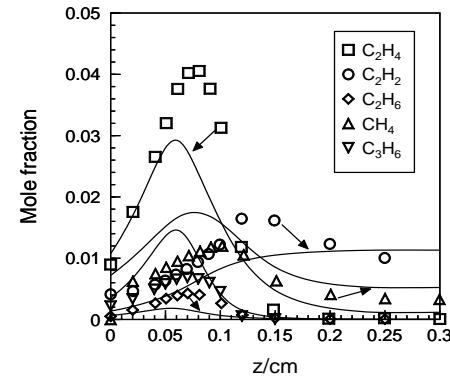
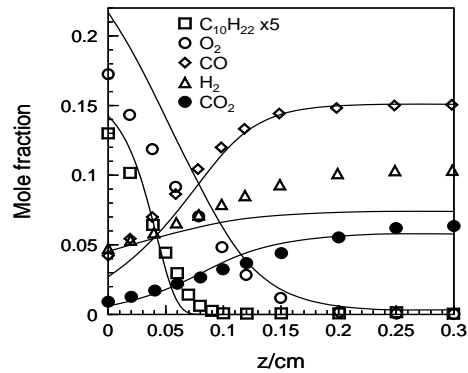
The rate constants for reverse reactions were computed from the corresponding forward rate constants and the appropriate equilibrium constants,

$$K_c = k_{\text{forward}} / k_{\text{reverse}}$$

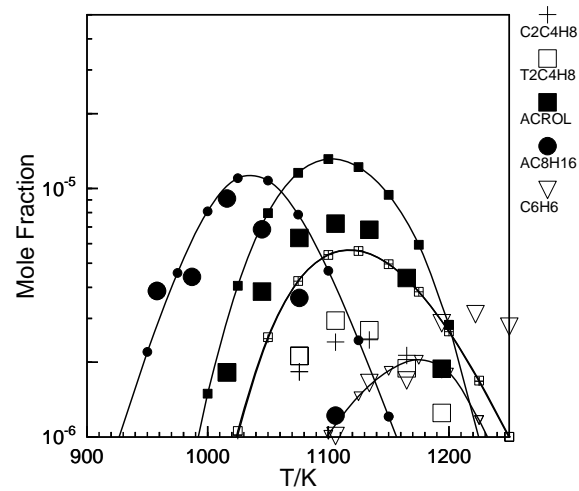
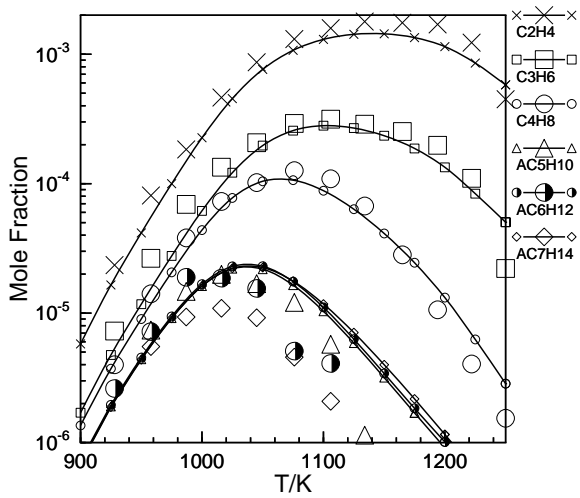
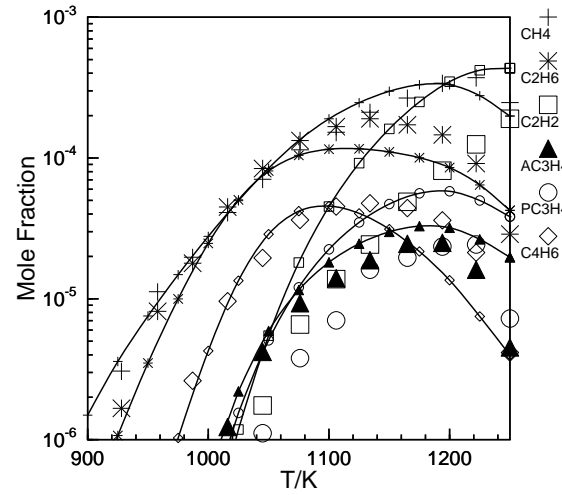
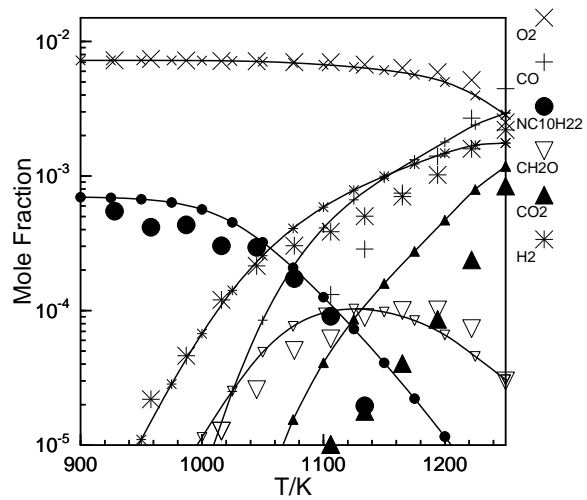
calculated using thermochemical data.

Results and Discussion: n-decane

The kinetic model was tested against the atmospheric pressure n-decane premixed flame data of Douté et al. to verify the validity of the proposed kinetic scheme in flame conditions. The experimental temperature profile reported by the authors was used in the computations.



Dagaut & Cathonnet, *PECS* **32**, 48-92, 2006



Oxidation of n-decane in a JSR: the experimental results consisted of the mole fractions of reactants, stable intermediates and final products measured at fixed residence time, as a function of T (example: 700 ppmv of n-decane, 7230 ppmv of O₂, in N₂; 0.07 s, 1 atm).

Dagaut & Cathonnet, *PECS* **32**, 48-92, 2006

Results and Discussion: Kerosene

For the oxidation of kerosene in a JSR, the experimental results consisted of the mole fractions of the reactants, stable intermediates and final products measured at fixed residence time, as a function of temperature.

They are compared to PSR simulations.

To test the effect of the model fuel composition on the computations, we modeled the oxidation of a stoichiometric mixture kerosene/O₂/N₂ using **four different model-fuels**:

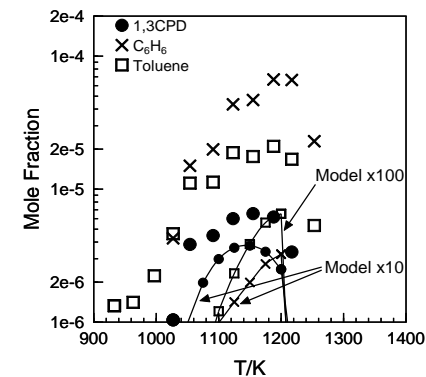
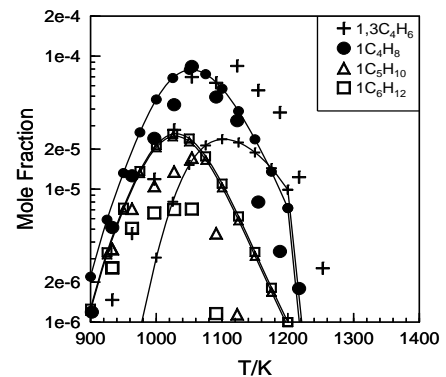
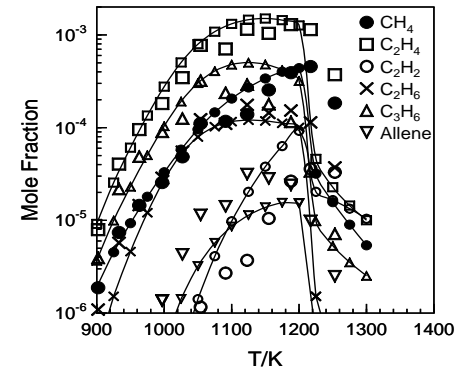
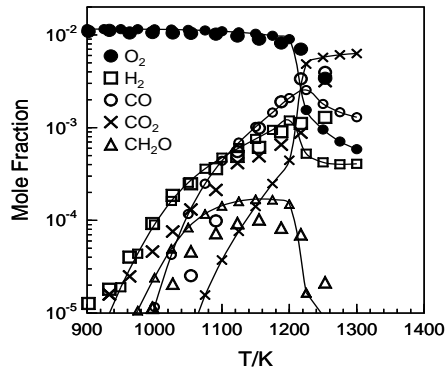
(1) n-decane

(2) n-decane/n-propylbenzene (74% / 26% mole) mixture

(3) n-decane/n-propylcyclohexane (74% / 26% mole) mixture

(4) n-decane/ n-propylbenzene/ n-propyl-cyclohexane (74% / 14% / 11% mole) mixture

n-Decane was used as a model fuel:



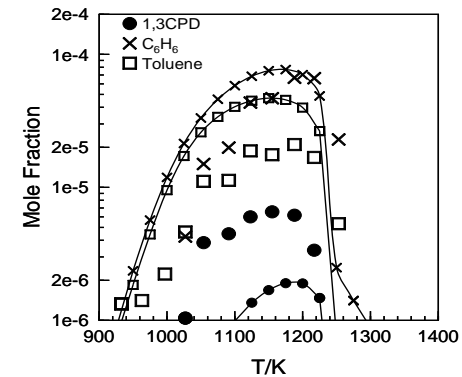
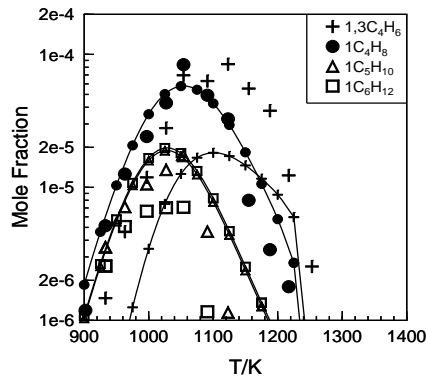
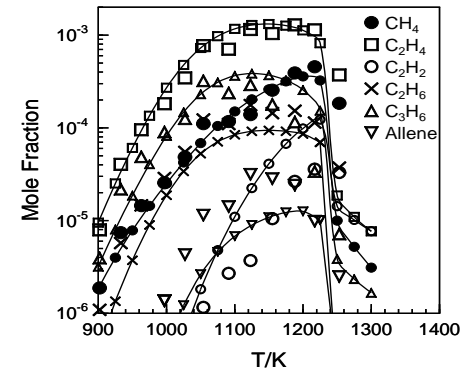
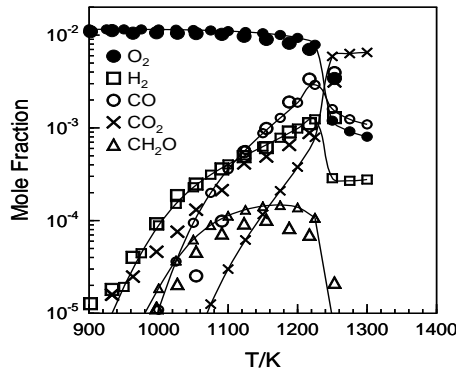
Kerosene oxidation of in a JSR (700 ppmv of kerosene, 11550 ppmv of O₂, N₂; 0.07 s, 1 atm).

1,3-Cyclopentadiene, benzene, and toluene are strongly underestimated!

- (1) These results confirm the similitude between n-decane and kerosene kinetics of oxidation
- (2) The inclusion of non-paraffin components in the model fuel is necessary to simulate the formation of aromatics from kerosene oxidation

Dagaut & Cathonnet, *PECS* **32**, 48-92, 2006

n-decane/n-propylbenzene (74% / 26% mole) mixture as model fuel



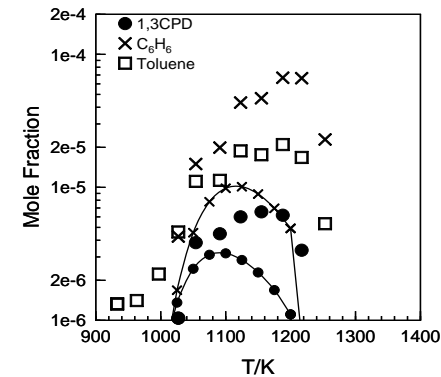
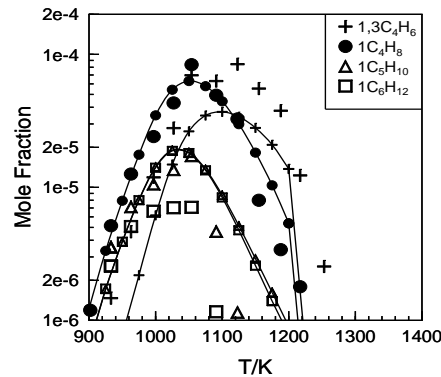
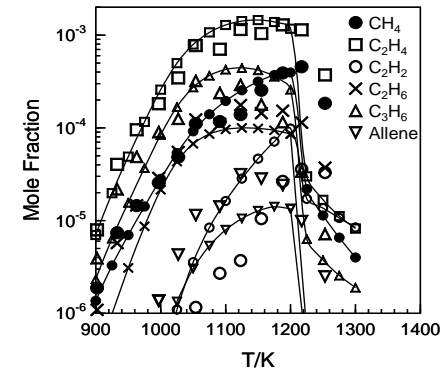
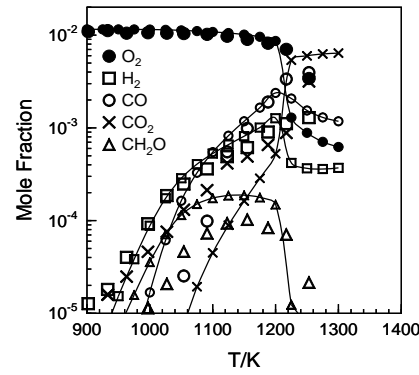
Kerosene oxidation in a JSR (700 ppmv of kerosene, 11550 ppmv of O_2 , N_2 ; 0.07 s, 1 atm).

A good agreement between the data and the modeling results for most of the species but 1,3-cyclopentadiene, benzene, and toluene: benzene and toluene are overestimated

Thus the inclusion of cycloalkanes in the kerosene model fuel is necessary

Dagaut & Cathonnet, *PECS* **32**, 48-92, 2006

n-decane/n-propylcyclohexane (74% / 26% mole) mixture as model fuel



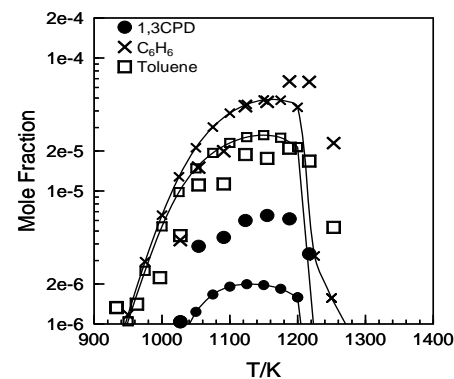
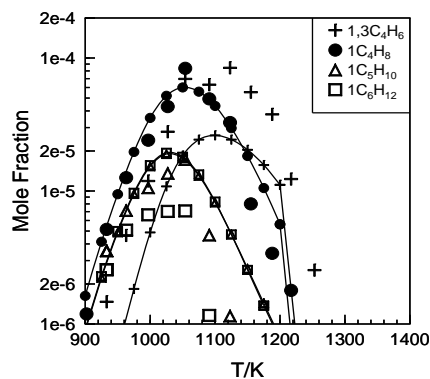
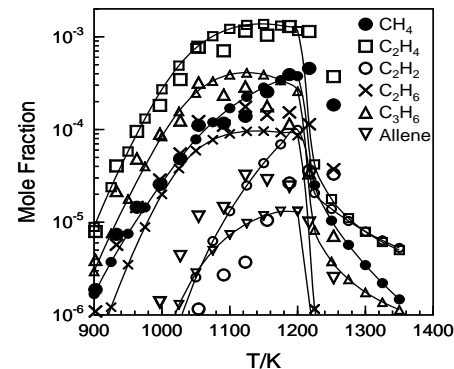
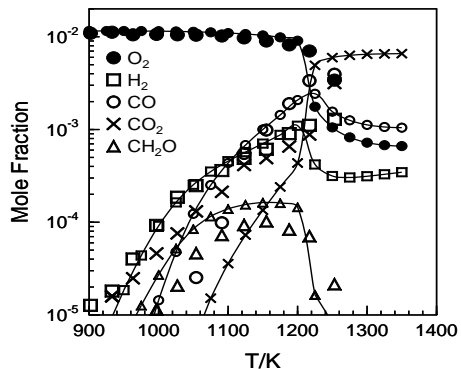
Kerosene oxidation in a JSR (700 ppmv of kerosene, 11550 ppmv of O₂, N₂; 0.07 s, 1 atm).

A good agreement between the data and the modeling for most of the species but benzene, and toluene which are strongly underestimated.

Expected: The oxidation of n-propylcyclohexane yields little benzene and toluene.

Dagaut & Cathonnet, *PECS* **32**, 48-92, 2006

n-decane/ n-propylbenzene/ n-propyl-cyclohexane (74% / 14% / 11% mole) as model fuel:



Kerosene oxidation in a JSR (700 ppmv of kerosene, 11550 ppmv of O_2 , N_2 ; 0.07 s, 1 atm).

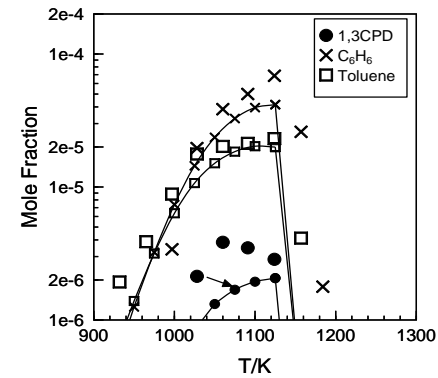
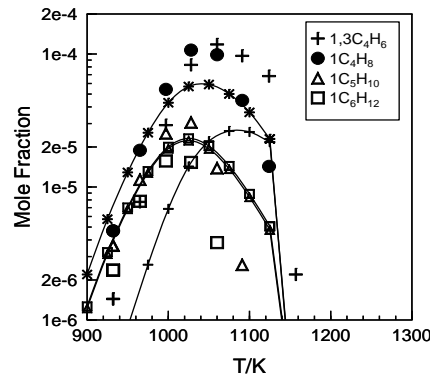
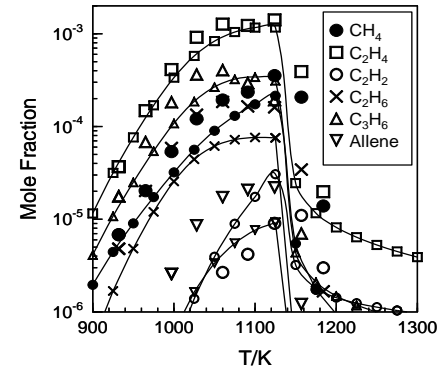
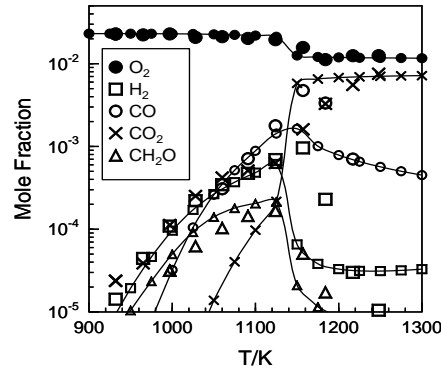
This mixture was more representative of the composition of kerosene: A good agreement between the data and the computational results for most of the species, including simple aromatics (benzene, toluene). Dagaut & Cathonnet, *PECS* **32**, 48-92, 2006

The three-component model fuel

n-decane/ n-propylbenzene/ n-propyl-cyclohexane (74% / 14% / 11% mole)

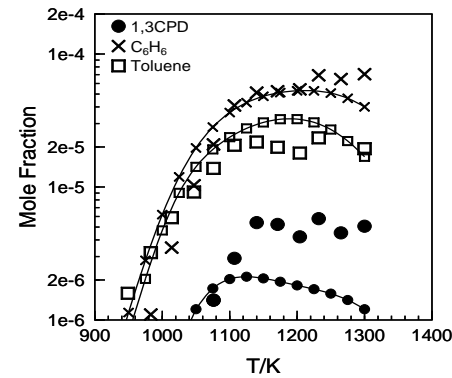
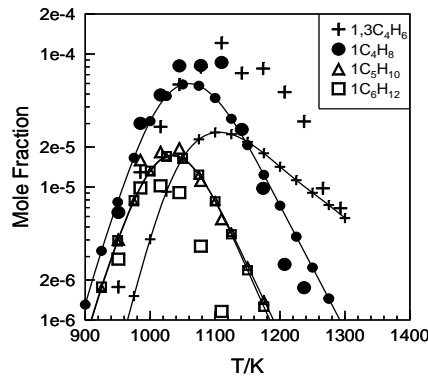
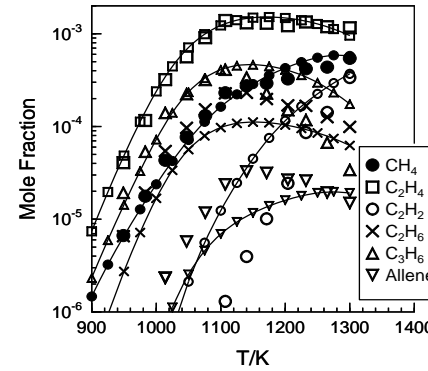
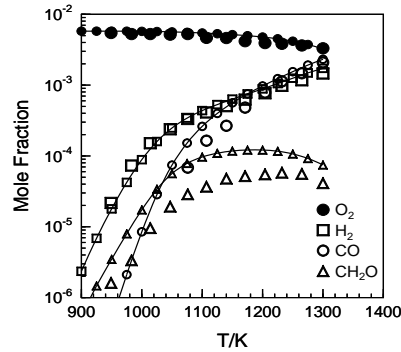
was selected for modeling the oxidation of kerosene in other experiments

n-decane/ n-propylbenzene/ n-propyl-cyclohexane (74% / 14% / 11% mole) as model fuel:



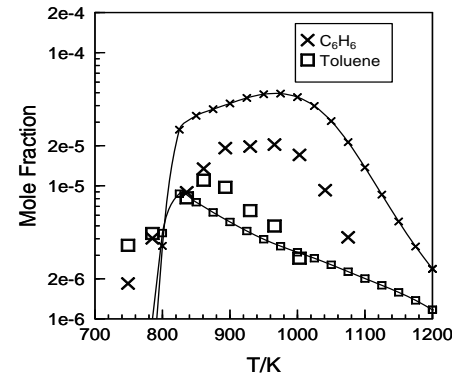
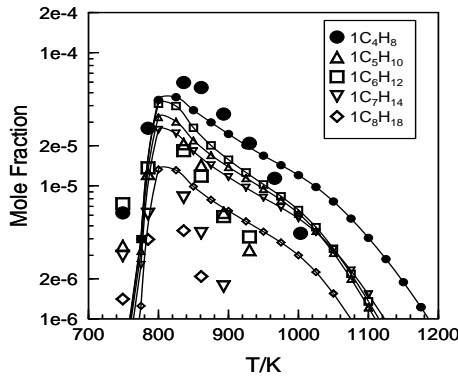
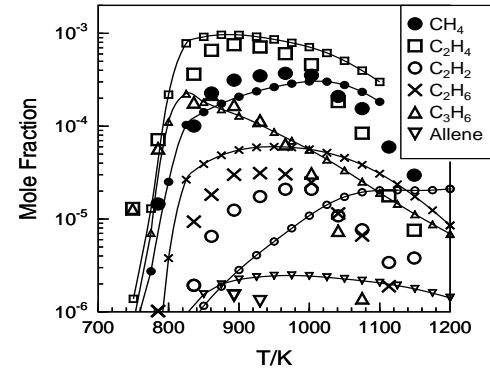
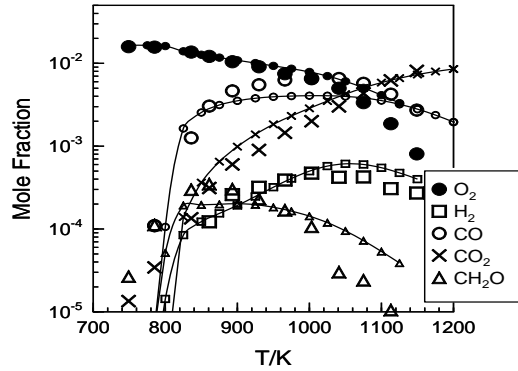
Kerosene oxidation (fuel lean) in a JSR (700 ppmv of kerosene, 23100 ppmv of O_2 , N_2 ; 0.07 s, 1 atm).
 Dagaut & Cathonnet, *PECS* **32**, 48-92, 2006

n-decane/ n-propylbenzene/ n-propyl-cyclohexane (74% / 14% / 11% mole) as model fuel:



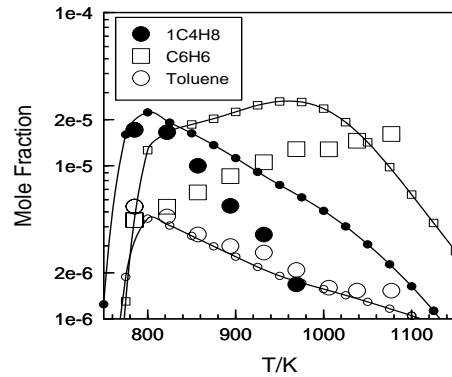
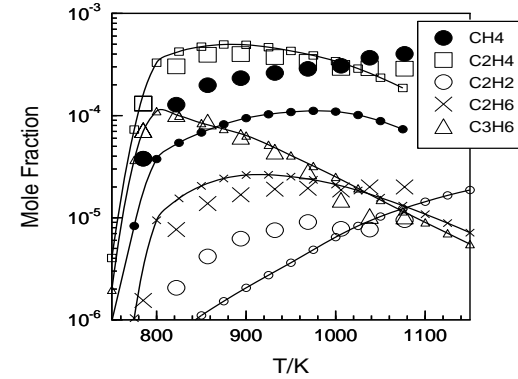
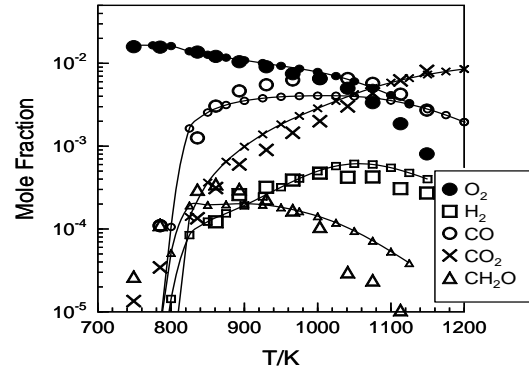
Kerosene oxidation (fuel rich) in a JSR (700 ppmv of kerosene, 5775 ppmv of O_2 , N_2 ; 0.07 s, 1 atm).
 Dagaut & Cathonnet, *PECS* **32**, 48-92, 2006

n-decane/ n-propylbenzene/ n-propyl-cyclohexane (74% / 14% / 11% mole) as model fuel:



Oxidation of kerosene in a JSR at **10 atm** and $t=0.5$ s (initial conditions: 1000 ppmv of kerosene TR0, 16500 ppmv of O_2 , diluent nitrogen)
 Dagaut & Cathonnet, *PECS* 32, 48-92, 2006

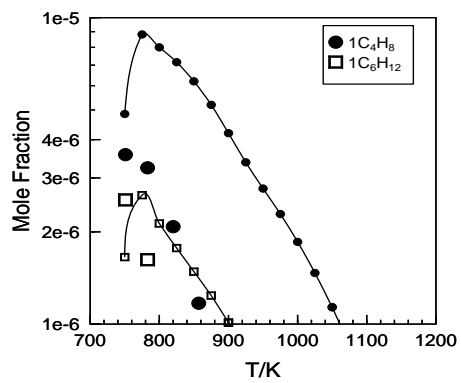
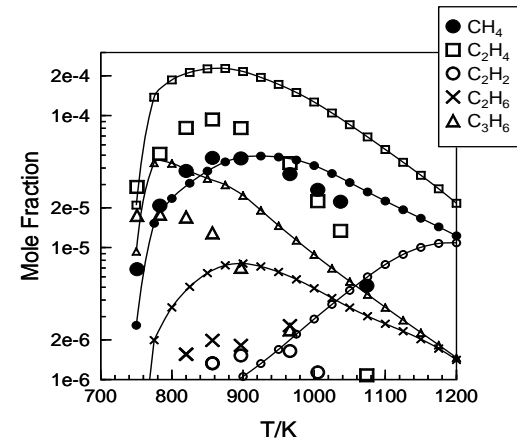
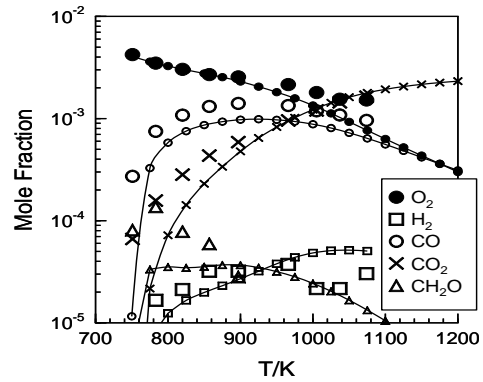
n-decane/ n-propylbenzene/ n-propyl-cyclohexane (74% / 14% / 11% mole) as model fuel:



Oxidation of kerosene in a JSR (500 ppmv of kerosene, 8250 ppmv of oxygen, nitrogen diluent; 1.0 s, **20 atm**).

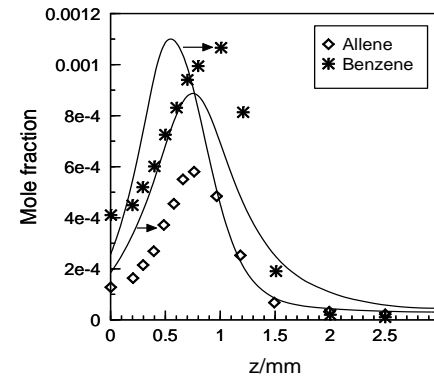
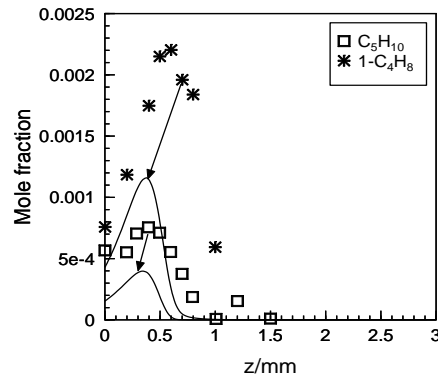
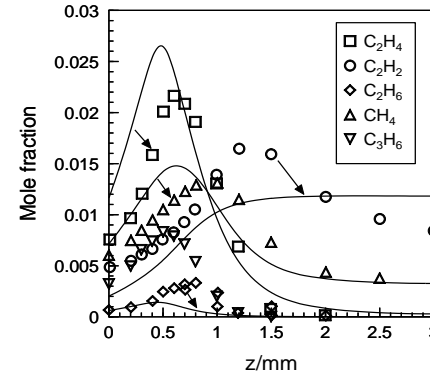
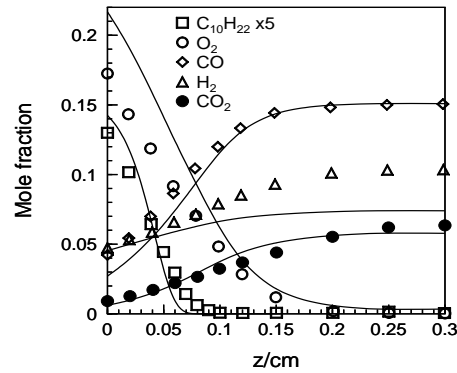
Dagaut & Cathonnet, *PECS* **32**, 48-92, 2006

n-decane/ n-propylbenzene/ n-propyl-cyclohexane (74% / 14% / 11% mole) as model fuel:



Oxidation of kerosene in a JSR at **40 atm** and $t=2.0$ s (initial conditions: 250 ppmv of kerosene TR0, 4125 ppmv of O_2 , diluent nitrogen)
 Dagaut & Cathonnet, *PECS* **32**, 48-92, 2006

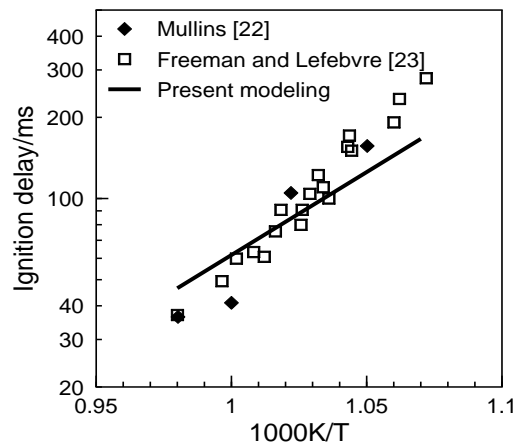
n-decane/ n-propylbenzene/ n-propyl-cyclohexane (74% / 14% / 11% mole) as model fuel:



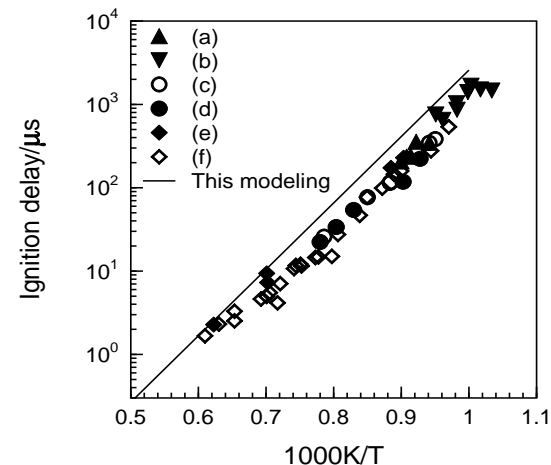
The oxidation of kerosene in premixed flame (Douté et al.) conditions: 1 atm, $0.010739794 \text{ g/cm}^2/\text{s}$, initial mole fractions: 0.0319 of kerosene, 0.28643 of oxygen.

Dagaut & Cathonnet, *PECS* 32, 48-92, 2006

The ignition delays of few kerosene-air mixtures at atmospheric pressure have been reported before; some of them have been used in several previous modeling efforts showing reasonable agreement with these data.



Ignition delay of kerosene/air mixtures at **1 atm**



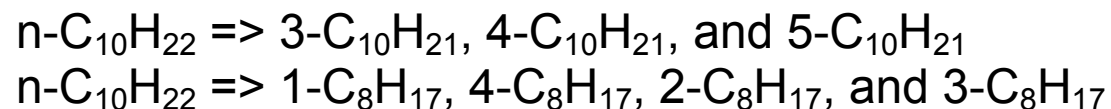
Ignition delay of kerosene/air mixtures at **20 atm**
 Data: Dean et al. 20th ICDEERS (2005); Starikovskii et al. (2003); Davidson and Hanson, 6th Int. Conf. on Chemical Kinetics, Gaithersburg, MD (2005).

Dagaut & Cathonnet, *PECS* **32**, 48-92, 2006

We performed a kinetic analysis of the reaction paths during the oxidation of the kerosene model-fuel at 10 atm, under stoichiometric conditions. It indicated that the overall oxidation of the fuel is mostly driven by n-decane oxidation.

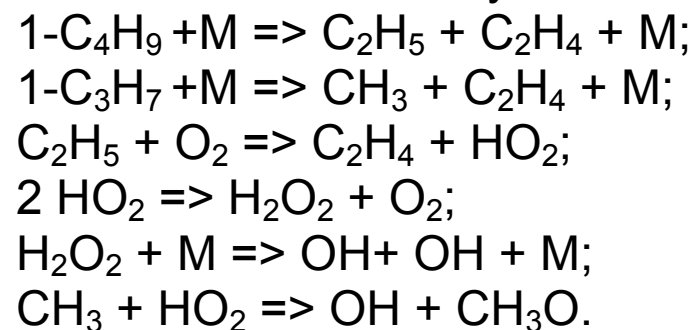
According to the model, at 900 K, the early stages of the fuel oxidation involve the oxidation of n-decane, n-propylbenzene, and n-propylcyclohexane.

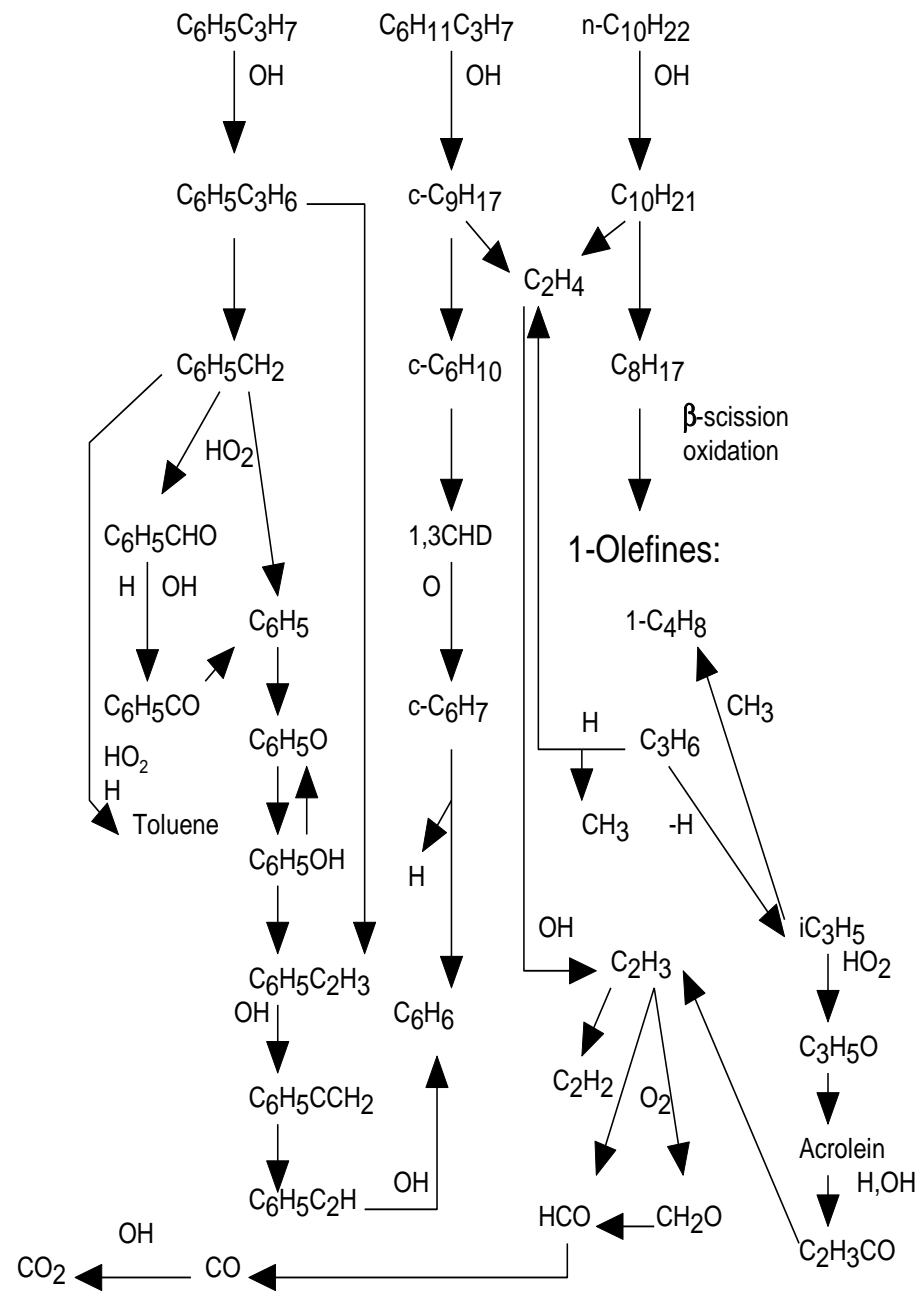
Hydroxyl radicals are the main species involved in the oxidation of the fuel mixture. The oxidation of n-decane is responsible for the production of these radicals via a complex reaction scheme that can be summarized as follows:



The decyl and octyl radicals isomerize and decompose. Their decomposition yields 1-butyl and 1-propyl radicals that in turn decompose.

The further reactions in turn yield OH radicals:

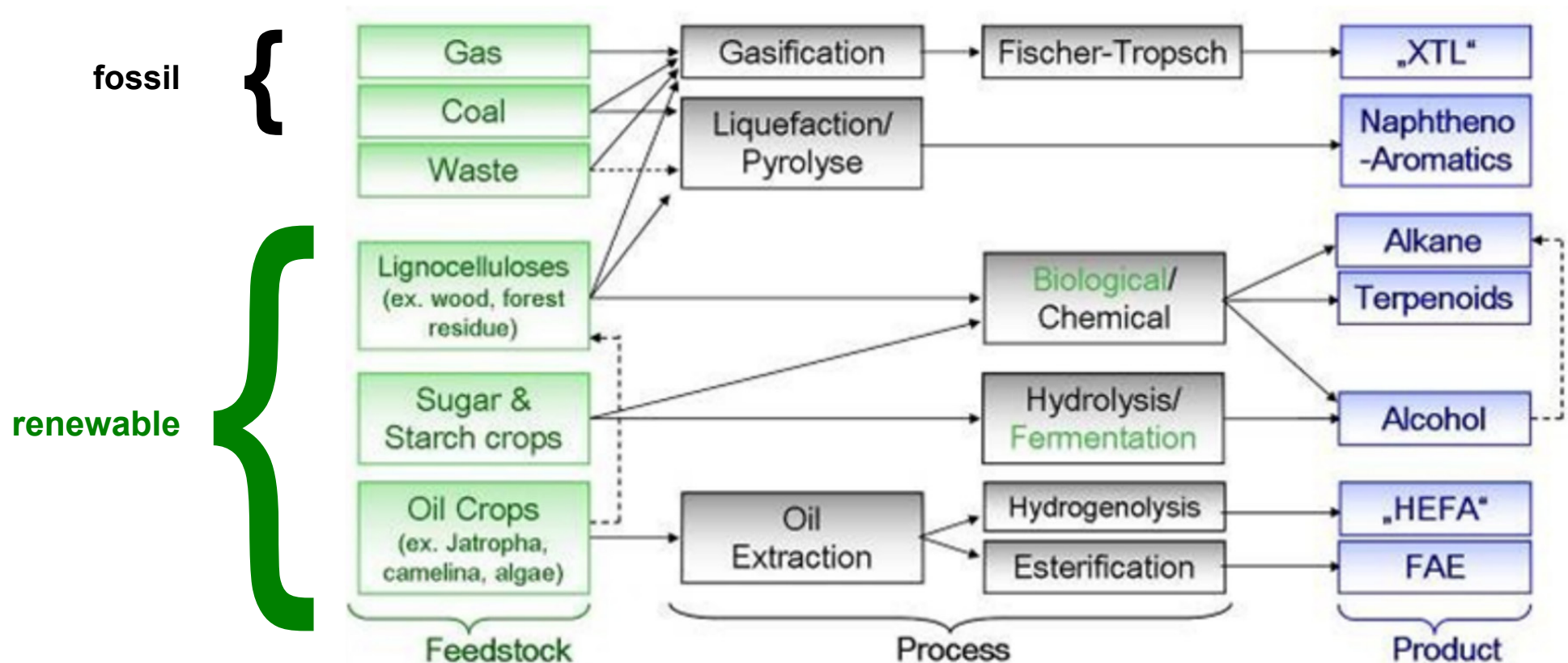




Dagaut & Cathonnet, *PECS* **32**, 48-92, 2006

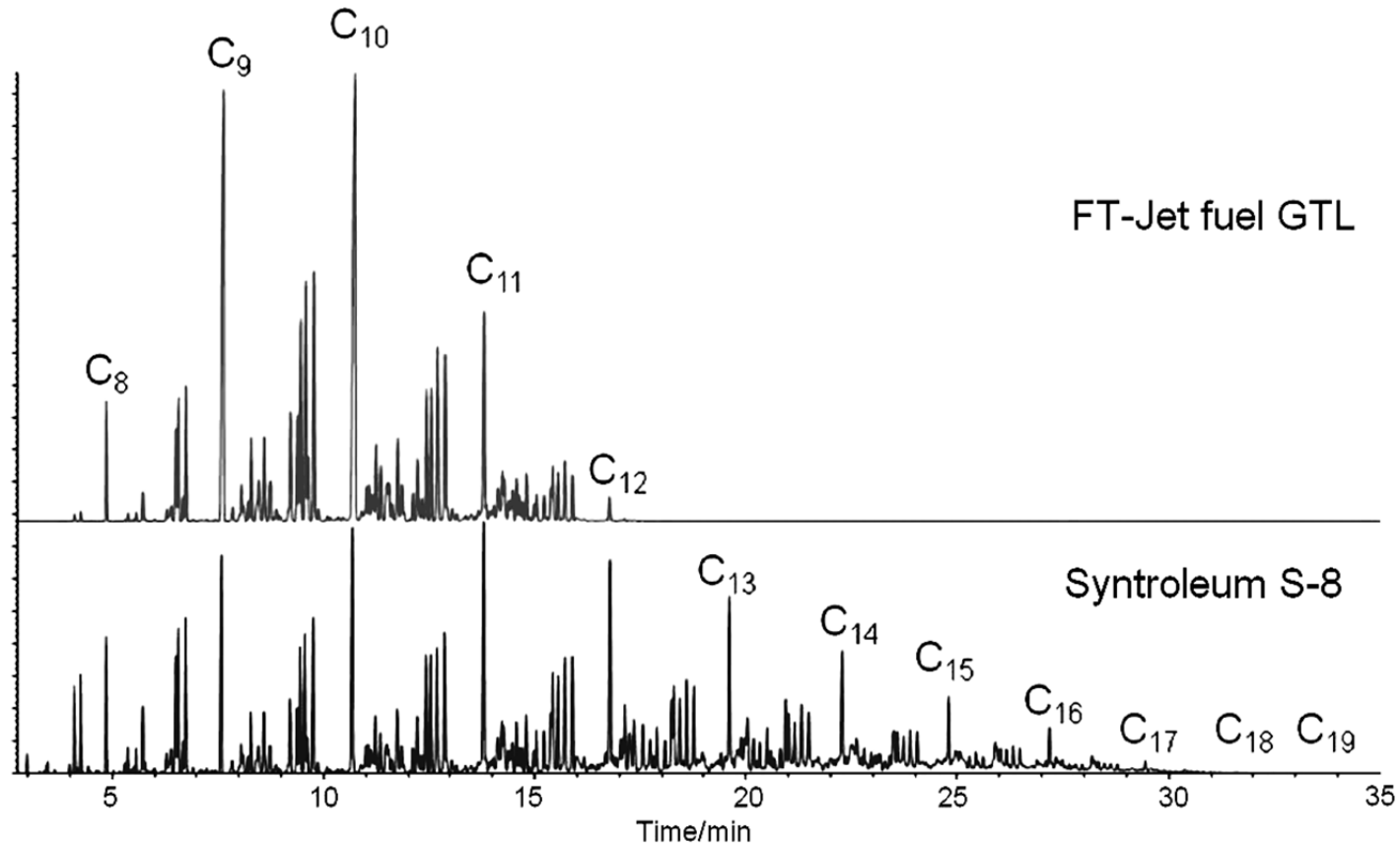
Synthetic jet fuels

In recent years, research activities on **synthetic and bio-derived jet fuels** have increased significantly in order to reduce dependence of air transportation on oil (petroleum).



*XTL: Gas/Coal/Waste/Renewable to Liquid

The Fischer-Tropsch (F-T) process allows the production of a kerosene type fuel from synthesis gas also called syngas (CO/H_2). Frequently, a **synthetic jet fuel** is mainly composed of ***n*-alkanes**, ***iso*-alkanes** and ***cyclo*-alkanes**, but **composition varies** from one source to another, e.g.:



Source: *Egolfopoulos et al. (USC)*

The very low proportion of aromatic compounds in GtL fuels causes a reduction in emissions of soot and unburned hydrocarbons*.

The composition of synthetic jet fuel allows also a decrease in emissions of carbon dioxide and soot**.

These fuels are a good alternative to current conventional oil-derived fuels.

* Corporan et al., 2007, *Energy & Fuels* 21, pp. 2615–2626; Kahandalawa et al., 2008, *Energy & Fuels* 22, pp. 3673–3679.

** Rye et al., 2010, *Energy & Environmental Science* 3, pp. 17–27

The kinetics of oxidation of **alternative jet fuels** and **representative surrogates** studied in a JSR under the same conditions (temperature, 550-1150 K; pressure, 10 bar; equivalence ratio, 0.5-2).

To **experimentally represent** the two synthetic fuels we have designed **surrogates** consisting of few representative species among **n-decane, iso-octane, decalin, n-propylcyclohexane, and n-propylbenzene**.

The **oxidation of 2 representative mixtures, 100% GtL** ($C_{10.45}H_{22.93}$; $H/C=2.20$; $M=148.28$ g mol⁻¹; $CN=56^*$; density=724 g L⁻¹, from Shell), **and 100% CtL** ($C_{11.06}H_{21.38}$, $H/C=1.934$; $M=154.12$ g mol⁻¹; $CN=41^*$; density=799 g L⁻¹, from Sasol) **was performed in a JSR at 10 atm**.

* ASTM D7668

A **detailed kinetic reaction mechanism** was developed and validated by comparison with the experimental results obtained here and previously*.

The current model was also evaluated under shock tubes conditions by using data from the literature**.

* Mzé Ahmed, A., Dagaut, P., Hadj-Ali, K., Dayma, G., Kick, T., Herbst, J., Kathrotia, T., Braun-Unkhoff, M., Herzler, J., Naumann, C., and Riedel, U., 2012, *Energy & Fuels*, 26(10), pp. 6070-6079.

Dagaut, P., Karsenty, F., Dayma, G., Diévar, P., Hadj-Ali, K., Mzé-Ahmed, A., Braun-Unkhoff, M., Herzler, J., Kathrotia, T., Kick, T., Naumann, C., Riedel, U., and Thomas, L., 2014, *Combustion and Flame*, 161(3), pp. 835-847

**Wang, H. W., and Oehlschlaeger, M. A., 2012, *Fuel*, 98(1), pp. 249-258.

MODELING

The CHEMKIN II computer code was used for the kinetic modeling of the oxidation of the two fuels studied in a jet-stirred reactor.

The chemical kinetic reaction mechanism used here contained **2,430 species and 10,962 reversible reactions.**

Surrogate model fuels were used for the kinetic modeling

MODELING

- The synthetic kerosene **GtL** was represented by a mixture of **28.1%w n-decane, 30% 2-methylheptane, 33.1% 3-methylheptane, and 8.8% decalin.**

This corresponds very well with the GtL composition (GtL%/surrogate% in mass: 28.1/28.1, 63.1/62.8, 8.8/8.8 in mass of n-alkanes, iso-alkanes, and naphthenes, respectively).

- The synthetic kerosene **CtL** was represented by a mixture of **5.7%w n-decane, 11.5% iso-octane, 24.8% 3-methylheptane, 16.1% n-propylcyclohexane, 28.3% decalin, 4% n-propylbenzene, and 9.6% tetralin.**

This corresponds very well with the CtL composition (CtL%/surrogate% in mass: 5.7/5.7, 36.3/36.3, 16.1/16.1, 28.3/28.3, 4/4, 9.6/9.6 of n-alkanes, iso-alkanes, mono-naphthenes, di-naphthenes, mono-aromatics, and naphtheno-aromatics, respectively).

MODELING

Sub-models for surrogates components were taken from our previous modeling efforts. *n*-Decane, iso-octane, 2-methylheptane and 3-methylheptane studied previously[#] were used to represent the *n*- and *iso*-paraffins present in the synthetic fuels. Naphthenes were represented by *n*-propylcyclohexane* and decalin** in the model. Mono-aromatics were represented by *n*-propylbenzene*** and tetralin****represented naphteno-aromatics.

Experimental data obtained in JSR were compared to simulations in order to validate the chemical kinetic mechanism developed in this work.

Sarathy et al., 2011, Combustion and Flame, 158(12), pp. 2338-2357.

Karsenty et al., 2012, Energy & Fuels, 26(8), pp. 4680-4689.

Mze-Ahmed et al., 2012, Energy & Fuels, 26(7), pp. 4253-4268.

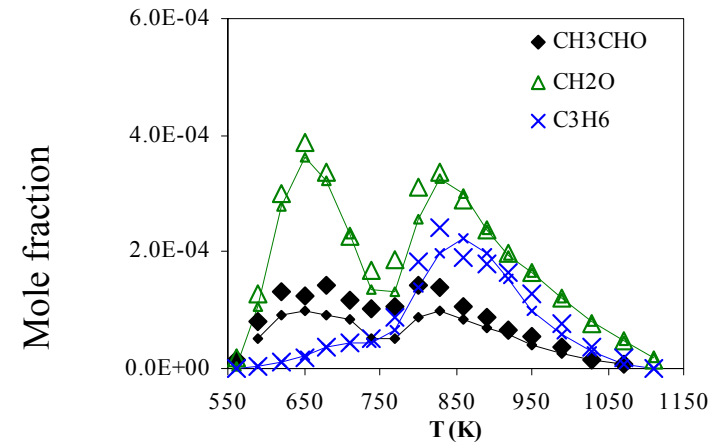
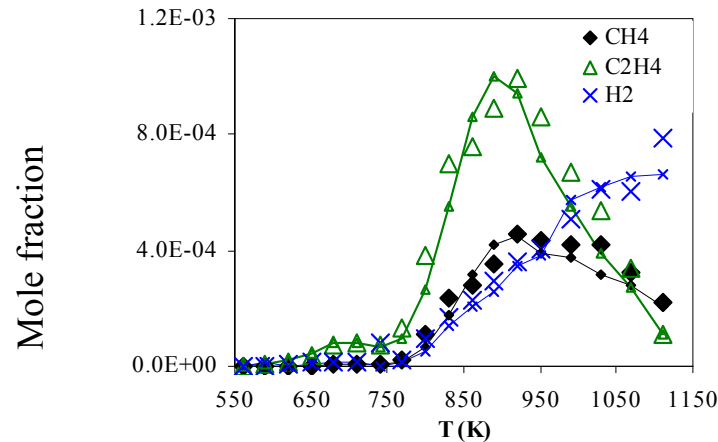
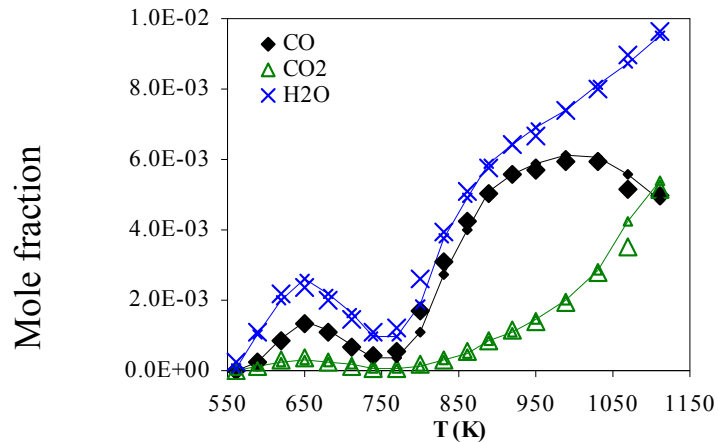
* Ristori, A et al., 2001, Combustion Science and Technology, 165(1), pp. 197-228.

** Dagaut et al., 2013, Proceedings of the Combustion Institute, 34(1), pp. 289-296.

*** Dagaut et al., 2002, Fuel, 81(2), pp. 173-184.

**** Dagaut et al., 2013, Energy & Fuels, 27(3), pp. 1576-1585.

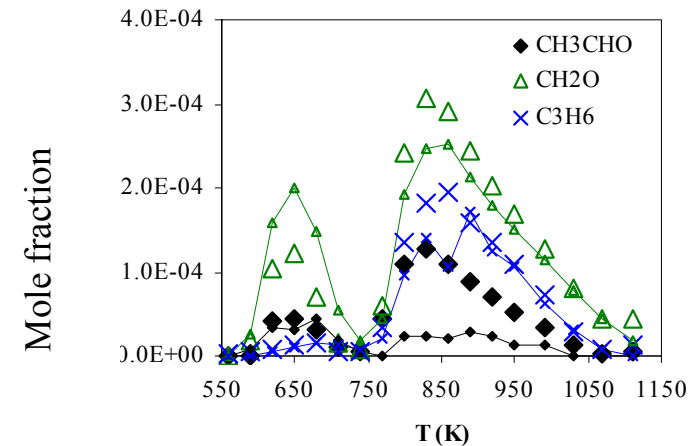
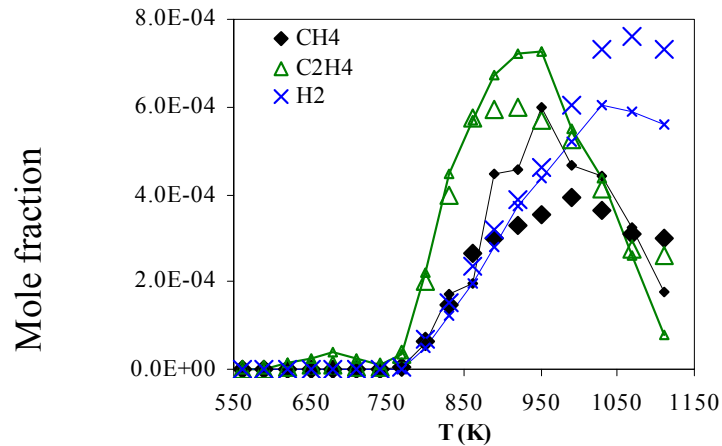
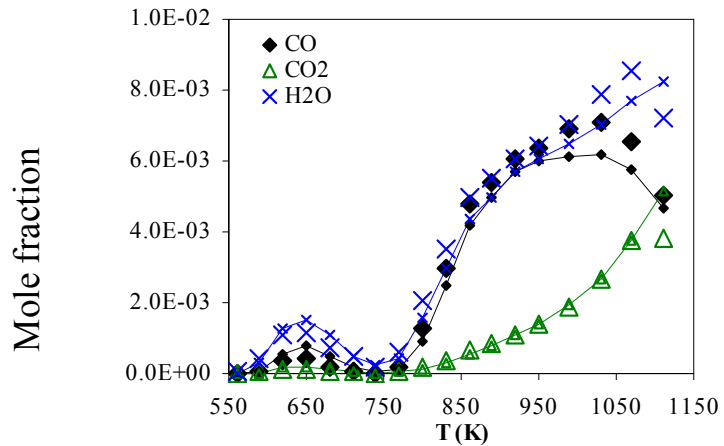
EXPERIMENTAL RESULTS GTL VS. SURROGATE



Concentrations profiles obtained from the **oxidation of the GTL and the representative mixture** in a JSR at 10 bar, $\tau = 0.7$ s and $\phi = 1$. The initial mole fractions were: $x_{\text{GTL}} = 0.1\%$, $x_{\text{O}_2} = 1.6\%$, $x_{\text{N}_2} = 98.3\%$ mole. The GTL data (large symbols) are compared to those for the surrogate (lines and small symbols, 650 ppm of **n-decane**, 375 ppm of **iso-octane**, and 95 ppm of **decalin**).

Dagaut et al., ICDERS 2015

EXPERIMENTAL RESULTS CTL VS. SURROGATE



Concentrations profiles obtained from the oxidation of the **CTL** and the **representative mixture** in a JSR at 10 bar, $\tau = 0.7$ s and $\phi = 1$. The initial mole fractions were: $x_{\text{CTL}} = 0.1\%$, $x_{\text{O}_2} = 1.5\%$, $x_{\text{N}_2} = 98.4\%$ mole. The CTL data (large symbols) are compared to those for the surrogate (lines and small symbols, 163 ppm of **n-decane**, 365 ppm of **iso-octane**, 197 ppm of **n-propylcyclohexane**, 317 ppm of **decalin**, and 175 ppm of **n-propylbenzene**).

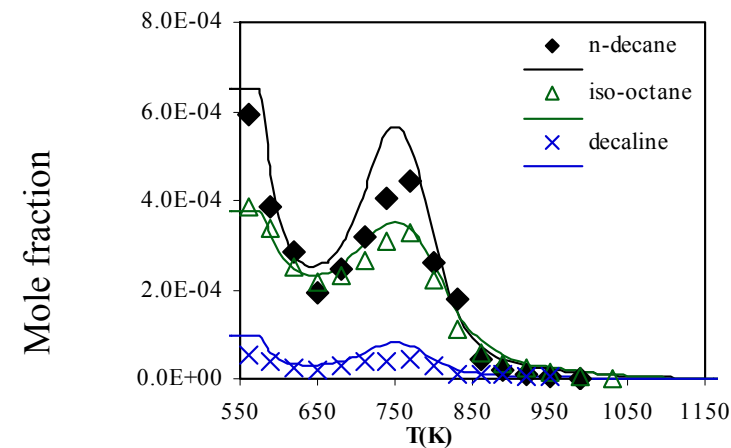
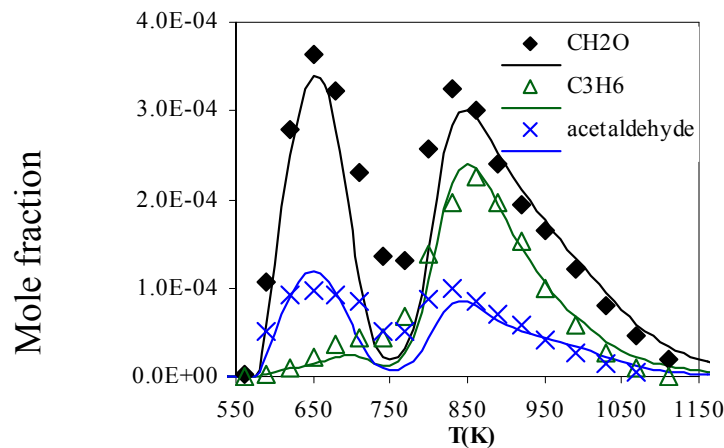
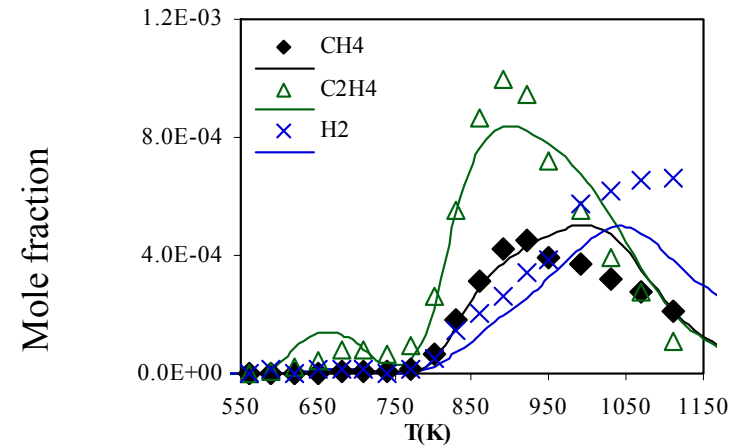
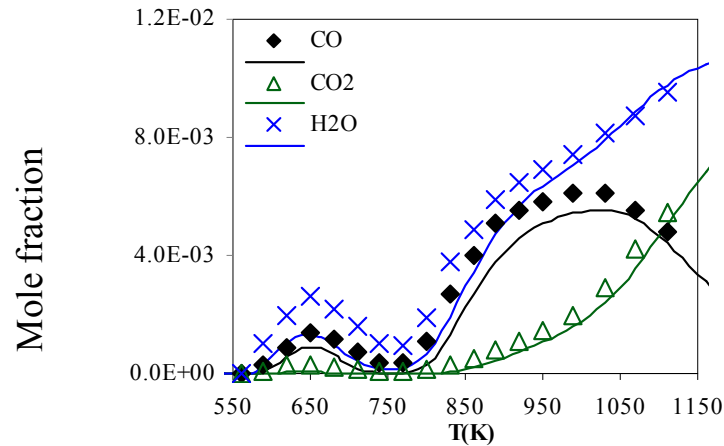
Dagaut et al., ICDERS 2015

EXPERIMENTAL RESULTS SPK VS. SURROGATE

Very similar **experimental** profiles obtained for the SPKs and their Surrogates

☞ Kinetic modeling of the oxidation of these surrogates for model validation

SURROGATE OX'n, EXPERIMENTAL VS. MODELING



Concentrations profiles obtained from the oxidation of a **GTL representative mixture** in a JSR at 10 bar, $\tau = 0.7$ s and $\phi = 1$. The data (large symbols) are compared to the **modeling** (lines).

Dagaut et al., ICDERS 2015

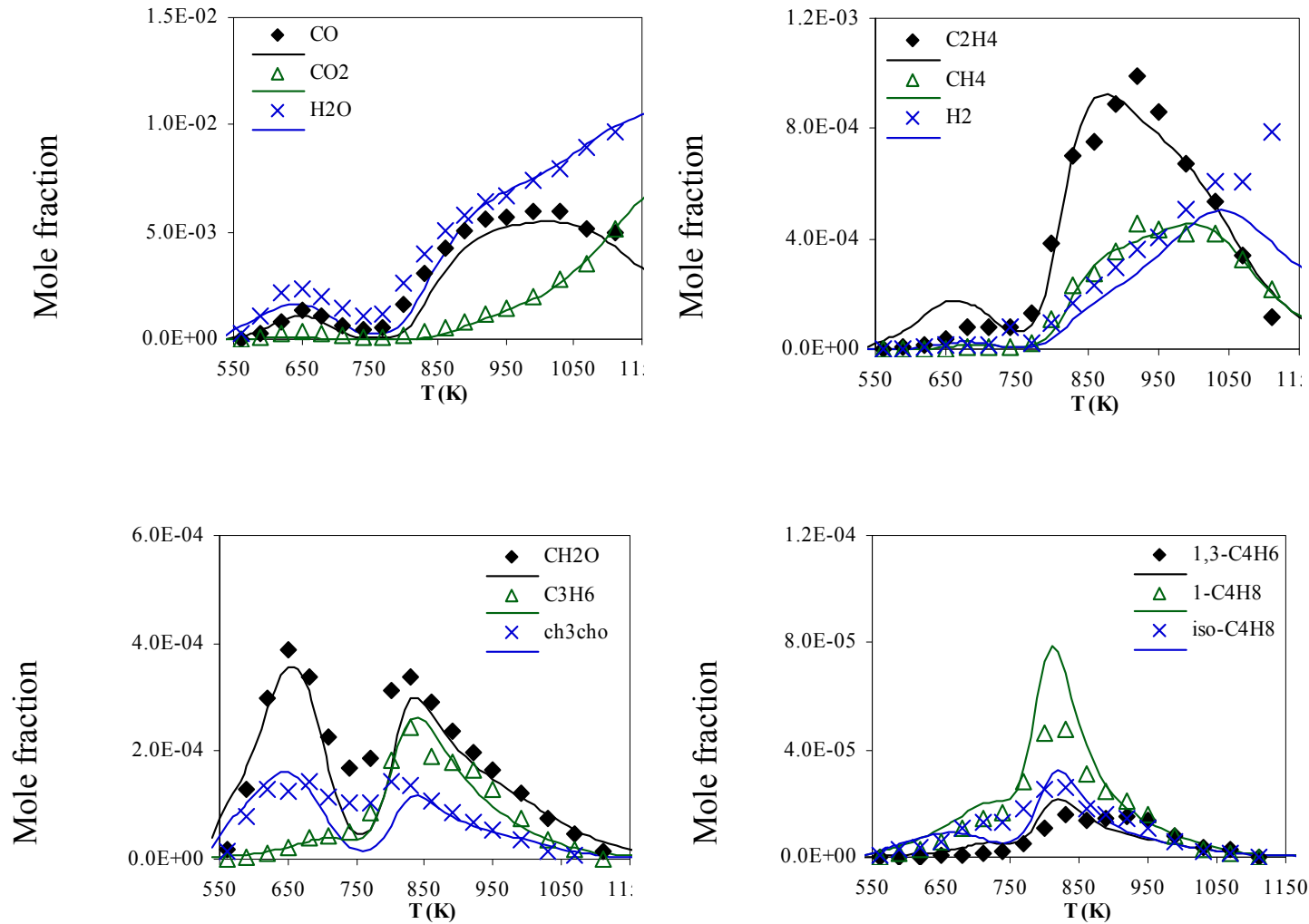
MODELING GTL OX'n

Composition of final model fuel to simulate the oxidation of the **GtL** fuel ($C_{10.45}H_{23.06}$; $H/C=2.20$; $CN= 57.94$; 737.7 g mol^{-1} ; $M=148.46 \text{ g mol}^{-1}$)^a

Component	Initial concentrations (ppm)
<i>n</i> -decane	294
2-methylheptane	390
3-methylheptane	431
decalin	94

^a $1.209 \times C_{8.64}H_{18.97}$ since we used 1209 ppm of model fuel to represent 1000 ppm of GtL

GTL OX'n, EXPERIMENTAL VS. MODELING

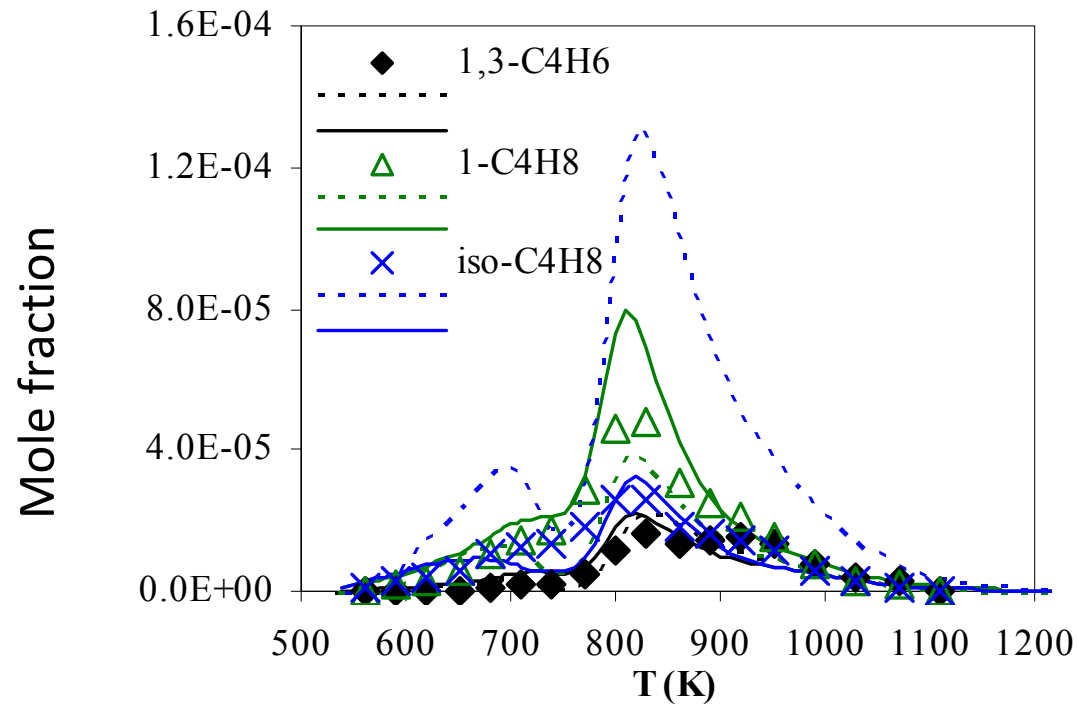


Concentrations profiles obtained from the oxidation of the **GTL fuel** in a JSR at 10 bar, $\tau = 0.7$ s and $\phi = 1$. The data (large symbols) are compared to the modeling (lines).

Dagaut et al., ICDERS 2015

GTL OX'n, EXPERIMENTAL VS. MODELING

Modeling improvements:



Comparison of computed and experimental concentrations profiles obtained from the oxidation of the **GTL** fuel in a JSR at 10 bar, $\tau = 0.7$ s and $\phi = 1$ (experimental data: large symbols; previous model (Dagaut et al., 2015, CNF, 161(3) 835-847): dotted lines; this model: continuous lines).

Dagaut et al., ICDERS 2015

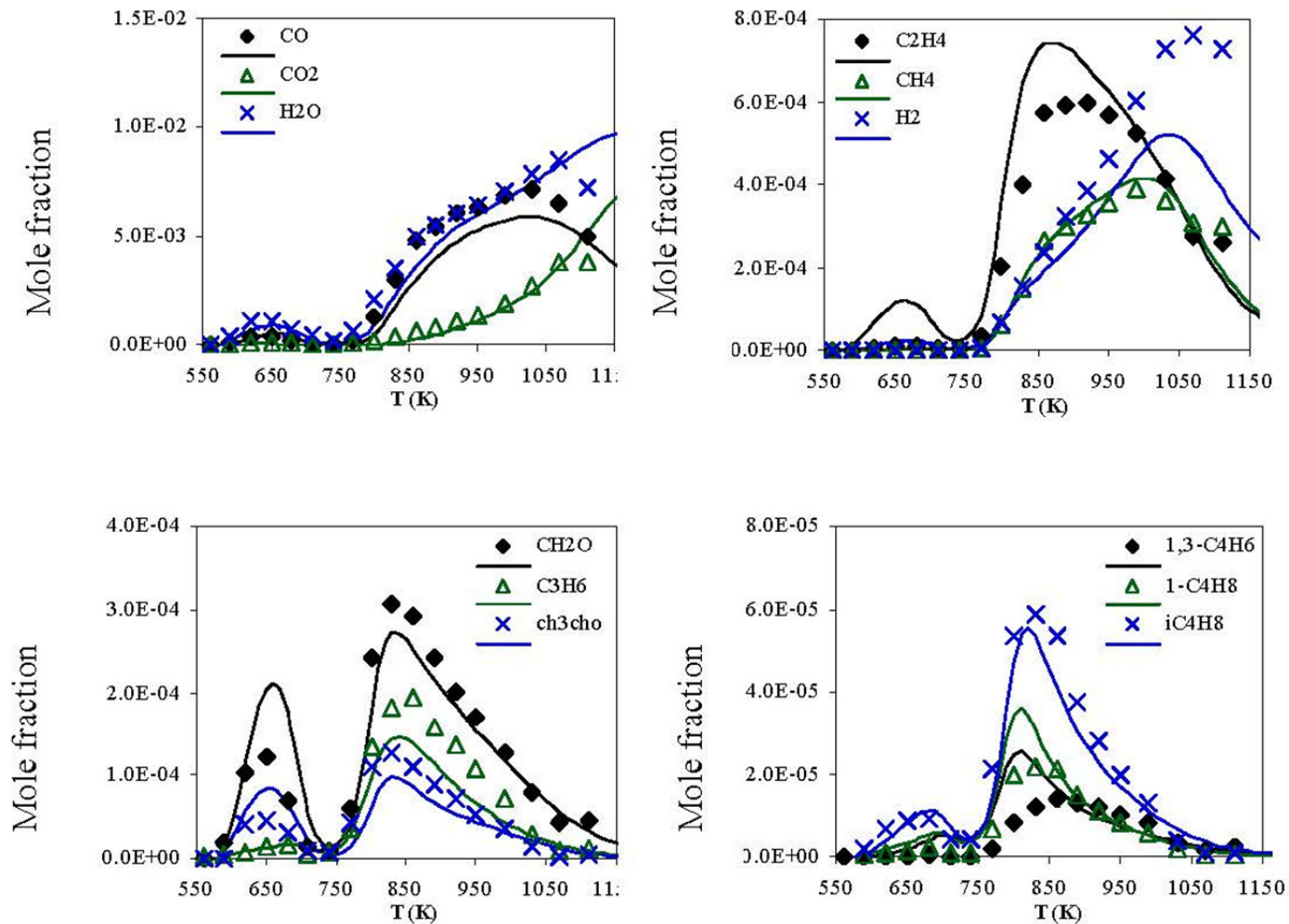
MODELING CTL OX'n

Composition of final model fuel to simulate the oxidation of the CtL fuel ($C_{11.06}H_{21.6}$; $H/C=1.953$; $CN= 32.7$; 815.7 g mol^{-1} ; $M=154.32 \text{ g mol}^{-1}$)^b

Component	Initial concentrations (ppm)
<i>n</i> -decane	62
<i>iso</i> -octane	155
3-methylheptane	335
<i>n</i> -propylcyclohexane	197
decalin	316
<i>n</i> -propylbenzene	52
tetralin	112

^b $1.229 \times C_9H_{17.4}$ since we used 1229 ppm of model fuel to represent 1000 ppm of CtL

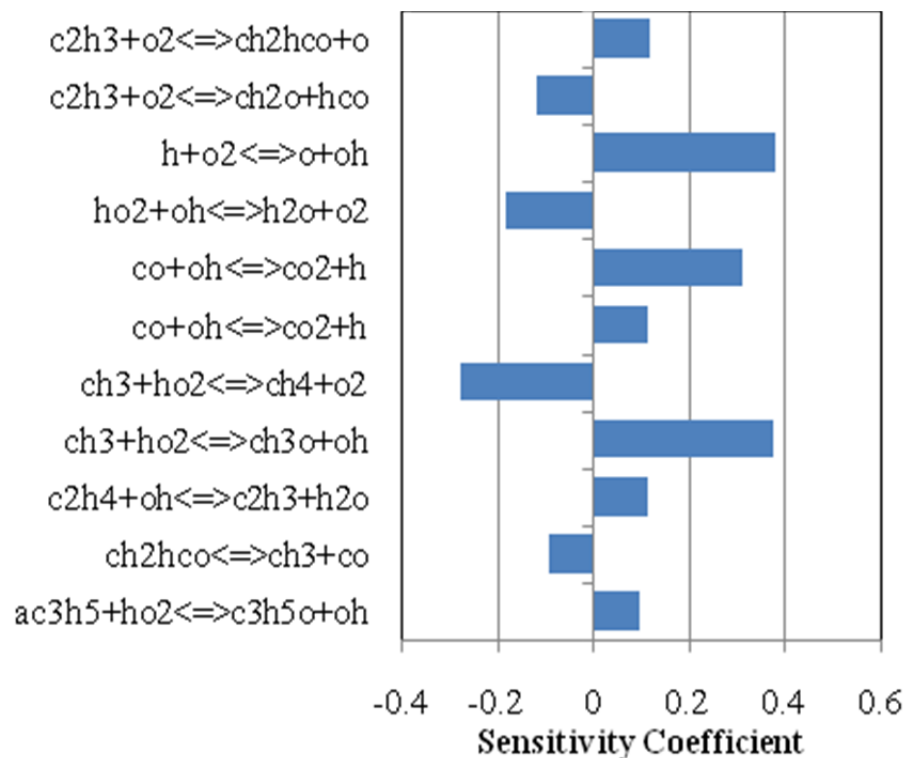
RESULTS AND DISCUSSION: CTL OX'n, EXPERIMENTAL VS. MODELING



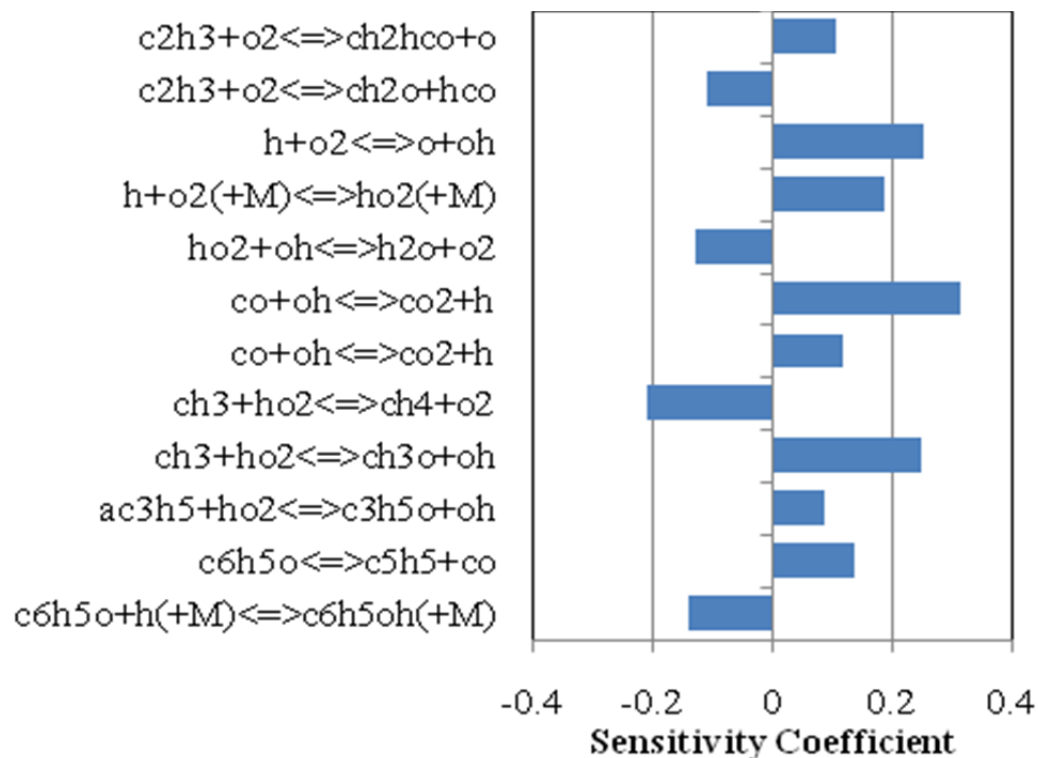
Concentrations profiles obtained from the oxidation of the **CTL fuel** in a JSR at 10 bar, $\tau = 0.7$ s and $\phi = 1$. The data (large symbols) are compared to the modeling (lines).

Dagaut et al., ICDERS 2015

Sensitivity analyses and reaction pathways analyses



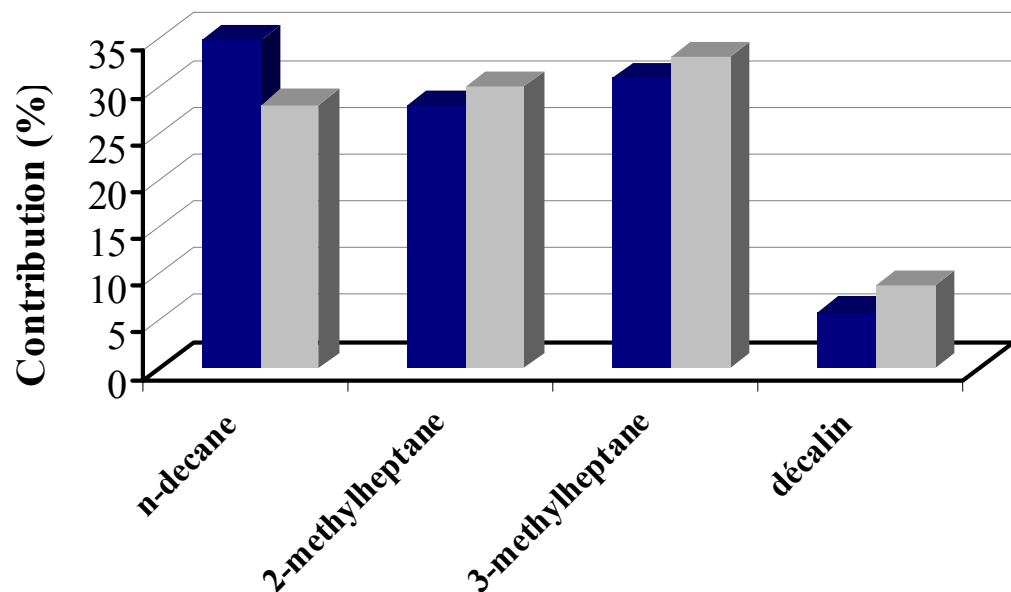
Sensitivity analyses for CO₂ at 1030 K during the oxidation of the **GtL** fuel in a JSR ($\phi = 1$, 10 bar, residence time of 0.7 s)



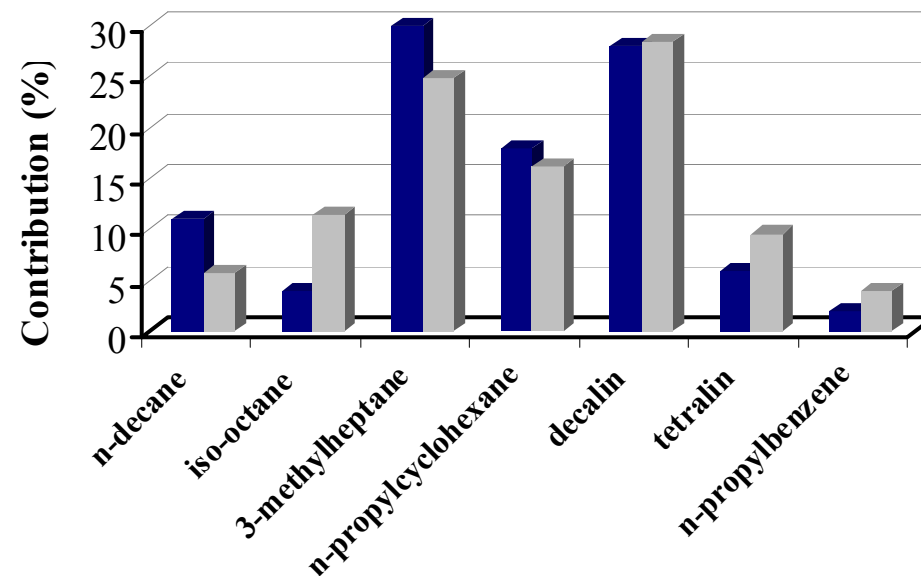
Sensitivity spectrum for CO₂ during the oxidation of the **CtL** fuel in a JSR at $\phi=1$ and $T=1030$ K ($P = 10$ bar and $\tau = 0.7$ s).

These computations show the influence of **OH radicals** during the oxidation of these fuels.

Sensitivity analyses and reaction pathways analyses



Contribution of the surrogate components to the **formation of OH** (blue) during the oxidation of the **GtL** fuel in a JSR ($\phi = 1$, 830 K, 10 bar, residence time of 0.7 s). For comparison, the concentrations of the surrogate components are shown in grey.



Contribution of the surrogate components to the **formation of OH** (blue) during the oxidation of the **CtL** fuel in a JSR ($\phi = 1$, 830 K, 10 bar, residence time of 0.7 s). For comparison, the concentrations of the surrogate components are shown in grey.

Ignition Delay Times

Wang and Oehlschlaeger* measured the ignition delay of a synthetic jet fuel derived from natural gas and provided by Shell ($C_{10.40}H_{22.88}$) in a heated shock tube between 650 and 1290 K at 20 atm and $\phi=1.0$ (1.286% fuel, 20.74% O_2 , 77.97% N_2). In order to simulate the high temperature regime ($T > 1000K$), they used the surrogate model developed by Naik et al.** (*n*-decane: 61%, *n*-dodecane: 11%, *iso*-octane: 28% in mole).

Their results showed that the data measured by Wang and Oehlschlaeger are similar to the model predictions at high temperature.

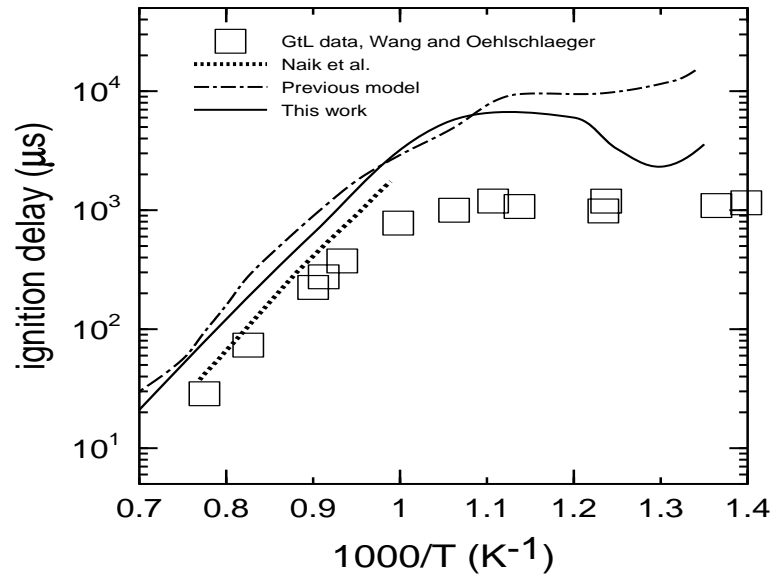
We verified the validity of our model for the ignition in shock tube using the experimental data* for GtL and the data of Vasu et al.*** for *n*-dodecane ignition.

*Wang and Oehlschlaeger, 2012, *Fuel* 98, pp. 249–258

**Naik et al., 2011, *Comb. Flame* 158, pp. 434–445

***Vasu et al. , 2009, *Proc. Combust. Inst.* 32, pp. 173-180

Ignition Delay Times in Air



Comparison between ignition delay times measurements by Wang and Oehlschlaeger (Shell GtL, open symbols) and Vasu et al. (*n*-dodecane, stars), modeling of Naik et al. (dotted line), the present modeling results for GtL (dashed dotted line) and *n*-dodecane predictions (solid line).

- The computed ignition delays $>$ Naik's computations.

Same trends as in the experiments but overestimation of ignition delays (ca. $\times 4$ @ 900K).

- The new computed ignition is in better agreement with the data than previously, but the model is too slow.

Further studies of synthetic jet fuels oxidation

The very low proportion of aromatic compounds in GtL fuels causes a reduction in emissions of soot and unburned hydrocarbons*. The composition of synthetic jet fuel allows also a decrease in emissions of carbon dioxide and soot**.

These fuels are a good alternative to current conventional oil-derived fuels.

* Corporan et al., 2007, *Energy & Fuels* 21, pp. 2615–2626; Kahandalawa et al., 2008, *Energy & Fuels* 22, pp. 3673–3679.

** Rye et al., 2010, *Energy & Environmental Science* 3, pp. 17–27

A GtL, a Naphthenic cut (NC) and a mixture NC/GtL were oxidized in a JSR:

Properties	GtL	NC*	NC/GtL
Formula	$C_{10.45}H_{23.06}$	$C_{12.64}H_{23.64}$	$C_{11.54}H_{23.35}$
M (g mol ⁻¹)	148.44	175.32	161.83
H/C ratio	2.20	1.87	2.02
DCN [‡]	58.0	39.3	45.8
Density (g l ⁻¹)	737.7	863.1	800.3

* Naphthenic cut: a representative commercial solvent that fits with typical chemical composition of product coming from coal or biomass liquefaction.

‡ measured by PAC Cetane ID 510, ASTM D7668

MODELING

A detailed kinetic reaction mechanism was developed and validated by comparison with the experimental results obtained here and previously*.

The CHEMKIN II computer code was used for the kinetic modeling of the oxidation of the two fuels studied in a jet-stirred reactor.

The chemical kinetic reaction mechanism used here contained **2,384 species and 10,368 reversible reactions.**

* Mzé Ahmed, A., Dagaut, P., Hadj-Ali, K., Dayma, G., Kick, T., Herbst, J., Kathrotia, T., Braun-Unkhoff, M., Herzler, J., Naumann, C., and Riedel, U., 2012, *Energy & Fuels*, 26(10), pp. 6070-6079.
Dagaut, P., Karsenty, F., Dayma, G., Diévar, P., Hadj-Ali, K., Mzé-Ahmed, A., Braun-Unkhoff, M., Herzler, J., Kathrotia, T., Kick, T., Naumann, C., Riedel, U., and Thomas, L., 2014, *Combustion and Flame*, 161(3), pp. 835-847

MODELING

Surrogate model fuels for the kinetic modeling:

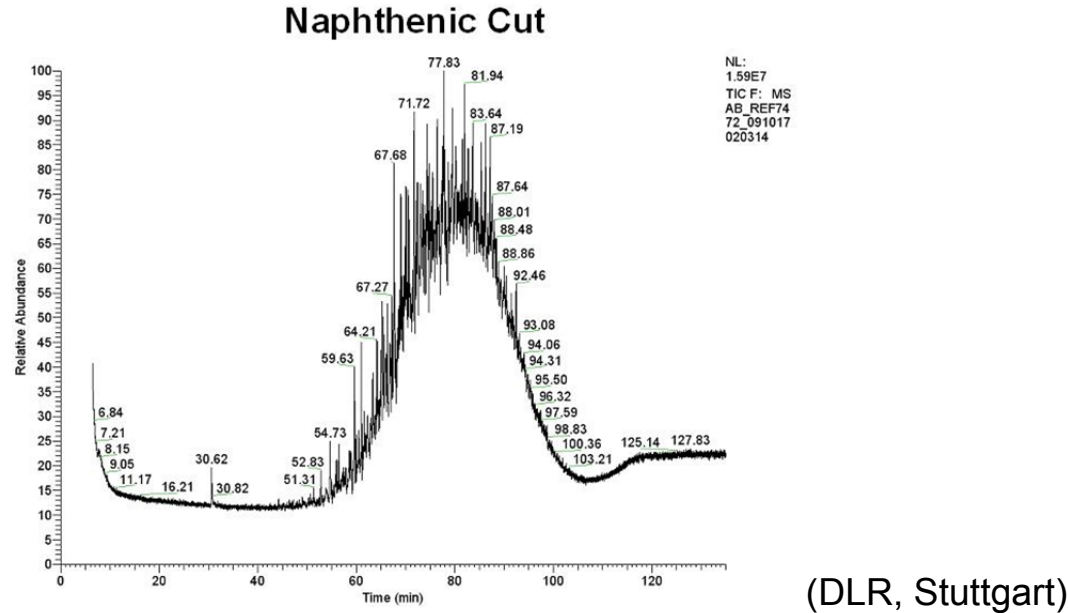
The GtL was represented by a mixture of **n-decane**, **2-methylheptane**, **3-methylheptane**, and **decahydronaphthalene** (28.1%, 30%, 33.1%, and 8.8% in mass, respectively) which corresponds very well with the GtL mass composition (28.1%, 62.8%, 8.8% of n-alkanes, iso-alkanes, and naphthenes, respectively). The model fuel matches well the GtL cetane number (57.94 vs. 58) and its H/C ratio (2.2 vs. 2.2).

The substitution of the highly branched iso-octane used in a previous model by weakly branched iso-alkanes (2-methylheptane and 3-methylheptane) is beneficial, particularly for better controlling iso-butene production.

MODELING

Surrogate model fuels for the kinetic modeling:

The naphthenic cut was represented by a mixture of **decahydronaphthalene**, **tetrahydronaphthalene**, **n-propylcyclohexane**, **2-methylheptane**, and **3-methylheptane** (27.6%, 23.5%, 10.8%, 12.1%, 25%, and 13% in mass, respectively) which is in line with the naphthenic cut composition (89.9% of paraffins and cycloparaffins and 10.1% of aromatics in mass).



MODELING

- Composition of the model-fuel to represent the GtL* fuel in the computations ($C_{10.45}H_{23.06}$; $H/C=2.20$; $DCN= 57.94$; $M=148.46 \text{ g mol}^{-1}$) ‡

Component	Initial concentrations (ppm)
<i>n</i> -decane	294
2-methylheptane	390
3-methylheptane	431
decahydronaphthalene	94

‡ $1.209 \times C_{8.64}H_{18.97}$ since we used 1209 ppm of model fuel to represent 1000 ppm of GtL

*GtL: 28.1% *n*-alkanes, 62.8% iso-alkanes, 8.8% cyclo-alkanes, and 0.2% aromatics. The composition of the fuels and their molecular weight were determined through gas chromatography (<http://www.alfa-bird.eu-vri.eu/>)

MODELING

- Composition of the model-fuel to represent the naphthenic cut* in the computations

($C_{12.63}H_{23.26}$; H/C=1.84; DCN= 39.7; M=174.82 g mol⁻¹) ‡

Component	Initial concentrations (ppm)
decahydronaphthalene	350
tetrahydronaphthalene	312
<i>n</i> -propylcyclohexane	150
2-methylheptane	384
3-methylheptane	200

‡ $1.396 \times C_{9.05}H_{16.66}$ since we used 1396 ppm of model fuel to represent 1000 ppm of NC

*NC: 4.7% paraffins, 85.2% cyclo-paraffins, 9.6% monoaromatics and 0.5% polyaromatics.

The composition of the fuels and their molecular weight were determined through gas chromatography (<http://www.alfa-bird.eu-vri.eu/>)

MODELING

- Composition of the model-fuel representing the GtL/naphthenic cut mix ($C_{11.54}H_{23.09}$; $H/C=2.0$; $DCN=48.8$; $M=161.57 \text{ g mol}^{-1}$)[‡] in the simulations

Component	Initial concentrations (ppm)
<i>n</i> -decane	147
decahydronaphthalene	222
tetrahydronaphthalene	156
2-methylheptane	387
3-methylheptane	316
<i>n</i> -propylcyclohexane	75

[‡] $1.3024 \times C_{8.86}H_{17.73}$ since we used 1302.4 ppm of model fuel to represent 1000 ppm of GtL/naphthenic cut mixture.

MODELING

Sub-models for surrogates components were taken from our previous modeling efforts. *n*-Decane, 2-methylheptane and 3-methylheptane studied previously[‡] were used to represent the *n*- and *iso*-paraffins present in the synthetic fuels. Naphthenes were represented by *n*-propylcyclohexane* and decahydronaphthalene ** in the model. Tetrahydronaphthalene ***represented naphtheno-aromatics.

Experimental data obtained in JSR were compared to simulations in order to validate the chemical kinetic mechanism.

‡ Sarathy et al., 2011, *Combustion and Flame*, 158(12), pp. 2338-2357.

Karsenty et al., 2012, *Energy & Fuels*, 26(8), pp. 4680-4689.

Mze-Ahmed et al., 2012, *Energy & Fuels*, 26(7), pp. 4253-4268.

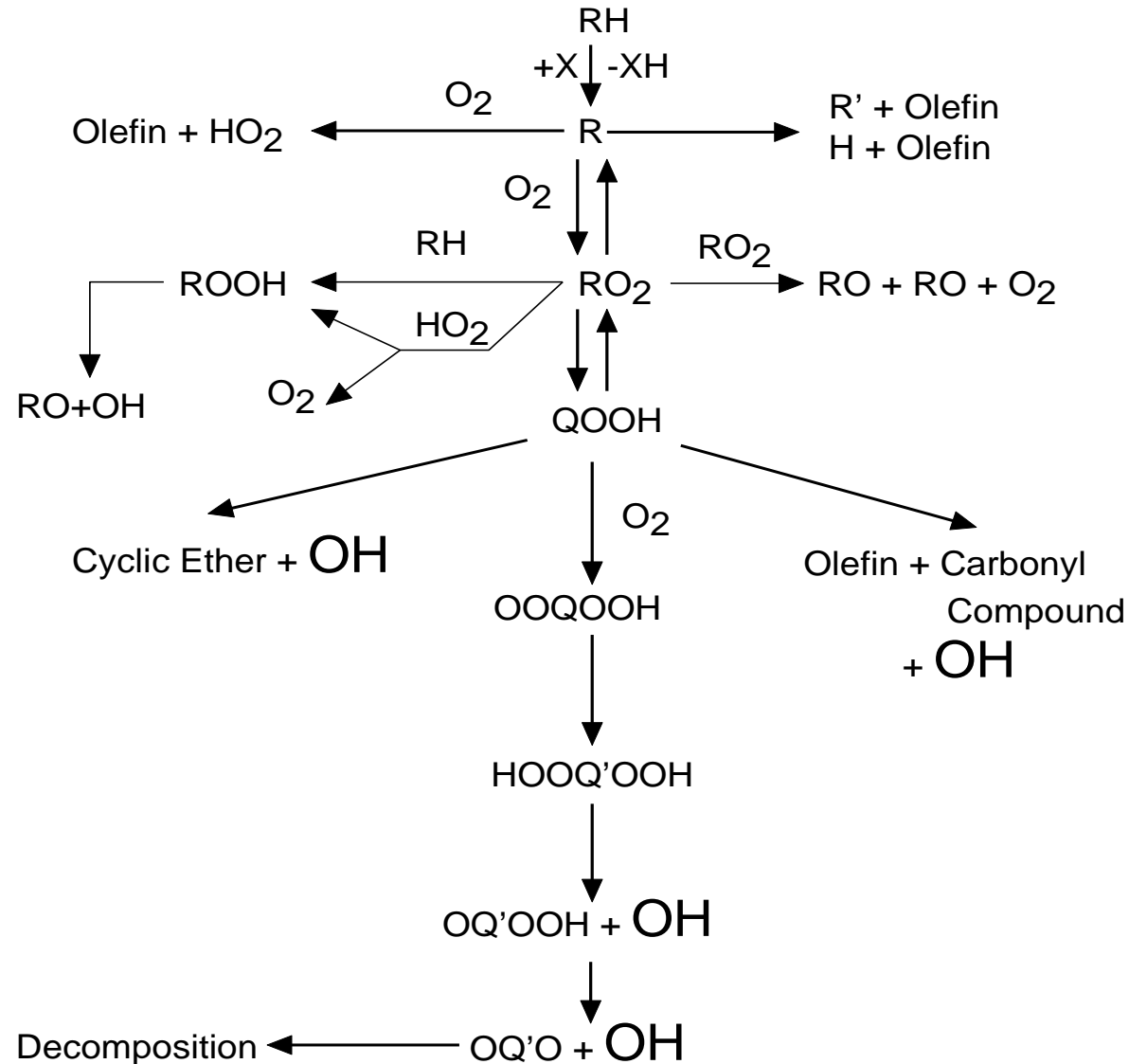
* Ristori, A et al., 2001, *Combustion Science and Technology*, 165(1), pp. 197-228.

** Dagaut et al., 2013, *Proceedings of the Combustion Institute*, 34(1), pp. 289-296.

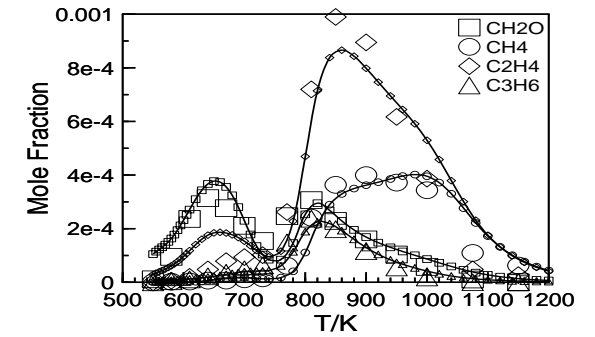
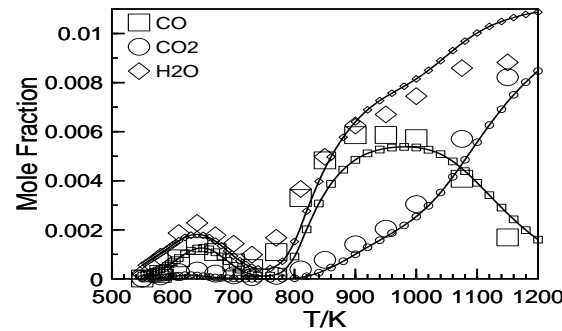
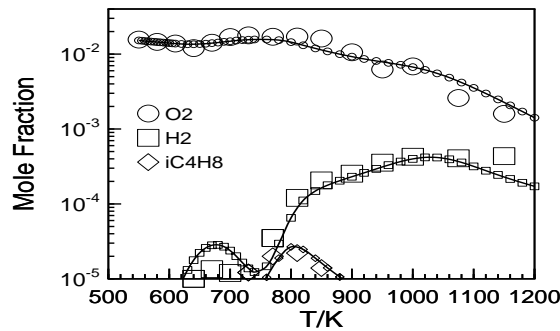
*** Dagaut et al., 2013, *Energy & Fuels*, 27(3), pp. 1576-1585.

RESULTS AND DISCUSSION

The data showed three regimes of oxidation: the cool flame regime ($T < \sim 750$ K), the negative temperature coefficient (~ 640 - 750 K) and the high-temperature regime (> 750 K).



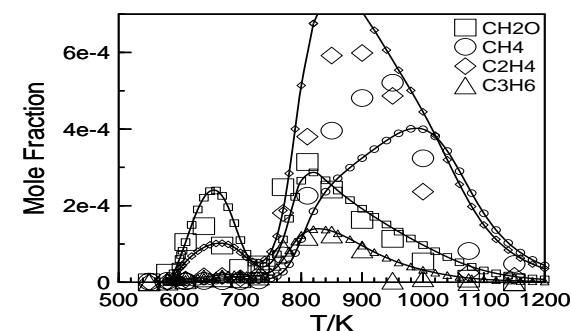
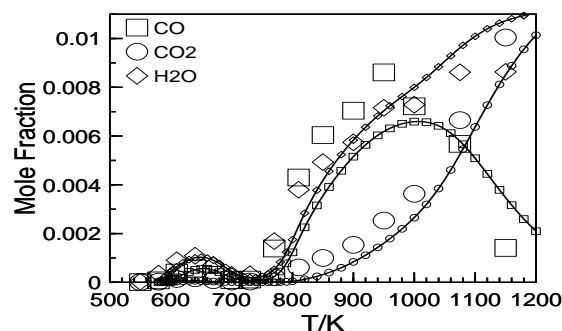
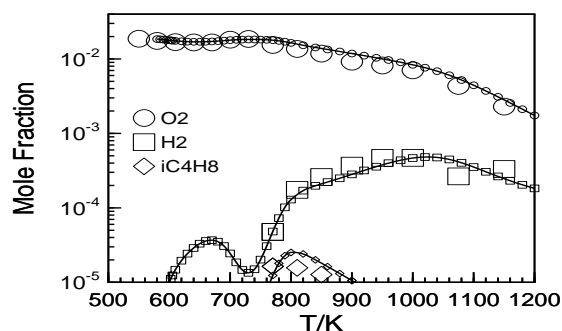
RESULTS AND DISCUSSION: GTL OX'n, EXPERIMENTAL VS. MODELING



Comparison of experimental and computed concentrations profiles obtained from the oxidation of 1000 ppm of the GtL fuel with 16215 ppm of O₂ in a JSR at 10 bar, $\tau = 1$ s and $\phi = 1$ (experimental data: large symbols; computations: lines; dilution by N₂).

P. Dagaut, P. Diévert. Proc. Combust. Inst. **36**, 433–440 (2017)

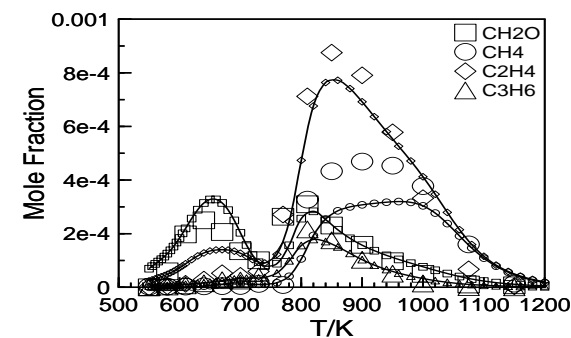
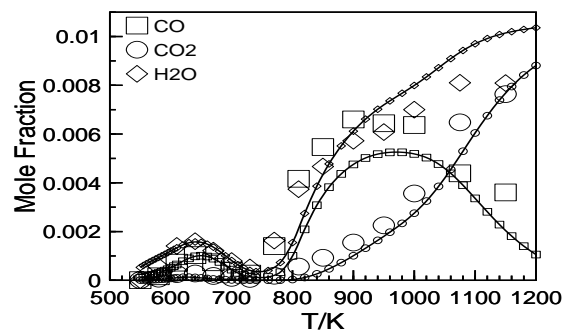
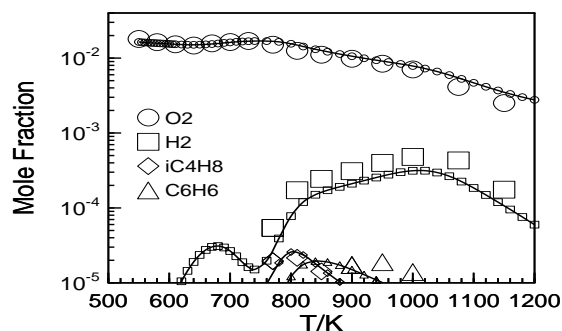
RESULTS AND DISCUSSION: NC OX'n, EXPERIMENTAL VS. MODELING



Comparison of computed and experimental concentrations profiles obtained from the oxidation of 1000 ppm of the naphthenic cut with 18570 ppm of O₂ in a JSR at 10 bar, $\tau = 1$ s and $\phi = 1$ (experimental data: large symbols; computations: lines; dilution by N₂).

P. Dagaut, P. Diévert. Proc. Combust. Inst. **36**, 433–440 (2017)

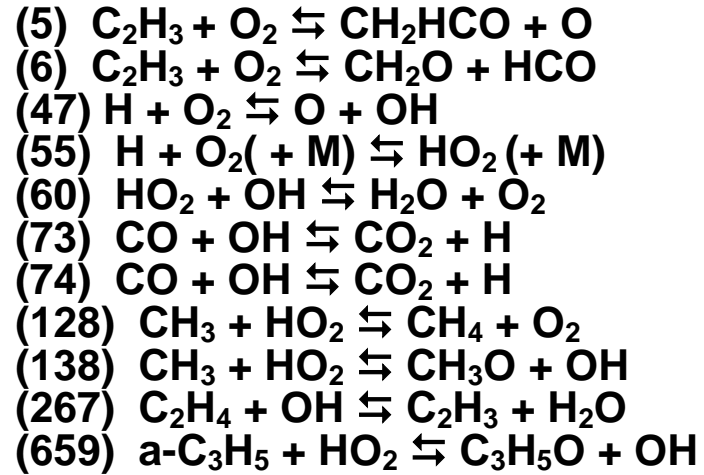
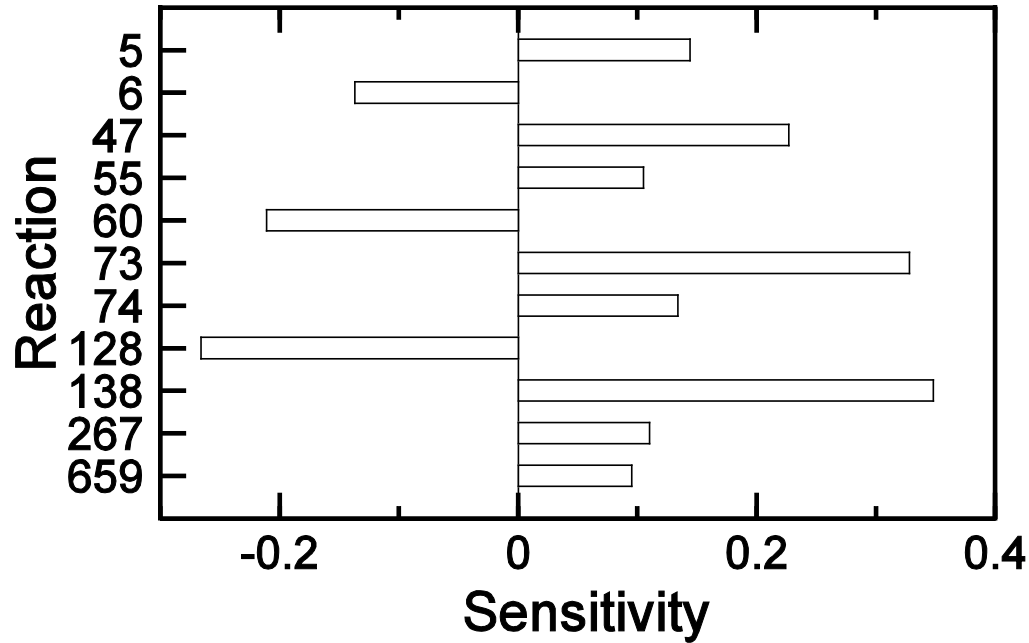
RESULTS AND DISCUSSION: NC/GTL OX'n, EXPERIMENTAL VS. MODELING



Comparison of computed and experimental concentrations profiles obtained from the oxidation of 1000 ppm of the naphthenic cut/GtL fuel mixture with 17378 ppm of O_2 in a JSR at 10 bar, $\tau = 1$ s and $\phi = 1$ (data: large symbols; computations: lines; dilution by N_2).

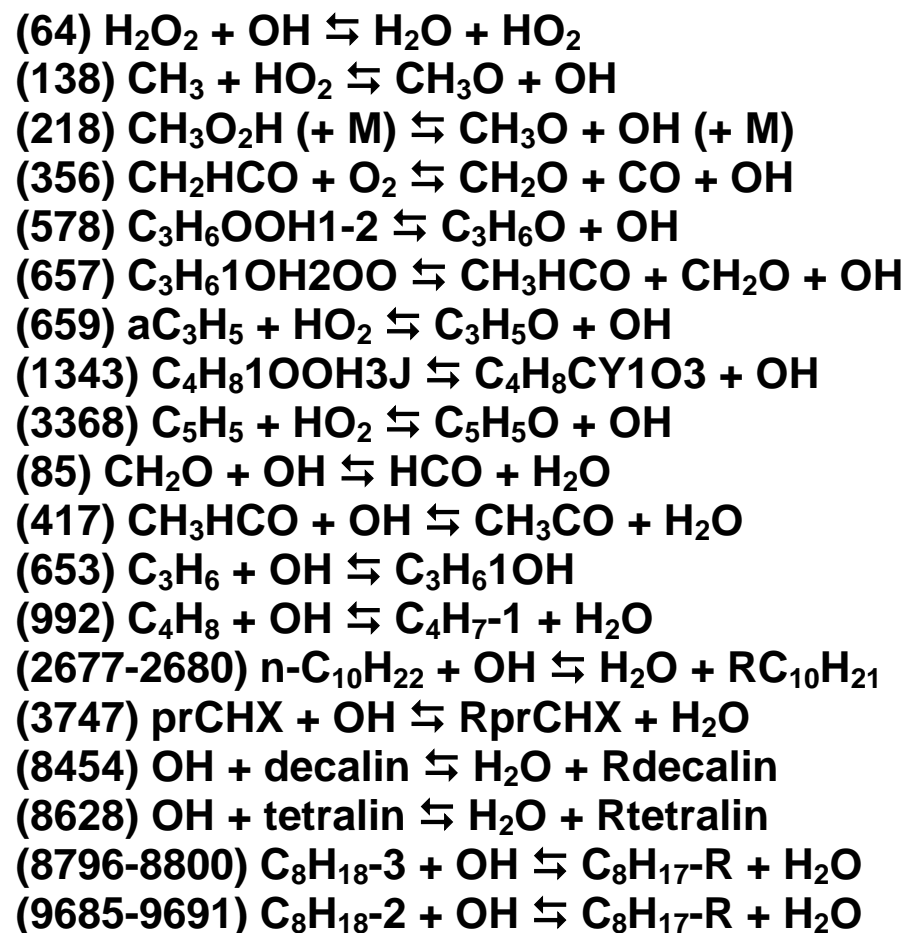
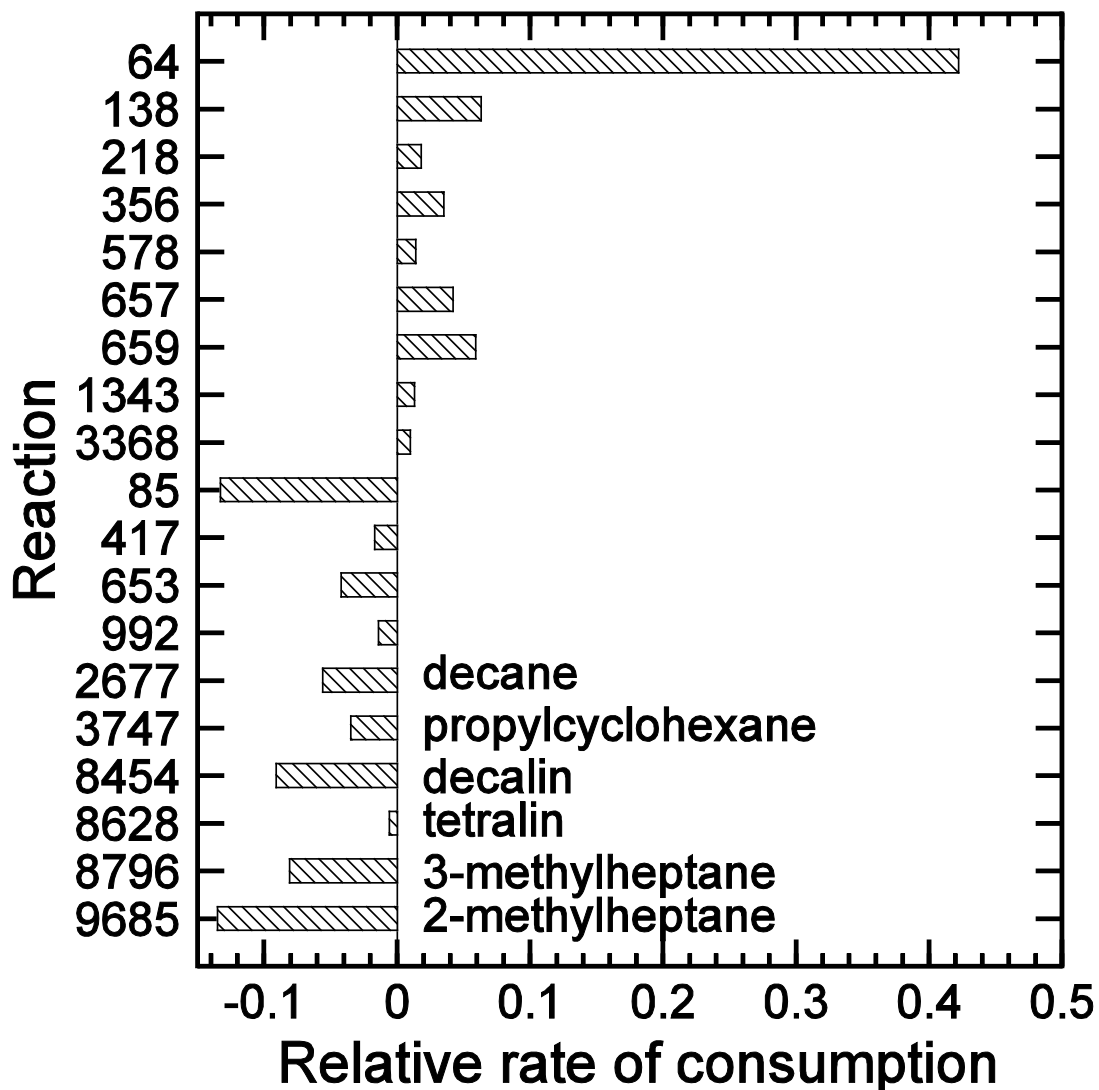
P. Dagaut, P. Diévert. Proc. Combust. Inst. **36**, 433–440 (2017)

RESULTS AND DISCUSSION: NC/GTL OX'n, MODELING



Sensitivity analyses for CO_2 at 1040 K during the oxidation of 1000 ppm of the naphthenic cut/GtL fuel mixture in a JSR ($\varphi = 1$, 10 bar, residence time of 1 s).

RESULTS AND DISCUSSION: NC/GTL OX'n, MODELING

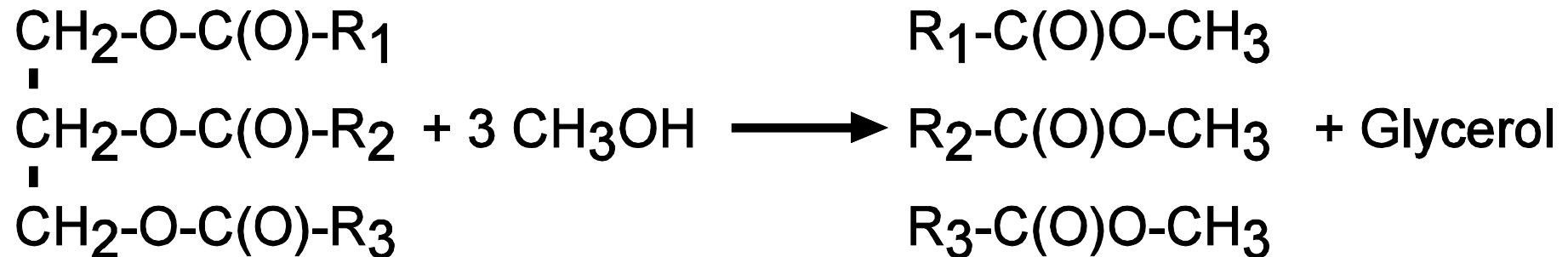


Consumption/Production of OH at 790 K during the oxidation of 1000 ppm of the naphthenic cut/GtL fuel mixture in a JSR ($\phi = 1$, 10 bar, residence time of 1 s).

5.4 Biofuels

5.4.1 RME (biodiesel)

Several vegetable oils have also been tested for transport purpose, but their high viscosity, low volatility, and low cetane number (>40) led to incomplete combustion. Therefore, the concept of using bio-diesel, consisting of alkyl esters of these vegetable oils obtained by transesterification with an alcohol (mostly methanol, but also ethanol)



Vegetable oil composition

Vegetable oil	Fatty acid composition (% weight)								
	16:1	18:0	20:0	22:0	24:0	18:1	22:1	18:2	18:3
Corn	11.67	1.85	0.24	0.00	0.00	25.16	0.00	60.60	0.48
Cottonseed	28.33	0.89	0.00	0.00	0.00	13.27	0.00	57.51	0.00
<u>Crambe</u>	20.7	0.70	2.09	0.80	1.12	18.86	58.51	9.00	6.85
Peanut	11.38	2.39	1.32	2.52	1.23	48.28	0.00	31.95	0.93
Rapeseed	3.49	0.85	0.00	0.00	0.00	64.4	0.00	22.30	8.23
Soybean	11.75	3.15	0.00	0.00	0.00	23.26	0.00	55.53	6.31
Sunflower	6.08	3.26	0.00	0.00	0.00	16.93	0.00	73.73	0.00
Castor	0.00	0.00	0.00	0.00	0.00	87.0	0.00	0.00	11.2
Palm	10.2	3.7	0.00	0.00	0.00	22.8	0.00	53.7	8.6

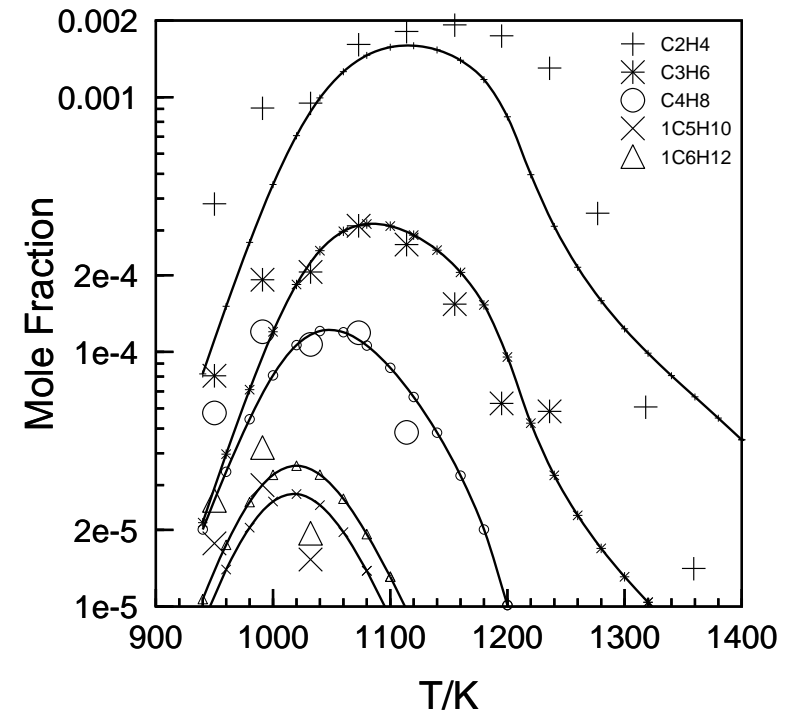
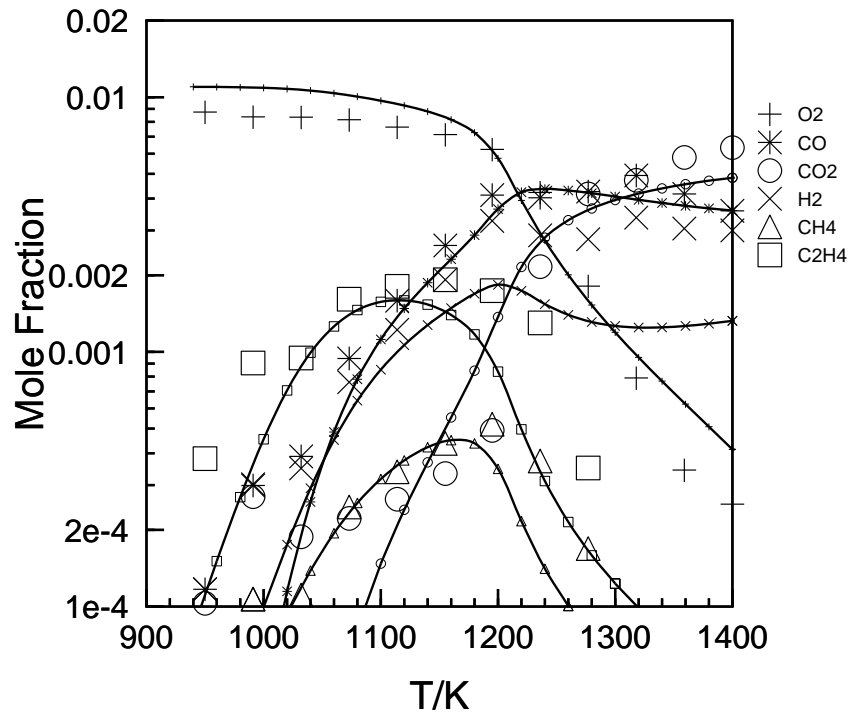


Early modeling efforts

To model combustion of fuels, to predict accurate combustion performance and emission characteristics, a good knowledge of their kinetics of combustion is essential. Since rapeseed is one of the main crop growing Europe, we focus our study on the kinetic of rapeseed oil methyl ester (RME) oxidation.

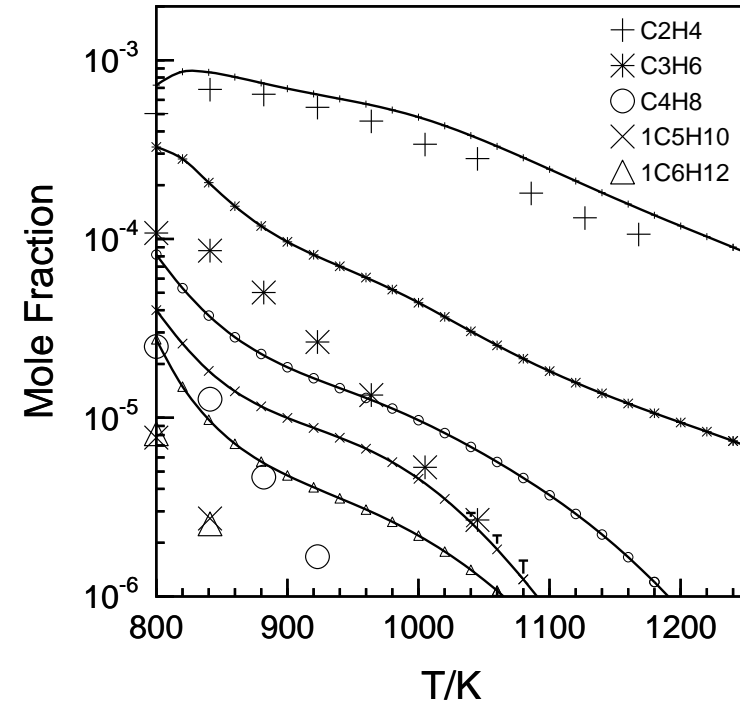
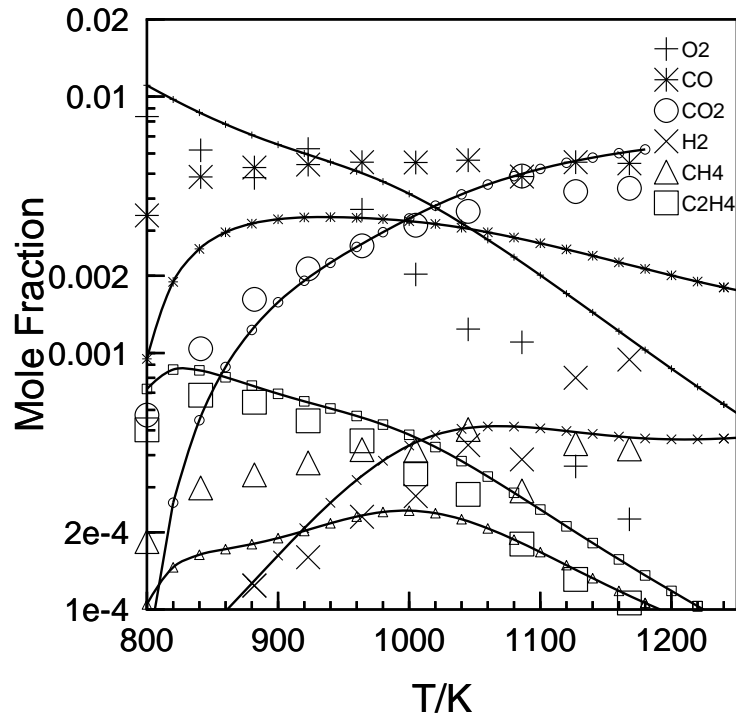
RME is a complex mixture of C_{14} , C_{16} , C_{18} , C_{20} , and C_{22} esters with highly saturated carbon chain. The composition of the fuel was 0.1% C_{14} , 5.4% C_{16} , 92.0% C_{18} , 2.0% C_{20} , and 0.5% C_{22} , with mostly one double bond on the acid chain. The equation for the oxidation of RME can be written as follows:

$C_{17.92}H_{33}O_2 + 25.17 O_2 = 17.92 CO_2 + 16.5 H_2O$. Because of the complexity of this fuel, it is difficult to propose a detailed kinetic scheme for its oxidation, although that could be achieved building on previous kinetics studies involving simpler esters



The oxidation of RME in a JSR at 1 atm ($\phi = 1$, 0.07 s). The data (large symbols) are compared to the computations (lines, small symbols), n-hexadecane as surrogate model-fuel, initial mole fractions: n-hexadecane, 0.0005625; oxygen, 0.011; nitrogen, 0.9884375).

P. Dagaut et al., Proc. Combust. Inst. 31, 2955–2961 (2007)



The oxidation of RME in a JSR at 10 atm ($\phi = 1$, 1 s). The data (large symbols) are compared to the computations (lines, small symbols), n-hexadecane as surrogate model-fuel, initial mole fractions: n-hexadecane, 0.0005625; oxygen, 0.012585; nitrogen, 0.9868525).

P. Dagaut et al., Proc. Combust. Inst. 31, 2955–2961 (2007)

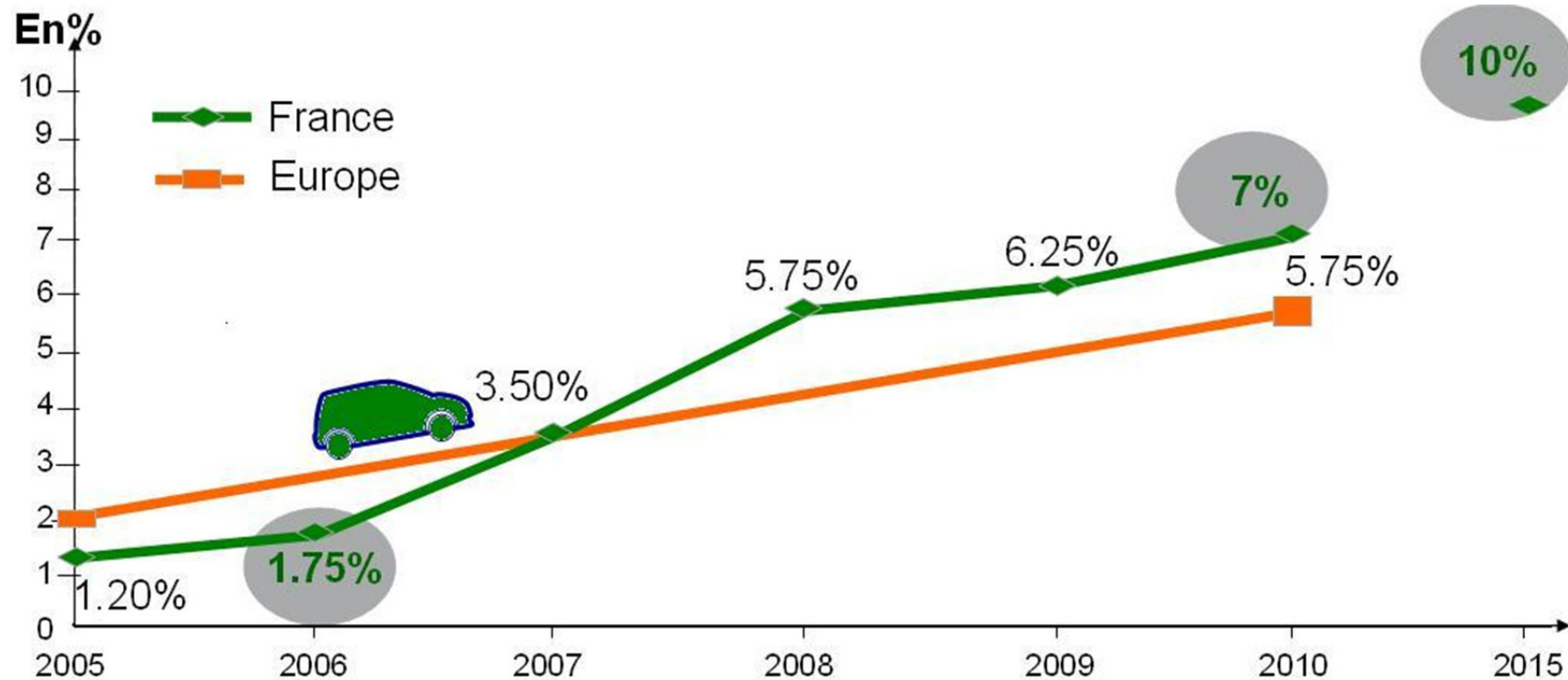
5.4.2 B30

Diesel engines contribute significantly to overall **carbon dioxide emissions** whereas concerns about green-house effect and air pollution favor the investigation of sustainable and environment-friendly Diesel fuels.

Biofuels such as fatty acid methyl esters (FAME) are **mixed** in variable quantities (e.g. B5 contains 5% in volume of FAME and B30 contains 5% in volume of FAME) **with fossil Diesel fuel**.

Introduction

Reduction of engines emissions in terms of carbon oxides and polyaromatic hydrocarbons (PAH) have been reported, indicating **bio-diesel** may help preserving our environment.



Reduction of carbon footprint in Europe by increased biodiesel fraction (EU 2010: 5.75% energy HV)

Introduction (cont'd)

The so-called bio-Diesel is a **mixture of FAME** produced from transesterification of triglycerides (oils) with methanol. Current biodiesel fuels are mixtures of ca. C₁₂-C₂₂ highly saturated carbon-chain esters. Their complex composition implies the use of surrogate model-fuels for simulating their combustion kinetics.

Whereas early kinetic studies have demonstrated a strong similitude between the oxidation of rapeseed oil methyl esters (RME) and that of n-hexadecane, long-chain methyl esters exhibiting cool-flames were also proposed as bio-Diesel model fuels.

Introduction (cont'd)

A fossil Diesel fuel consists of an even more complex mixture of thousands of medium-high molecular weight hydrocarbons that participate in thousands of pyrolysis and oxidation reactions. Therefore, **surrogates are needed** to represent Diesel fuel with a limited number of components.

In Europe, the 'IDEA' surrogate Diesel fuel (70% n-decane + 30% 1-methyl naphthalene) was formulated previously as part of the 'Integrated Development on Engine Action' (IDEA) program.

This fuel mixture **matches both the physicochemical properties and combustion behavior** of a **conventional Diesel fuel**. The IDEA fuel has properties similar to those of a conventional Diesel fuel, i.e. a normal density of 0.798 g/L at 20°C, a CN of ca. 53, and a hydrogen-to-carbon ratio of 1.8.

Introduction (cont'd)

The kinetics of oxidation of a **commercial B30 bio-Diesel fuel** and a **B30 surrogate bio-Diesel fuel** were measured and compared.

The experiments were performed in a jet-stirred reactor (JSR), in order to:

- (1) **provide** new information on the kinetic of oxidation of a B30 bio-Diesel fuel over a wide range of conditions,
- (2) **verify** the chemical kinetics of oxidation of a simple B30 surrogate can represent that of a commercial B30 Diesel fuel, and
- (3) **propose and validate** a detailed kinetic reaction mechanism for the oxidation of a B30 bio-Diesel fuel from low to high temperatures.

Experimental conditions in the JSR (10300 ppm of C, 560-1030 K, t=0.6 & 1s)

Initial concentrations (in ppm for the fuel, in mole fraction for O ₂ and N ₂)					φ	P/ atm
B30	n-C ₁₀ H ₂₂	C ₁₁ H ₁₀	C ₉ H ₁₈ O ₂	O ₂		
600	-	-	-	0.0574	0.25	10
600	-	-	-	0.0287	0.5	10
600	-	-	-	0.0144	1	10
600	-	-	-	0.0096	1.5	10
-	490	210	300	0.0597	0.25	10
-	490	210	300	0.0284	0.5	6, 10
-	490	210	300	0.0142	1	6, 10
-	490	210	300	0.0095	1.5	10

B30 bio-Diesel fuel surrogate: 49% n-decane, 21% 1-methyl naphthalene, and 30% methyl octanoate in mole, i.e. $C_{10.3}H_{18.4}O_2$

Commercial low-S B30 bio-Diesel fuel (CN 54.8, 84.1% C, 12.9% H, and 3% O by wt., d= 845 g/L at 15°C, FAME fraction was rapeseed oil methyl ester): $C_{16.47}H_{30.83}O_{0.5}$

Modeling

The computations were performed using the PSR computer code.

The detailed kinetic reaction mechanism is based on previous studies of the oxidation of methyl octanoate, large alkanes, 1-methylnaphtalene and diesel + IDEEA surrogate [H.P. Ramirez L, K. Hadj-Ali, P. Diévert, G. Moréac, P. Dagaut, *Energy Fuels* **24**(3) (2010) 1668-1676] where cross-reactions between the main fuel components were considered: metathesis of n-decane with phenyl, benzyl, 1-naphtylmethyl, 1-naphtyl, and indenyl radicals; reactions of decyl radicals with 1-naphtaldehyde; reactions of $\cdot\text{C}_{10}\text{H}_{21}\text{O}_2$ with toluene, 1-methylnaphtalene, 1-naphtylmethyl, 1-naphtaldehyde, benzyl, phenyl, and 1-naphtyl.

The proposed kinetic scheme (7748 reversible reactions and 1964 species) represents the 1st attempt to propose a kinetic scheme for the oxidation of Diesel-biodiesel fuel mixtures.

Experiment results

- Oxidation of a B30 bio-Diesel fuel surrogate, 49% n-decane, 21% 1-methyl naphthalene, and 30% methyl octanoate in mole
- Oxidation of a commercial low-sulfur B30 bio-Diesel fuel

They were studied in a jet-stirred reactor over a wide range of conditions: $\varphi=0.25-1.5$; temperature in the range 560–1030 K, mean residence time constant: 0.6 s at 6atm and to 1 s at 10atm.

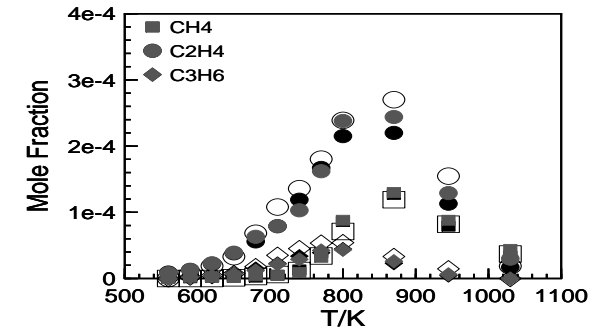
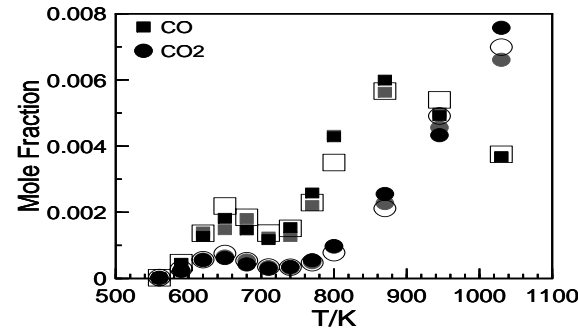
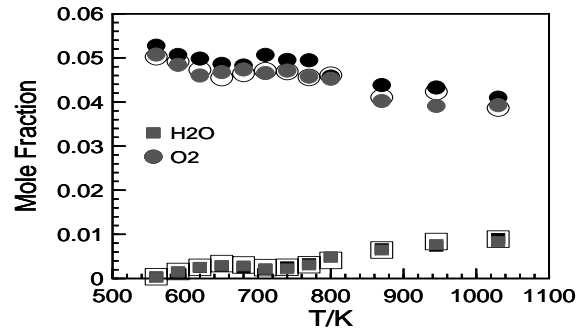
This allowed the observation of the cool-flame oxidation regime, the negative temperature coefficient (NTC) regime, and the high-temperature oxidation regime.

Experiment results (cont'd)

More than 20 species were identified and measured by FTIR, CG-MS/FID/TCD. Experimental concentration profiles were obtained for H_2 , H_2O , O_2 , CO , CO_2 , CH_2O , CH_4 , C_2H_6 , C_2H_4 , C_2H_2 , formaldehyde, acetaldehyde, C_3H_6 , 1- C_4H_8 , 1,3- C_4H_6 , 1- C_5H_{10} , 1- C_6H_{12} , 1- C_8H_{16} , n-decane, methyl octanoate, and 1-methylnaphthalene. Other minor species detected at ppm levels were not quantified nor used in the modeling.

The concentration profiles measured from the oxidation of the commercial B30 and the B30 surrogate over the low-, intermediate-, and high-temperature oxidation regimes were compared:

Experiment results (cont'd)



Experimental concentration profiles from the oxidation of a commercial Diesel fuel (filled symbols), the B30 fuel (grey symbols), the B30 surrogate (empty symbols) in a JSR at 10 atm, $\phi=0.25$, and $\tau=1$ s.

H.P. Ramirez L. et al., Proc. Combust. Inst. 33(1), 375–382 (2011)

The concentration profiles obtained for CO, CO₂, H₂O, and O₂ during the oxidation of the 2 biofuels are **very similar** over the entire range of experimental conditions; the commercial Diesel fuel used in the B30 mixture reacts **similarly**.

Modeling results

The concentration profiles obtained for the oxidation of the B30 surrogate fuel were compared to the model predictions.

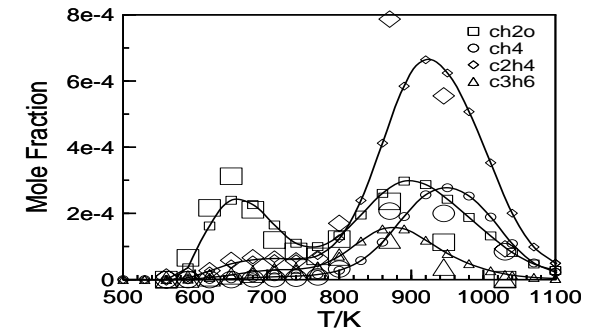
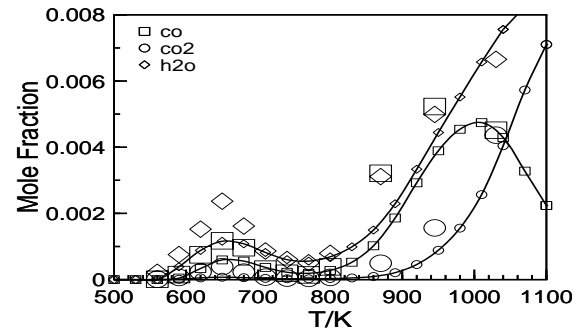
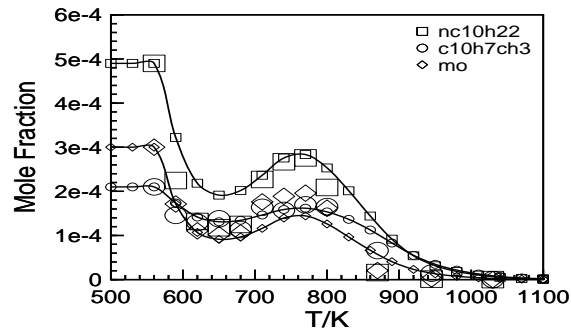
The present model was also successfully tested for the oxidation of pure n-decane, pure methyl octanoate, and pure 1-methylnaphtalene under similar JSR conditions.

Furthermore, the proposed model, not including the methyl octanoate chemistry, was used to simulate the oxidation of commercial and surrogate Diesel fuels [H.P. Ramirez L, K. Hadj-Ali, P. Diévar, G. Moréac, P.

Dagaut, Energy Fuels **24**(3) (2010) 1668-1676]

Modeling results (cont'd)

Results at 6 atm



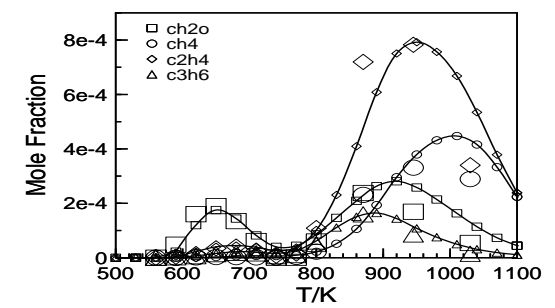
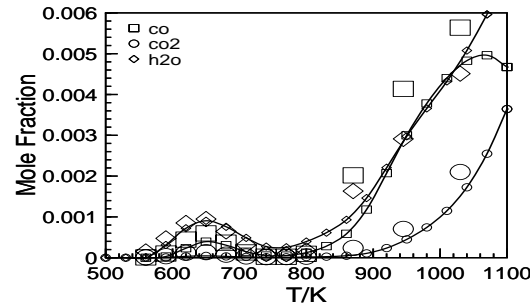
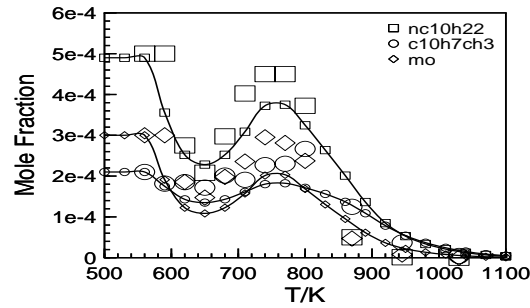
The B30 surrogate Diesel fuel oxidation in a JSR at 6 atm, $\tau = 0.6$ s, and $\phi = 0.5$. The experimental data (large symbols) are compared to the computations (lines with small symbols).

N.B. B30 Surrogate = 490ppm of n-decane + 210ppm of 1-methyl naphthalene + 300ppm of methyl octanoate

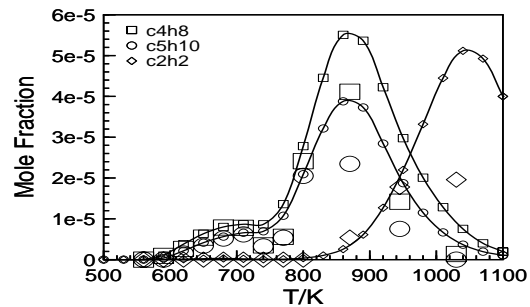
H.P. Ramirez L. et al., Proc. Combust. Inst. 33(1), 375–382 (2011)

Modeling results (cont'd)

Results at 6 atm



The B30 surrogate Diesel fuel oxidation in a JSR at 6 atm, $\tau = 0.6$ s, and $\phi = 1$. The experimental data (large symbols) are compared to the computations (lines with small symbols).

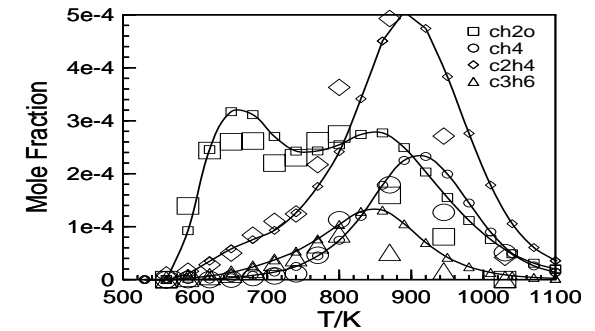
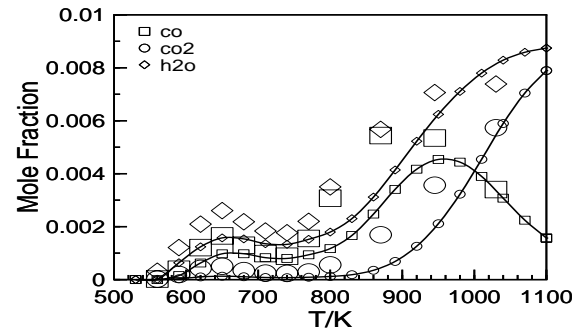
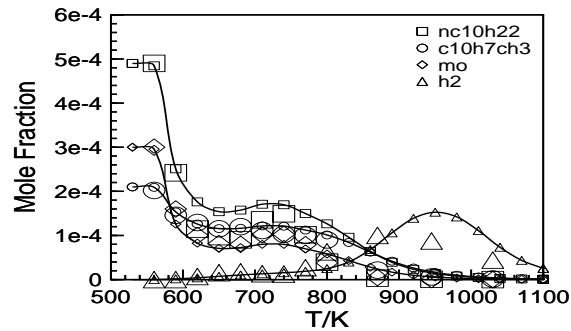


N.B. B30 Surrogate = 490ppm of n-decane + 210ppm of 1-methyl naphthalene + 300ppm of methyl octanoate

H.P. Ramirez L. et al., Proc. Combust. Inst. 33(1), 375–382 (2011)

Modeling results (cont'd)

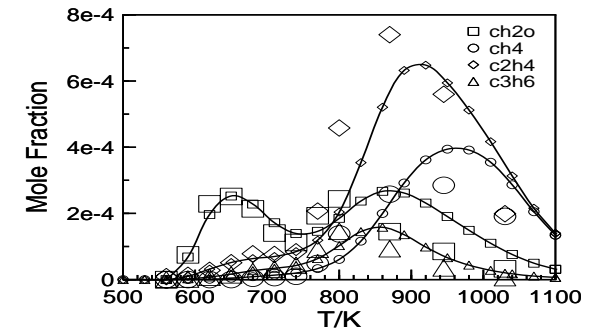
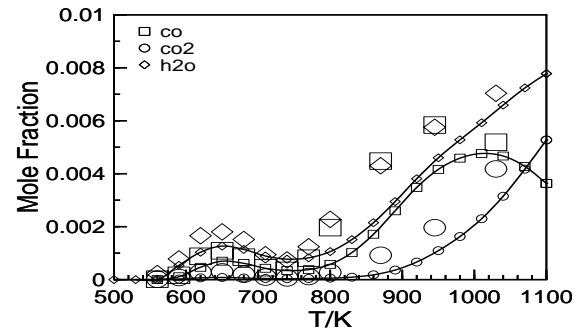
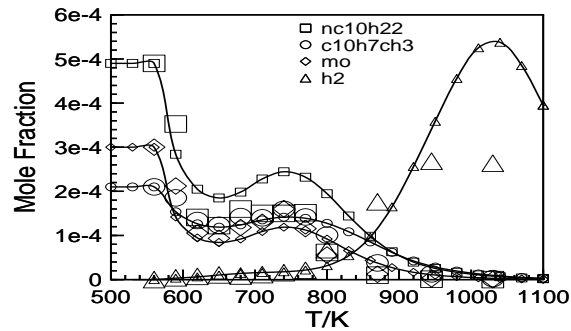
Results at 10 atm



The B30 surrogate Diesel fuel oxidation in a JSR at 10 atm, $\tau = 1$ s, and $\phi = 0.5$. The experimental data (large symbols) are compared to the computations (lines with small symbols).

N.B. B30 Surrogate = 490ppm of n-decane + 210ppm of 1-methyl naphthalene + 300ppm of methyl octanoate

H.P. Ramirez L. et al., Proc. Combust. Inst. 33(1), 375–382 (2011)



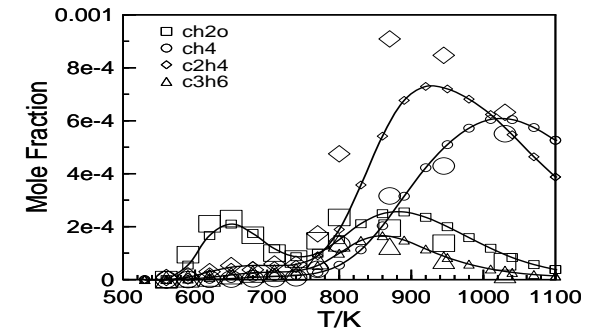
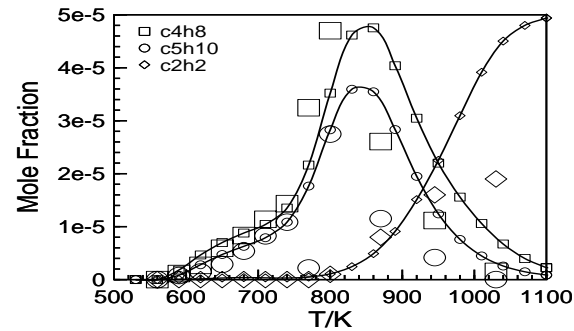
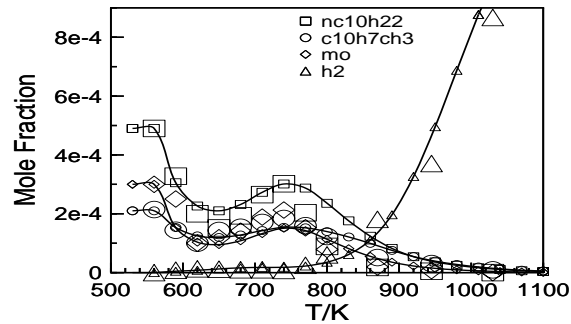
The B30 surrogate Diesel fuel oxidation in a JSR at 10 atm, $\tau = 1$ s, and $\phi = 1$. The experimental data (large symbols) are compared to the computations (lines with small symbols).

N.B. B30 Surrogate = 490ppm of n-decane + 210ppm of 1-methyl naphthalene + 300ppm of methyl octanoate

H.P. Ramirez L. et al., Proc. Combust. Inst. 33(1), 375–382 (2011)

Modeling results (cont'd)

Results at 10 atm

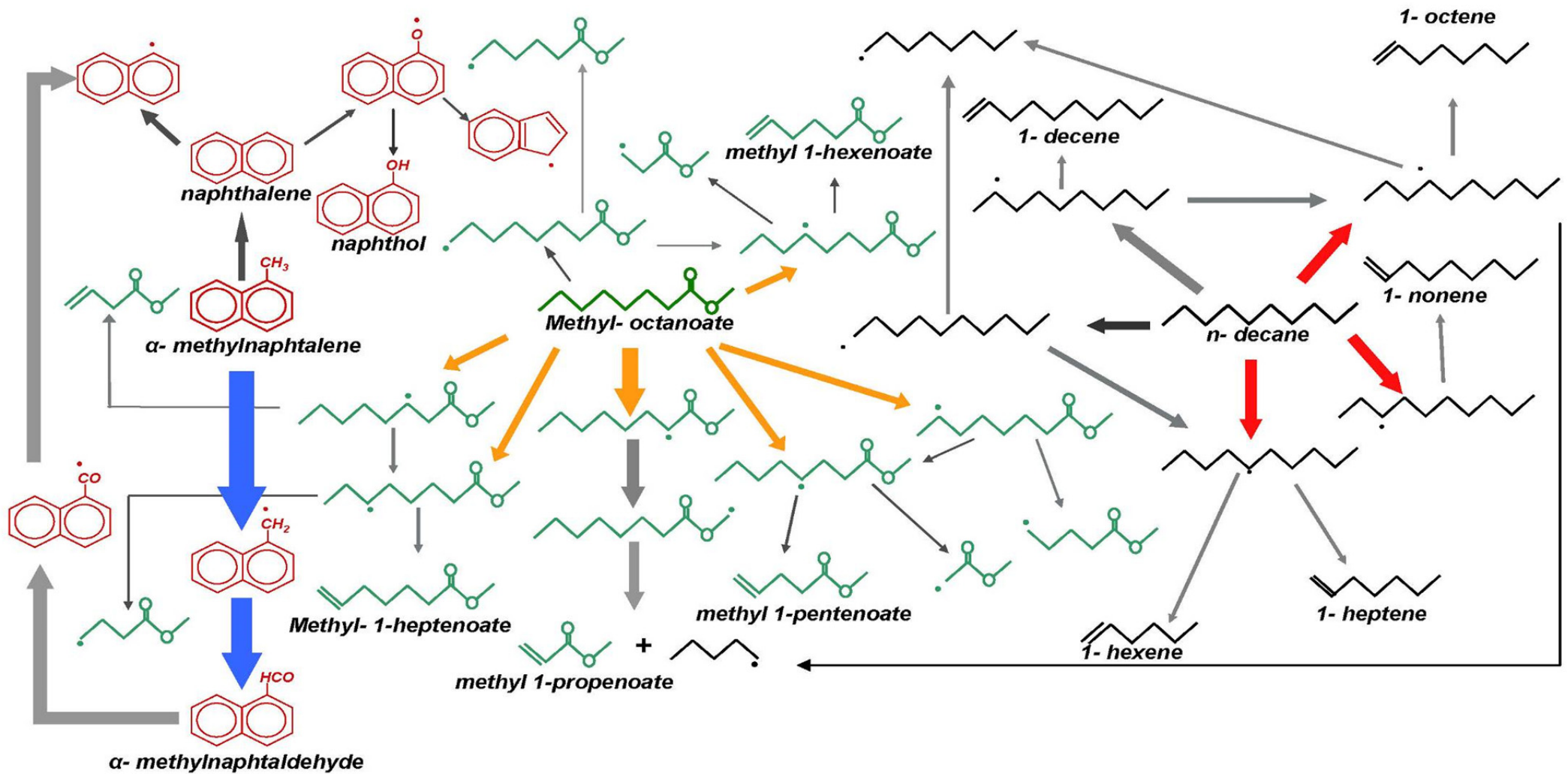


The B30 surrogate Diesel fuel oxidation in a JSR at 10 atm, $\tau = 1$ s, and $\phi = 1.5$. The experimental data (large symbols) are compared to the computations (lines with small symbols).

N.B. B30 Surrogate = 490ppm of n-decane + 210ppm of 1-methyl naphthalene + 300ppm of methyl octanoate

H.P. Ramirez L. et al., Proc. Combust. Inst. 33(1), 375–382 (2011)

Modeling results (cont'd)

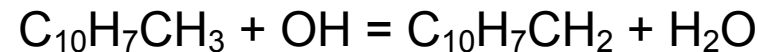
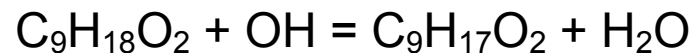
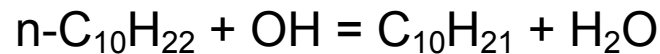


Rxn pathways analysis for B30 surrogate oxidation (10 atm, $\phi=1$, 1030K)

H.P. Ramirez L. et al., Proc. Combust. Inst. 33(1), 375–382 (2011)

Modeling results (cont'd)

According to the present computations, at 620 K and in fuel-lean conditions ($\phi=0.5$ at 10 atm), OH radicals are mostly responsible for the oxidation of n-decane (ca. 95%), methyl octanoate (ca. 89%), and 1-methylnaphtalene (ca. 80%) via



Under these conditions, their formation mainly occurs via the decomposition of alkylhydroperoxy (O_2QOOH and $\text{OQ}'\text{OOH}$) deriving from the oxidation of n-decane and methyloctanoate.

Modeling results (cont'd)

Above ca. 750 K, the transition to the high-temperature oxidation regime occurs. The fuel is rapidly consumed through metathesis reactions with OH and larger amounts of products are formed.

The model predicts the experimentally observed overall reactivity of the fuel and products' formation, although it tends to underestimate the overall rate of oxidation above ca. 800 K. This behavior results from the too strong inhibiting effect of 1-methylnaphtalene on n-decane and methyl octanoate oxidation.

We did not attempt to improve the present simulations by modifying the kinetic parameters used in previous modeling efforts in order to keep this model valid for representing the neat oxidation of the surrogate fuel components, i.e. n-decane, 1-methylnaphtalene, and methyl octanoate.

Modeling results (cont'd)

At 1040 K, OH radicals are still mostly responsible for the oxidation of n-decane (ca. 80%), methyl octanoate (ca. 80%), and 1-methylnaphtalene (ca. 89%) via the same reactions.

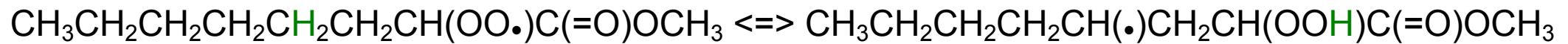
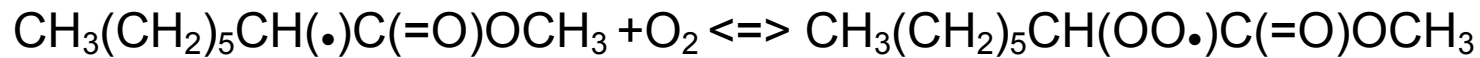
The reactions of n-decane with O (ca. 10%) and H (ca. 5%) also contribute to its consumption.

Also, methyl octanoate reacts with H (ca. 8%). Similarly, H-atoms also consume 1-methylnaphtalene (ca. 8%).

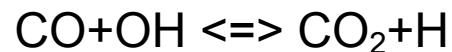
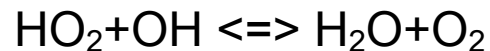
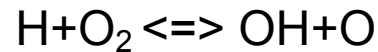
Under these conditions, the production of ethylene mainly occurs via β -scissions of alkyl radicals (1-butyl and 1-propyl 30%) whereas the oxidation of ethyl radicals by O_2 also contributes to ethylene formation (20%).

Modeling results (cont'd) *Local, first-order sensitivity analyses*

Sensitivity analyses showed that at 620K, besides the C₀-C₂ reactions, the overall reactivity is positively sensitive to the rates of oxidation of n-decane by OH, and the peroxidation of methyl octanoate radicals, i.e. to reactions



As expected, at 1040K, the system is mostly sensitive to the kinetics of the C₀-C₁ sub-scheme, i.e.



5.4.3-Pentanol

Because they are renewable, biofuels are attracting great interest as transportation fuels. They can be locally produced, may be less polluting, sometimes more biodegradable, and could reduce net greenhouse gas emissions [1].

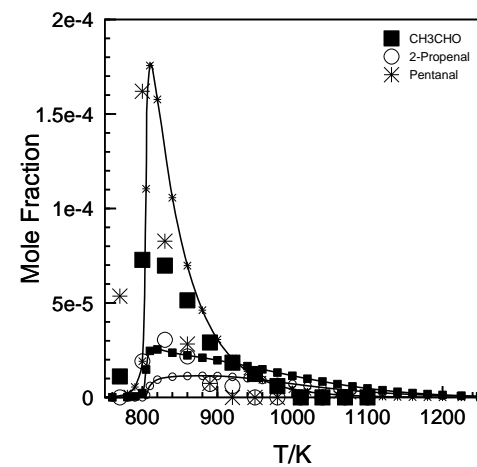
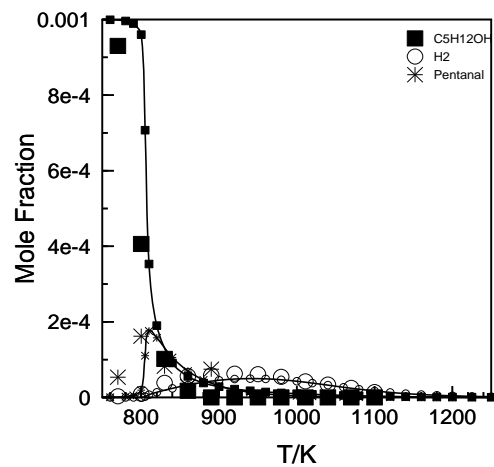
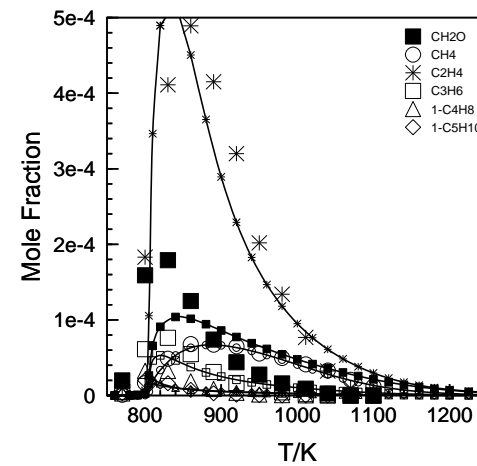
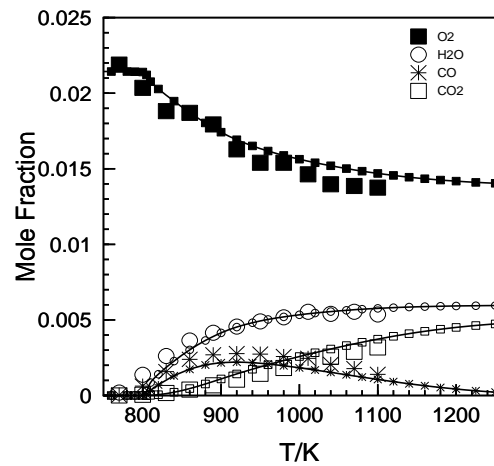
Ethanol accounts for over 90% of all biofuels' production worldwide [2]. However, mixing stability issues may appear with simple alcohols whereas larger alcohols would mix better with petrol-derived fuels thanks to their longer alkyl carbon chain.

Since 1-butanol was announced to be sold soon as a gasoline blending constituent [3], Dagaut and Togbé studied the oxidation of butanol-gasoline surrogate mixtures (85-15 vol%) in a JSR at 10 atm and a kinetic reaction mechanism was derived for modeling the oxidation of butanol-gasoline surrogate mixtures [4].

1. A. Demirbas, Prog. Energy Combust. Sci. 33 (1) (2007) 1-18.
2. IEA World Energy Outlook (2006), ISBN 92-64-10989-7, 500p.
3. Dupont Corp. (2006) available at http://www2.dupont.com/Biofuels/en_US/facts/BiobutanolFactsheet.html
4. P. Dagaut and C. Togbé, Energy and Fuels 22 (2008) 3499–3505.

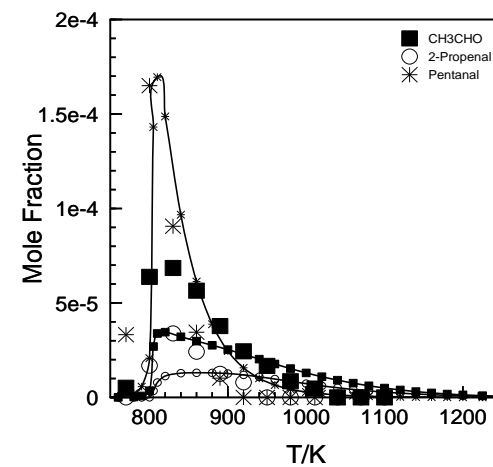
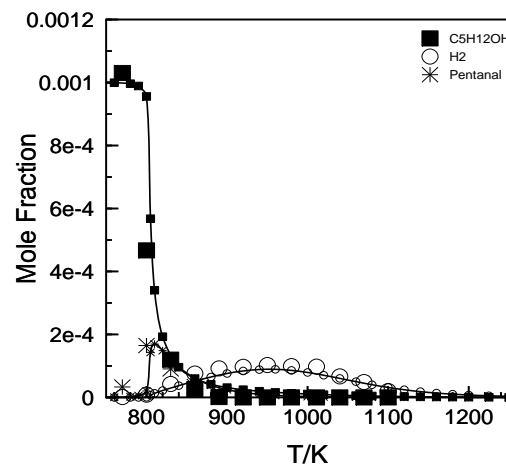
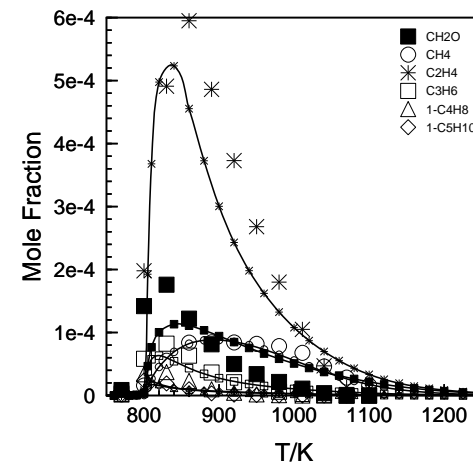
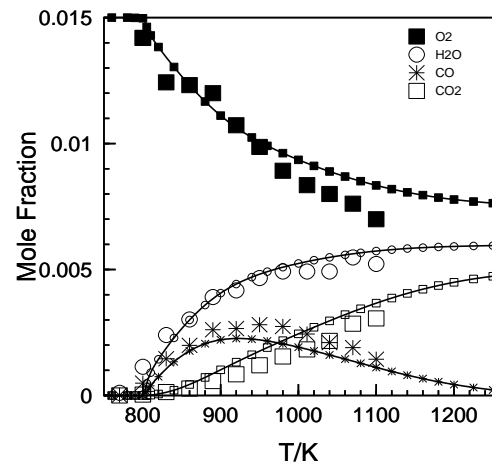
1-Pentanol is among the longer carbon-chain alcohols that could be blended with conventional fuels. However, so far, it received little attention since only engine experiments were reported in the literature [5,6] whereas bio-pentanol could be produced [7,8].

5. M. Gautam, D.W. Martin, Proc Instn Mech Engrs Part A 214 (2000) 165-182.
6. M. Gautam, D.W. Martin, D. Carder, Proc Instn Mech Engrs Part A 214 (2000) 497-511.
7. A. F. Cann, J.C. Liao, Appl. Microbiol. Biotechnol. 85 (2010) 893-899.
8. K. Zhang, M.R. Sawaya, D.S. Eisenberg, J.C. Liao, Proc. Natl. Acad. Sci. USA 105 (2008) 20653-20658.



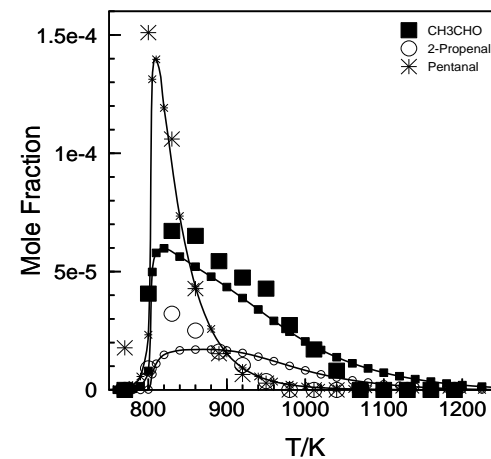
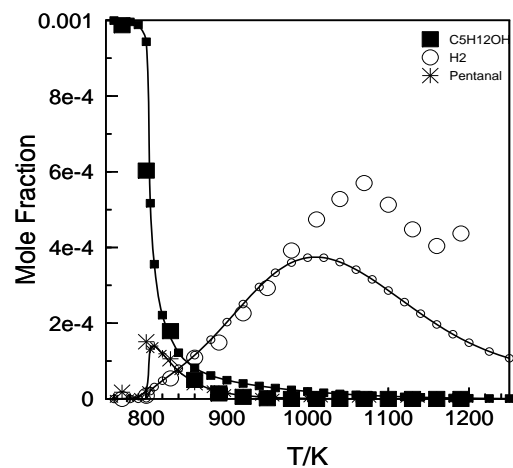
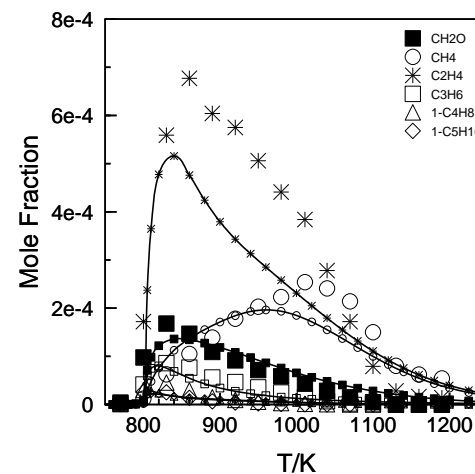
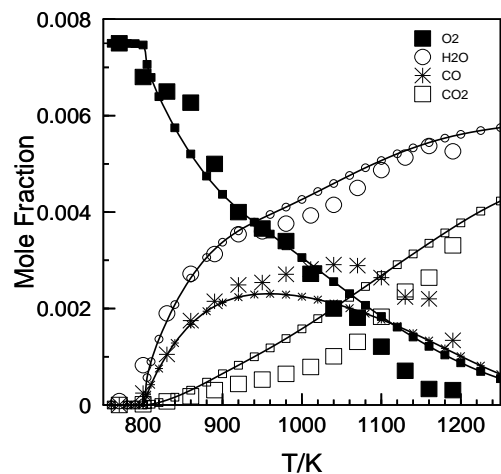
Experimental (large symbols) and computed (lines and small symbols) concentration profiles obtained from the oxidation of 1-pentanol in a JSR at $\phi = 0.35$, $P = 10$ atm, $\tau = 0.7$ s.

C. Togbé et al., Proc. Combust. Inst. **33**(1), 367–374 (2011)



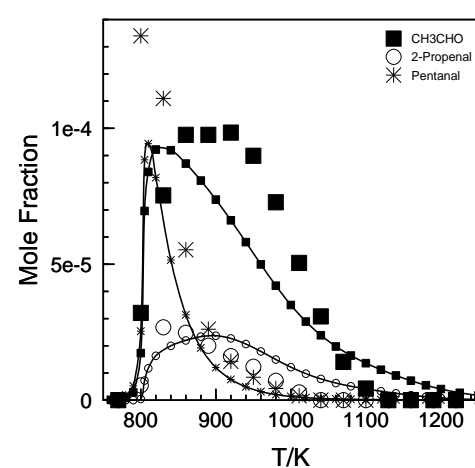
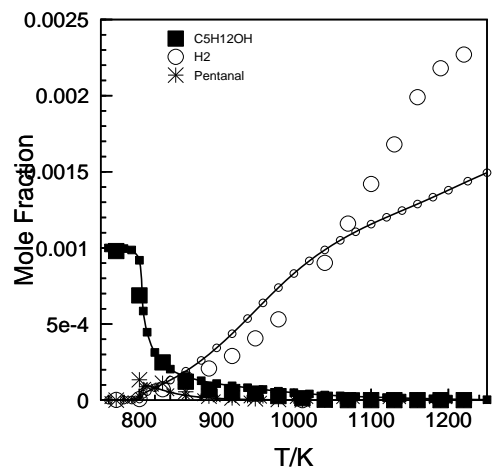
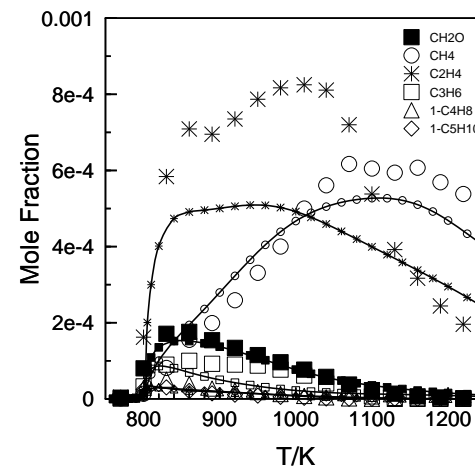
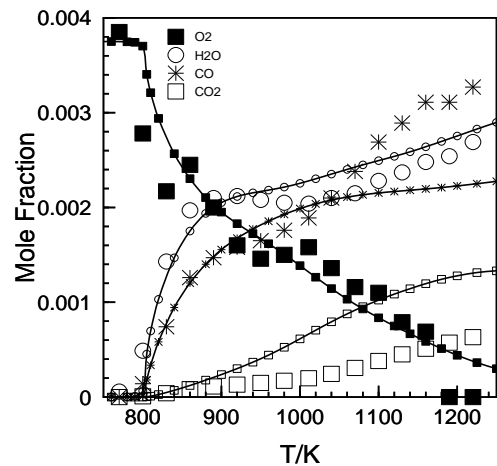
Experimental (large symbols) and computed (lines and small symbols) concentration profiles obtained from the oxidation of 1-pentanol in a JSR at $\phi = 0.5$, $P = 10$ atm, $\tau = 0.7$ s.

C. Togbé et al., Proc. Combust. Inst. **33**(1), 367–374 (2011)

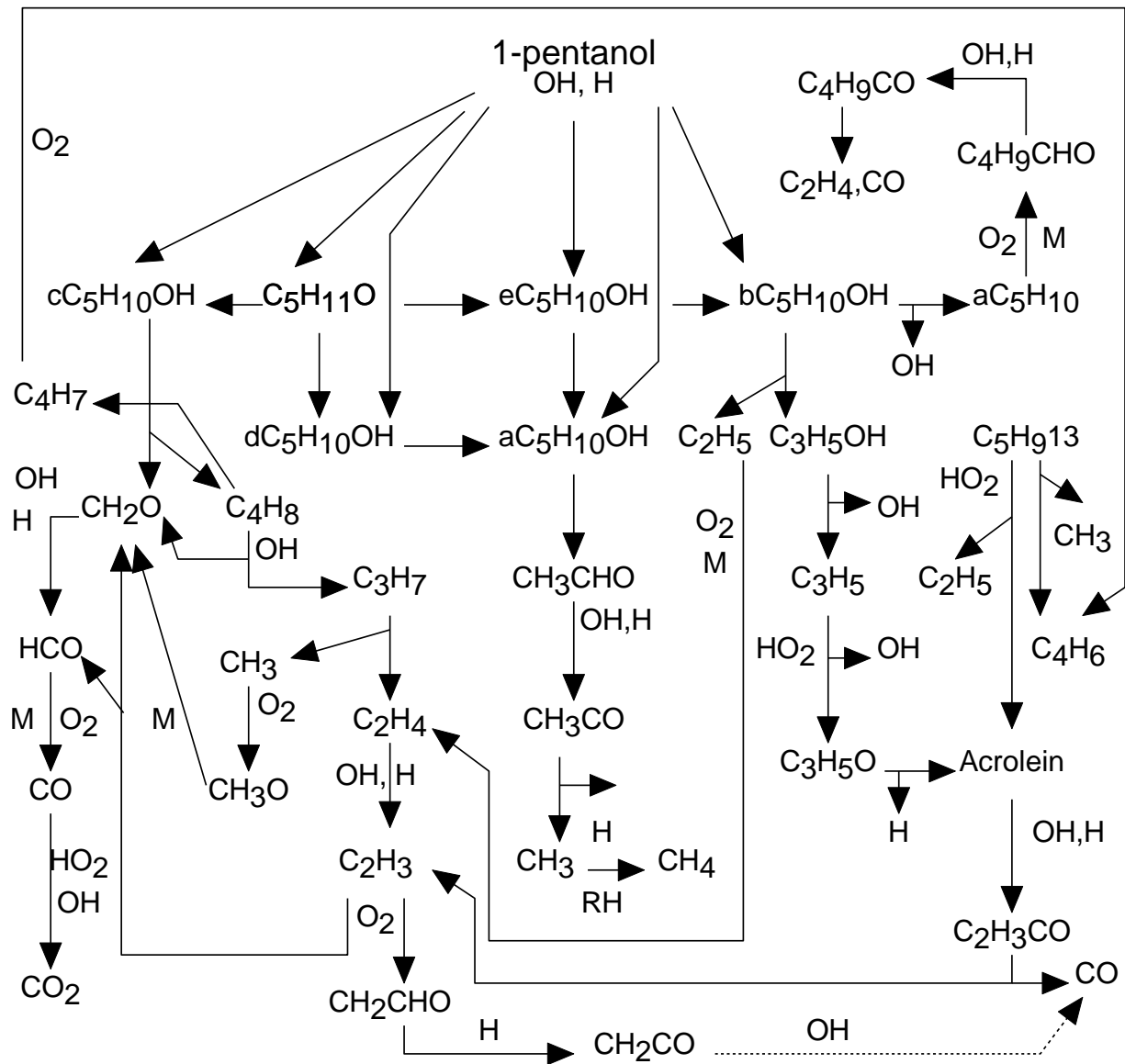


Experimental (large symbols) and computed (lines and small symbols) concentration profiles obtained from the oxidation of 1-pentanol in a JSR at $\phi = 1$, $P = 10$ atm, $\tau = 0.7$ s.

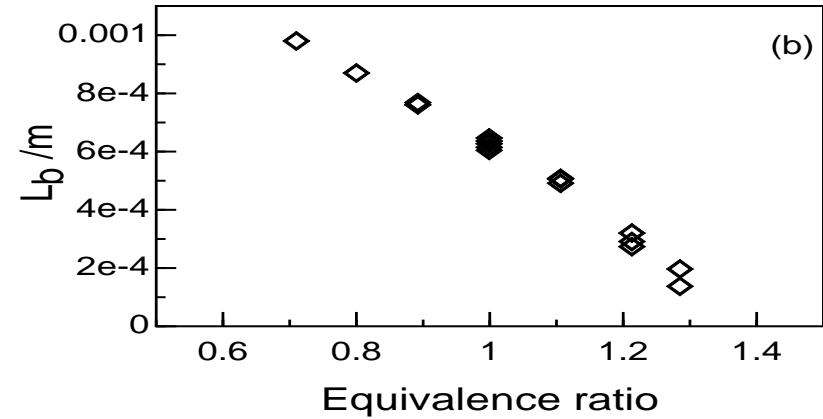
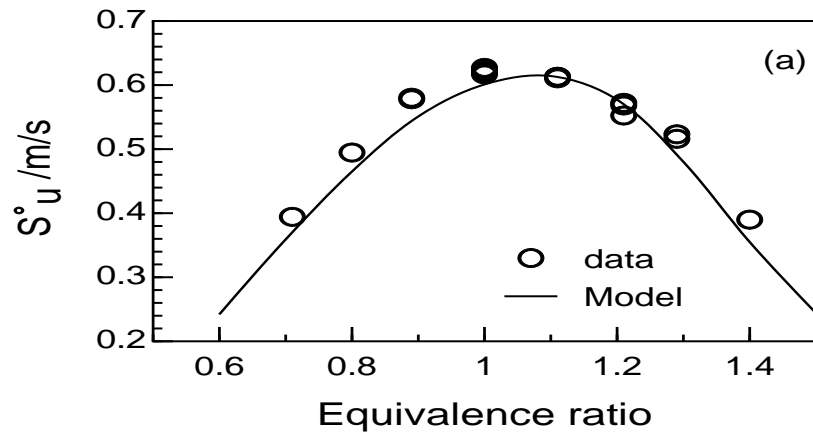
C. Togbé et al., Proc. Combust. Inst. **33**(1), 367–374 (2011)



Experimental (large symbols) and computed (lines and small symbols) concentration profiles obtained from the oxidation of 1-pentanol in a JSR at $\phi = 2$, $P = 10$ atm, $\tau = 0.7$ s.
C. Togbé et al., Proc. Combust. Inst. 33(1), 367–374 (2011)



Reaction paths from the kinetic modeling of 1-pentanol oxidation in a JSR at 10 atm.
C. Togbé et al., Proc. Combust. Inst. 33(1), 367–374 (2011)



Laminar burning velocities of 1-pentanol/air mixtures at $T=423$ K and 1 atm (a) and burnt gases Markstein lengths (b).

C. Togbé et al., Proc. Combust. Inst. **33**(1), 367–374 (2011)

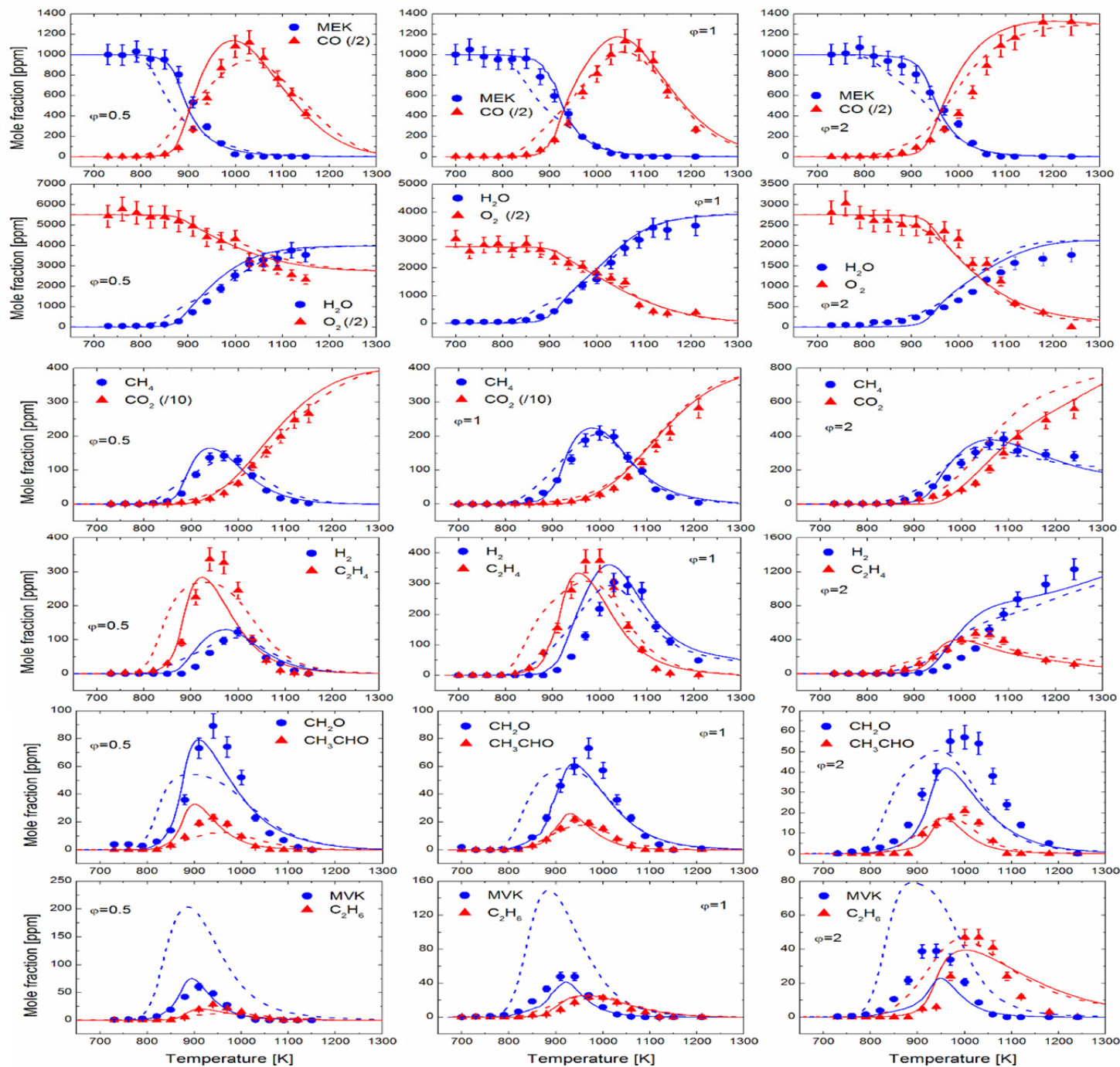
5.4.4-Butanone

Methyl Ethyl Ketone (MEK) is a four carbon linear ketone that can be produced through either chemical and biological conversion of furfural [1] or oxidation of 2-butanol. Besides its potential application as a fuel substitute [2], MEK is also used as solvent in the paint and adhesive industry.

With these considerations, and since MEK is the smallest ketone exhibiting secondary C-H bonds, this fuel is a molecule of choice to investigate the specificities of keto groups oxidation.

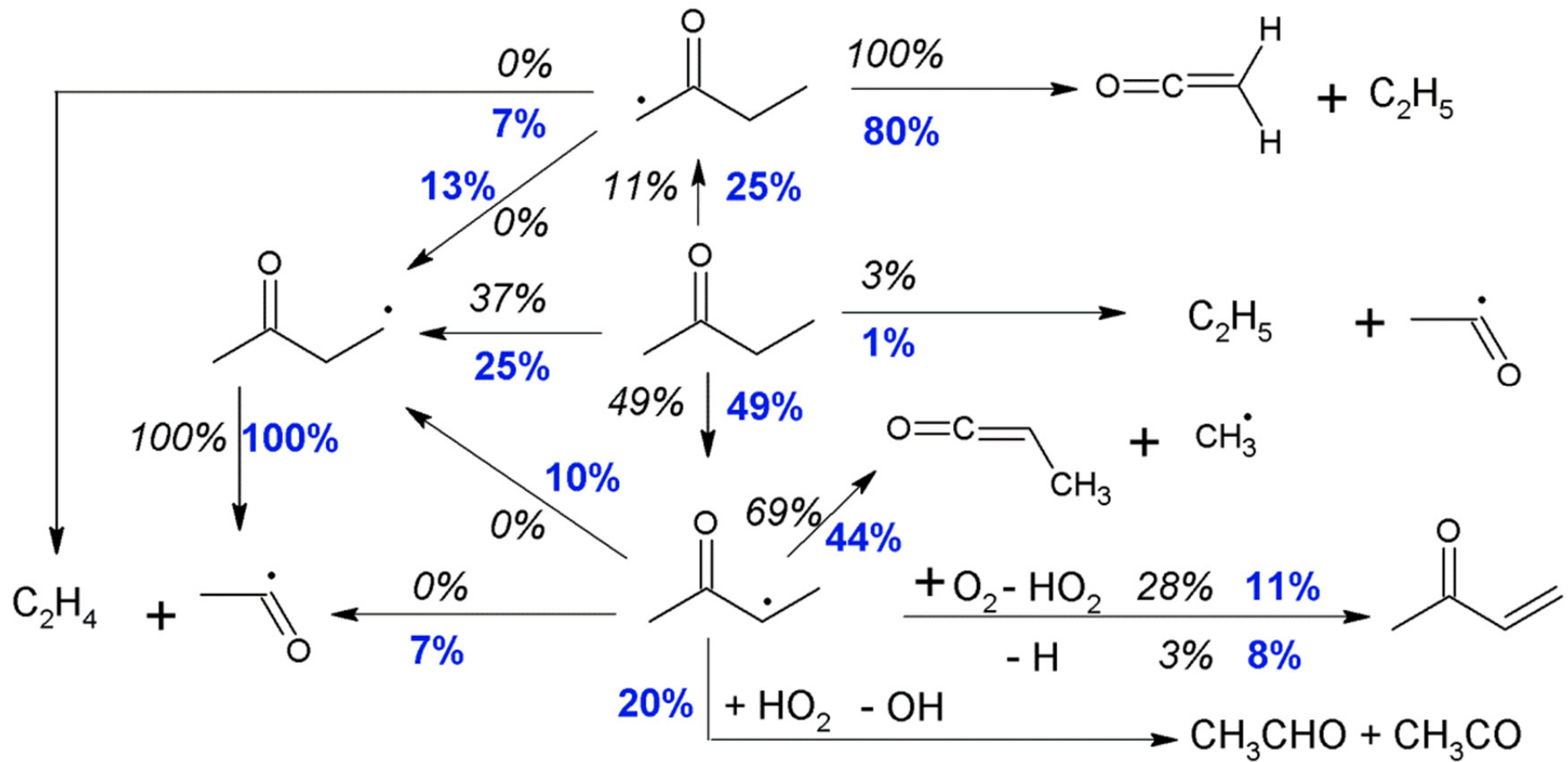
[1] E.R. Sacia, M. Balakrishnan, M.H. Deaner, K.A. Goulas, F.D. Toste, A.T. Bell, *ChemSusChem*, 8 (10)(2015) 1726-1736.

[2] F. Hoppe, U. Burke, M. Thewes, A. Heufer, F. Kremer, S. Pischinger, *Fuel*, 167 (2016) 106-117.



Comparison between experimental (symbols) and computed (Solid line: this work, dashed line: Serinyel et al. [10]) concentration profiles for the oxidation of MEK at 10 atm at different equivalence ratios.

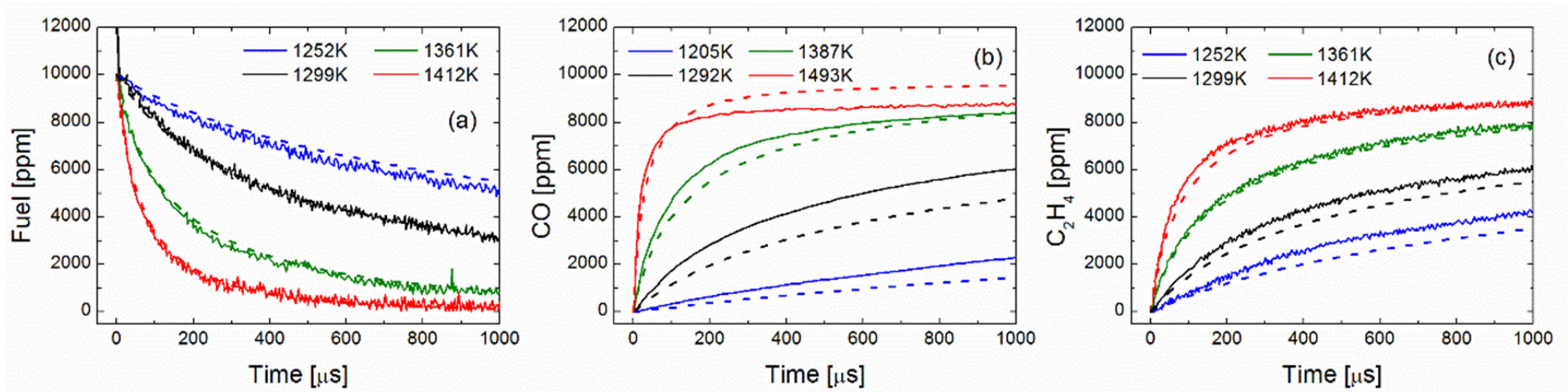
Rate of production analysis



Rate of production analyses of MEK oxidation at 950K, $\phi=1$ and 10 atm. Blue values: This work, black italic values: Serinyel et al. .

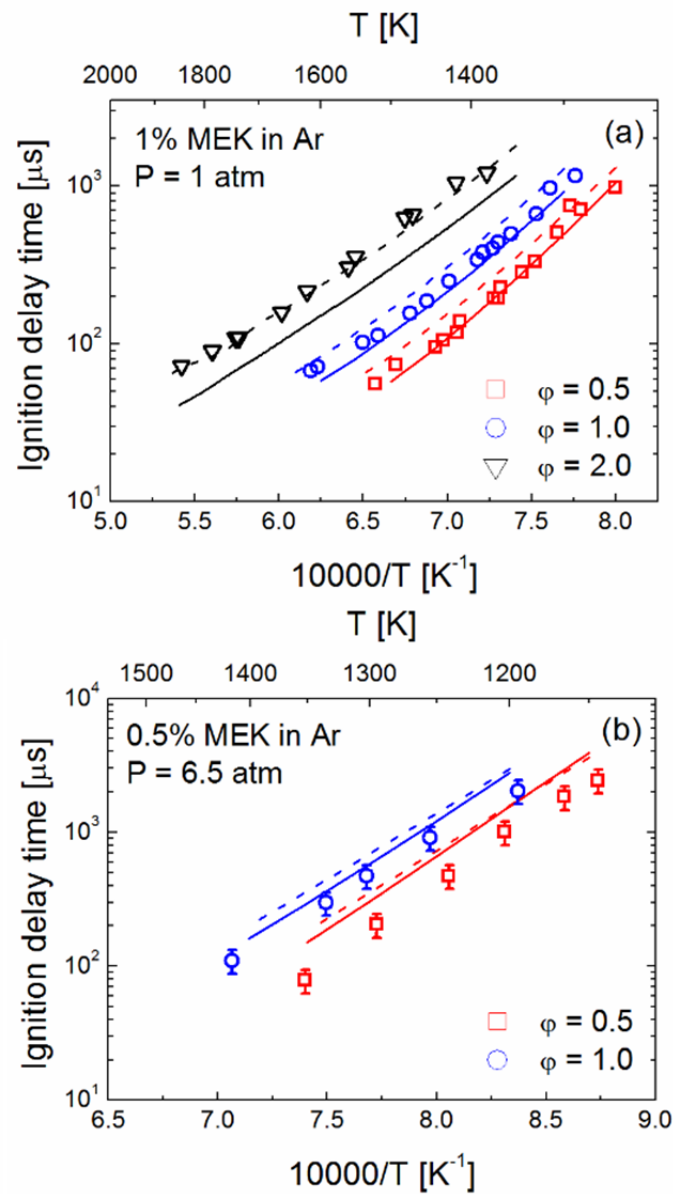
S. Thion, Proc. Combust. Inst. **36**, 459–467 (2017)

Pyrolysis and high temperature oxidation



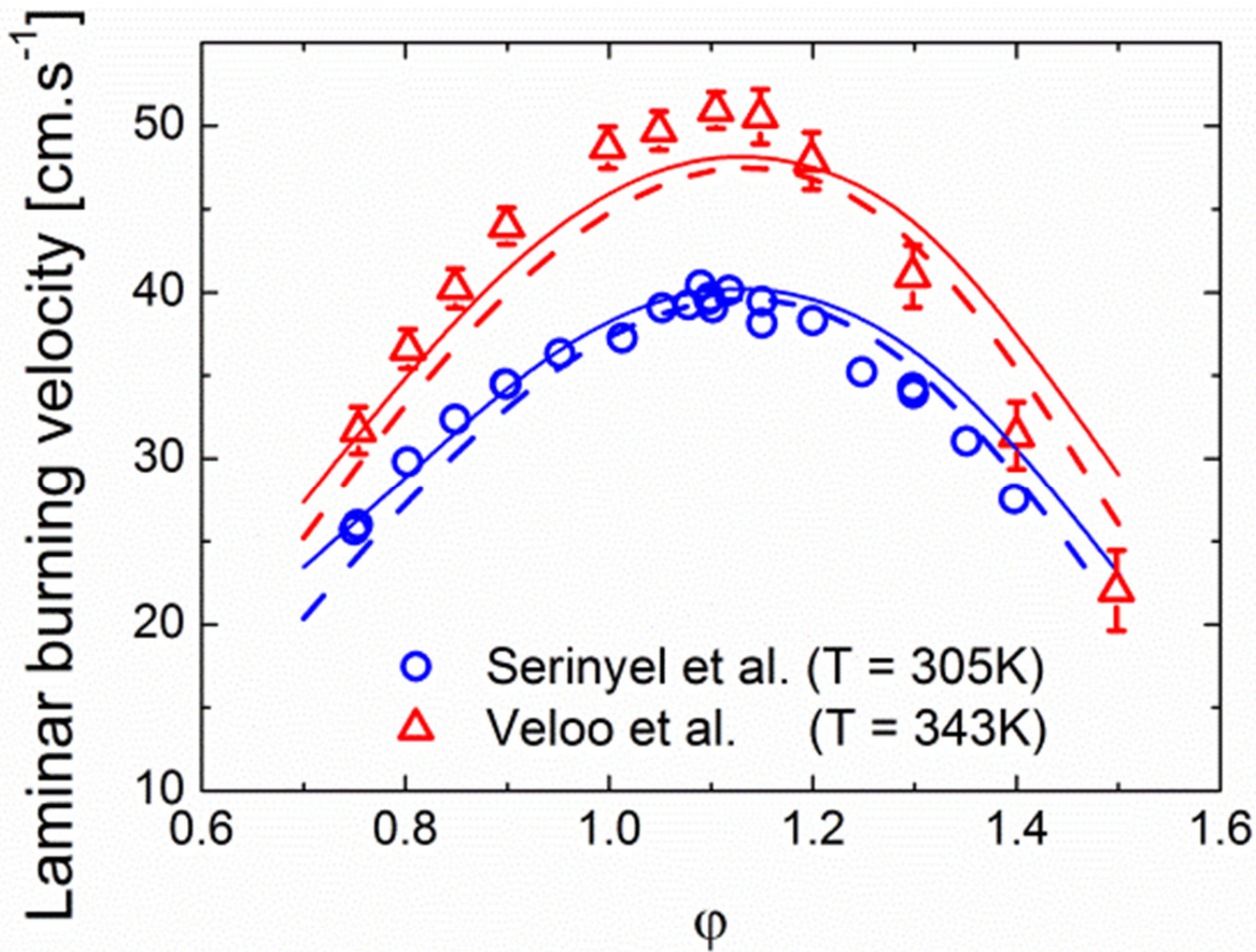
Species concentration profiles for the pyrolysis of 1% MEK in argon at an average pressure of 1.5 atm (solid line: experiments by Lam et al., dashed line: this work.)

S. Thion, Proc. Combust. Inst. **36**, 459–467 (2017)



Ignition delay times of MEK/ O_2 /Ar mixtures. Solid line: this work, dashed line: Serinyel et al.

S. Thion, Proc. Combust. Inst. **36**, 459–467 (2017)



Laminar burning velocities of MEK in air. Dashed line: Serinyel et al., solid line: this work.

S. Thion, Proc. Combust. Inst. **36**, 459–467 (2017)

5.4.5 ML and DEE

- Among proposed chemical platforms, levulinic acid is one of the most interesting

Alkyl levulinates produced from levulinic acid esterification contain keto and ester functional groups. The synthesis of these compounds starts with hemicellulose and cellulose hydrolysis to xylose and glucose, respectively. They can be converted to furfural and 5-hydroxymethylfurfural which in turn can be converted to levulinic acid.

Methyl levulinate (DCN ≈ 7.8) is considered here.

- Another interesting biofuels, produced via dehydration of bio-ethanol, is **diethyl ether** suitable for C.I. engines (CN > 125).

MODELING

The CHEMKIN II computer code was used for the kinetic modeling of the oxidation of the two fuels studied in a jet-stirred reactor.

The chemical kinetic reaction mechanism for ML oxidation contained **704 species involved in 3870 reversible reactions**; that for DEE oxidation contained **471 species involved in 2861 reversible reactions***.

Core mechanism: C₀-C₃ oxidation mechanism extended to model the oxidation of other oxygenates [a]

[a] S. Thion et al., Combust. Flame 185 (2017) 4-15; A.M. Zaras et al., Energy & Fuels 31 (6) (2017) 6194-6205.

* sub-mec included in DBE oxidation mechanism.

MODELING: ML Oxidation

We previously reported computed rate constants for H-abstractions by OH, H and CH₃ on ML [a].

H-abstraction reactions by other radicals were not found to be sensitive, and simple analogies were applied with no specific corrections for $k(T)$.

[a] S. Thion, A.M. Zaras, M. Szori, P. Dagaut, *Phys. Chem. Chem. Phys.* 17 (36) (2015) 23384-23391

MODELING: ML Oxidation

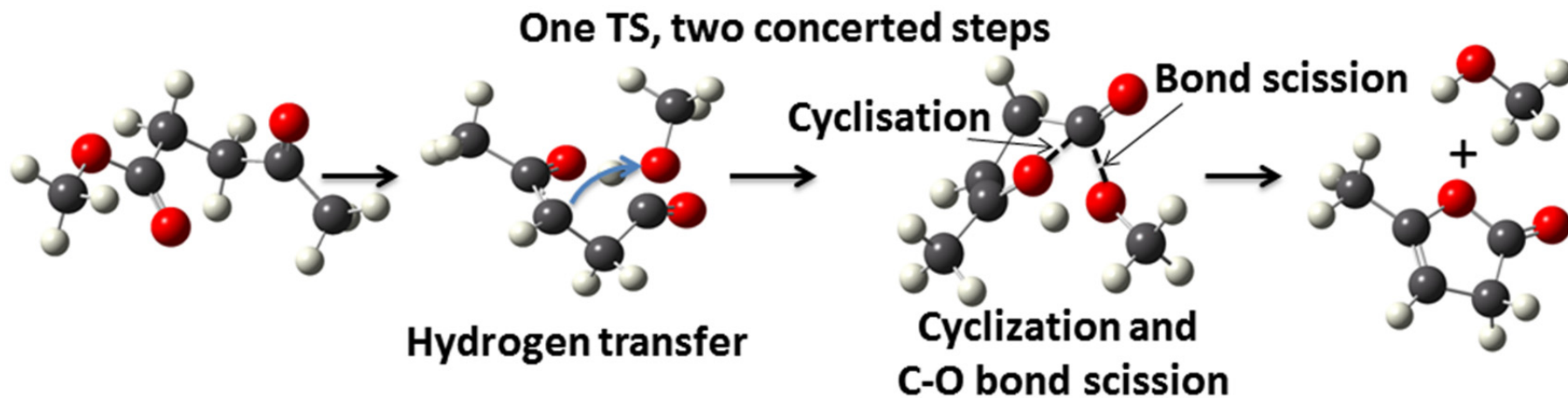
Additional theoretical calculations using the same computational strategy were performed in order to elucidate the decomposition pathways of ML and to obtain missing thermochemical properties.

These calculations were carried out using the Gaussian09 code [a] at the G3//MP2/aug-cc-pVDZ and G3B3 levels of theory.

[a] M.J. Frisch et al., Gaussian 09, Revision D.01; Wallingford CT, 2009

MODELING: ML Oxidation

The presence of oxygenated groups, and in particular of the ester group, favors molecular reactions. Ethyl (and larger) esters can easily decompose by H-transfer to produce an acid and an olefin. This type of reaction cannot take place here because a carbon chain is needed on the alcohol side, while methyl levulinate has only one carbon. Therefore, other possible pathways for the molecular reaction decomposition of methyl levulinate were explored by theoretical chemistry methods and a reaction similar to that of esters has been identified. It involves a complex TS:



Structure of the transition state during the molecular reaction yielding methanol and 5-methyl-2(3H)-furanone from ML.

MODELING: ML Oxidation

The high-pressure limit rate constant was computed at the G3B3 and G3//MP2/aug-cc-pVDZ levels of theory by following the strategy described in our previous work. We assumed hindered rotors cancel out, as in the work of Al Abbad et al.[a].

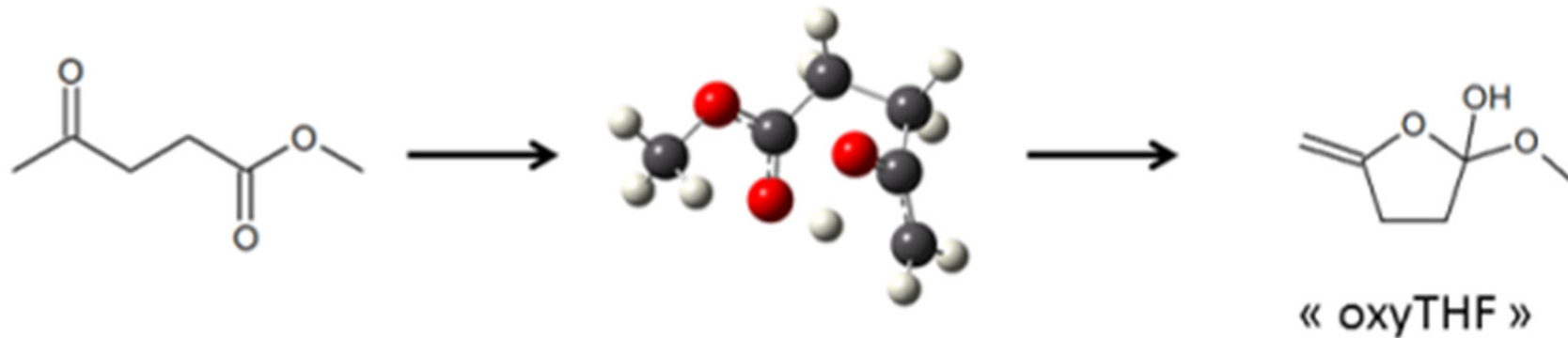
This molecular reaction is much slower than that observed in the case of esters: Its rate constant is 100 times lower at 1500 K and almost 200 times at 1000 K.

However, its low activation barrier allows it to play an important role.

[a] M. Al Abbad, B.R. Giri, M. Szori, A. Farooq, Proc. Combust. Inst. 36 (1) (2017) 187-193.

MODELING: ML Oxidation

A second reaction has also been identified. It involves another interaction between the two oxygenated groups in ML. It consists of a H-transfer from the C-"5" to the oxygen atom in C=O of the ester group. This transfer is accompanied by cyclization between the oxygen atom of the ketone group and C-"1" and the formation of a C=C double bond to give 2-methylene-5-methoxy-5-hydroxy-tetrahydrofuran ("oxyTHF"):

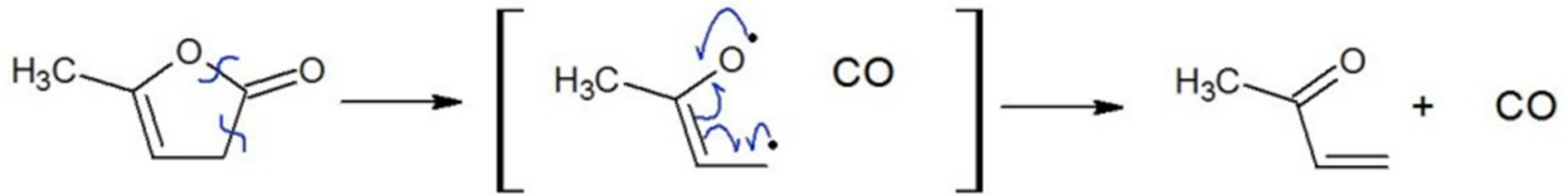


Formation of 2-methylene-5-methoxy-5-hydroxy-tetrahydrofuran.

The rate constant for this reaction was calculated with G3B3 and G3//MP2/aug-cc-pVDZ levels of theory.

MODELING: ML Oxidation

The α -angelica lactone is likely to undergo a molecular decomposition reaction similar to that of cyclopentanone yielding methyl vinyl ketone and CO:



Molecular decomposition of α -angelica lactone.

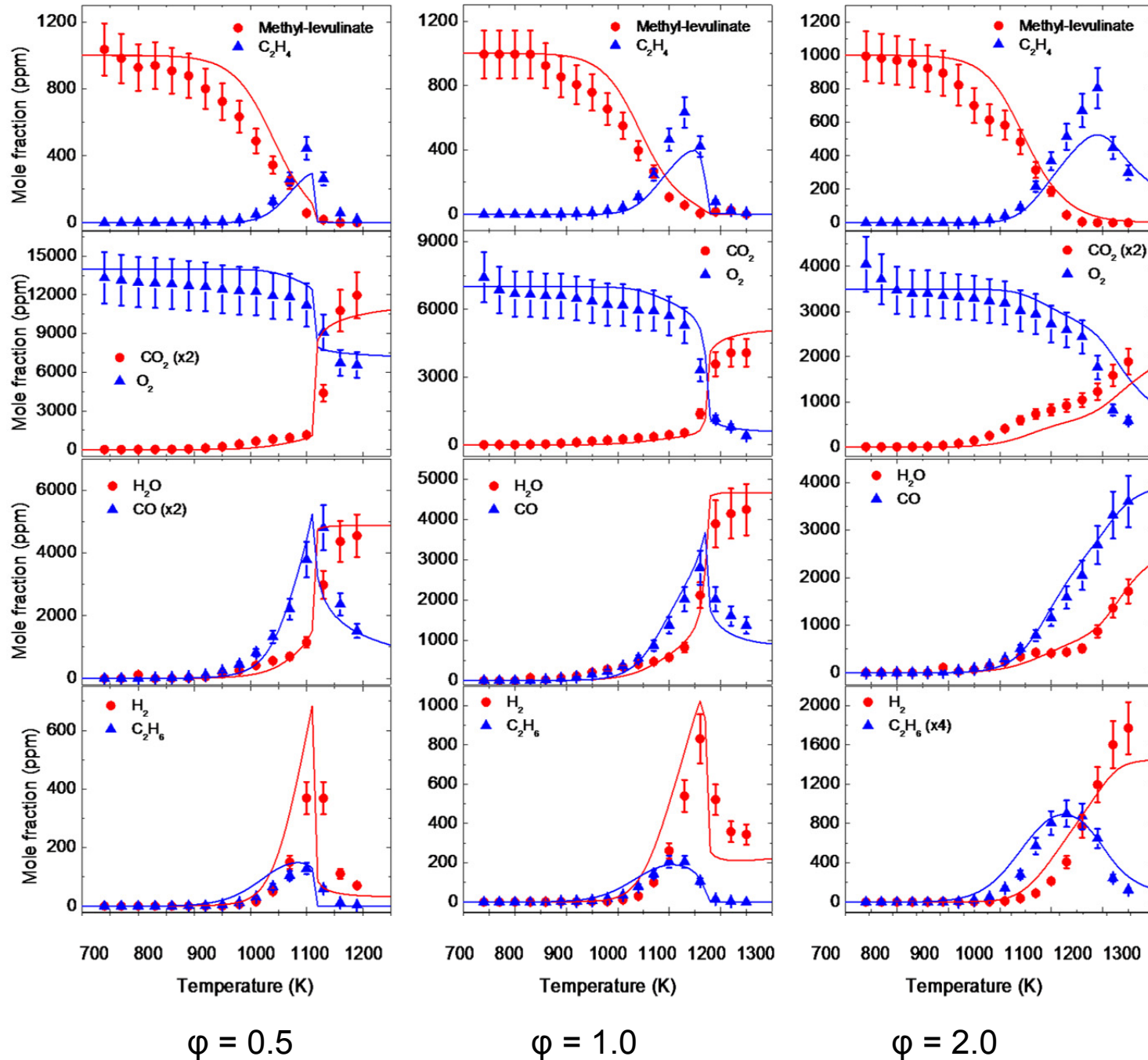
The rate constant for this reaction was calculated using the G3B3 method and the transition state theory.

RESULTS and DISCUSSION: ML Oxidation

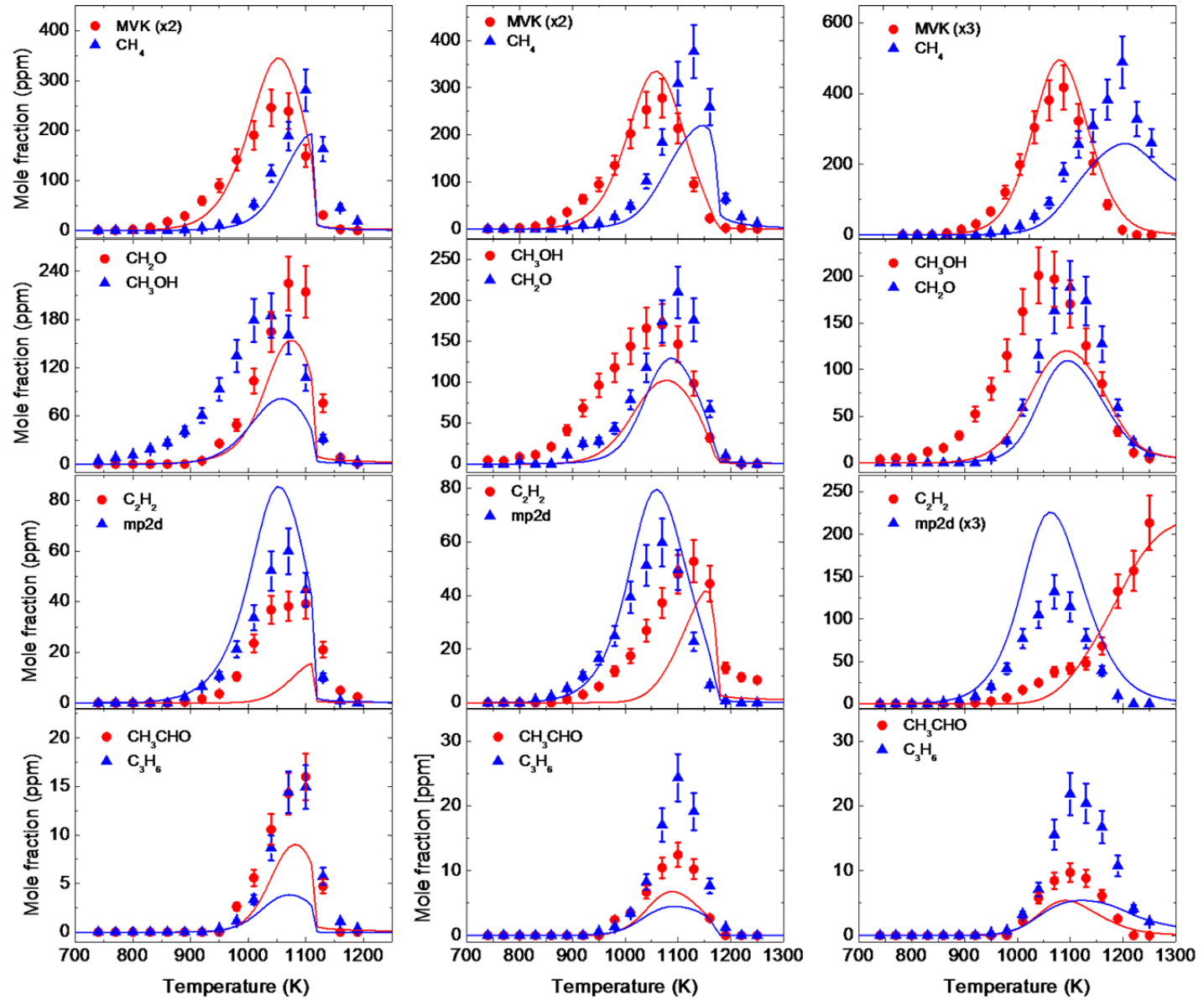
12 intermediate stable species were identified and quantified in addition to the reactants (O_2 , ML) and the final products (H_2O , CO_2).

No reactivity below 750K

RESULTS and DISCUSSION: ML Oxidation



RESULTS and DISCUSSION: ML Oxidation

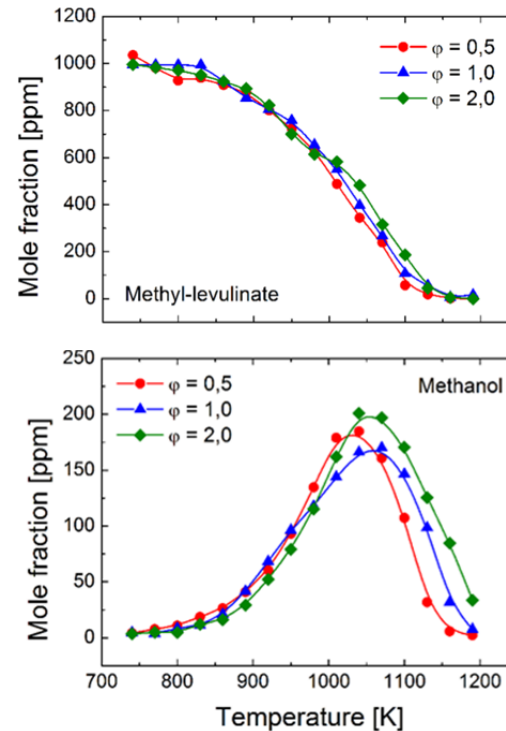


$\phi = 0.5$

$\phi = 1.0$

$\phi = 2.0$

RESULTS and DISCUSSION: ML Oxidation

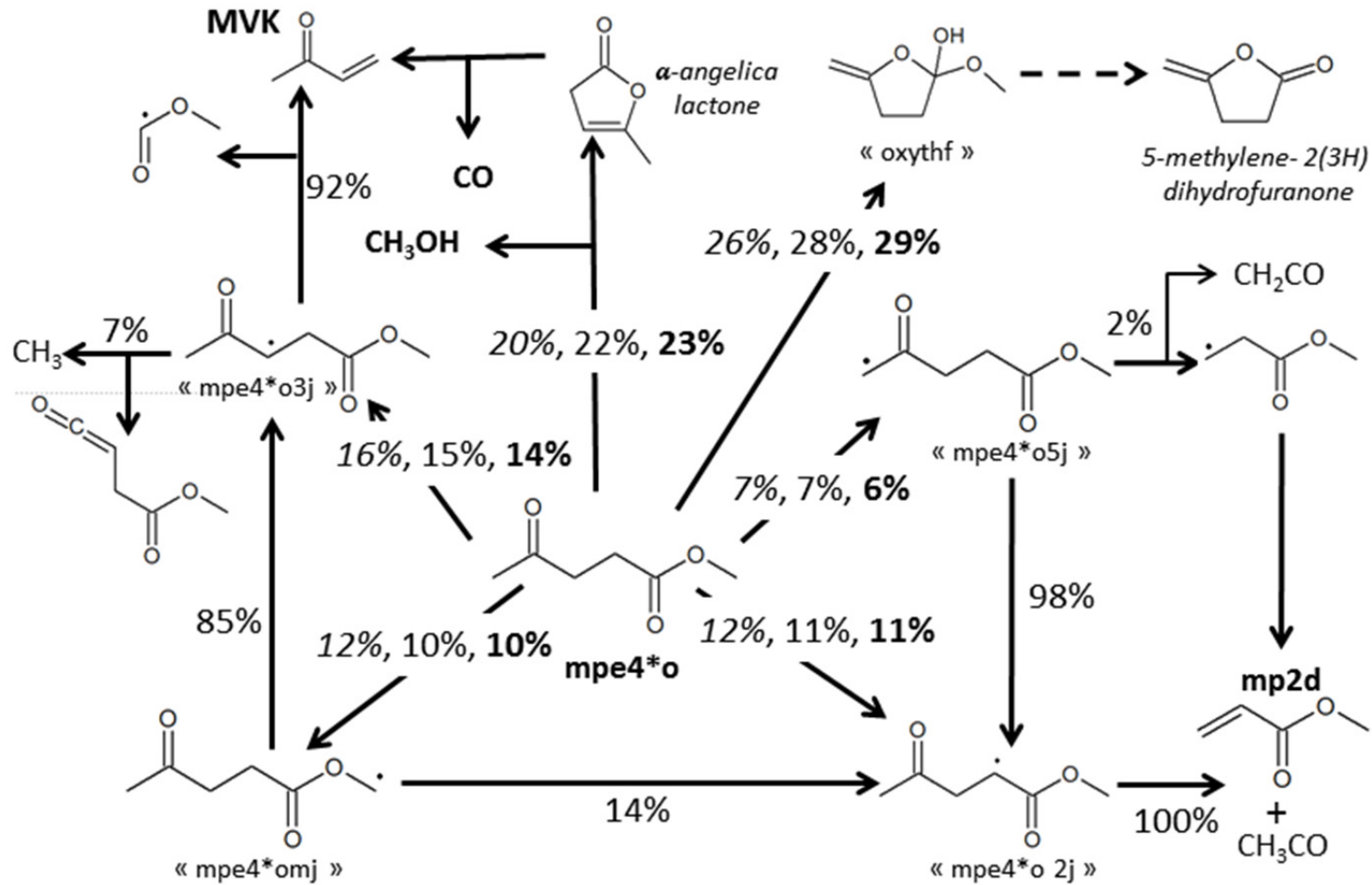


Consumption of ML and production of methanol during the oxidation of ML in a JSR.

Methanol production starts at the same temperature as fuel consumption (around 850 K) and in the same proportions for the 3 equivalence ratios.

Differences are observed ~ 1000 K, when the consumption of methanol $>$ formation. These experimental observations indicate that a large fraction of the fuel is consumed by molecular reactions yielding methanol.

RESULTS and DISCUSSION: ML Oxidation



Normalized rates of reaction analysis at $\phi = 1$, 1 atm and 1000 K corresponding to $\sim 50\%$ of fuel consumption. Values are also given at $\phi = 0.5$ (*italics*) and **2 (bold)** for the primary reactions. **Bold species are measured** and *italic species are detected* in trace amounts.

MODELING: DEE Oxidation

- Beta-scission reactions of fuel radicals and QOOH radicals are adopted from the CBS-QB3 calculations of Sakai et al. [a], and from our previous calculations on DBE [b].
- Other reactions related to low-temperature chemistry are taken analogous to our previous DBE study [b].
- Unimolecular decomposition reactions of DEE were taken from the study of Yasunaga et al. [c].
- Thermochemistry of the fuel, fuel radical as well as all related low-temperature species were taken from the theoretical study of Sakai et al. [a], and for other species these were calculated using using the group additivity method of Benson [d].

[a] Y. Sakai et al. Proceedings of the Combustion Institute 36 (2017) 195–202.

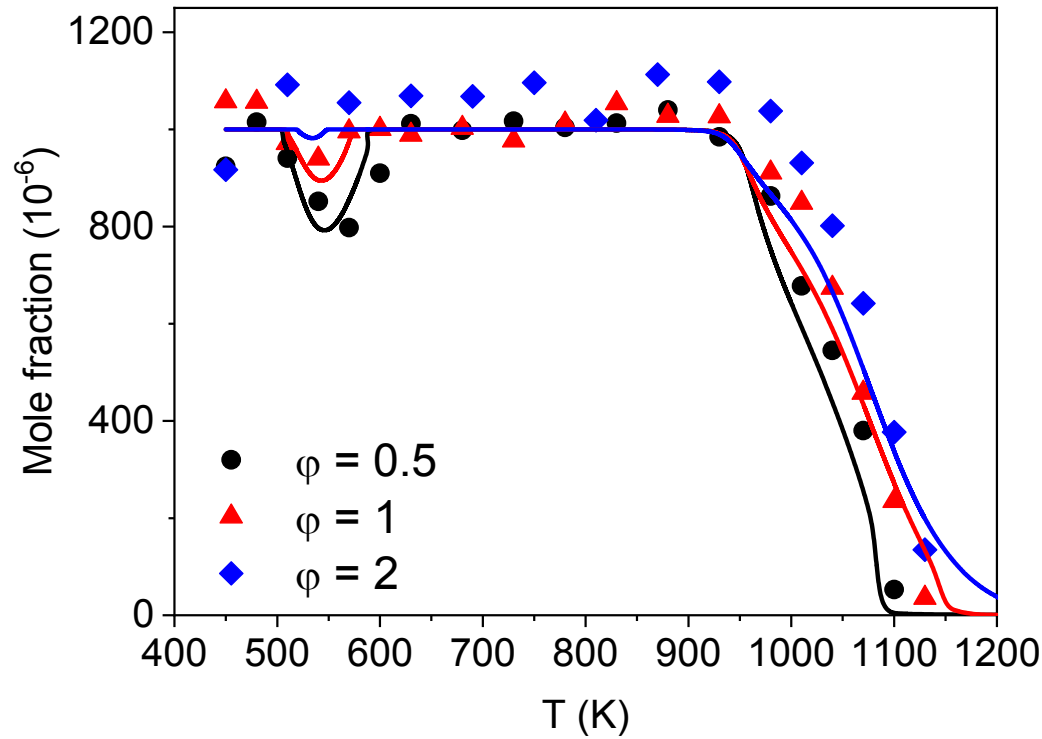
[b] S. Thion et al. Combustion and Flame 185 (2017) 4-15.

[c] K. Yasunaga et al. Journal of Physical Chemistry A 114 (2010) 9098-9109.

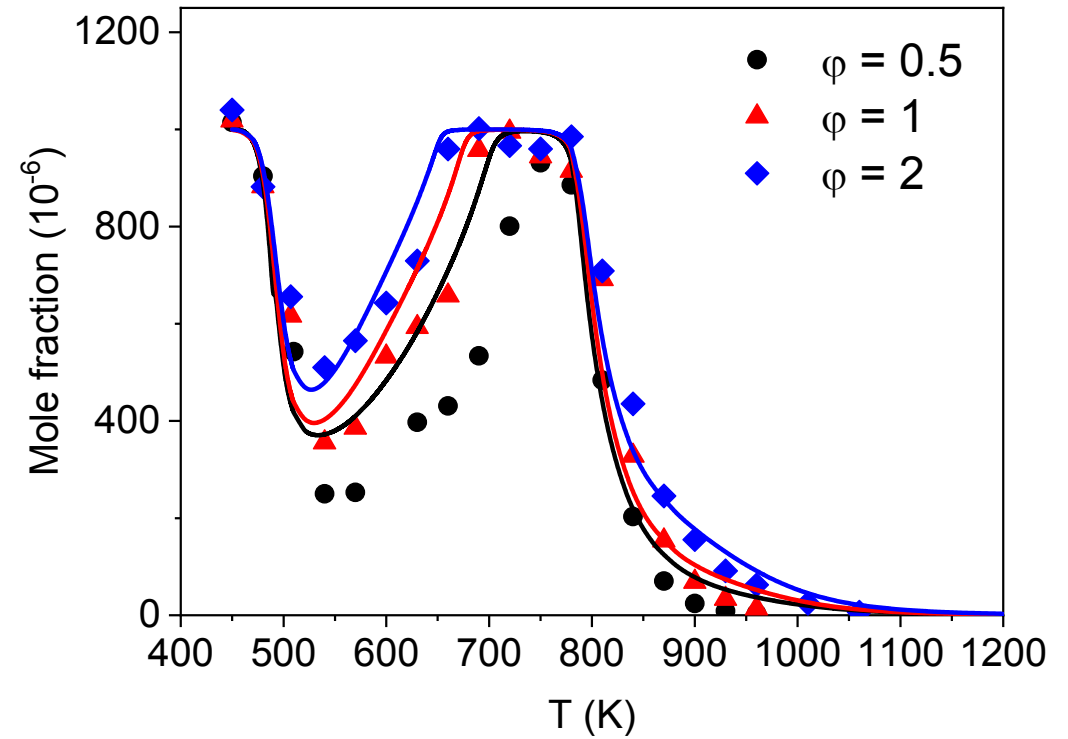
[d] S.W. Benson, Thermochemical Kinetics, Wiley, New York, 1976.

RESULTS and DISCUSSION: DEE Oxidation

1 atm



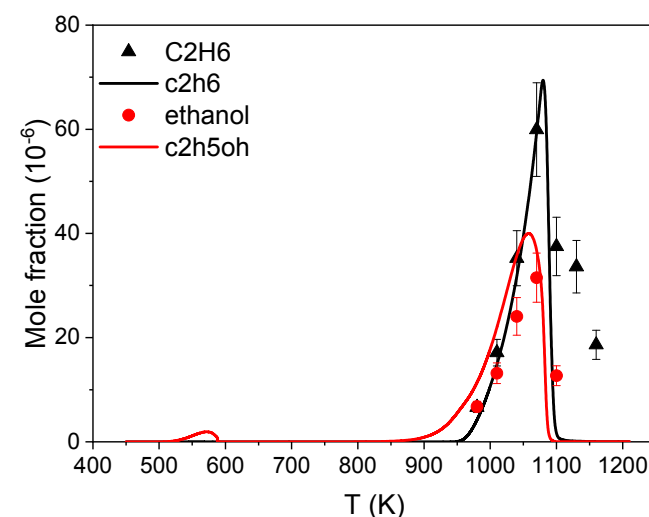
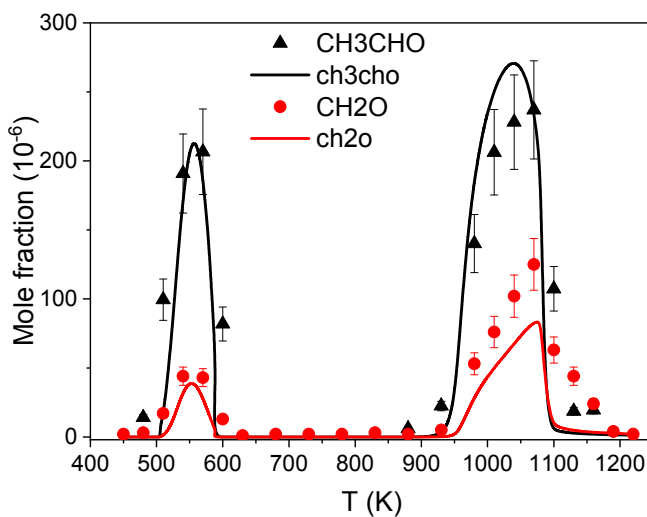
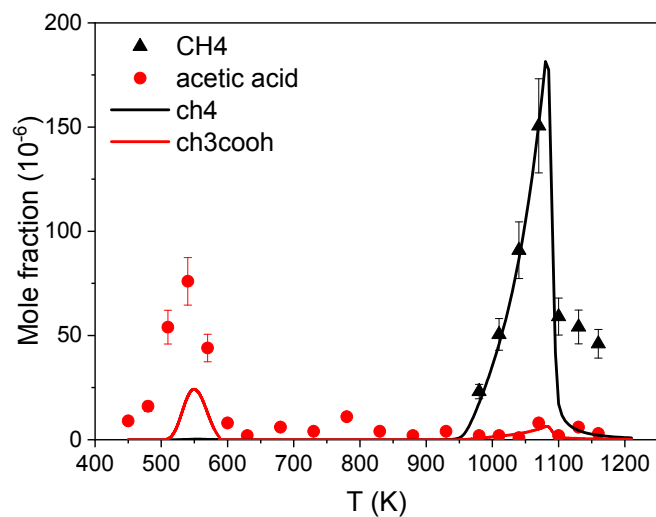
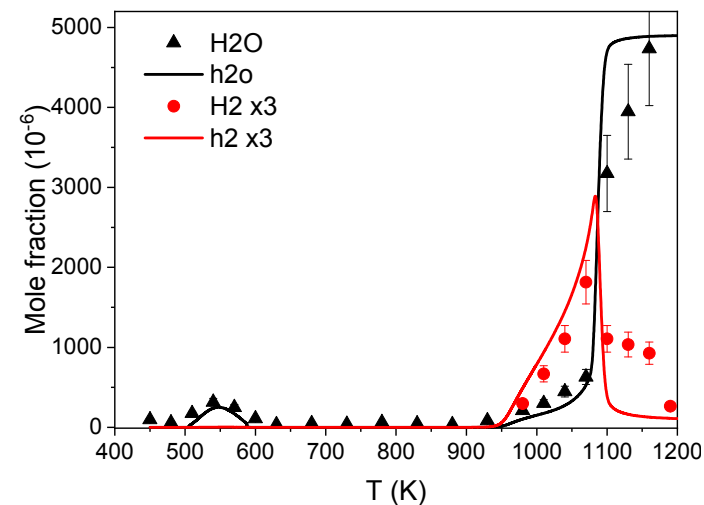
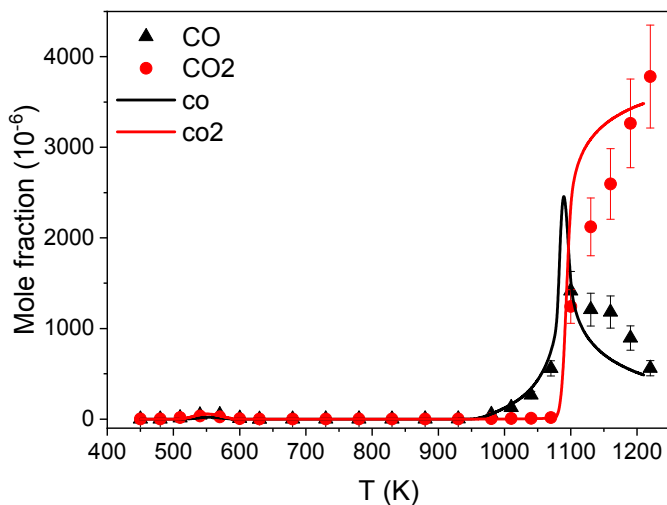
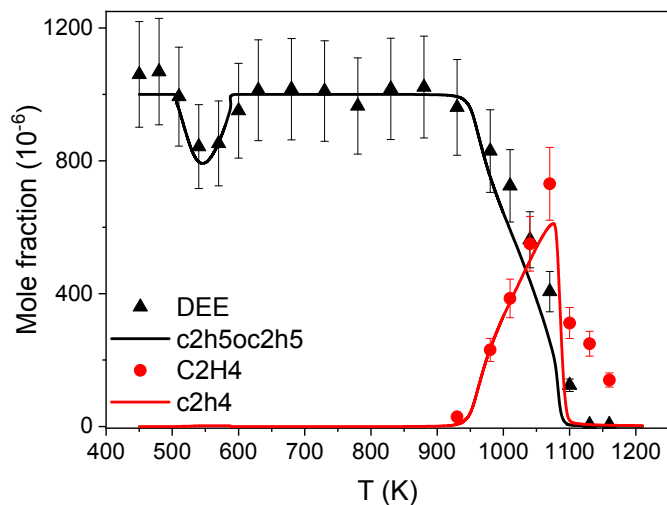
10 atm



DEE mole fraction evolution as a function of temperature; lines represent simulations.

Z. Serinyel et al., *Combust. Flame* 193, 453–462 (2018)

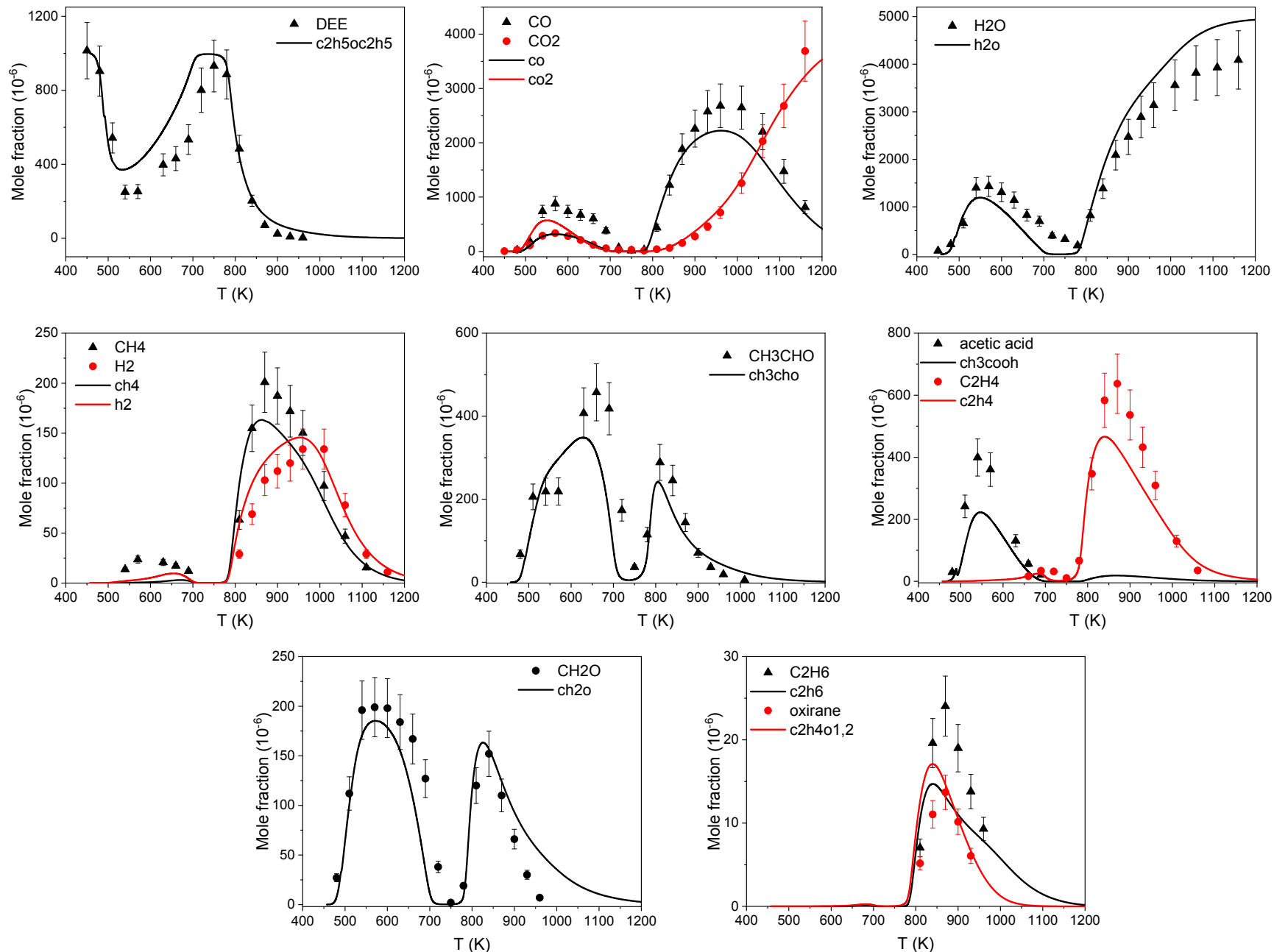
RESULTS and DISCUSSION: DEE Oxidation



Mole fraction for the $\phi = 0.5$ experiment at 1 atm, initial mole fraction of DEE: 1000 ppm, $t = 0.07s$.

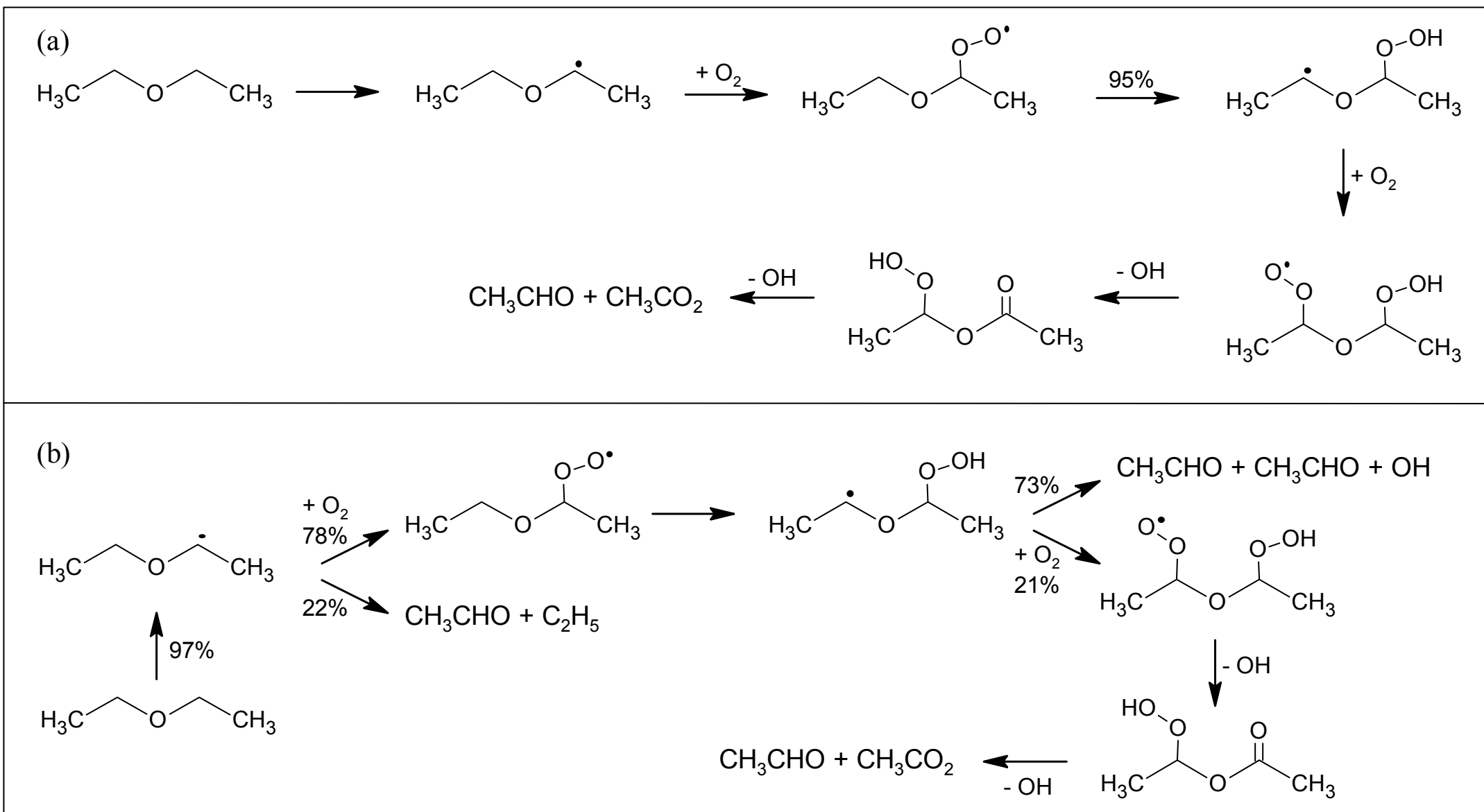
Z. Serinyel et al., Combust. Flame 193, 453–462 (2018)

RESULTS and DISCUSSION: DEE Oxidation



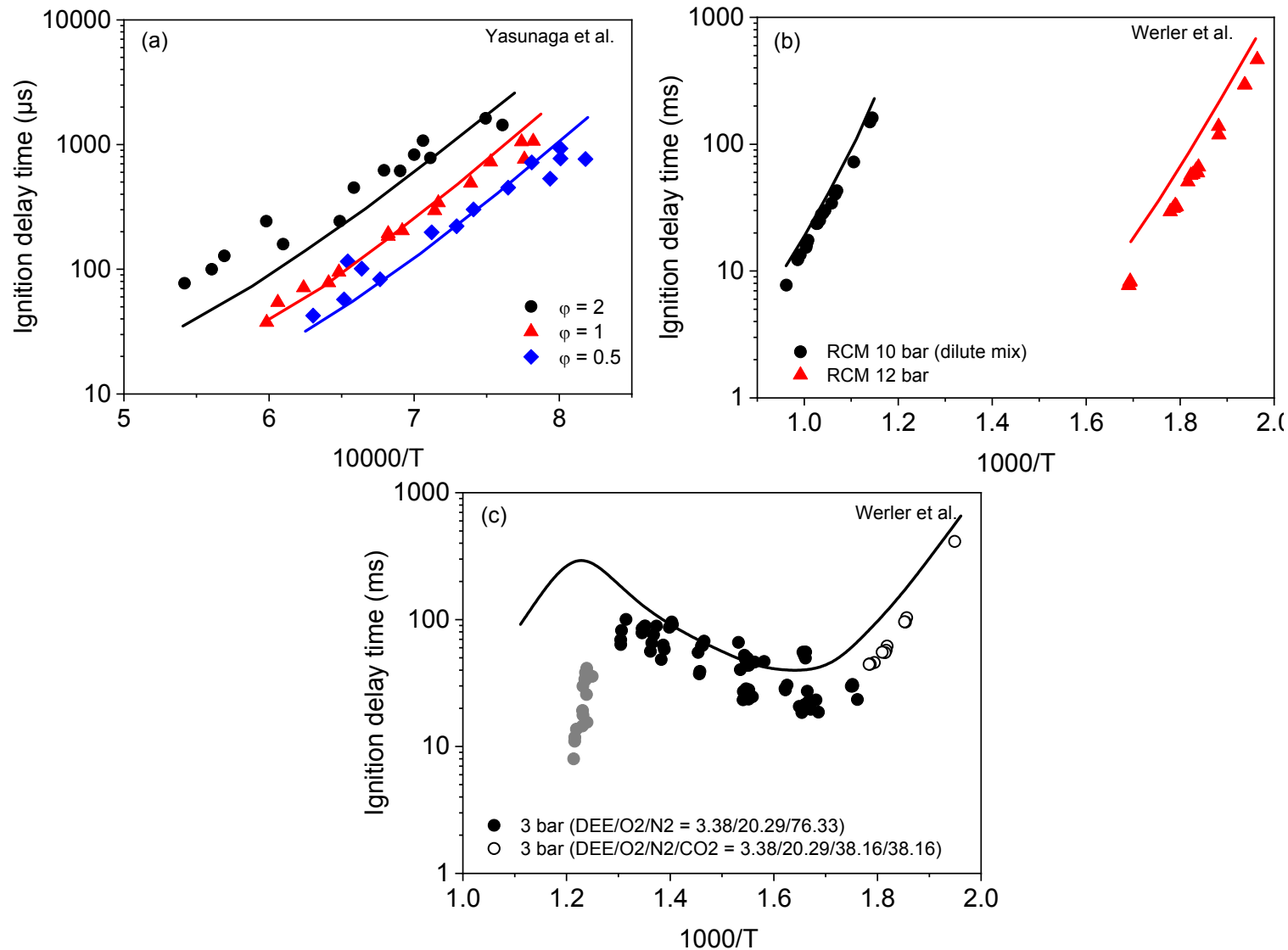
DEE oxidation $\phi = 0.5$ experiment at 10 atm, $t = 0.7s$.

RESULTS and DISCUSSION: DEE Oxidation



Reaction pathways at (a) 510 K and (b) 690 K (10 atm, $\phi = 0.5$)

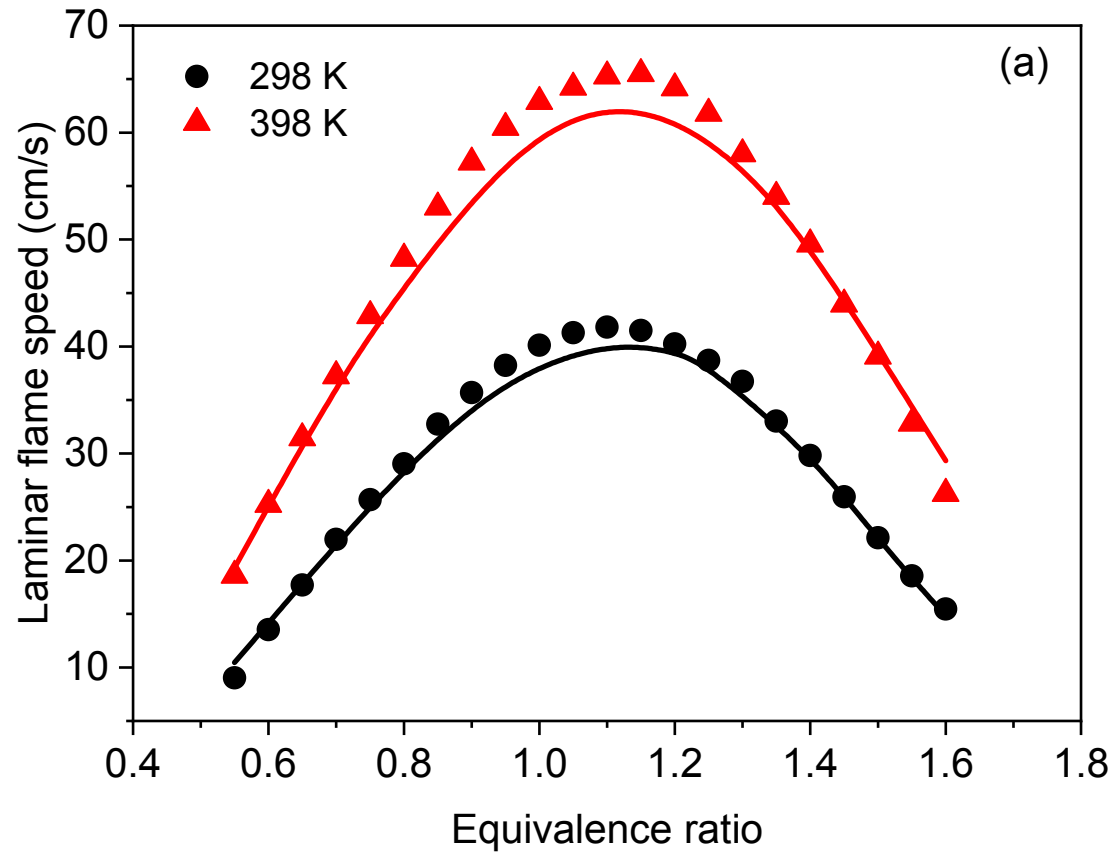
RESULTS and DISCUSSION: DEE Oxidation



Shock tube and RCM ignition (a) 1% DEE in Ar, $p = 1$ atm; (b) 0.698% DEE in Ar, $\phi = 1$, $p = 10$ – 12 bar; (c) DEE in air, $\phi = 1$, RCM by Werler et al. 2015

Z. Serinyel et al., Combust. Flame 193, 453–462 (2018)

RESULTS and DISCUSSION: DEE Oxidation



Laminar flame speed of DEE/air mixtures [a] as a function of ϕ at 1 atm, $T_u = 298$ and 398 K.

Z. Serinyel et al., *Combust. Flame* 193, 453–462 (2018)

[a] F. Gillespie et al. *Energy* 43 (2012) 140-145.